Broadband Microwave Push-Pull Power Amplifiers

Robert Martin Hooper Smith, BEng.

A thesis submitted to Cardiff University
in candidature for the degree of

Doctor of Philosophy

September 2013

Declaration

This work has not previously been accepted in substance for any degree and is not concurrently submitted in candidature for any other higher degree.

Signed: ..... (Candidate)

Date: .....

Statement 1

This thesis is being submitted in partial fulfilment of the requirements for the degree of PhD.

Signed: ..... (Candidate)

Date: .....

Statement 2

This thesis is the result of my own independent work/investigation, except where otherwise stated. Other sources are acknowledged by explicit references.

Signed: ..... (Candidate)

Date: .....

Statement 3

I hereby give consent for my thesis, if accepted, to be available for photocopying, inter-library loan and for the title and summary to be made available to outside organisations.

Signed: ..... (Candidate)

Date: .....

Abstract

The research work presented in this thesis aims to achieve high-power, high-efficiency amplification across substantial bandwidths at microwave frequencies. The push-pull topology was identified as a promising possible solution which had previously not been considered for this application.

The key component in the push-pull power amplifier is the balun, which converts between balanced and unbalanced signal environments. The novel use of ferrite materials allowed the half-wavelength resonance of a coaxial-cable transmission line balun to be suppressed, greatly extending its bandwidth. This was done by utilising the resistive properties of the ferrite material at frequencies greater than 1 GHz, at which these materials are not usually studied.

The multi-decade performance of the transmission line baluns opened up the possibility of realising push-pull power amplifiers across similar bandwidths. The measurement of these baluns revealed that they present a resistive impedance to the odd-harmonic frequencies, and an open circuit to the even-harmonic frequencies. This is a significant departure from the conventional view of the push-pull mode, and led to the modes of operation inside a microwave push-pull power amplifier being reconsidered.

Factorised waveform expressions were used to describe the new modes of operation, and these were verified through load-pull simulations and measurements. The waveforms were found to resemble the inverted modes of operation, with similar desirable characteristics such as high efficiency and an increase in output power compared to Class A.

The viability of the push-pull amplifier topology was demonstrated through two prototype amplifiers, which achieved high output power levels and efficiencies over multi-octave bandwidths. Measurement systems for characterising and analysing these amplifiers were developed, which should lead to improved understanding and better performance in future.

Key Contributions

Contribution 1

Demonstration of the viability of the push-pull amplifier topology as a method for obtaining high-power, high-efficiency operation across multi-octave bandwidths at microwave frequencies.

Contribution 2

Identification of and investigation into the modes of operation of a push-pull power amplifier using transmission line baluns.

Contribution 3

Novel use of ferrite materials to suppress the half-wavelength resonance of a coaxial-cable transmission line balun.

Contribution 4

Development of a measurement system for investigating the push-pull power amplifier with differential input ports.

Acknowledgements

First and foremost, I would like to thank Professor Steve Cripps for his dedicated supervision throughout my PhD. His enthusiasm for the subject and renowned expertise have been inspirational. I am honoured to have worked with him.

I am grateful for the insight of Professor Paul Tasker, whom it has been a pleasure to work with, and to Professor Johannes Benedikt for securing the funding that made my PhD possible in the first place. I would like to extend a special thanks to Dr Jonny Lees for always finding time to offer me practical expertise and advice. I have learnt a great deal from him and for that I am extremely grateful.

Thanks to Steve Wales of Roke Manor Research (recently renamed to Chemring Technology Solutions) and Mark Walden, formerly of Roke, for acting as industrial supervisors and offering a different perspective on the work conducted during the project. Thanks also to Dr Jason Devaney for his support and guidance throughout my time working with and for Roke.

I would like to thank everyone I had the pleasure of working with at the Centre for High Frequency Engineering at Cardiff University. In particular, Pete Wright, Vincenzo Carrubba, Randeep Saini and Jack Naylon taught me a lot about RF and microwave engineering when I started and helped me 'learn the ropes'. Thanks also to Will McGenn, James Bell and Tim Canning for the useful discussions throughout the years.

Thanks to all my friends outside of university, who have always been there with welcome distractions from work. Amy, James, Dave, Ollie and Kev, cheers!

I owe a great deal to my parents; Lesley and Martin, for their continuous support and encouragement. They have always offered advice and wisdom when I have needed it. Thanks to my brother Phil for always being there and pushing me to do the best I can.

Finally, I owe a special thanks to Emma for her endless patience and understanding. Thank you for believing in me.

List of Publications

First-author papers

1. R. M. Smith, J. Lees, P. J. Tasker, J. Benedikt, and S. C. Cripps, "A Design Methodology for the Realization of Multi-Decade Baluns at Microwave Frequencies," in *Microwave Symposium Digest (MTT), 2011 IEEE MTT-S International*, pp. 1 - 3, June 2011.

2. R. M. Smith, J. Lees, P. J. Tasker, J. Benedikt, and S. C. Cripps, "A Novel Formulation for High Efficiency Modes in Push-Pull Power Amplifiers using Transmission Line Baluns" *Microwave and Wireless Components Letters, IEEE*, vol. 22, no. 5, pp. 257 - 259, May 2012.

3. R. M. Smith and S. C. Cripps, "Design of High Efficiency, Multi-Octave Microwave Push-Pull Power Amplifiers" in *Automated RF and Microwave Measurement Society Conference*, April 2012.

4. R. M. Smith, J. Lees, P. J. Tasker, J. Benedikt, and S. C. Cripps, "A 40W Push-Pull Power Amplifier for High Efficiency, Decade Bandwidth Applications at Microwave Frequencies, in *Microwave Symposium Digest (MTT), 2012 IEEE MTT-S International*, pp. 1 - 3, June 2012.

5. R. M. Smith and S. C. Cripps, "Broadband Push-Pull Power Amplifier Design at Microwave Frequencies," in *Automated RF and Microwave Measurement Society Conference*, April 2013.

   Winner of the Steve Pugh Memorial Prize for Best Paper.

Additional papers

- V. Carrubba, J. J. Bell, R. M. Smith, Z. Yusoff, J. Lees, J. Benedikt, P. J. Tasker and S. C. Cripps, "Inverse Class-FJ: Experimental Validation of a New PA Voltage Waveform Family," *IEEE Asia Pacific Microwave Conference (APMC)*, pp. 1254 - 1257, December 2011.

Contents

Chapter 1

Introduction

1.1 Broadband Microwave Push-Pull Power Amplifiers

A microwave power amplifier is a device that converts DC energy into microwave energy in order to increase the amplitude of an input signal. This concept is simple enough, and yet designing a power amplifier for a modern communications system is a complicated task. This is due to the numerous requirements that are placed on the power amplifier, many of which will become apparent throughout this thesis.

As a starting point, it is worth expanding on the title of the thesis in order to clarify some of the terms contained within it.

Although **'broadband'** is a commonly used term in RF and microwave engineering, its definition varies significantly depending on perspective. For cellular network applications, for instance, broadband could refer to a relative bandwidth of less than 10%. For this thesis, broadband is taken to mean 'greater than one octave of relative bandwidth' (66.7%).

'Microwave' is defined in the Oxford English Dictionary as "an electromagnetic wave with a wavelength between about one millimetre and 30 centimetres (corresponding to a frequency between 300 gigahertz and one gigahertz)" [1]. The work presented in this thesis focusses on the low-end of this range, and also below 1 GHz, but the concepts can be extended to higher frequencies.

'Push-pull' is a well-known amplifier topology which is described in Chapter 2. It has many advantages, as well as a number of design challenges, and until now has not been widely investigated as a method of achieving broadband performance at microwave frequencies.

And finally, the **'power amplifier'** itself is briefly introduced in the next section.

1.2 The Power Amplifier

The power amplifier (PA) is a crucial component in the transceiver, a simplified form of which is shown in Fig. 1.1. Of all the components in the transmitter and receiver chain, it is generally the power amplifier that consumes the most power, and so largely determines the power efficiency of the transmitter.

Power amplification was originally achieved through the use of vacuum device (or 'valve') amplifiers. These devices can operate at high power levels and high frequencies, however have relatively short lifespans compared to solid-state amplifiers. They also require high voltages and high temperatures to operate, which makes them unsuitable for mobile applications.

Solid-state amplifiers have replaced vacuum tubes in most applications, and have been integrated into billions of fixed and portable communications devices as well as military hardware and systems for industrial, scientific and medical (ISM) applications. It is worth noting that vacuum tubes are still used in certain high-power applications, typically above 1 kW, and so the transition to solid-state amplifiers is not yet entirely complete.

A number of transistor structures have been developed, based on either the field-effect transistor (FET) or the bipolar junction transistors (BJT). The most-used semiconductor material of recent years has been silicon (Si), firstly in the implementation of BJTs and later as the laterally-diffused metal-oxide semiconductor (LDMOS) FET. The other widely used semiconductor material has been gallium arsenide (GaAs), a 'III-V' compound semiconductor used in high electron mobility transistors (HEMTs) and heterojunction bipolar transistors (HBTs). Other semiconductor materials have been utilised in solid-state power amplifiers, including silicon germanium (SiGe), silicon carbide (SiC) and indium phosphide (InP), however silicon and gallium arsenide are used for the majority of applications.

In the last decade, the emergence of another III-V compound semiconductor mate-

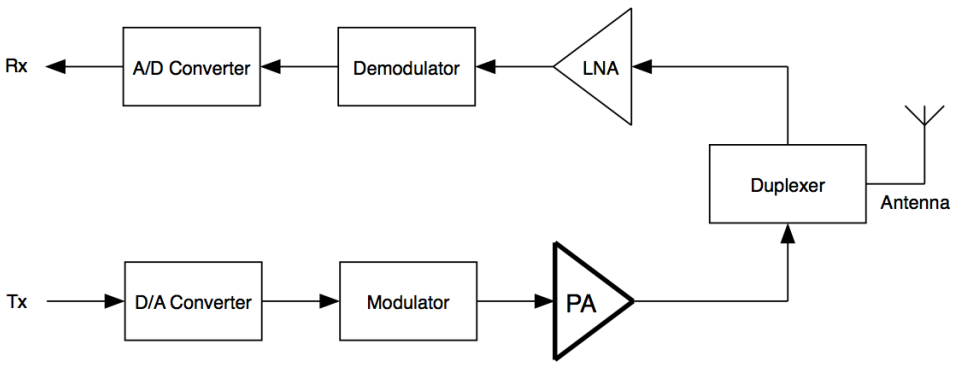

Figure 1.1: Simple transceiver block diagram

rial, gallium nitride (GaN), has opened up the possibility of replacing vacuum tubes in high-power, high-frequency applications where solid-state amplifiers had previously been unsuitable. Gallium nitride transistors feature heavily in this thesis, and are introduced in Chapter 2.

The power amplifier is a key component in the transmitter chain, and any improvements that can be made to it will have a profound effect on the overall system. As a result, there is a large incentive to conduct research into improving the power amplifier.

1.3 Research Motivation

If the ideal power amplifier were to be defined, it would have the following characteristics;

- Broadband operation
- High output power
- High power efficiency
- High gain
- Linear
- Reliable
- Minimal size, weight and cost

Simultaneously achieving the first three of these characteristics is the key motivation behind the research in this thesis.

Having an amplifier that can cover a wide range of operating frequencies is desirable for several reasons. It requires fewer amplifiers to cover the desired bandwidth, and thus removes the need for switching systems to select the appropriate amplifier. This makes transmitters smaller, cheaper and simpler. The techniques developed for multi-octave bandwidth amplifiers can also find use in narrower band applications.

High output power levels (where permitted) are useful for communications signals in order to increase the signal-to-noise ratio (SNR) and hence the information capacity of the communication channel. For radar and jamming applications, increased power will increase the range that the systems can operate over and improve their effectiveness. Being able to realise a single high-power amplifier means that it is unnecessary to combine the output power from several low-power amplifiers, and this again reduces cost and complexity, as well as eliminating the power loss in the combiners and hence improving efficiency.

DC-to-RF conversion efficiency a measure of how much energy is converted to 'useful' RF energy, and how much is 'wasted' as heat. Improving efficiency means that less energy is required to achieve a desired output power, and for portable devices this has a

direct impact on battery life. For systems such as cellular base-stations, reducing energy consumption results in lower operating expenditure (OPEX) for the network provider, and is more environmentally friendly. If the DC-to-RF conversion efficiency of the power amplifier can be improved, the reduced heat dissipation also means that it requires less cooling. This further reduces power consumption of the overall transmitter, as well as size, weight, cost and complexity.

One of the key applications for this work is in the field of jamming. Jamming is the transmission of signals to purposely lower the signal-to-noise ratio of another signal, with the intention of disrupting the communication link. High power levels are required to reduce the signal-to-noise ratio to the extent that the target signal cannot be received.

One method to counteract jamming is frequency hopping. This involves regularly changing the frequency at which a signal is broadcast, such that the jammer cannot determine the broadcast frequency and hence cannot disrupt the signal. An effective jammer is therefore required to operate over wide bandwidths in order to be able to block the signal at any frequency it may be broadcast at. In addition, it is desirable for high power efficiencies to be achieved in order to reduce the overall size and weight of the jammer.

In the wireless communications space, modern systems can operate across a wide range of frequencies, although the signal bandwidths are typically narrow. Long Term Evolution (LTE), for example, has portions of frequency spectrum allocated between 698 MHz and 3.8 GHz [2], and it is desirable to cover as many of these frequency bands as possible in order to maximise the number of countries that the equipment can be used in. In addition, both base-stations and handsets are likely to have to support multiple generations of cellular communications systems.

Whilst a mobile handset is limited to relatively low power levels, a base-station's output power requirements are much higher. As previously mentioned, power efficiency is important to reduce operating expenses. Again, the three requirements of high output power, good power efficiency and broadband operation are present.

Instrumentation is another potential application for broadband power amplifiers. A modern Vector Network Analyser (VNA) can cover a frequency range of 10 MHz to 26.5 GHz [3], and a driver PA that could cover this bandwidth would be extremely useful for large-signal measurements.

1.4 Research Objectives

Two key objectives for the research were set;

1. Investigate the push-pull topology as a method for achieving high-power, high efficiency power amplification over multi-octave bandwidths.

2. Deliver a prototype power amplifier with performance figures that match or exceed previously published work.

1.5 Thesis Organisation

The basic modes of operation of RF power amplifiers are outlined in Chapter 2, along with the existing literature on broadband amplifier topologies, including the push-pull configuration.

A novel method for extending the bandwidth of the microwave transmission line balun is introduced in Chapter 3. A multi-decade balun is presented that opens up the possibility of broadband push-pull power amplifiers at microwave frequencies.

As a result of measurements on the transmission line balun, it was necessary to reconsider the modes of operation that are present inside a push-pull power amplifier. These newly-recognised modes are presented in Chapter 4 and verified through simulation and measurement.

The potential of the push-pull topology is demonstrated through the design, manufacture and test of two prototype power amplifiers in Chapter 5. Bespoke measurement systems were used to gain additional insight into the amplifiers' operation.

The work presented in this thesis is concluded in Chapter 6, and areas for future work are described in Chapter 7.

Chapter 2

Literature Review

2.1 Introduction

This chapter introduces many of the concepts that will be expanded upon later in the thesis and reviews the existing work that has been conducted on developing high-efficiency, high-power amplifiers over significant bandwidths.

The essence of power amplifier design is in the selection of a bias point for the transistor and the design of input and output matching networks, in order to achieve the required performance. Particular bias points and matching impedances are classified as power amplifier modes and assigned an alphabetic designation. As can be seen in Fig. 2.1, the purpose of the matching network is to present the required impedances to the transistor whilst presenting the system impedance to external components.

The chapter begins with a brief review of 'conventional' PA modes as a foundation on which to build later work. Fundamental limitations in the ability to design matching networks that operate over large bandwidths are identified. Having introduced the traditional approach to PA design and some of its limitations, continuous modes, also known as 'extended' modes, are shown to be able to maintain highly power-efficient operation over significantly extended bandwidths.

An introduction to gallium nitride (GaN) transistors and their suitability to broadband, high-power applications is presented, along with some of the challenges that they

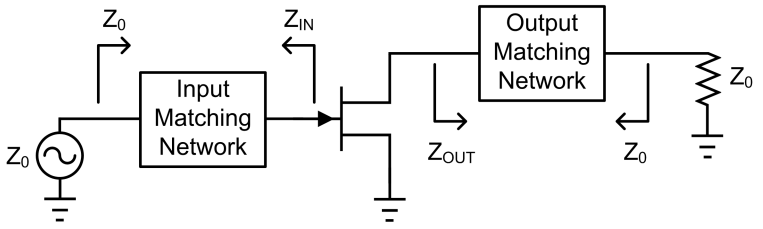

Figure 2.1: Basic single-ended amplifier configuration

present to amplifier designers. The different topologies used to achieve broad bandwidth operation, namely balanced and distributed amplifiers, are then outlined along with their shortcomings.

Finally, the push-pull topology, which will form the basis of the work in this thesis, is introduced. Its advantages and challenges are explained, and the current state-of-the-art papers are reviewed. As will become evident throughout the thesis, the balun component is the key component in the push-pull amplifier, and the many techniques for implementing baluns are categorised.

2.2 Power Amplifier Modes of Operation

In this section, a brief introduction to the various power amplifier operating modes is presented. There is no point 'reinventing the wheel', seeing as many excellent texts on RF PA design already exist [4–6], however it will provide a useful point of reference for later work.

Classes A through to C are regarded as the 'conventional' modes of operation. Figure 2.2 shows an idealised transistor transfer characteristic with the bias points associated with each mode. A common characteristic of the conventional modes of operation is that the output voltage waveform is sinusoidal, achieved by presenting the harmonics with a short circuit.

Classes D, E and S are known as 'switched' modes, as they rely on the transistor acting as a switch. Switched mode amplifiers require a resonator to be included as part of their output matching network, and this makes them unsuitable for broadband applications. Details of these modes can be found in the PA textbooks previously identified.

Classes F and F^{-1} (inverse Class F) are known as 'harmonically tuned' modes, whose efficiency is improved compared to other modes by shaping the output waveforms. They require more complicated matching networks due to their harmonic impedance requirements, however very high efficiencies are possible over modest bandwidths.

Class J, the Class JB continuum and the continuous modes of operation are recent developments in power amplifier design. Unlike other modes of operation, they account for the transistor's intrinsic output capacitance (described in Section 2.3.2) and compensate for its effects to achieve high levels of performance across wider bandwidths than other modes.

In discussing the theory of all of these modes, the effect of the transistor's knee region is ignored. The effect of the knee region is to reduce the RF output voltage swing, and hence output power and drain efficiency. It is shown analytically in [4] that for Class B operation the knee region causes a decrease of approximately 1 dB in output power and 10% in efficiency.

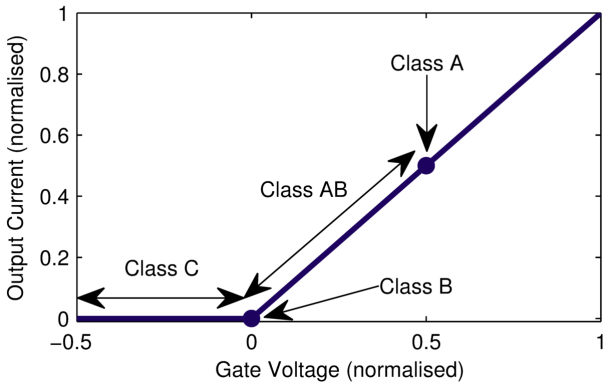

Figure 2.2: Ideal transistor transfer characteristic

2.2.1 Class A

A Class A amplifier has a conduction angle of 360°, i.e. it is always conducting. Because the DC power is always non-zero, its efficiency is low compared to the other modes of operation. Figure 2.2 shows that Class A PAs are biased halfway between the maximum output current and zero output current. The maximum theoretical drain efficiency for a Class A amplifier is 50%. As shown in Fig. 2.3, Class A has purely sinusoidal waveforms for both current and voltage. The current has been normalised to I_{MAX}, the maximum drain current that can be supplied by the transistor. The output voltage has been normalised with respect to its DC value, which remains constant.

Class A has a linear power back-off characteristic, such that a 3 dB reduction in input power results in a 3 dB reduction in output power. Most modulation schemes employ some form of amplitude modulation (AM), whereby the carrier signal amplitude varies with time. Whenever the signal is not at its peak value, the RF output power of the Class A PA is reduced but its DC power consumption remains constant. Under these conditions, the Class A mode exhibits low values of efficiency.

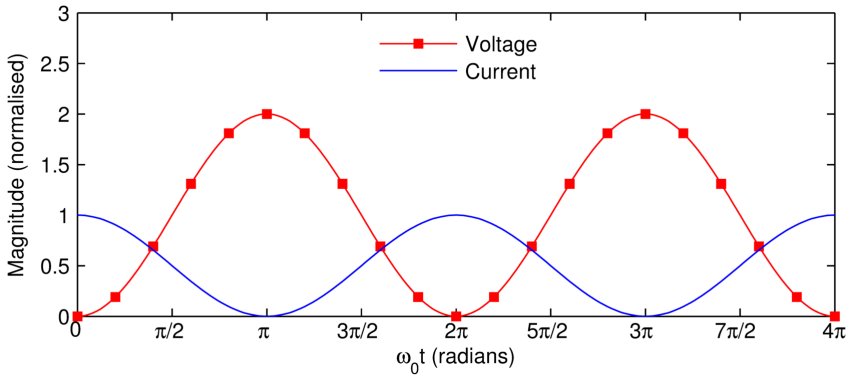

Figure 2.3: Class A voltage and current waveforms

2.2.2 Class B

In Class B the transistor is biased at its threshold voltage, so that the current only conducts for half of the cycle, producing a half-wave rectified sinusoid. In order to achieve the half-wave rectified shape, even-order harmonics are generated but the odd-order harmonic components are zero. Class B amplifiers produce the same maximum output power as Class A amplifiers, but have to be driven with more input power, as the theoretical gain is 6 dB lower. The load resistance is the same as for Class A, and the power back-off relationship is also linear.

The maximum theoretical efficiency for a Class B amplifier is 78.5%, and its time-domain waveforms are shown in Fig. 2.4. Because the harmonic frequencies are short-circuited, none of the harmonics present in the current waveform appear in the output voltage waveform, hence it is a pure sinusoid.

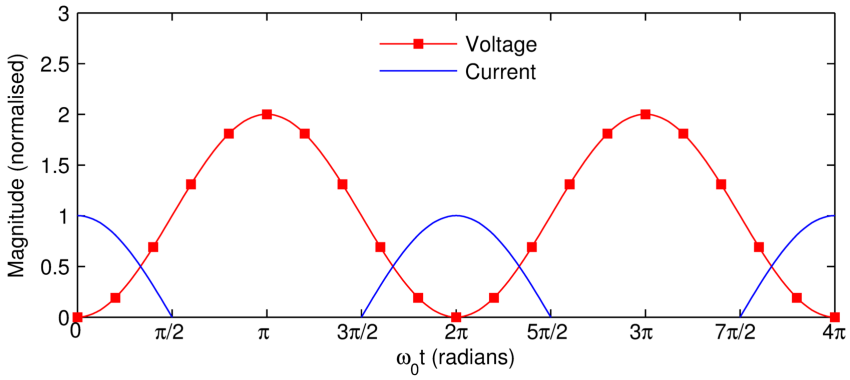

Figure 2.4: Class B voltage and current waveforms

2.2.3 Class AB

As opposed to Classes A and B, Class AB is not defined at a single bias point but instead as the range between Class A and Class B. Bias points closer to Class A are generally referred to as 'light' or 'shallow' Class AB, with bias points closer to Class B referred to as 'deep' Class AB. It is possible to achieve slightly higher maximum output power with Class AB compared to Class A (typically 0.25 dB [4]), but the trade-off is a reduction in gain. The optimum load resistance is slightly lower than for Class A operation. As the conduction angle depends on the input (drive) power [4], as well as the biasing conditions, the output power and drain efficiency do not decrease with power back-off as rapidly as in Classes A and B. This is advantageous for applications where the amplifier will not be constantly operating at full output power, such as when amplifying amplitude-modulated signals. As the transistor is biased into 'deep' Class AB, the harmonic content of the current waveform increases.

2.2.4 Class C

In Class C amplifiers the conduction angle is very small (less than one-half of the RF cycle) so the drain current is shaped as a narrow pulse, as shown in Fig. 2.5. As with the other 'conventional' modes of operation, the harmonics are shorted and so the output voltage is always sinusoidal. In theory, the maximum efficiency of a Class C amplifier tends towards 100%, as the conduction angle tends towards zero. However, this higher efficiency is achieved at the expense of both output power and gain. Class C amplifiers have a reduced gain compared to Classes A, AB and B, which makes this mode unfeasible in applications where the maximum available gain (MAG) of the transistor is low, for example at X-band frequencies.

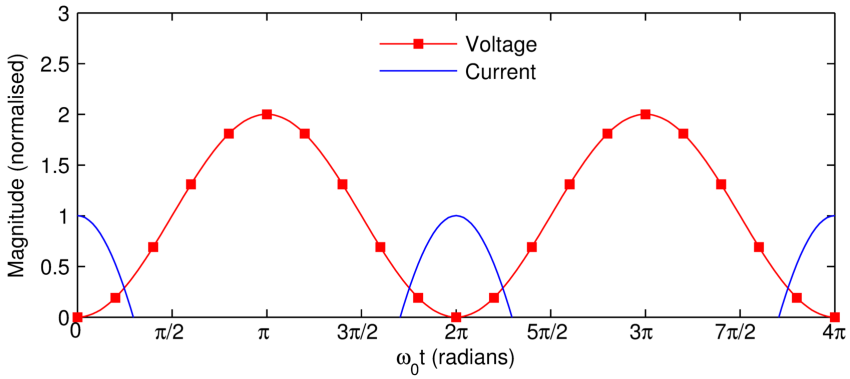

Figure 2.5: Class C voltage and current waveforms

Amplifier Class	Conduction Angle	Maximum Efficiency	Z_{f_0}	Z_{2f_0}	Z_{3f_0}
Class A	$\theta = 2\pi$	50%	1	n/a	n/a
Class AB	$\pi < \theta < 2\pi$	50% - 78.5%	0.93	0	0
Class B	$\theta = \pi$	78.5%	1	0	0
Class C	$\theta < \pi$	78.5% - 100%	≥ 1	0	0
Class F	$\theta = \pi$	90.7% - 100%	1.154	0	∞
Class F^{-1}	$\theta = 2\pi$	90.7% - 100%	1.22	∞	0
Class J	$\theta = \pi$	78.5%	$1 + j$	$-j\frac{3\pi}{8}$	0

Table 2.1: Summary of power amplifier modes of operation

2.2.5 Class F

'Waveform engineering' is the modification of a transistor's time-domain voltage and current waveforms through the manipulation of the harmonic impedances that are presented to it [7]. The Class F mode can be realised using waveform engineering by shaping the output current and voltage into highly power-efficient waveforms. The transistor is driven into compression and the voltage waveform is 'flattened' by presenting the odd-order harmonics with an open circuit. By flattening the voltage waveform, the fundamental voltage swing can be increased, and hence output power is increased without increasing the DC power consumption. As additional higher-order odd harmonics are tuned, the voltage waveform tends towards a square wave shape, and the efficiency increases. Tuning lower-order harmonics is more effective at improving efficiency than tuning higher-order harmonics, so lower-order harmonics are tuned first.

The current waveform approaches the shape of a half-rectified sinewave by short-circuiting the even harmonics. Again, tuning the lower-order harmonics has a greater effect than tuning the higher-order harmonics. Typical Class F waveforms are shown in Fig. 2.6.

Some key results are contained within Table 2.2. The number of even harmonics considered is represented by m, and n represents the number of odd harmonics considered. When m and n are 1, both current and voltage are sinusoidal and the maximum efficiency is 50%. This is the Class A mode. When the even harmonics are all shorted but the odd-order harmonics are not tuned, the maximum efficiency is 78.5% (Class B). If the third harmonic is then tuned (keeping the ideal current waveform) the maximum efficiency then increases to 90.7%. This is the most commonly quoted maximum efficiency for the Class F amplifier. If it were possible to tune an infinite number of harmonics, the Class F amplifier would theoretically be 100% efficient.

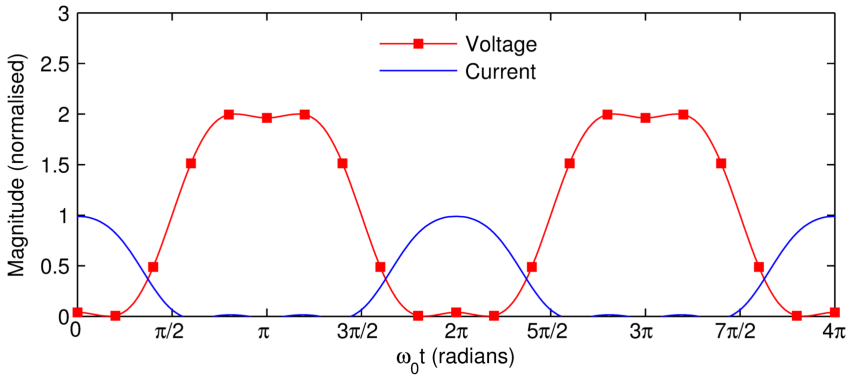

Figure 2.6: Class F voltage and current waveforms ($m = 4$, $n = 5$)

	n = 1	n = 3	n = 5	n = ∞
$m = 1$	50.0%	57.7%	60.3%	63.7%
$m = 2$	70.4%	81.6%	85.3%	90.0%
$m = 4$	75.0%	86.6%	90.5%	95.4%
$m = \infty$	78.5%	90.7%	94.8%	100.0%

Table 2.2: Maximum efficiency of the Class F mode with m even harmonics and n odd harmonics considered (from [8])

2.2.6 Inverse Class F

Inverse Class F amplifiers (commonly denoted as Class F^{-1}) are based on the same principle of operation as Class F, but are biased at the Class A bias point. Rather than the voltage waveform being flattened, the current waveform is flattened and the voltage waveform tends towards a half-wave rectified sinusoid. The waveforms are shown in Fig. 2.7.

To realise the inverse Class F mode, the second harmonic is open-circuited and the third harmonic is shorted. A characteristic of the inverse Class F mode that is not commonly noted is that the theoretical maximum output power of this mode is 2.1 dB higher than for Class A, a notable increase. Later on in this thesis, a similar advantage will be shown to be present in the modes of operation present in a push-pull power amplifier. The inverse Class F mode results in higher peak voltages than other modes, which could be problematic for transistors with relatively low breakdown voltages, but is acceptable for wide-bandgap semiconductor materials such as GaN, which have high breakdown voltages.

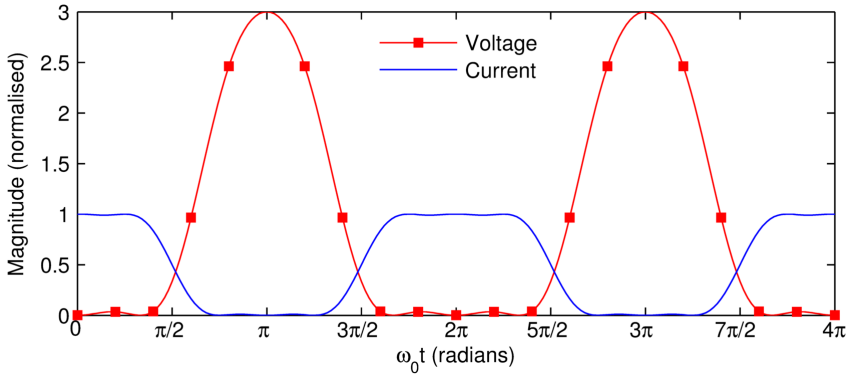

Figure 2.7: Inverse Class F voltage and current waveforms

2.3 Bandwidth Limitations in Power Amplifier Design

In this section, three major obstacles to achieving broadband power amplifier operation using conventional matching networks are outlined. It will be shown that the limitations of the conventional single-ended power amplifier in achieving large bandwidths necessitates the investigation into alternative approaches.

2.3.1 Matching Network Limitations

As stated in the introduction, the purpose of a matching network is to transform a system impedance, typically 50 Ω, into an impedance that will result in the circuit element giving the desired performance. In the case of power amplifiers, the desired output impedance is dependent on the operating mode of the amplifier and the size of the transistor. Higher-power transistors are physically larger and have lower optimum output impedances.

When matching is only required at a single frequency, this can be done fairly easily through appropriate design [9]. However, maintaining an impedance transformation over a range of frequencies is a significant challenge. The main reason for this is that the impedance presented by the matching network varies with frequency, which is unsurprising given that the matching network is constructed from frequency-dependent elements such as transmission lines, capacitors and inductors. Broadband matching can be achieved through careful design, but becomes increasingly complicated as the required bandwidth increases.

Because of the difficulties of matching to a single impedance across a range of frequencies, it is common to target a range of impedances, for example where the output power is within 1 dB of the output power achieved at the optimum impedance. These contours can be predicted by theory [10], measured directly using a load-pull measurement system or obtained by simulation, if a nonlinear model is available. This approach helps to take into account the variation of the presented matching network impedance with frequency.

When designing a matching network, there is a fundamental limit to the bandwidth that a matching network can achieve for a given transformation ratio. A greater impedance transformation ratio reduces the achievable bandwidth. As smaller transistors have larger output impedances, they can generally be matched over wider bandwidths than higher power transistors. One approach to achieving high-power, broadband amplifiers could therefore be to combine many low-power transistors that are matched over a wide bandwidth. Unfortunately, the losses associated with the power combining components, as well as the bandwidth of these components, are a major obstacle to this particular approach.

The limitations of matching arbitrary impedances over bandwidth have been dis-

cussed first by Bode [11] and later expanded on by Fano [12]. It can be shown that there is a maximum achievable bandwidth for a specified tolerance of match, and vice versa. Fano provides a set of integral relations for determining the realisability of matching networks for a given specification, and later provides a method for designing these matching networks. It should be noted however that the mathematical analysis for complex matching networks quickly becomes cumbersome, and that the widespread use of CAD (computer-aided design) tools means that in reality the equations developed are rarely used when designing matching networks.

Additional challenges result from the use of lumped-element components, which cannot be considered to be ideal components, especially at microwave frequencies where they have distributed effects. Complicated, multi-element matching networks also have the disadvantage that the additional components will increase the loss of the matching network, and also increase its physical size.

2.3.2 Reactive Output Impedances

In the previous section the difficulties of matching two fixed impedances over a wide bandwidth have been discussed. These difficulties are due to the fundamental trade-off between bandwidth and matching tolerance when designing matching networks.

However, the output impedance of the transistor also varies with frequency, further complicating the task of designing a matching network. There are a number of reactive components contained within the transistor and its packaging that cause its output impedance to vary with frequency. The most influential of these reactive components is the capacitance between the drain and the source (C_{DS}) that is inherent to the transistor. Bond wire inductances and other reactances introduced by the transistor package also serve to complicate the problem. It can be seen in Fig. 2.8 how a normalised output impedance is shifted by reactances inherent to the transistor so that the resulting impedance varies significantly across a decade of bandwidth. In addition, it can be observed that the impedance at the high-frequency end of the band is much lower than the original impedance, increasing the matching ratio and further limiting the bandwidth.

The effect of the transistor's reactive components is even more pronounced at the harmonic frequencies. This makes it very difficult to present the desired harmonic terminations over bandwidth, and this has a detrimental effect on performance. In Section 2.4.3 it is shown that the Class J mode and continuous modes can alleviate this problem through waveform engineering.

2.3.3 Harmonic Impedances

In addition to the matching restrictions at the fundamental frequency, outlined in Sections 2.3.1 and 2.3.2, the matching network is also required to present appropriate

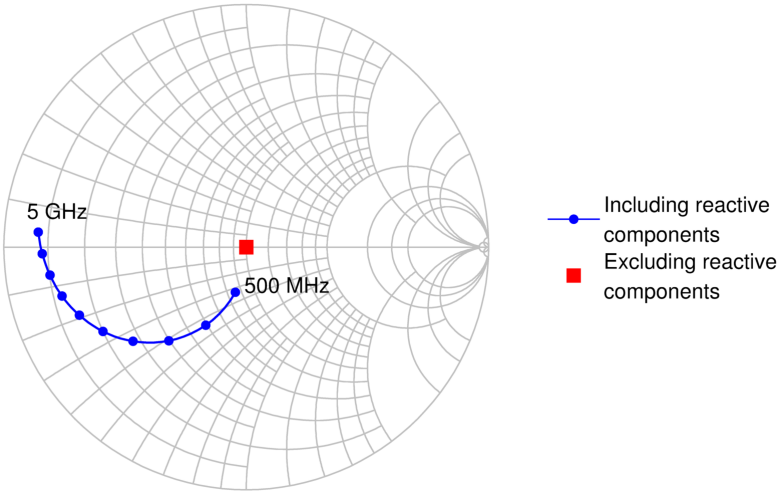

Figure 2.8: Output impedance as transformed by device and package reactances

impedances at the harmonic frequencies. This creates a further bandwidth limitation at the frequencies at which there are conflicting requirements placed on the matching network. As the bandwidth of an amplifier increases, eventually the high end of the fundamental band and the low end of the second harmonic band will meet, as shown in Fig. 2.9. In a conventional PA mode, this would require a specific impedance to be presented at the fundamental frequency and a short circuit to be presented at the second harmonic. As can be seen in Fig. 2.9, the theoretical bandwidth limitation for conventional PA modes is one octave (66%).

For harmonically-tuned, high efficiency modes, the bandwidth limitation can also be identified. Figure 2.10 shows the limitations in implementing the Class F mode of operation. As Section 2.2.5 outlined, the second harmonic is required to be presented with a short circuit and the third harmonic requires an open circuit. At the normalised frequency of $2.4f_C$, the matching network is required to simultaneously present a short circuit to the second harmonic and open circuit to the third harmonic, which is not possible. Figure 2.10 demonstrates that the theoretical bandwidth limitation for a high-efficiency mode with three tuned harmonics is 40%. In reality, a matching network would not be able to maintain a perfect short or open circuit over any significant bandwidth in any case, so this bandwidth limitation is rarely a practical concern. However, it is worth noting as a theoretical limitation of conventional matching networks.

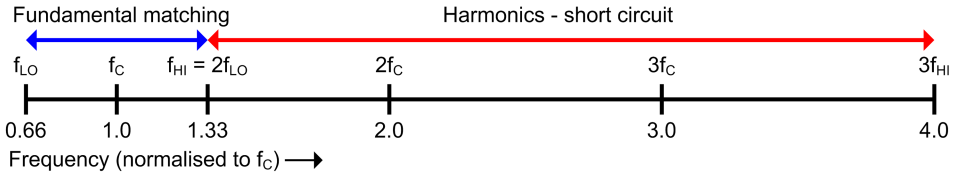

Figure 2.9: Bandwidth limitation of a conventional PA mode of operation

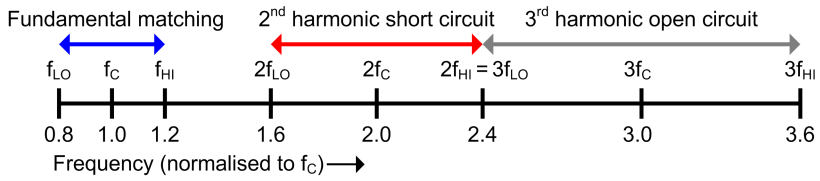

Figure 2.10: Bandwidth limitation of the Class F PA mode of operation

2.4 Class J and Continuous PA Modes

2.4.1 Class J

The Class J mode can be used to compensate for the effects of reactive components on the harmonic output impedances discussed in Section 2.3.2. When designing a Class B power amplifier, the second harmonic impedance can be shifted a significant distance away from an ideal short circuit due to the transistor's drain-source capacitance. This means that the output voltage waveform is no longer sinusoidal and may have a negative value at certain points of the waveform (known as 'zero-crossing'), leading to a decrease in both output power and efficiency. Because C_{DS} is inherent to the transistor, the PA designer cannot remove this effect and has to compensate by reducing the voltage swing or modifying the matching network.

The Class J mode introduces a reactive element to the fundamental matching impedance [13] to shape the time-domain voltage into a waveform with the same efficiency and output power as Class B. This is a remarkable result that, unlike the conventional PA modes, recognises and compensates for non-ideal effects inside a transistor. The Class J voltage and current waveforms shown in Fig. 2.11 have the same output power as Class B and the same theoretical 78.5% drain efficiency. It can be seen that the Class J voltage waveform has a higher peak value than the Class B voltage waveform, however when used with transistor technologies which have high breakdown voltages, such as GaN, this is not a significant problem. It can be seen that the Class J amplifier displays approximately half-wave rectified sinusoidal output current and voltage waveforms, but with a shift in phase.

2.4.2 Class JB Continuum

The time-domain voltage waveform of Class J can be described mathematically as the sum of cosinusoidal and sinusoidal components. The cosinusoidal components represent the real components of the complex waveform, and the sinusoidal components represent the reactive components. It was recognised that these expressions could be factorised [14], and the factorised voltage waveform for the Class J mode is described by (2.1). The parameter α can be varied between -1 and 1 to produce a family of waveforms with the same power and efficiency. Because α can take any value between -1 and 1, this

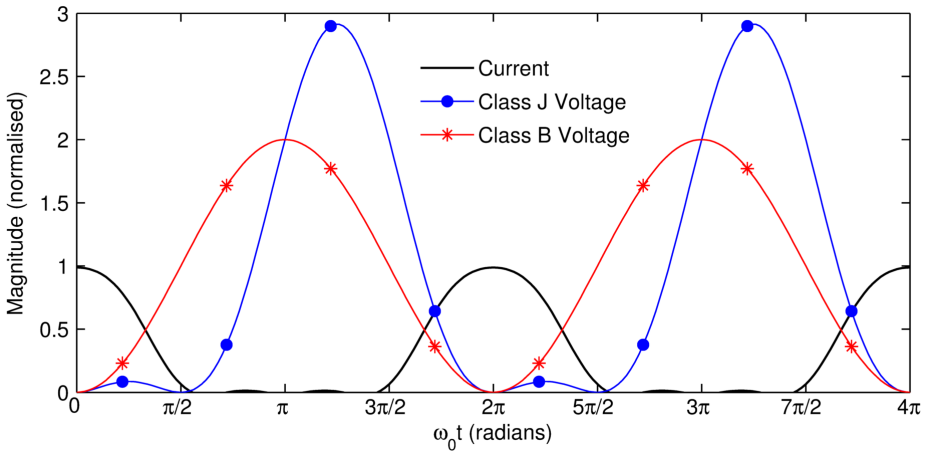

Figure 2.11: Class J voltage and current waveforms, with Class B voltage waveform for comparison

set of waveforms is termed the Class JB continuum. A number of these waveforms are shown in Fig. 2.12. Note that when α is zero the output voltage waveform is sinusoidal, corresponding to the Class B mode of operation, and that $\alpha = 1$ corresponds to the Class J mode.

The corresponding Class JB impedances are shown in Fig. 2.13, and it can be observed that the reactive components of the fundamental and second harmonic have opposite signs. The equations ensure that the voltage remains above zero (known as non-zero crossing). This is an important consideration, as a zero-crossing voltage would result in current collapse and low output power and efficiency.

$$v(\omega t) = (1 - \cos(\omega t))(1 - \alpha \sin(\omega t)) \tag{2.1}$$

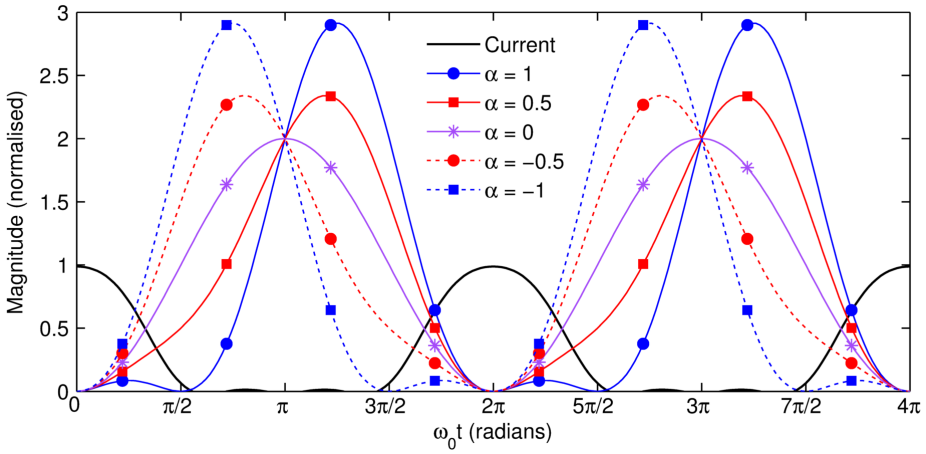

Figure 2.12: Class JB waveforms for various values of α including Class J ($\alpha = 1$), Class B ($\alpha = 0$) and Class J* ($\alpha =$ -1), where α is defined in (2.1)

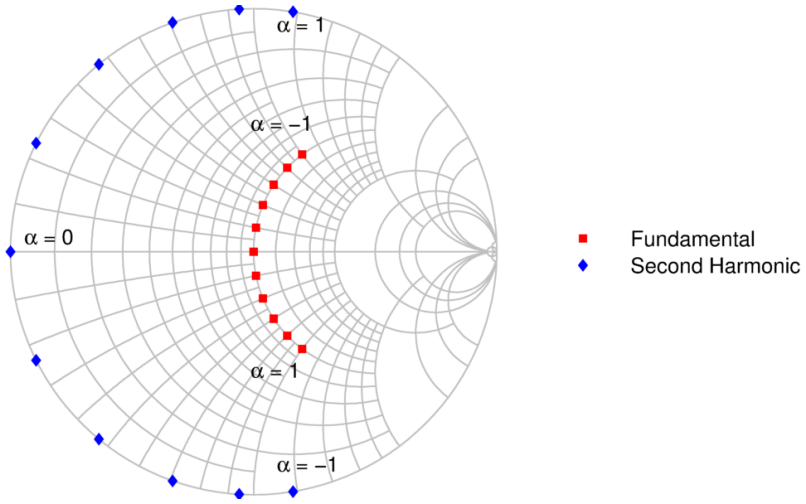

Figure 2.13: Fundamental and second harmonic impedances for the Class JB continuum

2.4.3 Continuous Modes

Using the voltage factorisation method, other PA modes that exhibit high drain efficiencies over narrow bandwidths can be extended to a continuum of waveforms with the same output power and drain efficiency. The significance of this is that the modes can be maintained over a much wider range of impedances and therefore frequencies.

High-efficiency, harmonically-tuned modes such as Class F require the harmonic impedances to remain constant and preferably at an ideal short- or open-circuit, depending on the mode. This is difficult to achieve in practice, due to transistor output reactances and non-ideal matching networks, and is virtually impossible to maintain over significant bandwidths. The continuous modes allow the harmonic reactances to vary with frequency, and provide a mechanism for compensating for this variation through the introduction of a suitable reactive component in the fundamental impedance.

The continuous mode approach has been extended to the Class F mode [15, 16], inverse Class F mode and Class A mode [17]. As an example, (2.2) describes the continuous Class F mode of operation, where the parameter γ is analogous to α in the Class JB equation.

$$v(\omega t) = (1 - \frac{2}{\sqrt{3}}\cos(\omega t))^2(1 + \frac{1}{\sqrt{3}}\cos(\omega t))(1 - \gamma\sin(\omega t)) \tag{2.2}$$

As with the Class JB continuum, these modes are enabled by factorising the time-domain waveform expressions and including a $(1 - \sin(\omega t))$ multiplier. Furthermore, for each 'base' mode that the extended modes are derived from, there are two sets of continuous modes, specified by a -I or -V suffix. The difference between the two is that for -I modes the voltage waveform remains constant and the current waveform varies, and for -V modes the opposite occurs. The mode that is present in the PA depends on

the harmonic at which the impedance varies reactively.

Despite the advantages of the continuous modes, of which there are many, they are still based on conventional matching networks and their inherent bandwidth limitations, and suffer from conflicting harmonic termination requirements at certain frequencies, as outlined in Section 2.3.3. Therefore, although continuous modes can provide excellent performance up to one octave of bandwidth [15], they would not be a suitable solution for targeting larger bandwidths.

2.5 Gallium Nitride RF Transistors

In this section a brief overview of gallium nitride (GaN) transistors is presented. Its key properties that make it suitable for broadband, high power applications are identified and compared to those of the other two primary transistor technologies, silicon (Si) and gallium arsenide (GaAs).

Gallium nitride is a wide band gap compound semiconductor material whose use in RF power amplifiers has been rapidly increasing in recent years. A compound semiconductor is made up of two or more elements, one of which is typically a Group III element in the periodic table, with the other being a Group V element. Gallium nitride is a III-V semiconductor, as is gallium arsenide, but GaN has a much wider band gap (3.4 eV compared to 1.43 eV). This means that GaN has a higher breakdown voltage and hence can be operated with a higher drain supply voltage, typically 28 V compared to 10 V for GaAs [18]. A higher operating voltage requires lower current for the same output power level, and this results in a higher output impedance, which is advantageous for matching high-power devices into 50 Ω. Compared to a GaAs device at the same power level, both input and output impedance transformation ratios are greatly reduced, which means the transistor can be matched over a wider range of frequencies. A high breakdown voltage is especially advantageous for PA modes of operation which produce high peak voltages, such as Class J.

Gallium nitride transistors also exhibit a higher power density than either GaAs or LDMOS. Cree's 0.4 µm 28 V process, used extensively in this thesis, gives a power density of 4.5 W/mm [19], but experimental GaN has been shown to achieve greater than 30 W/mm [20]. In comparison, the power density for GaAs and LDMOS transistors is typically around 1 W/mm [21]. A high power density means a smaller device is needed for a specified output power. A device's capacitance is proportional to both its area and its dielectric constant. A smaller gate area therefore results in a lower drain-source capacitance (C_{DS}), which reduces the shift in output impedance described in Section 2.3.2. In addition, as can be seen in Table 2.3, GaN has the lowest dielectric constant when compared to GaAs and Si. The smaller device sizes and lower dielectric constant mean that GaN devices' capacitance-per-Watt is lower than either GaAs or

Parameter	Symbol (unit)	Si	GaAs	GaN
Band gap	E_g (eV)	1.12	1.43	3.4
Thermal conductivity	K (W/°K-cm)	1.5	0.54	1.3
Dielectric constant	ε_r (unitless)	11.9	12.5	9.5
Electric field for breakdown	E_c (V/cm)	3×10^5	4×10^5	2×10^6

Table 2.3: Material properties of GaN compared to GaAs and SiC (values from [18])

silicon, another significant advantage for wide bandwidth applications. By using GaN transistor technology, two of the three bandwidth limitations identified in Section 2.3 can be improved upon.

High-power, broadband power amplifiers are an application well suited to gallium nitride given its high power density, high breakdown voltages and low output capacitance per Watt. Gallium nitride transistors are also competing with GaAs transistors in areas where GaAs has traditionally excelled, for example in low noise amplifiers (LNAs) [22]. In addition, gallium nitride is challenging vacuum electron devices in high power applications where solid-state devices have not been suitable until now.

It is not currently possible to make wafers out of gallium nitride, so substrates must be made out of a different material, on which GaN layers are then grown. Silicon carbide (SiC), sapphire and silicon can all be used as substrates for GaN devices. The high power density of GaN transistors means that they require careful thermal management. Gallium nitride itself has reasonable thermal conductivity, slightly lower than silicon, however silicon carbide has excellent thermal conductivity (4 W/°K-cm). It should be noted that because of GaN transistors' high power density, conducting heat away from the underside of the die is still a challenge .

An additional advantage is that GaN can operate at higher channel temperatures than GaAs, which means that less cooling equipment will be needed to keep the device within its operating limits, reducing the size and power demands of the overall system.

As with most new technologies, one of the barriers to adoption that GaN faces is cost. Silicon transistors are extremely inexpensive to manufacture, and as such are used wherever possible. However, as GaN increasingly replaces GaAs and, in certain applications, vacuum tubes, its demand will increase and this generally leads to a reduction in price.

As a relatively immature technology, GaN has experienced a number of technical issues such as trapping effects, reliability and current collapse. One problem that GaN has experienced is the issue of knee-voltage 'walk-out' [23]. Knee walk-out is the problem of the transistor knee voltage being greater at RF than at DC [7]. This can cause difficulties for loadline matching based on DC I-V measurements.

Current collapse is the problem that the maximum drain current is reduced under RF drive compared to that observed under DC [7]. There is a reversible and nondestructive reliability problem with AlGaN/GaN HFETs that is due to electrons leaking from the gate electrode to the surface of the semiconductor. This results in a degradation of the DC drain current, gain and RF output power, and an increase in gate leakage current.

It should be noted that whilst GaN is a promising and increasingly popular choice of transistor technology, GaAs transistors can operate at higher frequencies, and that for many high power applications vacuum tube amplifiers remain the only choice. However, for implementation of decade bandwidth power amplifiers with output power levels in the tens of Watts, GaN appears to be the best choice.

2.6 Broadband Power Amplifier Topologies

Apart from the single-ended power amplifier topology, there are three main topologies that can be used to achieve broadband operation for solid-state devices; distributed, balanced and push-pull amplifiers. Because of the importance of the push-pull topology to this thesis, it will be considered separately in the next section. The distributed amplifier and balanced amplifier are discussed in this section, along with the 'resistive Class B' mode.

2.6.1 Distributed Amplifiers

A brief introduction to the distributed amplifier is presented here, due to its inherently broadband characteristics and its coverage in a number of classic textbooks. However, its low efficiency, output power and gain, notwithstanding the fact it is better suited to monolithic microwave integrated circuit (MMIC) implementation, meant that it was quickly deemed unsuitable for the requirements previously outlined.

Distributed power amplifiers have long been known as a technique to achieve very broad bandwidths. The distributed amplifier topology is shown in Fig. 2.14. Traditionally, distributed amplifiers exhibit low efficiencies, but recently a number of papers report relatively high efficiencies over multi-octave bandwidths using GaN devices. These are summarised in Table 2.4.

The basic principle of the distributed amplifier is that a standing wave is created along the length of the amplifier, and the input signal is gradually amplified along the length of the PA. First suggested for vacuum tubes, this technique allows for very broadband operation. There are, in effect, two transmission lines, a drain line and a gate line. The distributed amplifier is an inefficient use of device periphery [6], due to the low gain of the overall amplifier, although it does achieve flat gain and a reasonable match across very wide bandwidths.

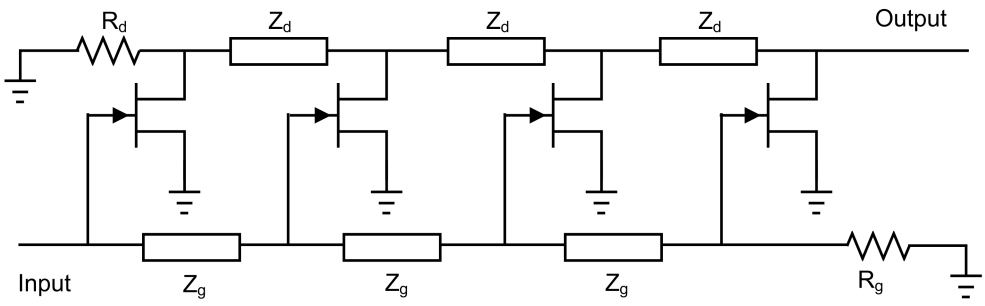

Figure 2.14: Distributed amplifier topology

There have been a number of modifications to the basic distributed topology including the non-uniformly distributed power amplifier (NDPA), capacitive coupling and tapered drain lines. The highest output power reported for the distributed amplifiers in Table 2.4 is 15 W, and the highest power-added efficiency (PAE) is 38%, showing that although distributed amplifiers are extremely broadband, there are still challenges to overcome for high-power, high-efficiency performance.

2.6.2 Balanced Amplifiers

The balanced amplifier consists of two identical single-ended amplifiers with quadrature (90°) couplers at the input and output, as shown in Fig. 2.15. This topology has advantages for both narrow- and broadband applications, and shares some similarities with the push-pull topology. The key advantage of the balanced configuration is that, as long as the amplifiers are identical, and reasonably well matched, any input and output reflections are absorbed in the 50Ω coupler terminations [6]. The input coupler divides the input signal into two equal amplitude signals of -3 dB power, with a 90° phase difference between the two. When any reflected waves travel back through the coupler, they are in anti-phase and cancel each other out [28]. The consequence of this is that the individual amplifiers can be mismatched for better performance whilst the overall balanced amplifier presents a 50 Ω impedance at its input and output ports. This is especially useful for multi-stage amplifiers, where gain stages can be designed

Ref.	Freq. Range	Output Power	Device Tech.	Efficiency
[24]	1.5 GHz - 17 GHz	9 W - 15 W	GaN on SiC	20 - 38% PAE
[25]	4 GHz - 18 GHz	4 W	GaN & GaAs	23 / 15.6% PAE
[26]	20 MHz - 3 GHz	5 W	GaN	27% PAE
[27]	100 MHz - 20 GHz	1 - 3 W	GaN	10 - 15% PAE

Table 2.4: Summary of published distributed amplifiers

individually and cascaded to form a complete amplifier.

Like the push-pull amplifier, the gain of the balanced amplifier is the same as one of its constituent single-ended amplifiers, but the output power is doubled. Unlike push-pull however, which transforms the transistors' impedance environment down to 25 Ω, the balanced configuration offers no impedance transformation to aid with the matching of high-power transistors. In addition, the balanced configuration does not solve the problem of conflicting harmonic impedances outlined in Section 2.3.3.

The balanced amplifier does, however, have a couple of other advantages. In the event that one amplifier fails, the other continues to operate and the overall amplifier still produces output power, albeit with a reduction of 6 dB in gain. Balanced amplifiers also have considerable in-band stability benefits when compared to single-ended amplifiers. The stability factor is increased in a balanced amplifier as reflected waves in the passband are cancelled in the quadrature couplers.

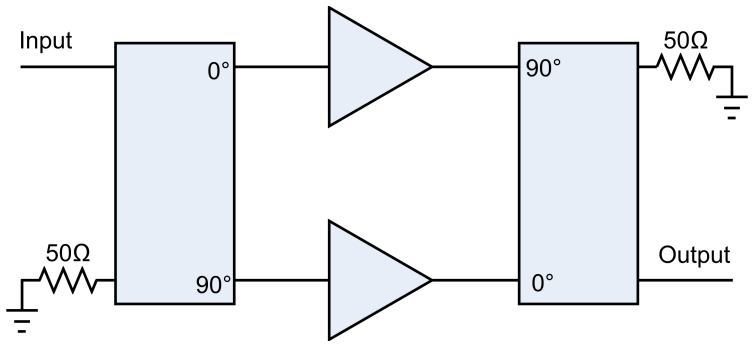

Figure 2.15: Balanced amplifier topology

As with baluns in push-pull amplifiers, the quadrature coupler is the key component in the balanced amplifier and is often the limiting factor for broadband operation. For wide-band couplers, multiple sections are needed, which require a large area [29]. Because microwave-frequency quadrature couplers are based on a pair of coupled quarter-wave transmission lines, couplers cannot be manufactured at low frequencies without becoming very long and consuming a lot of space. Detailed analysis of quadrature couplers can be found in [30], with an emphasis on VHF/UHF lumped element couplers. The effects of over- and under-coupling can be shown to have little impact on the amplifier output power [4]. There are a number of commercially-available quadrature couplers which operate over wide bandwidths, such as a 0.5 to 7 GHz coupler [31] and 1 to 18 GHz coupler [32], both from Krytar. These have relatively high loss (1.5 - 2.0 dB), but lower loss couplers with narrower bandwidths are readily available. As with push-pull amplifiers, the insertion loss in the power dividing and combining components is critical to the overall amplifier efficiency.

Considering the numerous advantages of the balanced amplifier topology, the bal-

anced amplifier does not feature heavily in the broadband PA literature at L- and S-band, although there are some examples of its use at X-band frequencies [33,34]. Physical size is generally a primary practical consideration in PA design, which would limit the use of this type of amplifier at lower frequencies.

2.6.3 Resistive Class B

The resistive Class B mode is described in [4] as a wideband variant of the standard Class B mode. 'Standard' Class B is limited in bandwidth due to the need for the harmonics to be short-circuited, either using short circuit stubs or a high-Q resonator [35]. The resistive Class B mode relaxes the need for short-circuited harmonics by terminating the fundamental and harmonics in the same load resistance. This results in the waveforms shown in Fig. 2.16. Unlike Class B, this mode can be sustained over a very broad bandwidth whilst still achieving a higher theoretical drain efficiency than the Class A mode (57.6% compared to 50%). Compared to Class B however, the drain bias voltage must be increased in order to maintain the same level of output power, and the efficiency is significantly lower. A practical implementation of this mode of operation has been shown to operate between 0.4 - 4.1 GHz [36], a greater than decade bandwidth. Drain efficiency varied between 40% and 62%, with an output power of 10 W. As the impedance transformation is achieved by conventional matching networks, it is doubtful as to whether this approach could be applied to larger bandwidths or higher output powers while still maintaining similar efficiencies. When compared to Class A, the resistive Class B mode exhibits lower gain with only a modest efficiency improvement. This has probably prevented this particular PA mode from being more widely adopted.

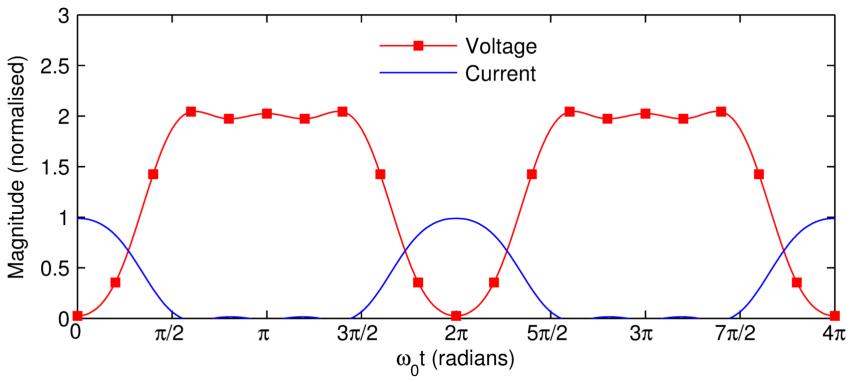

Figure 2.16: Voltage and current waveforms for the resistive Class B mode

2.7 Push-Pull Power Amplifiers

In this section the push-pull implementations documented in the existing literature are reviewed. It is shown that the push-pull topology has been implemented in silicon, GaAs and GaN over a range of frequencies and power levels. Unlike other broadband topologies such as distributed amplifiers, push-pull amplifiers have been demonstrated at high output power levels. Excellent performance has been achieved at VHF/UHF, with very broadband microwave amplifiers operating at frequencies up to 1.8 GHz.

However, it will be shown that the three requirements of high output power, high efficiency and decade bandwidth performance have not yet been achieved at microwave frequencies. This necessitates the further investigations that will be presented in this thesis.

The push-pull configuration is familiar to most electronic engineers, as it is a topology generally introduced at undergraduate level. In its classical form, shown in Fig. 2.17, it consists of two identical amplifiers, each operating in Class B bias, whose input signals are 180° out of phase and whose output currents are combined to reconstruct a sinusoidal output current. The commonly cited advantage of this arrangement is that the linear output waveforms of Class A can be obtained whilst achieving Class B efficiency (78.5%), albeit by using two transistors rather than one. The push-pull amplifier requires a balun at both input and output to split the input signals (with 180° offset between them) and recombine them at the output.

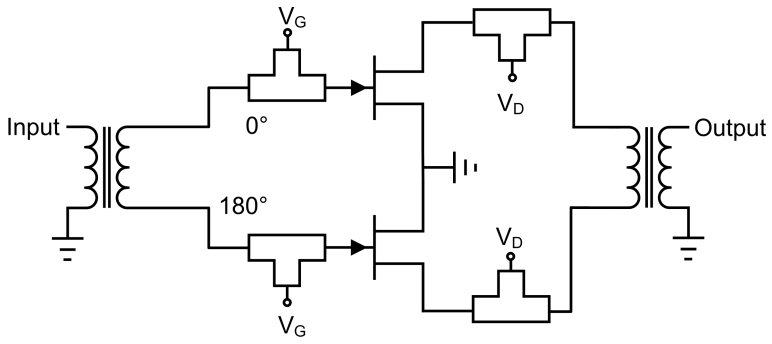

Figure 2.17: Push-pull amplifier topology

The other commonly cited advantages of push-pull are even-mode cancellation, assuming an ideal second harmonic short circuit, reduced common lead inductance and impedance transformation.

Whilst commonly used at lower frequencies, push-pull amplifiers are very uncommon at microwave frequencies. As will be shown in Section 2.8, baluns that make use of magnetic materials are used at at VHF and below to perform the balun function (convert balanced signals to unbalanced, and vice versa), impedance transformation and power combining and splitting. Limitations in magnetic material properties prevent the use of

magnetically coupled and VHF transmission line baluns much above 1 GHz.

There have been a range of frequencies and bandwidths at which push-pull power amplifiers have been designed and manufactured. They have been categorised into three groups; VHF/UHF amplifiers, above octave microwave amplifiers and narrowband amplifiers.

2.7.1 VHF / UHF Push-Pull PAs

Ref.	Freq. Range	Output Power	Device Tech.	Efficiency
[37]	100 MHz - 1 GHz	104 - 121 W	GaN	61.4 - 76.6% D.E.
[38]	100 MHz - 1 GHz	82.2 - 107.5 W	GaN	51.9 - 73.8% D.E.
[39]	50 MHz - 500 MHz	100 W	LDMOS	60% PAE
[40]	30 MHz - 500 MHz	100 W	LDMOS	30 - 38% PAE
[41]	10 MHz - 500 MHz	100 W	GaN	>43% PAE

Table 2.5: VHF/UHF push-pull power amplifiers

As already identified, push-pull amplifiers are commonly used at VHF and UHF frequencies, where excellent performance is achievable. A selection of VHF and UHF power amplifiers are presented in Table 2.5. A 30 MHz to 500 MHz 100 W push-pull power amplifier is described in [40] using LDMOS transistors. Two stages of Guanella 1:1 baluns (in balun configuration, see Section 2.8) were used to transform down to a characteristic impedance of 12.5 Ω. Reasonable PAE figures of around 30% were achieved under 1 dB of gain compression.

A common design approach is to take four single-ended transistors that have been designed into 50 Ω, then connect two pairs of parallel connected devices to match to 25 Ω, presented at each half of the balanced port [37]. Whilst this is a quick method of converting an existing amplifier into a push-pull configuration, this requires twice as many devices as are necessary. In addition, if this is done at microwave frequencies, the individual PAs will not have been designed for the open-circuit even harmonic impedance presented by a transmission line balun. This open-circuit even-mode impedance will be identified in Chapter 3, and its consequences on the operation of push-pull amplifiers will be studied in Chapter 4.

High power (100 W), high efficiency performance was achieved across a decade bandwidth from 100 MHz to 1 GHz, with the GaN transistors operated at a drain supply voltage of 48 V in order to increase output impedance [37].

Ref.	Freq. Range	Output Power	Device Tech.	Efficiency
[42]	20 MHz - 3 GHz	40 dBm (10 W)	GaAs	22 - 30%
[43]	0.1 - 1.8 GHz	50 dBm (100 W)	GaN	40.6% - 74.0% D.E.
[44]	4 - 8.5 GHz	36 dBm (4.0 W)	GaN	42% PAE
[45]	3.5 - 10.5 GHz	30 dBm (1.0 W)	GaN on SiC	15 - 25% PAE
[46]	6 - 18 GHz	31 dBm (1.3 W)	GaAs	Not disclosed

Table 2.6: Broadband (greater than one octave) push-pull PAs

2.7.2 Above Octave Push-Pull PAs

One of the earliest implementations of GaN in a push-pull configuration was presented in 2003 covering a 4 GHz to 8.5 GHz frequency range [44]. A power added efficiency value of 42% was achieved with 36 dBm output power at the 3 dB gain compression point. Interestingly, analysis of the three-coupled line balun reveals that the balun presents a short-circuit termination to the even-order harmonics. As will be shown in Chapter 3, the coaxial cable transmission line balun presents an open circuit to the even harmonics. This paper recognises that a 50 Ω balanced load is equivalent to two 25 Ω terminations to ground, and that this can be utilised to provide an impedance transformation ratio of 2:1. The GaN push-pull PA demonstrates improved linearity compared to a single-ended device.

A push-pull power amplifier with operation up to 1.8 GHz and excellent performance figures is reported in [43]. This is notable for using ferrite materials as a choking reactance at higher frequencies than previously reported. However, it is suspected that this is the upper frequency limit of this particular technique without further advances in ferrite materials.

Because the balun provides an impedance transformation across significant bandwidths, and the impedance transformation ratio can be increased using different topologies, in some cases it is possible to minimise or even eliminate conventional matching elements entirely. The concept of matching the output impedance of the device directly to the impedance presented by the balun, thus eliminating the need for a matching network, was used in [42] for a GaAs-based PA. Output power levels of 10 W were achieved between 20 MHz and 3 GHz with reduced performance up to 4 GHz. Fair-Rite ferrite beads are used to improve low frequency performance. Efficiencies between 22% and 30% were observed across the bandwidth, although it is not specified whether this was drain efficiency or power added efficiency (PAE).

Second harmonic cancellation is demonstrated between 6 GHz and 18 GHz in [46] using GaAs MMICs, subject to achieving good amplitude and phase balance in the baluns.

2.7.3 Narrowband (sub-octave) Push-Pull PAs

Although narrowband amplifiers are not the focus of this work, there are a number of notable papers that are worth discussing.

An example of a high-power microwave push-pull power amplifier is presented in [47] using GaAs transistors. It exhibits 112 W output power with 42% PAE, albeit at a spot frequency of 2.2 GHz. Whilst narrowband, it shows that high power levels can be achieved at microwave frequencies using the push-pull topology.

Stameroff et. al. [48] presented a push-pull PA with both transistors operating in inverse Class F mode. The power-added efficiency was 63% at 10 GHz, with saturated output power at 33 dBm (2 W). This paper is notable for recognising the open-circuit even-mode termination presented at the balanced port of a transmission line balun. The effects of reflection coefficient phase of the second and third harmonics on drain efficiency and output power are measured using load-pull. The prototype power amplifier is compared to a conventional single-ended AB amplifier. However, no details on the balun design were provided, and neither was a photo of the prototype circuit. The decision to implement a band-stop filter to short-circuit the third harmonic limits the frequency range of the power amplifier.

Later work by the same group [49] extended the operating bandwidth of the technique by eliminating the harmonic trap and instead using a broadside-coupled Marchand balun to provide the required inverse Class F impedances. Higher output powers of 40.5 dBm were achieved with reasonable efficiency across the whole X-band frequency range.

A pair of Doherty amplifiers in push-pull configuration is reported in [50], implemented at 2.14 GHz.

Ref.	Freq. Range	Output Power	Device Tech.	Efficiency
[47]	2.2 GHz	50.5 dBm	GaAs	46% PAE
[48]	10 GHz	33 dBm	GaAs	63% PAE
[49]	8 - 12 GHz	40.5 dBm	GaN	>55% PAE

Table 2.7: Narrowband (below one octave) push-pull PAs

2.8 Baluns

The input and output signals of the push-pull amplifier are 'unbalanced' (also known as single-ended), which means that one conductor carries the signal and the other is grounded. However, the transistors themselves are fed by a balanced signal, in which one conductor is positive and the other is negative. The transformation between unbalanced and balanced signal environments is achieved through the use of a balun.

The word balun is composed of the words that describe its function; BALanced-to-UNbalanced transformation. There are a number of different ways of achieving this function; the main ones will be introduced here.

A balun is a three port device, where one port is unbalanced (single-ended), and the other two ports form a balanced port. Baluns are used in a variety of applications including balanced antenna feeds and mixers, as well as push-pull power amplifiers. As would be expected, different applications place different requirements on the balun. For example, balanced mixers require good phase balance, whereas push-pull PAs require baluns with low loss for high efficiency operation.

There are three main types of balun. At frequencies up to 10 MHz, magnetically coupled coils of wire can be used as transformers or baluns [30]. These are similar to the transformers that are used in electrical systems for the step-up and step-down of voltages. They are usually, but not always, wrapped around a piece of ferrite material to increase the magnetic coupling. The parasitic capacitances between the windings and inductance due to long wire lengths limit the frequency response of these devices. Because of their low-frequency operation, it is not necessary to consider the magnetically-coupled balun further.

There are two types of transmission line balun which will be referred to as VHF transmission line baluns and microwave transmission line baluns.

Most of the time, the term 'transmission line transformer' refers to a VHF transformer or balun. A VHF balun can be made from coaxial cable or twisted wires and always makes use of some sort of ferrite component. In contrast to the magnetically-coupled balun, the ferrite is not used to increase the magnetic coupling but instead as a high impedance choke to increase the impedance of the outer transmission line. The high permeability of the ferrite results in a large inductance, which presents a high reactive impedance that blocks current. The ferrite can provide a high impedance without the loss that would be introduced by a resistive element. It is worth noting that in both magnetically-coupled baluns and VHF baluns the desirable property of the ferrite material is high real permeability.

The main reference work on the design of transmission line transformers at HF and VHF is [51]. At these frequencies, a lot of the practical knowledge has stemmed from the amateur ('ham') radio community. Because of the number of parameters that affect the ferrite's characteristics, and therefore the balun's performance, VHF transmission line balun design using ferrite materials is regarded as "mostly empirical" [52].

Microwave transmission line baluns, in contrast, rarely make use of ferrite materials. This is due to the fact that most ferrite materials display rapidly decreasing real permeability at 100 MHz and above [53]. Transmission line baluns can be implemented as three-dimensional structures using coaxial cable, or as two-dimensional planar structures. The coaxial cable transmission line balun is shown in Fig. 2.18.

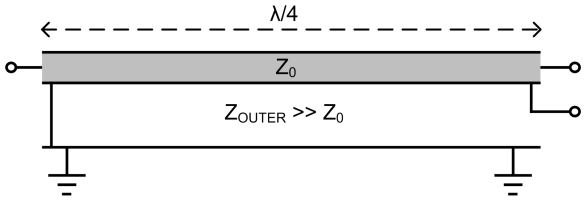

Figure 2.18: Coaxial cable transmission line balun

Further complication in categorising baluns stems from the three most common ways in which the balun structure can be connected. The first is the 'true' balun mode, shown in Fig. 2.19, where an unbalanced load at one end is converted into a balanced load at the other end.

The second is the 'transformer' mode, shown in Fig. 2.20, where the unbalanced-to-balanced transformation is not actually implemented. However, by choosing an appropriate value of Z_0, an impedance transformation can be realised. Occasionally in the literature, a transformer is referred to as an 'unun' (UNbalanced-to-UNbalanced), but this term will not be used here.

The third mode will be termed the 'push-pull mode'. Walker notes in [30] that when used in a push-pull amplifier, a balun is not actually converting to a balanced load but actually to two unbalanced loads, each with half the impedance of the balanced load. This configuration is shown in Fig. 2.21. He therefore suggests a more appropriate name for a balun in this scenario is an 'anti-phase power splitter'. This serves to differentiate the use of baluns for push-pull power amplifiers compared to true balanced loads, such as a balanced antenna. However, recognising that all the baluns that are discussed here are to be used in push-pull power amplifiers, they will continue to be referred to as baluns.

It should be noted that the balun function could also be implemented with a 180° hybrid coupler at microwave frequencies, however this component has a number of crucial differences compared to a balun. The balun is a three port device whereas the hybrid coupler has an additional port that combines the two signals in phase (designated the Σ port). A balun achieves a 2:1 impedance transformation ratio, which means that its balanced ports should be terminated into 25 Ω. In comparison, the 180° hybrid coupler has all of its ports terminated into 50 Ω. Another, less well recognised difference between the two is the isolation achieved between the two differential ports. The ideal 180° hybrid coupler has complete isolation between the two halves of the balanced port, whereas the ideal balun has 6 dB coupling between the two halves of its balanced port. The implications of this coupling on the output balun of a push-pull power amplifier will be considered in Chapter 5.

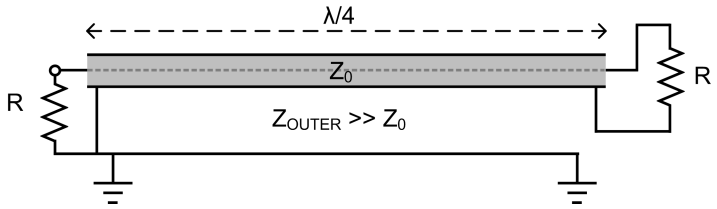

Figure 2.19: Balun connection

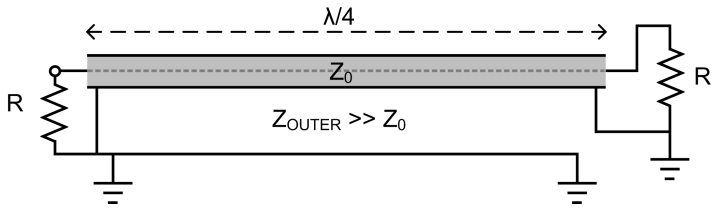

Figure 2.20: Transformer connection

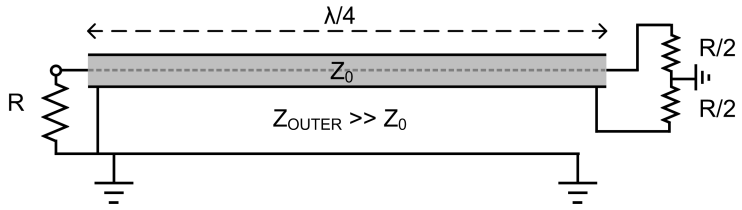

Figure 2.21: Push-pull connection (anti-phase power splitter)

2.8.1 Microwave Transmission Line Transformers & Baluns

It will be seen in Chapter 3 that one of the main bandwidth limitations in a microwave transmission line balun is the half-wavelength resonance. An interesting balun structure that avoids this problem is presented in [54]. By tapering the coils of the coaxial cable, and filling the low-frequency end of the tapered coil with ferrite, an operational bandwidth is achieved from kHz to 26 GHz. This is an extremely impressive bandwidth, however the design has a number of limitations. The balun exhibits high insertion loss at the high-frequency end of the bandwidth (4 dB), and the power handling capability of the structure is limited due to the narrow diameter (0.35 mm) of the coaxial cable used. In addition, the author acknowledges that the ground plane is required to be as far away from the structure as possible for optimum performance, limiting the practical use of the device. Back-to-back measurements were made, which means that the amplitude and phase balance of the balun cannot be determined.

Planar transmission line baluns generally do not achieve the same level of performance as coaxial cable baluns, primarily because of the reduced isolation between the primary transmission line and the ground plane compared to coaxial baluns. However, planar baluns are easier to mass-produce compared to coaxial cable transmission line

baluns. Planar baluns are either edge coupled (two transmission lines side-by side) or broadside coupled (on top of each other, i.e. multilayer) [28]. Low-loss, broadband baluns have been implemented in planar form [55], although these usually require complicated, multilayer processes. A transmission line transformer has been implemented in planar form between 200 MHz and 5.5 GHz [56]. Low loss is achieved for a 4:1 impedance transformation ratio, however three metal layers are required for implementation.

2.8.2 VHF Transmission Line Transformers & Baluns

The use of ferrimagnetic materials to improve the low frequency performance of transmission line baluns is widespread and described in [37,56]. A model for the ferrite-loaded balun at low frequencies is presented in [57]. At low frequencies, multi-octave bandwidths can be achieved through the use of ferrite materials [51], however the decreasing permeability of these materials greatly reduces the effectiveness of this technique at microwave frequencies.

Transmission lines wound on ferrite cores are analysed in [58] and good agreement is shown between theory and measurement. Low frequency, ferrite-loaded baluns are also analysed in [57], however as transmission line length and stray reactances are neglected in the analysis, this cannot be utilised at microwave frequencies.

Ferrite-and-wire based baluns with less than 1 dB insertion loss between 5 MHz and 2.5 GHz are presented in [52]. This is the highest frequency observed for transmission line baluns that use a ferrite component as a high reactance choke.

2.8.3 Marchand and Other Compensated Baluns

The basic concept of the compensated balun, of which the Marchand balun is most popular, is to introduce a compensating line to the inner conductor which has the same characteristic impedance as the outer transmission line, such that each half of the balanced port presents the same impedance. In the same way, it also improves the amplitude balance between the two halves of the balanced port. The basic circuit model of the Marchand balun is shown in Fig. 2.22.

Marchand's original paper was published in 1944 [59]. One of the key works in understanding the Marchand balun is [60], which also claims that Marchand's original optimisation criterion is not in fact optimum. The Marchand balun was reinvented by Roberts [61] and was presented after Marchand's design, but has the same structure. A Marchand planar balun with a very wide bandwidth is presented in [62]. A 'defected ground plane' structure helps to increase the characteristic impedance of the transmission line and hence widen the bandwidth. An operating bandwidth of 4 GHz to 20 GHz is achieved with insertion loss values of 0.5 to 0.7 dB.

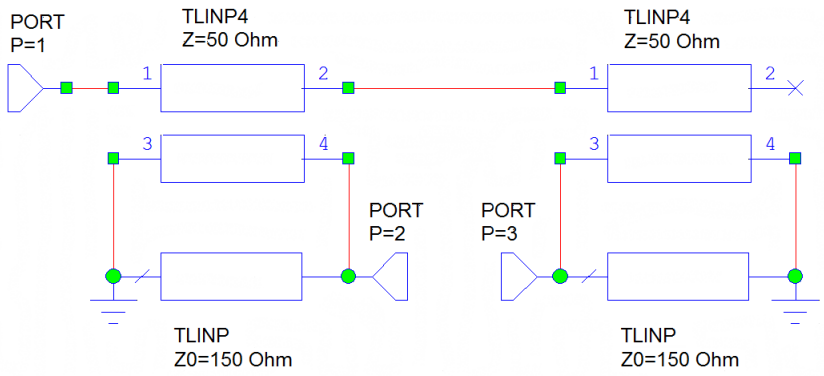

Figure 2.22: Marchand balun basic topology

2.9 Chapter Summary

In this chapter the main concepts that are relevant to this thesis have been introduced. It has been shown that there are several limitations to achieving broadband, high-power and high-efficiency performance using single-ended power amplifiers. These limitations include the fundamental ability of matching networks to present the necessary impedances across significant bandwidths, the variation in optimum impedances due to transistor and package reactances and the conflicting requirements for harmonic terminations.

The conventional modes of operation in a power amplifier have been outlined, as well as newer, broadband modes such as Class J and the continuous modes.

The basic properties of gallium nitride make it suitable for the applications discussed in this thesis. It has been shown that, compared to silicon or GaAs, GaN is the most appropriate semiconductor material for implementing broadband, high-efficiency power amplifiers.

Several alternative topologies to the single-ended amplifier have been discussed, including the distributed and balanced amplifier. The push-pull topology appeared to have the greatest potential for achieving high performance at microwave frequencies across significant bandwidths.

The many implementations of baluns and push-pull power amplifiers have been reviewed, with clarification on the differences between balun structures at different frequencies. It can be seen from the existing literature that there is plenty of scope for further research into this topic, as will be seen in the following chapters of this thesis.

Chapter 3

Design Methodology for Multi-Decade Baluns at Microwave Frequencies

3.1 Introduction

As identified in the previous chapter, the balun is key to the overall performance of a push-pull power amplifier. The requirements for the balun is that a 180° phase offset, 2:1 impedance transformation and even power split between the balanced ports is achieved across the entire operational bandwidth of the amplifier. Insertion loss is critical and should be kept to a minimum, as it directly affects the output power and efficiency of the amplifier. Secondary considerations include size and power handling capabilities. Multi-decade bandwidths are readily achievable at VHF and UHF but are much harder to realise at microwave frequencies.

In this chapter, a new methodology is presented for designing baluns exhibiting multi-decade bandwidths at microwave frequencies. The bandwidth limitations of coaxial cable transmission line baluns are identified and overcome through the use of ferrite beads. The novel aspect of the work is the observation that ferrite beads can perform a dual role of not only improving performance at low frequencies but also suppressing resonances at higher frequencies. The concept of using ferrite beads for resonance suppression was first introduced in [63], a copy of which is included in Appendix A.

The design methodology is comprised of a number of different elements, namely the circuit model for the balun, the effect of the physical dimensions of the balun on its outer characteristic impedance and the measurement of ferrite beads at microwave frequencies. These are discussed individually. The use of 3D electromagnetic (EM) simulations in designing the balun was also investigated, although this was not part of the original design procedure. The design methodology is then described and applied to

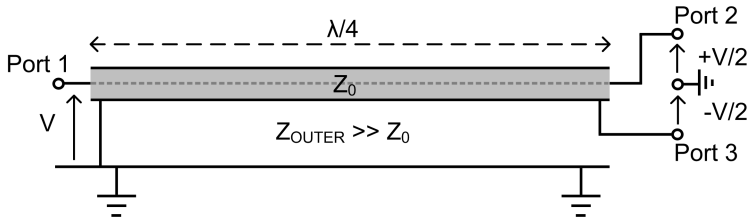

Figure 3.1: Coaxial cable transmission line balun

the design of a prototype multi-decade microwave balun.

The prototype balun achieves low-loss operation over a bandwidth greater than two decades. The measured results validate the design methodology and demonstrate that ferrite beads can be used to realise high-performance transmission line baluns.

3.2 Basic Transmission Line Balun Operation

The basic structure of the coaxial cable transmission line balun is again shown in Fig. 3.1. The properties of the transmission line force the voltage difference between the inner and outer conductor of the coaxial cable to remain constant along its length, so that a differential voltage appears across the balanced termination at the remote end. The balanced termination is in fact split into two unbalanced loads with half the impedance of the equivalent balanced load. This is the 'push-pull' configuration previously outlined in Section 2.8. There are two transmission lines; the coaxial cable and a 'parasitic' transmission line formed between the outer conductor and the ground plane. The simulated frequency response of this structure is shown in Fig. 3.2. This response was obtained using the circuit model of Fig. 3.4, which will be described in Section 3.3. A linear (S-parameter) circuit simulator was used with a frequency sweep between 10 MHz and 6 GHz.

It can be seen in Fig. 3.1 that the outer conductor of the coaxial cable is connected directly to ground at the unbalanced end of the cable (corresponding to Port 1). This short circuit to ground is transformed by the parasitic transmission line to a different impedance when viewed from the other end of the cable, in accordance with standard transmission line theory [28]. At the frequency at which the transmission line length is a quarter of a wavelength ($\lambda/4$), the short circuit is transformed to an open circuit. At this frequency (1.875 GHz in Fig. 3.2), the voltage at the balanced end of the cable is split equally between Ports 2 and 3.

When the transmission line length is half the wavelength, the short circuit is rotated 360°, back to a short circuit. This forms a series resonator, which limits the usable bandwidth of the balun. The frequency that is occurs at is termed the half-wavelength frequency (f_{res}). It should be noted that resonances occur every n*f_{res} where n is a

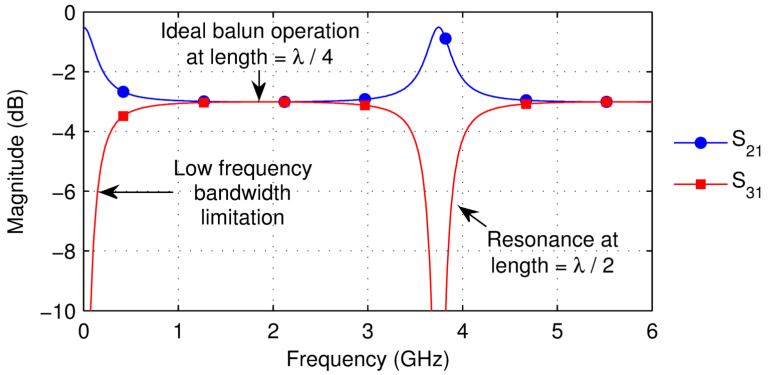

Figure 3.2: Simulated frequency response of the balun of Fig. 3.1 (1:1 transformation ratio)

positive integer. In Fig. 3.2 f_{res} is 3.75 GHz, calculated using (3.1). As the dielectric of the parasitic transmission line is air, it is assumed that the phase velocity is equal to the speed of light in free space, denoted by c.

$$f_{res} = \frac{c}{2l} \tag{3.1}$$

The second bandwidth limitation occurs when the outer conductor appears as a short circuit on the unbalanced input at the lower end of the frequency band. As the wavelength becomes much greater than the length of the transmission line, the transmission line can no longer be considered as distributed and the 'parasitic' transmission line appears as a short circuit. This bandwidth limitation can be overcome through the use of ferrite materials, which effectively act as 'choking reactances' to increase the impedance of the 'parasitic' transmission line and maintain balun operation. This is a standard technique that is widely used at VHF and below.

The length of the coaxial cable is chosen to be a quarter of a wavelength at the centre frequency of the operational bandwidth. This is necessary to transform the short circuit to ground into an open circuit, in order to realise an equal voltage split between the two balanced ports. This length of cable also means that the balun can be used as a quarter-wave impedance transformer, the operation of which is described in [28]. The quarter-wave balun can be used as an impedance transformer by selecting an appropriate value of Z_0 using (3.2). For example, a 50 Ω input impedance (Z_{IN}) can be transformed to a 12.5 Ω balanced impedance (Z_{OUT}) using a piece of coaxial cable with a characteristic impedance of 25 Ω.

$$Z_0 = \sqrt{Z_{IN} Z_{OUT}} \tag{3.2}$$

The tradeoff is that a larger transformation ratio results in a reduction in bandwidth. As can be seen in Fig. 3.3, an ideal 3 dB power split is achieved at the quarter-wavelength

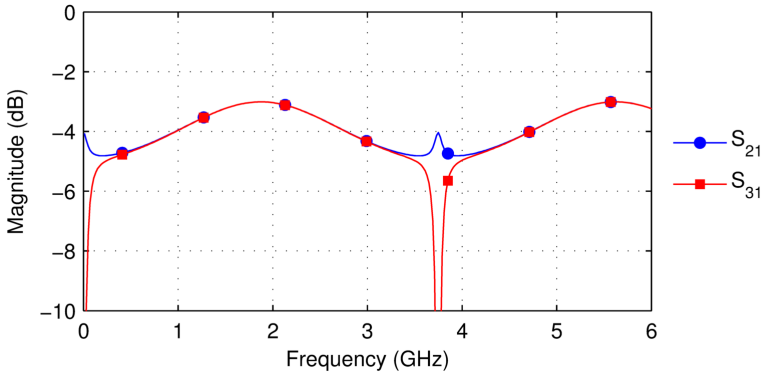

Figure 3.3: Frequency response of 4:1 impedance transforming balun

frequency, 1.875 GHz, but the insertion loss rapidly increases either side of this frequency. For this reason, it was decided to design a balun with an impedance transformation ratio of 1:1 in order to achieve maximum bandwidth. It should be noted that even in the 1:1 case there is effectively a 2:1 transformation at each half of the balanced port, due to the balanced load being split into two unbalanced loads.

3.3 Transmission Line Balun Circuit Model

3.3.1 Transmission Line Balun with Resonance

The coaxial cable transmission line balun can be modelled by the circuit shown in Fig. 3.4. It comprises two parallel transmission lines; one is formed between the centre and the outer conductors of the coaxial cable, the other between the outer conductor and the ground plane. The characteristic impedance of the 'inner' transmission line is equal to the characteristic impedance of the coaxial cable (typically 50 Ω). The characteristic impedance of the 'outer' transmission line is referred to as Z_{OUTER}, and is set to 150 Ω in Fig. 3.4. It will be seen later in this chapter that 150 Ω is a realistic value of Z_{OUTER} that can be achieved in practical baluns. The outer transmission line resonates at the half-wavelength frequency, limiting the bandwidth. Using typical values, the simulated response of the circuit in Fig. 3.4 is shown in Fig. 3.2. This circuit model provides a suitable yet simple model of a transmission line balun. Both transmission lines are modelled, with the connections between the two representing the shared conductor (the outer conductor of the coaxial cable). It will be seen throughout this chapter that this simple circuit model provides a valuable tool for investigating transmission line balun operation, and that it provides reasonable agreement with measured results.

It can be seen in Fig. 3.5 that a higher value of Z_{OUTER} increases the Q-factor of the resonance and hence increases the bandwidth. This demonstrates that the performance of the balun is improved by making the ground plane as far away as possible. If the

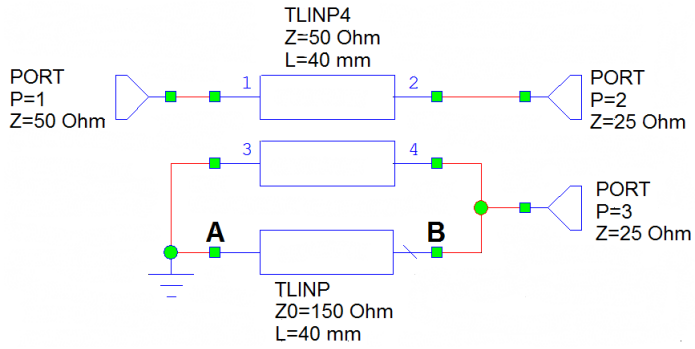

Figure 3.4: Basic transmission line balun circuit model

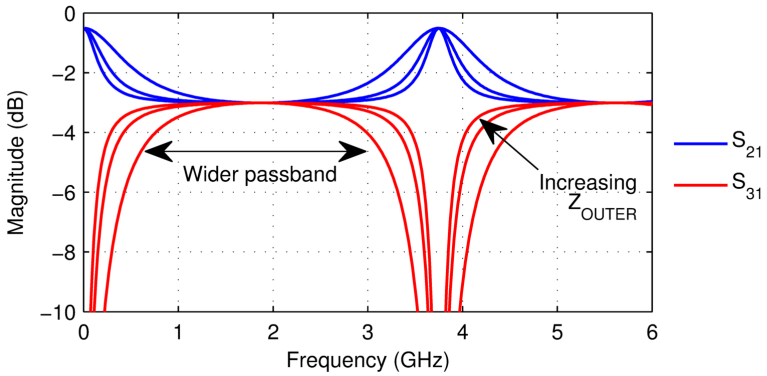

Figure 3.5: Effect of Z_{OUTER} on balun passband bandwidth (Z_{OUTER} = 50 Ω, 100 Ω and 150 Ω)

ground plane was not present, the parasitic transmission line could be ignored and the half-wavelength resonances would not appear. This would result in a near-ideal balun with an equal power split and a high-pass filter response, as described in [30].

The impedances presented to the two halves of the balanced port are shown in Figs. 3.6 and 3.7 between 10 MHz and 6 GHz. When the balun is excited at the balanced port, it presents different impedances depending on whether the excitation is odd-mode or even-mode. When considering coupled lines, there are two possible excitations. If the currents in the two conductors are equal in magnitude but opposite in direction, this is termed 'odd-mode' [28]. If the currents are equal and in the same direction, this is 'even-mode'. It can be seen that in the passband region both Ports 2 and 3 are presented with 25 Ω when excited in odd-mode, as expected, but at the half-wavelength resonance frequency Port 3 is presented with a short circuit. At the half-wavelength frequency Port 2 is presented with 50 Ω, and the balanced-to-unbalanced transformation does not take place. For even-mode excitation, the impedances are open-circuited except around the half-wavelength resonance frequency. The identification of the open-circuit even-mode impedance is an important observation, the implications of which will be discussed in Chapter 4.

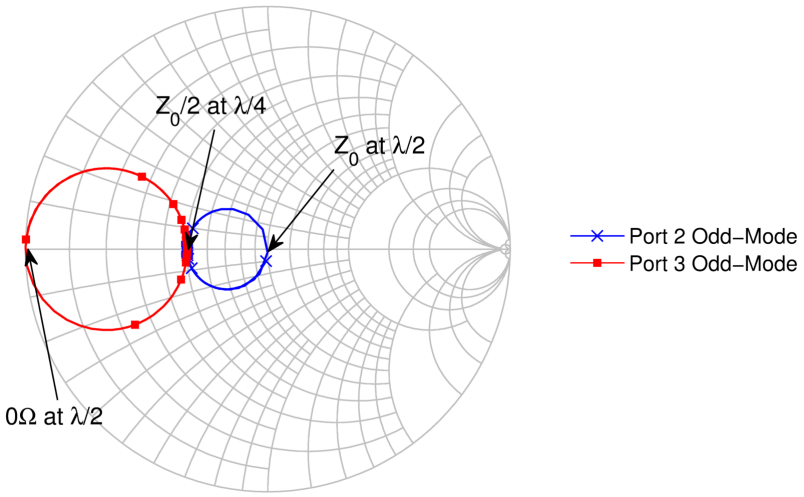

Figure 3.6: Odd-mode impedances presented to balanced ports of balun model of Fig. 3.4

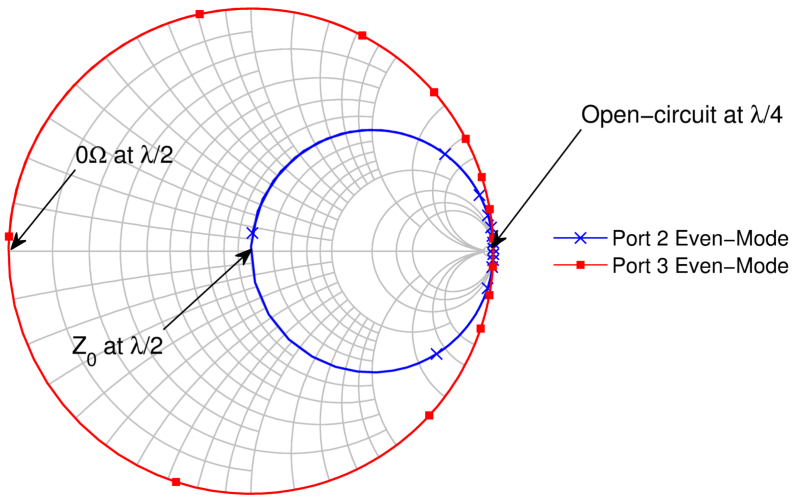

Figure 3.7: Even-mode impedances presented to balanced ports of balun model of Fig. 3.4

For the realisation of extremely broadband power amplifiers, it is desirable to extend the operational bandwidth of the balun to a decade or more. The existing technique of adding ferrite to the balun removes the low-frequency limit, however the half-wavelength resonance has proved to be the limitation at the high-end of the frequency band.

3.3.2 Suppression of Half-Wavelength Resonance

The key innovation in this work is the introduction of a terminating resistor at the unbalanced end of the outer transmission line (position A in Fig. 3.4). Figs. 3.8 and 3.9 show that when the resistance is equal to the characteristic impedance of the outer transmission line (Z_{OUTER}) the resonance is eliminated entirely and a flat frequency response is achieved over a wide bandwidth. S_{21} and S_{31} are plotted separately for clarity. The resistor ensures that at the half-wavelength frequency the transmission line appears as a finite resistance rather than a short circuit, and so a resonance is avoided. This is a significant result, as it opens up the possibility of greatly increasing the usable bandwidth of a microwave transmission line balun. It should be noted that when $R > Z_{OUTER}$, the frequency response actually worsens, as is the case for $R = 200\ \Omega$ in Figs. 3.8 and 3.9.

Although it may appear from the circuit model of Fig. 3.4 that a physical resistor could be placed between the outer conductor and ground, this is not possible in practice. A resistor placed between the outer conductor and ground would prevent the coaxial transmission line from being properly grounded. It will be seen later in this chapter that a ferrite bead can act as a terminating resistor whilst allowing the outer conductor to remain grounded. This is due to its geometry, which allows it to modify the characteristics of the outer 'parasitic' transmission line. However, a resistor provides a suitable model for the effect of the ferrite, so this will be referred to throughout the remainder of this section.

The disadvantage of adding resistance to the parasitic transmission line is that the insertion loss of the overall balun structure is increased. In all the simulations, the coaxial cable is assumed lossless, in order to directly evaluate the loss caused by the resonance-suppressing resistor. When the resistor is excluded, and the half-wavelength resonance is present, the insertion loss in the passband region is 0 dB, i.e. the balun has no loss. Once the resistor is included, and $R = Z_{OUTER} = 150\ \Omega$, the insertion loss increases to 0.33 dB. Fig. 3.10 shows that insertion loss decreases as Z_{OUTER} increases, indicating that for optimum balun performance the outer characteristic impedance should be as high as possible with an equal value of resistance in order to suppress the resonance.

It should be noted that introducing resistance at the unbalanced end of the outer transmission line also affects the amplitude balance between the balanced ports in the passband region. When the resistance is not present, the amplitude balance between the two halves of the balanced port is 0 dB, i.e. there is an equal power split. However, when

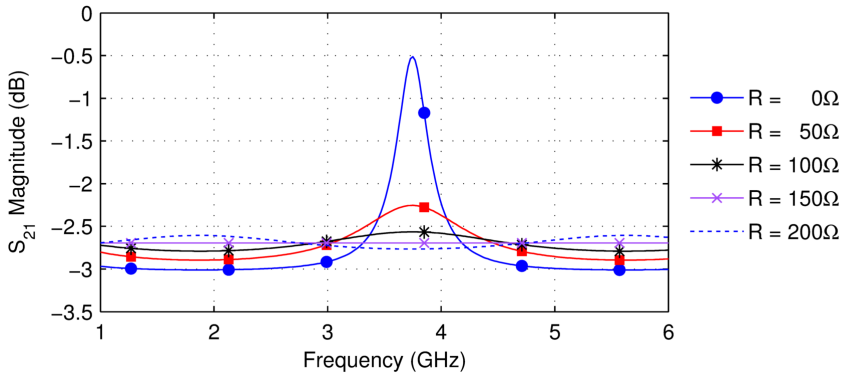

Figure 3.8: S_{21} of simulated balun with various terminating resistor values (Z_{OUTER} = 150 Ω)

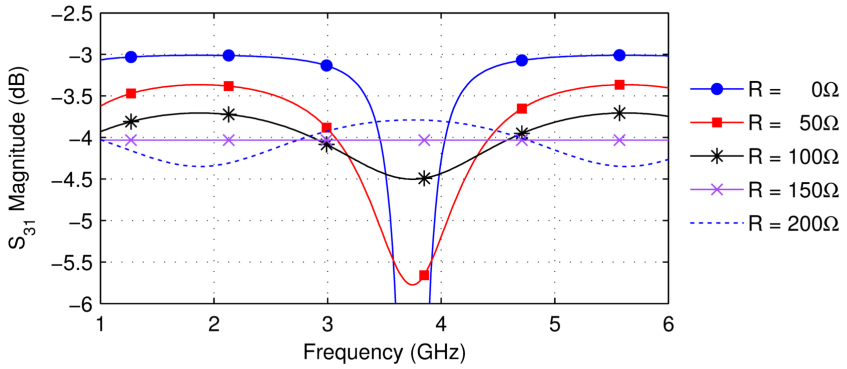

Figure 3.9: S_{31} of simulated balun with various terminating resistor values (Z_{OUTER} = 150 Ω)

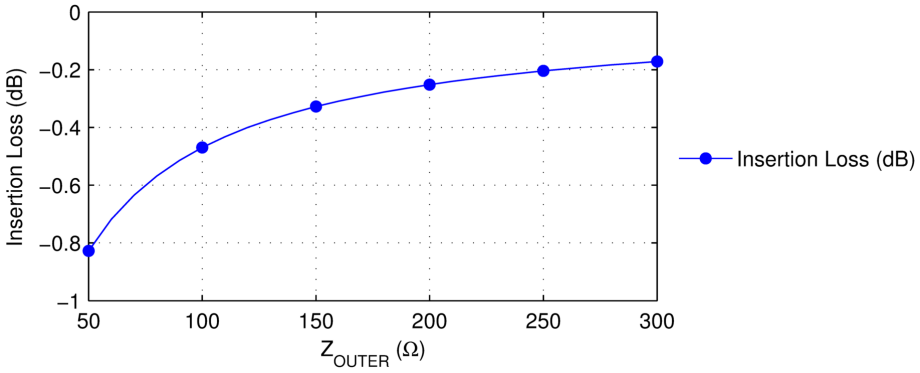

Figure 3.10: Insertion loss variation with Z_{OUTER} (with $R = Z_{OUTER}$)

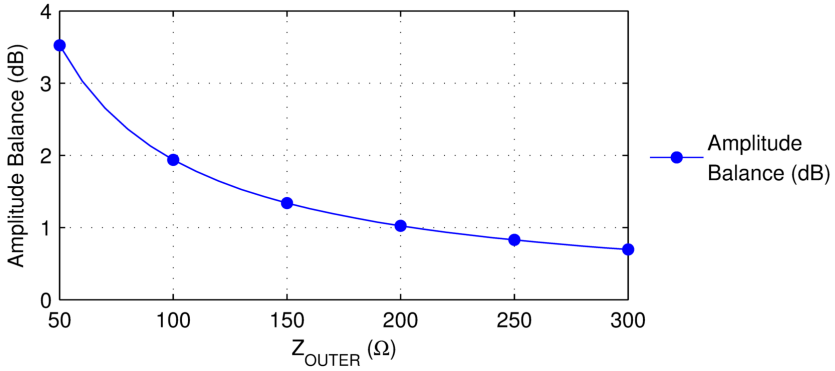

Figure 3.11: Amplitude balance variation with Z_{OUTER} (with $R = Z_{OUTER}$)

$R = Z_{OUTER} = 150\ \Omega$, the resonance is completely suppressed but there is a 1.34 dB difference in amplitude balance between the two halves of the balanced ports. As can be seen in Fig. 3.11, when the half-wavelength resonance is suppressed a higher value of Z_{OUTER} improves the amplitude balance between the balanced ports.

The effect of the terminating resistor on the odd- and even-mode impedances is shown in Fig. 3.12. It can be seen that over a very broad bandwidth the impedances do not vary with frequency, and neither odd- nor even-mode impedances pass through a short circuit.

Once a resistance equal to Z_{OUTER} has been placed at position A, it is possible to investigate the effect of including additional resistance at the balanced end of the outer transmission line (position B in Fig. 3.4). Figs. 3.13 and 3.14 demonstrate the effect of this additional resistance on insertion loss and amplitude balance respectively. The resistor at position B serves to increase the shunt impedance terminations between the two transmission lines, and thereby helps to improve the amplitude balance. According to simulation, the resistance at position B should be as high as possible. The increased impedance of the overall outer transmission line also results in a reduced insertion loss, as shown in Fig. 3.13.

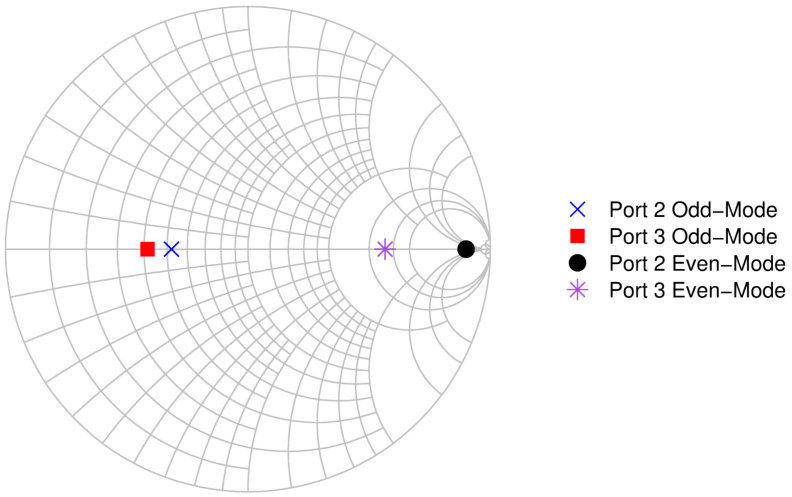

Figure 3.12: Odd- and even-mode impedances presented to balanced ports of balun model with terminating resistor suppressing resonance ($R = Z_{OUTER}$) between 0.5 GHz and 6 GHz

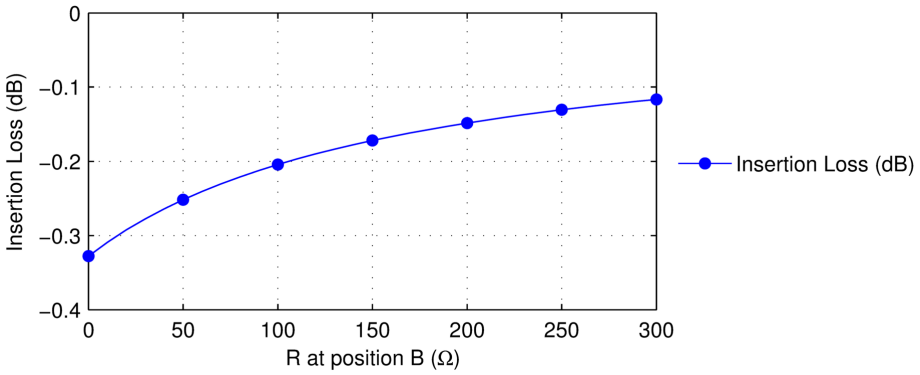

Figure 3.13: Insertion loss variation with resistance at position B

It can be seen through simulation that the bandwidth-limiting half-wavelength resonance can be eliminated using a resistor. It is apparent that for optimum performance, Z_{OUTER} should be as high as possible with an equal value of resistance at position A. In addition, a high value of resistance should be placed at position B to improve both the insertion loss and the amplitude balance. Both the values of Z_{OUTER} and resistance are limited by what can be achieved in practice. The implementation of the resonance-suppressing resistor for use with coaxial cable baluns is discussed in the next section.

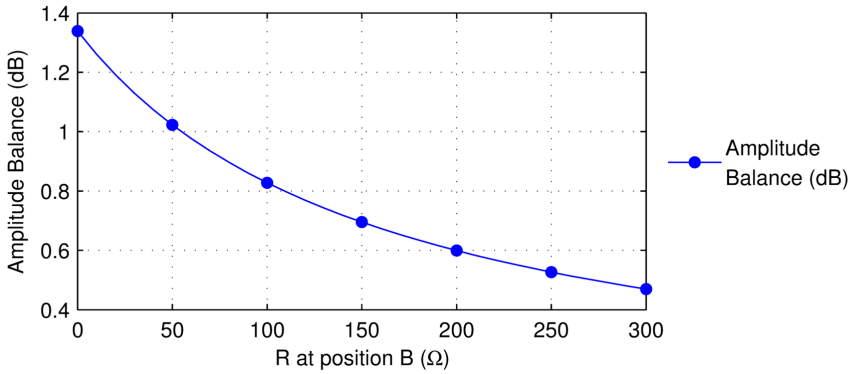

Figure 3.14: Amplitude balance variation with resistance at position B

3.4 Ferrite Measurements

In this section it is shown that the terminating resistors introduced in Section 3.3 can be realised in practice using one or more ferrite bead(s). Before illustrating that ferrite can be used to suppress a balun's half-wavelength resonance, it is necessary to briefly explain some of the properties of ferrite materials.

3.4.1 Introduction to Ferrite Materials

Ferrite materials are magnetic materials composed of oxides containing ferric (iron) ions as the main constituent [30]. The chemical formula for iron oxide is Fe_2O_3. Other elements such as cobalt (Co), manganese (Mn), nickel (Ni) and zinc (Zn) can be added to modify the properties of the ferrite.

The most important property of a ferrite material is its permeability. Permeability is a complex parameter, where the real part (μ') represents the reactive component and the imaginary part (μ") represents the resistive component (loss). Ferrite materials have high reactive permeabilities, which means that they can be used to increase the coupling between transformer coils and realise high-value inductors.

Ferrites are used in VHF transmission line baluns at low frequency to provide a 'choking' reactance, which increases the characteristic impedance of the unwanted parasitic transmission line to ground at low frequencies and hence extends the balun's performance.

Other uses for ferrite include chokes, EMI (electromagnetic interference) suppression beads and circulators. Ferrite materials are available in a number of geometries, such as toroids or rods. Three geometries which are relevant to the current discussion are shown in Fig. 3.15. These are the single aperture ferrite core, referred to in this work as a ferrite 'bead', the dual aperture core and the 'bead-on-lead' ferrite.

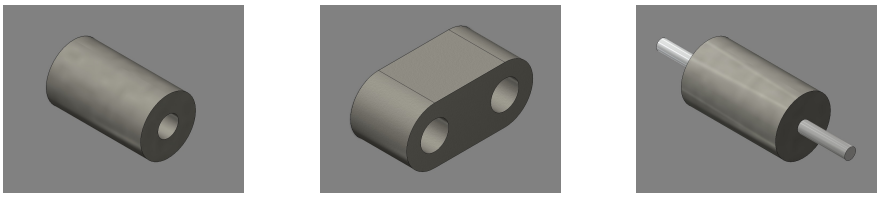

(a) Single aperture core ('bead') (b) Dual aperture core (c) 'Bead-on-lead'

Figure 3.15: Ferrite geometries

The conventional reason for using ferrite materials is due to their high values of reactive (real) permeability. The variation of this permeability with frequency is investigated using data provided by Fair-Rite, a leading ferrite manufacturer. Figs. 3.16 and 3.17 show the permeabilities of three different materials from Fair-Rite. These materials

are #61, #43 (both NiZn ferrites) and #73 (MnZn ferrite). At very low frequencies (below 1 MHz), the real permeability remains constant with frequency. However, above a certain frequency both the real and imaginary permeabilities decrease rapidly. This frequency is known as the ferroresonance frequency, which is the frequency at which loss (imaginary permeability) is highest (μ''_{max}) [64]. For #61 material, μ''_{max} occurs at around 30 MHz, for #43 material μ''_{max} occurs around 3 MHz and for #73 material μ''_{max} occurs around 1 MHz. μ''_{max} has an inversely proportional relationship to initial permeability [30], and this is visible in Fig 3.16.

For conventional ferrite applications, a high reactive permeability and low resistive permeability is generally desired. As Figs. 3.16 and 3.17 show, different materials are suitable for different frequency ranges. It can be observed that #73 material is a relatively low frequency ferrite, and #61 material is a relatively high frequency ferrite. Although #61 material is one of the highest frequency ferrite materials available, it can be seen that its reactive permeability falls below 1 at around 600 MHz. This explains why VHF transmission line baluns almost universally make use of ferrite materials whilst microwave transmission line baluns do not. It should be noted however, that at 1 GHz the ferrite materials still exhibit some resistive permeability. This is generally not considered to be useful in the conventional applications for ferrite materials, but as has been shown in Section 3.3 a resistor can be used to suppress a transmission line balun's half-wavelength resonance. The use of ferrite materials as resistive terminations is an exciting and novel observation, and the logical progression was to investigate its application in microwave transmission line balun design.

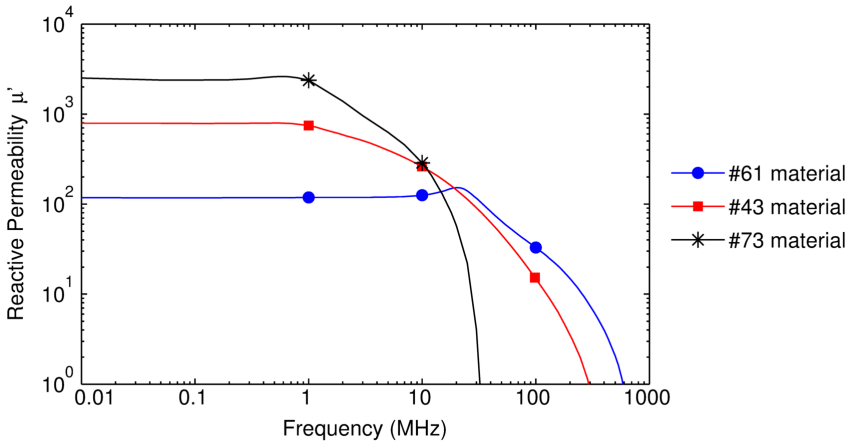

Figure 3.16: Real permeability of different Fair-Rite materials

From Figs. 3.16 and 3.17, it was decided to choose Fair-Rite #61 material as the ferrite material to investigate further. It has low resistive permeability, and hence low loss, at lower frequencies, but has suitable loss between 100 MHz and 1 GHz to suggest it could be used as a terminating resistor at the half-wavelength frequencies.

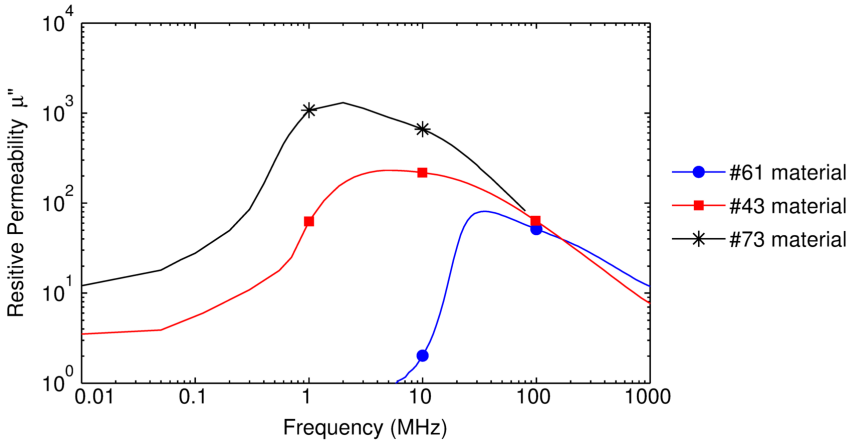

Figure 3.17: Imaginary permeability of different Fair-Rite materials

Unfortunately, because ferrite materials are rarely perceived to be useful above 1 GHz, manufacturer data is generally unavailable above this frequency. In the next section, however, it is shown that ferrite beads can be characterised at microwave frequencies using simple S-parameter measurements.

3.4.2 Ferrite Bead-on-Lead Measurements

S-parameter measurements made using a Vector Network Analyser (VNA) can be used to characterise ferrite beads at microwave frequencies. Ferrite beads are assumed to be linear under small-signal excitation, so S-parameters can be considered to be valid. Figure 3.18 shows the test fixture for measuring a 'bead-on-lead', which itself is shown in Fig. 3.15(c). The VNA was calibrated to the interface between the measurement cables and test fixture using a thru-open-short-match (TOSM) calibration. The 50 Ω microstrip lines of the test fixture were then de-embedded to shift the reference plane, as shown in Fig. 3.19. It should be noted that as S_{11} is being measured, 50 Ω should be subtracted from the measured resistive value of S_{11} to obtain the bead's true resistance.

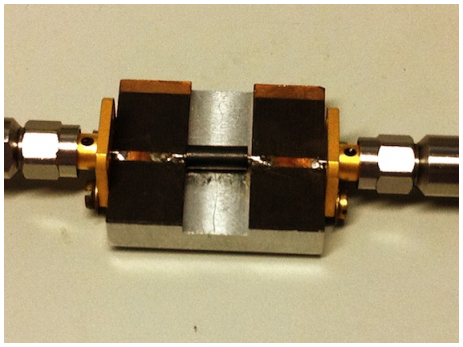

Figure 3.18: Test fixture for measuring ferrite beads-on-leads

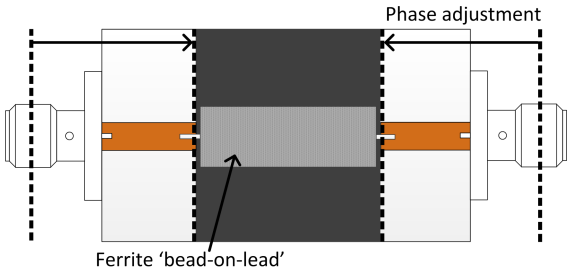

Figure 3.19: Bead-on-lead test fixture showing the shift in the measurement plane

Initially, the three different types of ferrite material from Fair-Rite were compared by measuring different lengths of 'beads-on-leads' between 30 MHz and 6 GHz. As Fig. 3.21 shows, the inductive properties of the ferrite bead-on-lead decrease, and essentially vanish, at higher frequencies. This shows that the imaginary permeability, which manifests itself as a resistance, becomes much higher than the real permeability at microwave frequencies. As noted in [57], the reactance becomes capacitive at the higher end of the frequency range. This can be explained by noting that in Fig. 3.20, the *permittivity* of #61 material appears to be steady up to 3 GHz and does not appear to be decreasing with frequency in the same way as permeability does. Crucially, these measurements show that at higher frequencies the bead-on-lead behaves like a resistance with a small series resonant reactance. As expected, in Fig. 3.21 the longest bead length results in the highest resistive value.

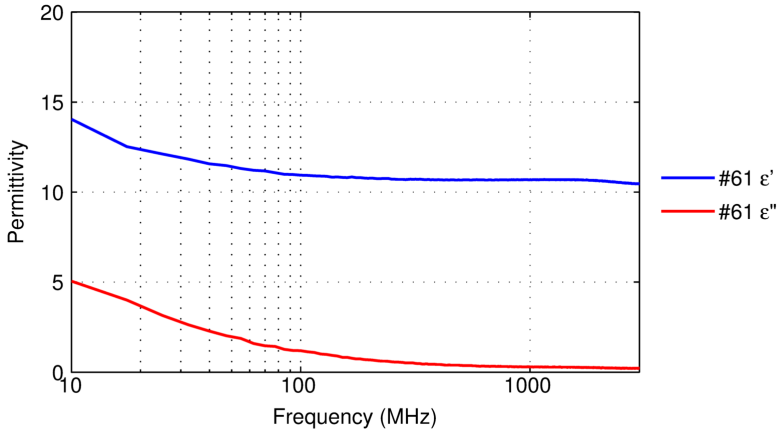

Figure 3.20: Permittivity of #61 material

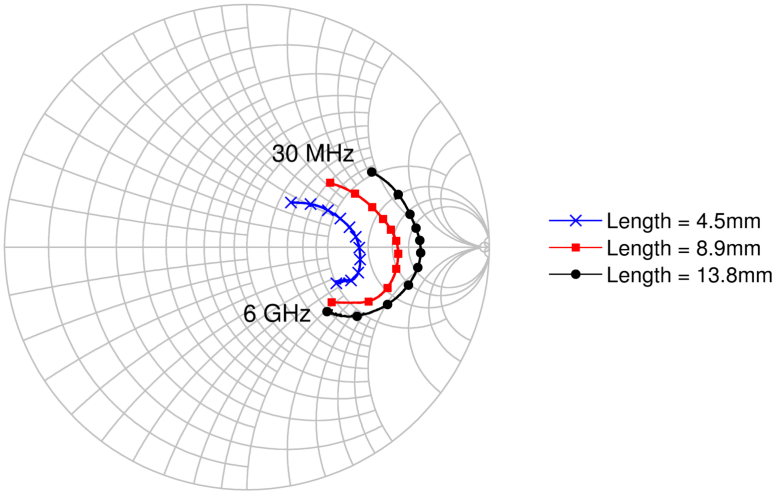

Figure 3.21: Frequency response of different lengths of #61 material beads-on-leads

The measurements of #43 and #73 material beads-on-leads are shown in Figs. 3.22 and 3.23 respectively. These beads-on-leads do not behave as expected; at low frequencies the shorter beads have a higher resistive component than the longer beads, a counterintuitive result. Their resistive components also decrease fairly rapidly with frequency compared to #61 material. The unexpected behaviour of these beads and the higher resistive values offered by #61 material led to the decision to use #61 material.

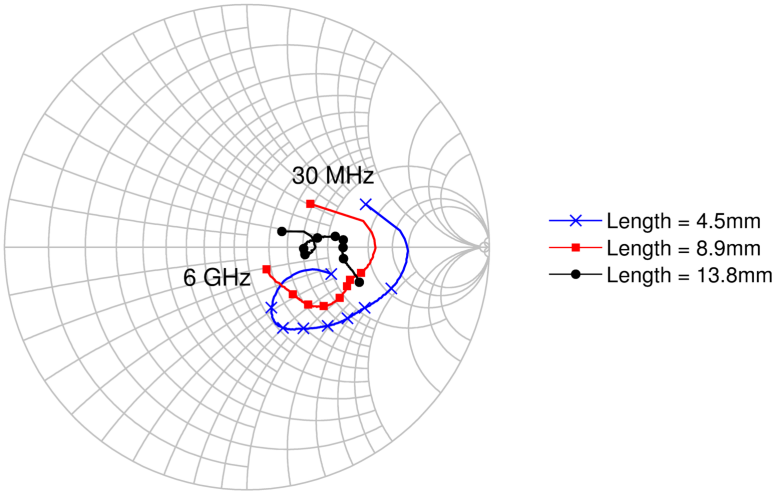

Figure 3.22: Frequency response of different lengths of #43 material beads-on-leads

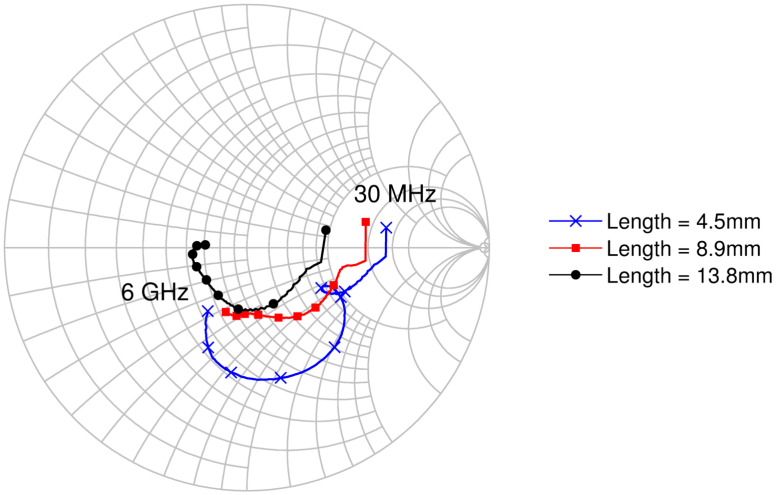

Figure 3.23: Frequency response of different lengths of #73 material beads-on-leads

3.4.3 Ferrite Bead Measurements

As mentioned in Section 3.3.2, any component added between the outer conductor of the coaxial cable and the ground plane would affect the grounding of the coaxial cable transmission line. As the beads-on-leads measured in the previous section are attached to a length of wire and cannot be separated from it, they cannot be used as terminating resistors for coaxial cable baluns.

However, ferrite beads, shown in Fig. 3.15(a), can be used as terminating resistors by passing the coaxial cable through the hole in the middle of the bead. This allows the outer coaxial cable conductor to be grounded whilst still suppressing the resonance.

S-parameter measurements can be made on the ferrite beads by placing them on a piece of wire so that they resemble a 'bead-on-lead'. However, there is a slight difference between measuring the ferrite beads and the 'beads-on-leads', as can be seen in Figs. 3.24 and 3.25. Because the hole in the bead is larger than the diameter of the wire, there is an air gap that exists between the ferrite and the wire. It is uncertain what the effect of this air gap is, but it is speculated that it will reduce the resistance of the bead and hence its resonance-suppressing effect. It should also be noted that when the bead is placed on a piece of coaxial cable, as in Fig. 3.26, the coaxial cable is thicker than the wire and the air gap is reduced. The measured S_{11} of a #61 material bead (model number 2661000101) is shown in Fig. 3.27, and it can be seen that it behaves in a similar manner to the beads-on-leads made from the same material. The length of this bead was 3.25 mm. Another ferrite bead made from #61 material (model number 2661021801) was measured, and its frequency response is shown in Fig. 3.28. The length of this bead was 11.1 mm, and it can again be seen that the bead behaves as expected across a wide frequency range. The advantage of shorter beads is that several can be stacked in series in order to get closer to the necessary value of resistance required to suppress the resonance.

The measurements of ferrite beads and beads-on-leads has shown that they can act as the resonance-suppressing terminating resistors introduced in Section 3.3.2 for coaxial cable transmission line baluns. This is in addition to the high choking reactance they exhibit at low frequency which significantly improves the low frequency response of the balun. It was identified that of the ferrite materials available, #61 material was most suitable for the application. It will now be shown how the value of Z_{OUTER} can be measured in order to determine the value of resistance that the ferrite bead is required to provide.

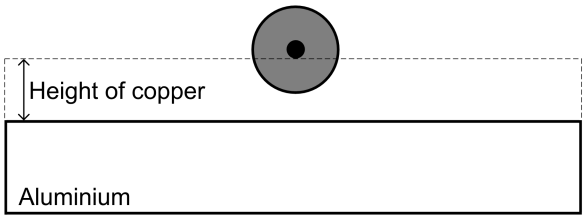

Figure 3.24: Bead on lead measurement cut through

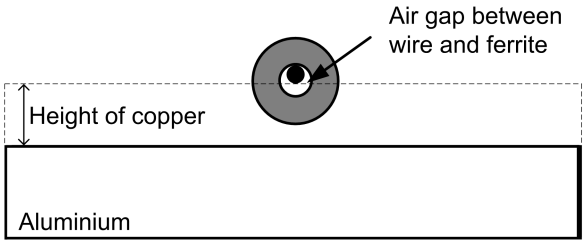

Figure 3.25: Ferrite bead on wire cut through

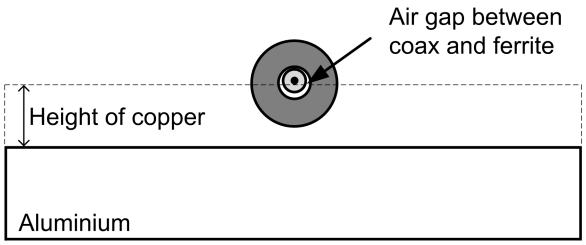

Figure 3.26: Ferrite bead on coaxial cable cut through

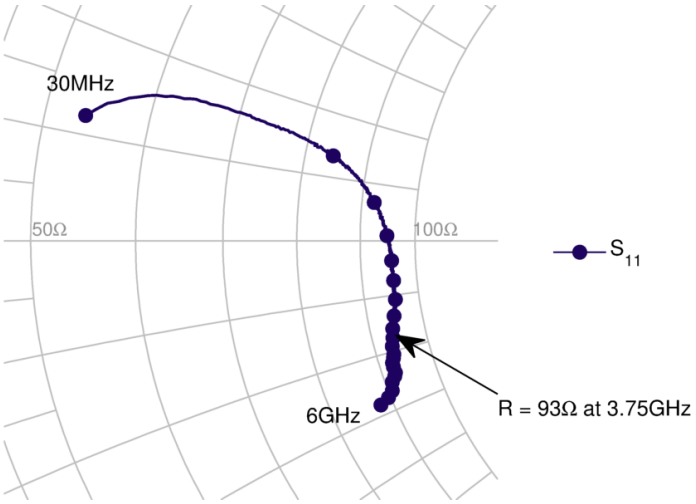

Figure 3.27: Frequency response of Fair-Rite 2661000101 ferrite bead

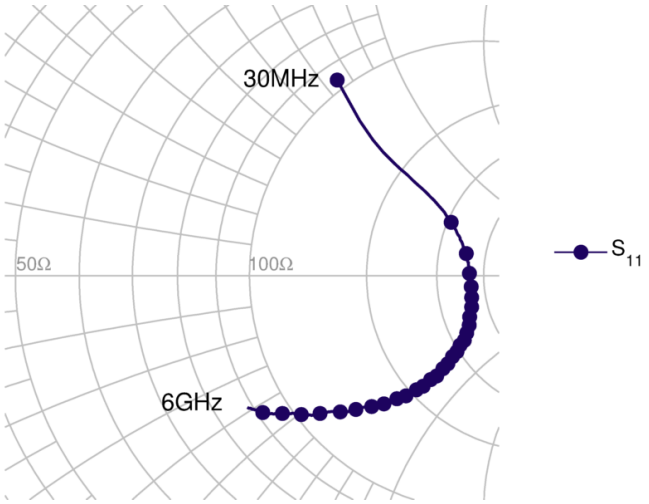

Figure 3.28: Frequency response of Fair-Rite 2661021801 ferrite bead

3.5 Outer Characteristic Impedance (Z_{OUTER}) Measurements

The design methodology requires knowledge of the characteristic impedance of the 'parasitic' transmission line to ground (Z_{OUTER}). This value is dependent on three physical parameters; the depth and width of the milled gap and the outer diameter of the coaxial cable. Using specially constructed test fixtures, S-parameter measurements were made to establish the relationship between the physical parameters and the characteristic impedance. A cut-through of the test fixture is shown in Fig. 3.29. It was constructed from Rogers RT/duroid 5880 circuit board backed with a 6.35 mm layer of aluminium. RT/duroid 5880 is a PTFE-based low-loss material with a dielectric constant (ε_r) of 2.20. By milling a gap in the aluminium layer, the characteristic impedance between the outer conductor of the coaxial cable and the ground plane could be set. Two-port S-parameter measurements were made to test the effect of varying depth on Z_{OUTER}. Using (3.3), Z_{OUTER} was calculated from the measured value, Z_{meas}, and Z_{load}, which was 50 Ω. Z_{meas} is plotted in Fig. 3.31.

$$Z_{OUTER} = \sqrt{Z_{meas} Z_{load}} \tag{3.3}$$

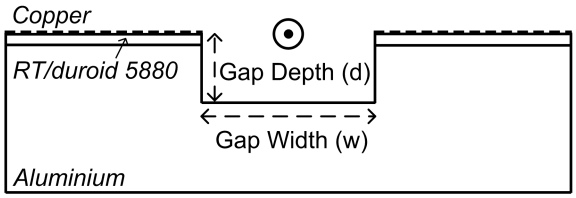

Figure 3.29: Cut-through view of coaxial cable test fixture and prototype balun

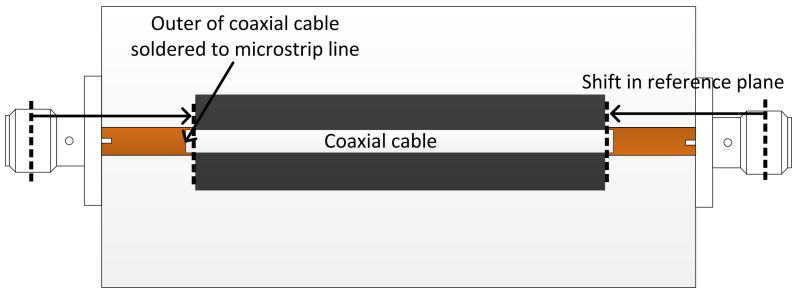

Figure 3.30: Coaxial cable test fixture

Table 3.1 shows that thinner coaxial cable and greater test fixture depth result in a higher characteristic impedance. As identified in Section 3.3, increased characteristic impedance (Z_{OUTER}) improves the balanced port amplitude balance when terminating resistors are present. These measurements show that a trade-off is needed between test fixture size and balun power loss, which increases for smaller coaxial cable diameters.

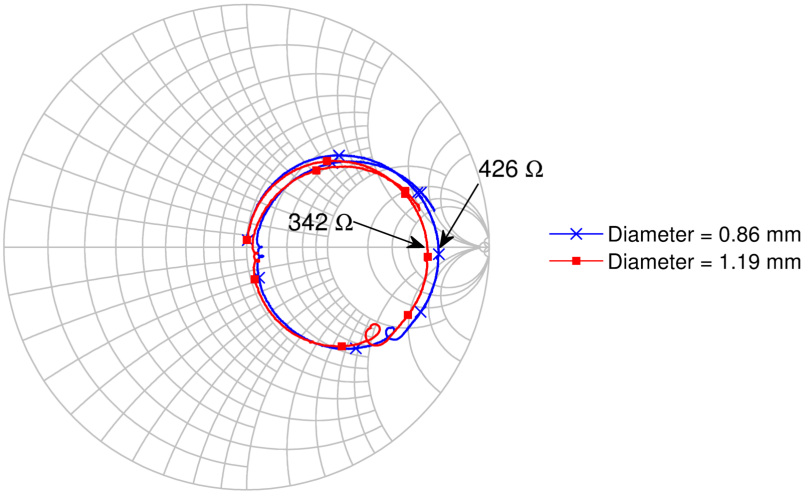

Figure 3.31: Measured S_{11} for two diameters of coaxial cable with gap width of 7.5 mm and depth of 3 mm

	Outer Coaxial Cable Diameter	
Gap Depth	0.86 mm	1.19 mm
2 mm	136 Ω	117 Ω
3 mm	146 Ω	136 Ω

Table 3.1: Variation of Z_{OUTER} for a gap width of 7.5 mm

3.5.1 3D FEM Electromagnetic Coaxial Cable Simulations

As demonstrated in Section 3.5, test fixtures can be constructed and measured to determine the width and depth of the milled channel for a given Z_{OUTER} and coaxial cable diameter. However, it can be a time-consuming process to build and measure many test fixtures, and an alternative method is to use a 3D electromagnetic (EM) simulator. The coaxial cable test fixture was modelled and simulated using COMSOL, a multiphysics finite element modelling (FEM) simulator. As can be seen in Fig. 3.33, the agreement between simulation and measurement is good. This suggests that 3D FEM simulations could be used to determine the required width and depth of the milled channel for a specified characteristic impedance.

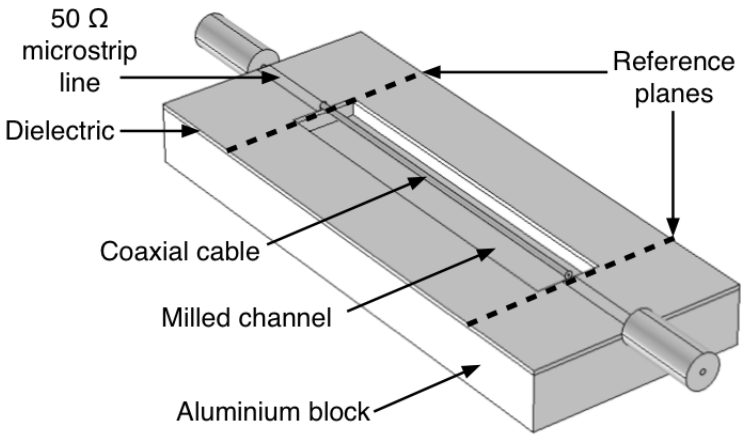

Figure 3.32: Coaxial cable test fixture as modelled in COMSOL

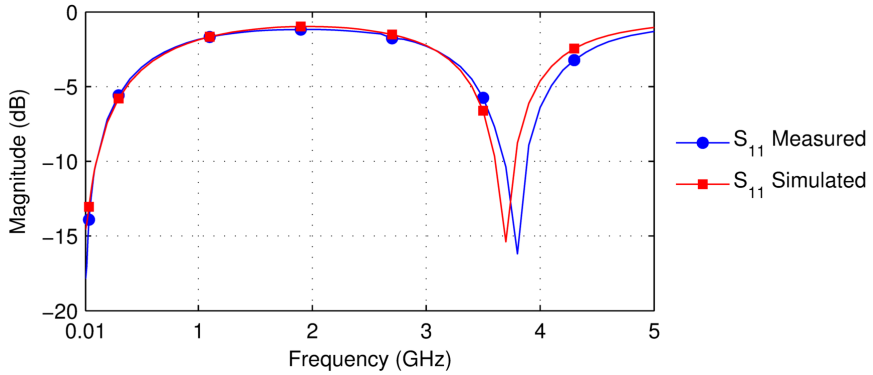

Figure 3.33: S_{11} of coaxial cable test fixture simulated in COMSOL compared to measured data

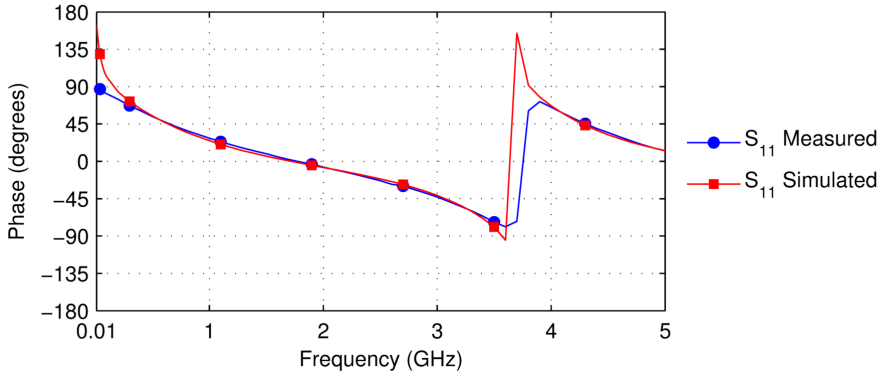

Figure 3.34: S_{11} of coaxial cable test fixture simulated in COMSOL compared to measured data

3.6 Design Methodology

The circuit model, ferrite and coaxial cable measurements described in Sections 3.3 to 3.5 are used in a design procedure to increase the usable bandwidth of a coaxial-cable balun to multiple decades. To verify this design procedure a balun was constructed with a target frequency range of 30 MHz to 6 GHz, a greater than double-decade bandwidth. The assumption made in the design methodology is that that commercial off-the-shelf (COTS) ferrite beads and coaxial cable are used. The balun was constructed using the same method as the coaxial cable test fixture in Section 3.5, shown in Fig. 3.29.

The design process can be summarised as follows;

1. Select coaxial cable based on power handling and Z_{OUTER} requirements.
2. Choose length of coaxial cable based on resonant frequency and low-frequency performance.
3. Select width and depth of channel milled in aluminium to set Z_{OUTER}.
4. Select ferrite beads such that $R_{ferrite} = Z_{OUTER}$ in order to suppress half-wavelength resonance.

This design procedure is now followed in order to implement a prototype balun that validates the design methodology.

3.6.1 Selection of Coaxial Cable

The first stage in the design is to select the coaxial cable diameter and length. The loss of the coaxial cable should be minimised as much as possible, as it will have a direct effect on the insertion loss of the overall balun. If used in a push-pull power amplifier, this loss would decrease the gain and output power of the power amplifier, and hence also its efficiency. It can be shown that the primary loss mechanism in the coaxial cable at these frequencies is due to conductor loss. Dielectric loss also contributes, but has a much smaller impact on the coaxial cable loss compared to conductor loss.

Conductor loss can be reduced by increasing the diameter of the coaxial cable and by choosing a metal with high conductivity per unit length. Coaxial cable with a larger diameter is also capable of handling higher power levels, as the electric field strength is reduced and dielectric breakdown will occur at a higher voltage.

The disadvantage of using coaxial cable with a greater diameter is that as the coaxial cable increases in diameter, the milled gap in the aluminium must become larger to maintain the same value of Z_{OUTER}. This could lead to an increase in the outer dimensions of the balun, which may be a problem for applications where available space is constrained. Instead of increasing the dimensions of the milled gap, it would also be

possible to accept a reduction in Z_{OUTER}, with reduced performance as shown in the simulations of Section 3.3. Thinner coaxial cable also has the advantage that a wider range of ferrite beads will be available for resonance suppression compared to thicker cable.

For the prototype balun, coaxial cable CSR034T from AtlanTec was chosen. This cable has a characteristic impedance (Z_0) of 50 Ω and a diameter of 0.86 mm.

3.6.2 Choice of Coaxial Cable Length

In order for the transmission line to be regarded as distributed, its length is required to be a "considerable fraction of a wavelength" [28] at the lowest frequency of operation. A length of cable one-tenth of the wavelength and above can be considered to be a considerable fraction of a wavelength. A longer cable therefore exhibits better low frequency performance, but the longer length increases the insertion loss. In a conventional balun design, the length of the balun would be highly dependent on making sure that the half-wavelength resonance was not in the passband region. However, this is not so much of a consideration in this case, as the resonance will be suppressed by ferrite beads at a later stage.

The cable was selected to be 40 mm long, which sets its half-wavelength resonant frequency at 3.75 GHz. The resonance was deliberately selected to be within the targeted bandwidth of the balun in order to demonstrate resonance suppression. This cable length also gives reasonable low frequency performance that can be further improved by the addition of ferrite.

3.6.3 Width and Depth of Milled Channel

Once the cable diameter has been selected, Z_{OUTER} is set by the width and depth of the gap. Whilst a high value of Z_{OUTER} is preferable, as described in Section 3.3.2, this requires a greater ferrite resistance to suppress the resonances. With commercial-off-the-shelf (COTS) components this may require multiple ferrite beads, which when connected in series could degrade the performance. It is speculated that using multiple beads would cause the magnetic fields of the individual beads to interact with each other, which may lead to the partial demagnetisation of the beads. As described in Sections 3.5 and 3.5.1, either measured data or 3D electromagnetic simulations can be used to calculate the required width and depth of the gap.

For the prototype balun, the width of the milled gap was 7.5 mm and the depth was 2 mm, giving a Z_{OUTER} of 136 Ω. This value was determined from the coaxial cable Z_{OUTER} measurements of Section 3.5.

3.6.4 Ferrite Bead Selection

Using measurements made in Section 3.4, it is then possible to select ferrite beads to place at the unbalanced end of the outer transmission line and hence eliminate the resonance. The resonant frequency can be calculated from the cable's length using (3.1), then a ferrite bead which satisfies the condition $R{=}Z_{OUTER}$ at that frequency can be chosen.

Three ferrite beads, which as Fig. 3.27 shows have a resistive value of 43 Ω at 3.75 GHz, were placed in series to give a combined resistance of 129 Ω. The beads provide a terminating resistance approximately equal to Z_{OUTER}.

3.7 Measurement of Prototype Balun

In this section it will be shown that ferrite beads have been successfully used to suppress the half-wavelength resonance and improve the low frequency performance of the prototype balun. It will also be shown that the design methodology results in the optimum number of ferrite beads needed to suppress the resonance. The circuit model used for the transmission line balun without the resonance-suppressing resistors is compared to measured results and refined to provide good agreement.

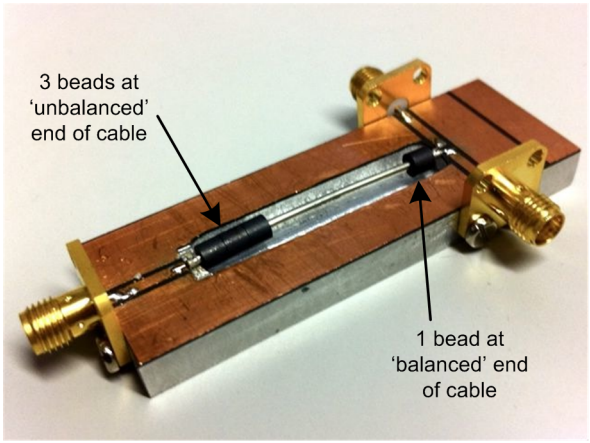

Figure 3.35: Prototype balun with ferrite beads attached

3.7.1 Measurement Technique

The prototype balun is shown in Fig. 3.35. Three-port S-parameter measurements were made between 30 MHz and 6 GHz, with both balanced ports terminated into 25 Ω. This was implemented in practice using the superposition properties of S-parameters. As Fig. 3.36 shows, all the ports were calibrated into 50 Ω, and then port extensions were used to measure the phase length to the end of the balanced-end microstrip lines. Once the

reference plane has been appropriately shifted, the system impedance of S-parameters can be changed to an arbitrary impedance, in this case 25 Ω. Note that this procedure is not necessary for the unbalanced port.

This method of measuring baluns gives a much greater insight into their operation compared to the standard 'back-to-back' configuration shown in Fig. 3.37. Back-to-back measurements are generally carried out as they only require a two-port VNA, rather than the three ports required to measure an individual balun. However, the only information that can be gained by back-to-back measurements is the balun's insertion loss (S_{21}) and input reflection coefficient. No knowledge of the amplitude or phase balance between Ports 2 and 3 is available, and the odd- and even-mode impedances presented to each half of the balanced port cannot be measured.

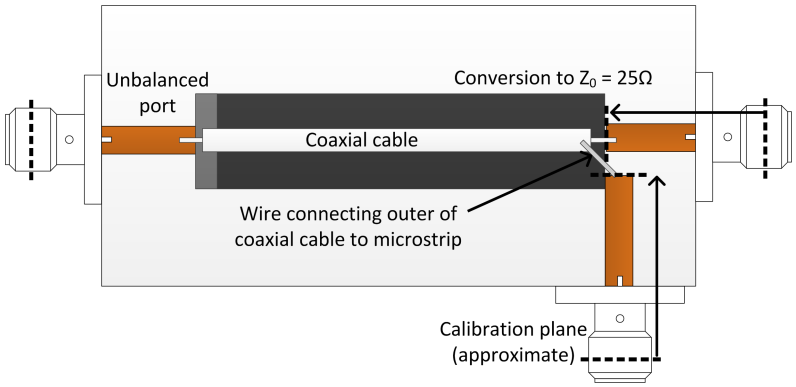

Figure 3.36: Port extensions used to shift measurement plane at balanced ports

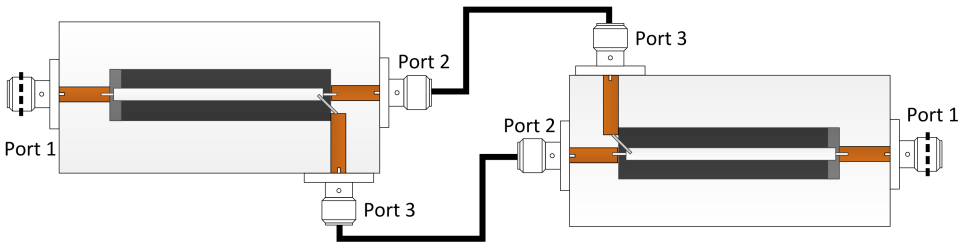

Figure 3.37: Baluns in 'back-to-back' measurement configuration

3.7.2 Demonstration of Resonance Suppression

Figure 3.38 shows the magnitude response of the prototype balun without ferrite beads attached, and it can be seen that it exhibits the classic bandwidth limitations at the low-end of the frequency band and at the half-wavelength resonance frequency. Comparing the magnitude responses in Figs. 3.38 and 3.39 it should be noted that the resonance has been eliminated entirely, and the performance at the low-end of the band has been greatly improved. The insertion loss of the balun is relatively flat across the full 30 MHz to

6 GHz bandwidth. It is possible that the series connection of ferrite beads is diminishing the performance at higher frequencies, as mentioned in Section 3.6.3. The results of Fig. 3.39 represent the optimum configuration of ferrite beads to achieve a flat frequency response whilst keeping insertion loss to a minimum. The optimum configuration was found to be three ferrite beads at the unbalanced end of the balun, equivalent to position A in Fig. 3.4, with one ferrite bead with a resistance of 43 Ω at the balanced end of the cable to increase the shunt impedance. Although simulations showed that making the balanced-end ferrite resistance as high as possible was beneficial, in practice it was found that doing this significantly increased the power loss at 3 GHz and above.

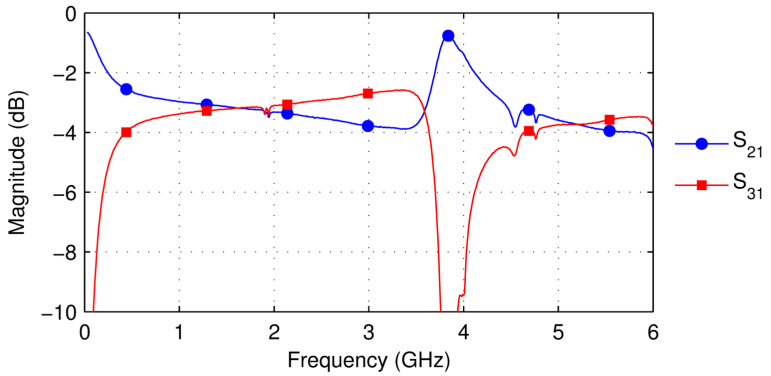

Figure 3.38: Magnitude response of balun without ferrite beads attached

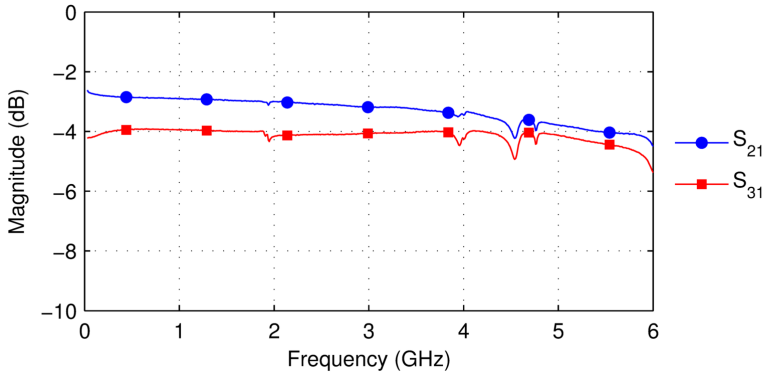

Figure 3.39: Magnitude response of balun with ferrite beads attached

Figure 3.40 shows the phase performance of the ferrite-loaded balun compared to the balun without ferrite. It can be seen that the addition of ferrite improves the phase response around the resonant frequency. A 180° phase difference between S_{21} and S_{31} can be observed across the entire 30 MHz to 6 GHz bandwidth.

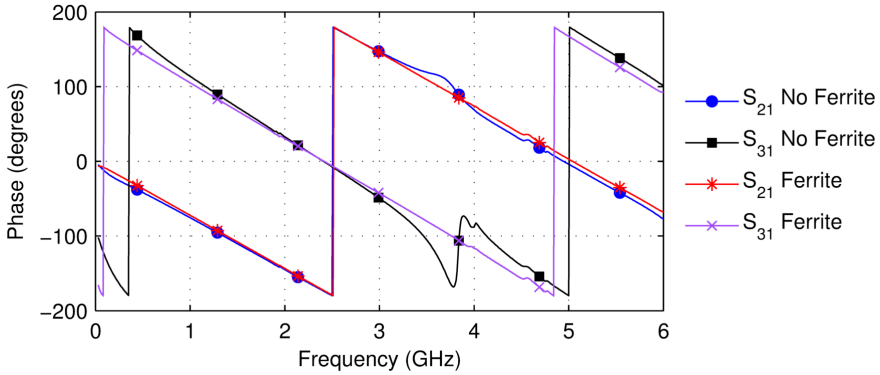

Figure 3.40: Phase response of balun with and without ferrite beads attached

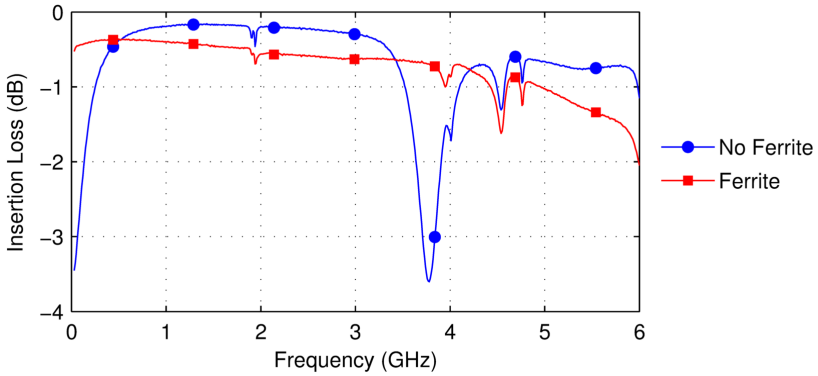

Figure 3.41: Insertion loss of balun with and without ferrite beads attached

It can be seen in Fig. 3.41 that the power loss is less than 1 dB up to 4.4 GHz, and the balun remains usable up to 6 GHz. The insertion loss of the balun increases with frequency, which is due in part to the coaxial cable's loss increasing with frequency. Adding ferrite increases the insertion loss between 0.5 GHz and 3.4 GHz by a typical value of 0.3 dB, a necessary compromise in order to obtain performance over such a broad frequency range.

It can be seen that there is a slight 'glitch' in performance at 4.54 GHz, where both S_{21} and S_{31} display a slight increase in loss. It is possible that this results from the assembly of the balun, which is done manually, and could be removed by more precise assembly. It is also possible that it results from a calibration error from the VNA.

Figure 3.39 shows that when the resonance is suppressed, there is an uneven power split between the inner and outer transmission lines, which could be reduced by increasing Z_{OUTER}. The amplitude balance would not have been measurable if back-to-back measurements had been conducted, as is often the case in published balun measurements.

3.7.3 Measured Balun Impedances

Figure 3.42 shows the measured odd-mode impedances of the balun without ferrite beads, and Fig. 3.43 shows the even-mode impedances. Fig. 3.42 shows that the Port 3 odd-mode impedance is close to a short circuit at 30 MHz, as would be expected. It then approaches 25 Ω across much of the bandwidth, except at the half-wavelength frequency where it again appears close to a short circuit.

Fig. 3.44 shows that when the resonance is suppressed through the use of ferrite beads the impedances are significantly less frequency-dependent. Over a bandwidth greater than two decades, the odd-mode impedances remain in the region of 25 Ω, and the even-mode excitations are presented with high impedances. The low-frequency even-mode impedance at Port 3 could be further increased with the addition of low-frequency ferrite material such as #43 or #73 materials.

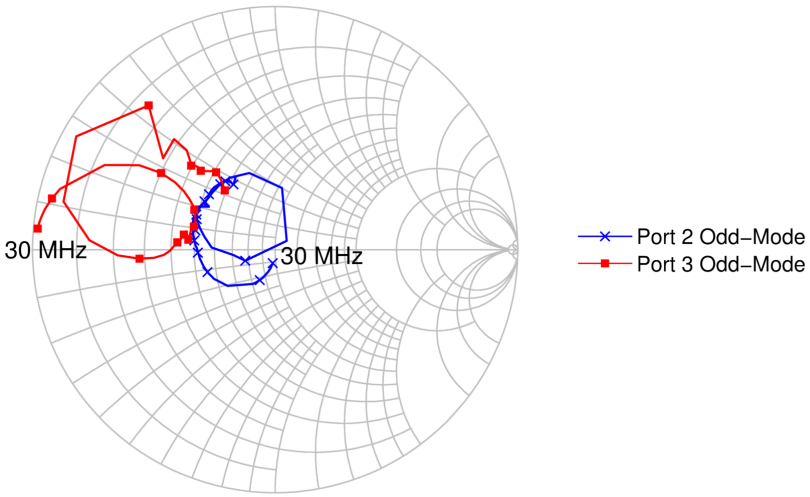

Figure 3.42: Measured odd-mode impedances presented to balanced ports of balun without resonance suppressed

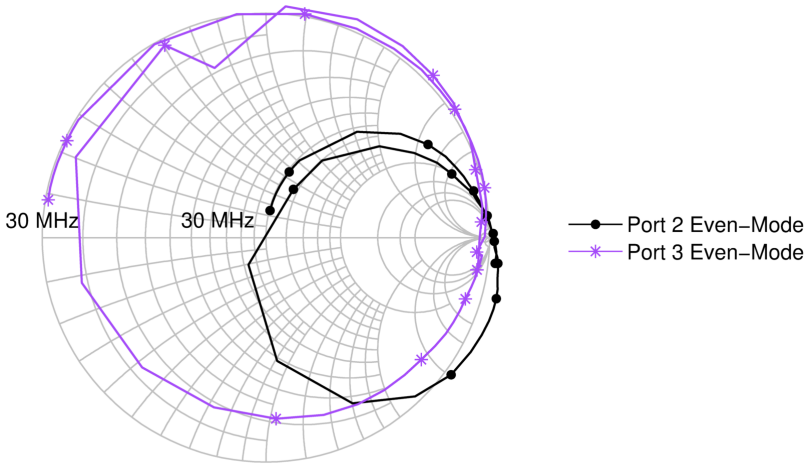

Figure 3.43: Measured even-mode impedances presented to balanced ports of balun without resonance suppressed

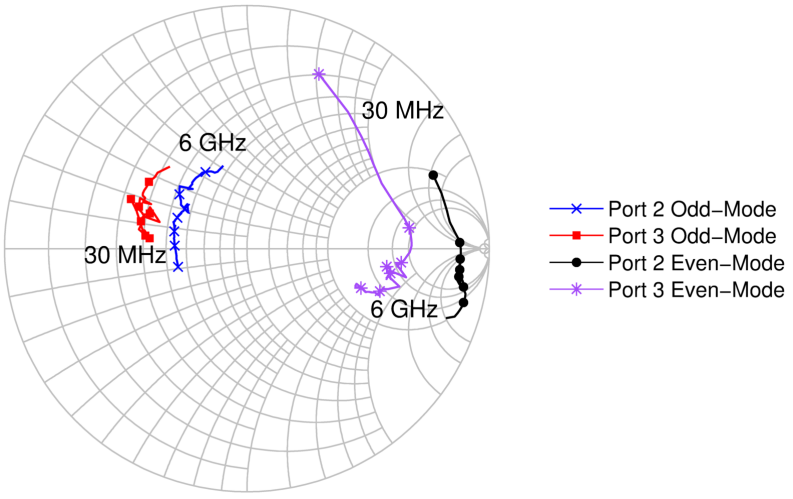

Figure 3.44: Measured odd- and even-mode impedances presented to balanced ports of balun with resonance suppressed

3.7.4 Circuit Model Validation

The simulated performance of the balun, without ferrite beads attached, was compared to its measured performance. Although the half-wavelength resonance and low frequency roll-off was accurately modelled, the measured balun exhibited a 'crossover' in the S_{21} and S_{31} traces in the passband region that was not present in simulation. This is marked on Fig. 3.45.

It was found that this 'crossover' was caused by the small length of wire that is soldered between the microstrip line of Port 3 and the outer conductor of the coaxial cable in order to connect them. This length of wire is labelled in Fig. 3.36. If this length of wire is modelled as an inductor with a value of 0.6 nH and included in the circuit model, and the loss of the coaxial cable is included, the response of Fig. 3.45 is obtained, which shows excellent agreement between simulation and measurement. This also indicates that making the connecting length of wire as short as possible improves the amplitude balance of the balun.

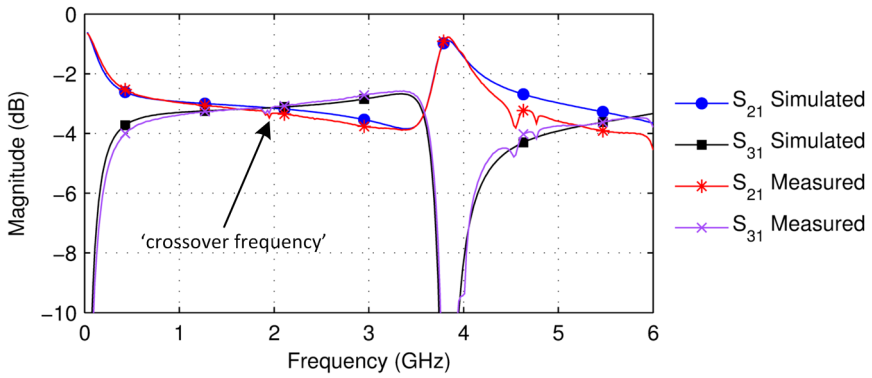

Figure 3.45: Simulated response of balun with 0.6 nH inductor added at Port 3

3.7.5 Validation of Design Methodology

Figure 3.46 shows measured results with different numbers of Fair-Rite 2661000101 beads attached at the unbalanced end. It can be seen that with only one bead the resonance is reduced but not suppressed entirely. As further beads are added the resonance is suppressed further but the two traces become more separated, as would be expected from simulation. The optimum case is when three beads are used and S_{31} is comparatively flat across the entire bandwidth. This agrees with the design procedure in Section 3.6, which identified that three beads would give the overall resistance value that was closest to Z_{OUTER}. When four beads are present, the flatness of the frequency response worsens as $R_{ferrite}$ is greater than Z_{OUTER}. This could also be observed in the simulated results of Figs. 3.8 and 3.9. At the low frequency end of the band, the performance improves as more beads are added. If the half-wavelength resonance were suppressed

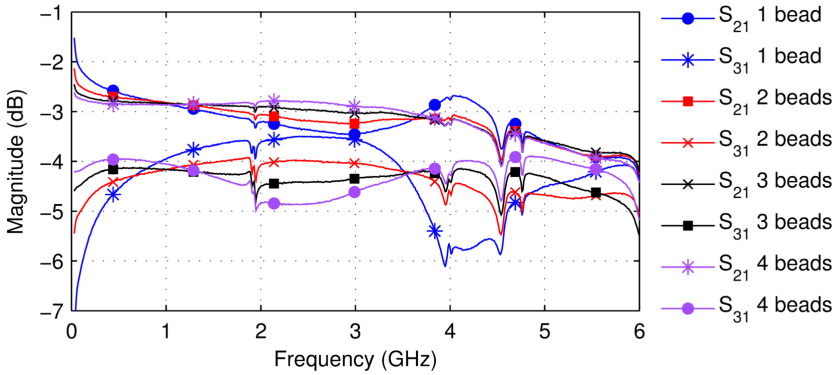

Figure 3.46: Comparison of different bead configurations

but the low-frequency performance was not sufficient, further beads of a lower-frequency ferrite material such as #43 or #73 could be added to improve the low-frequency performance without having a significant effect on the resonance suppression. In this case, however, this was not necessary.

3.8 Chapter Summary

In this chapter a novel design procedure is presented for multi-decade coaxial cable baluns based on a new understanding of the dual role of ferrite beads. Measured ferrite beads are shown to act as series resistors at microwave frequencies, and so can be used to suppress resonances on the outer transmission line. At VHF and UHF, the established practice of using ferrite beads as high impedance chokes is used.

Using this new design methodology, a balun was constructed that exhibits flat, low-loss performance between 30 MHz and 6 GHz. The power loss in the balun is less than 1 dB up to 4.4 GHz. It is shown that the design methodology can be used to select the optimum number of ferrite beads needed to suppress the half-wavelength resonance.

The balun serves as a power combiner and matching network in a push-pull amplifier, providing an effective 2:1 impedance transformation over the entire bandwidth and a 180° phase difference. The development of the balun opens up the possibility of a push-pull power amplifier operating over a bandwidth greater than two decades. It will be shown in Chapter 5 that the baluns introduced in this chapter can be successfully integrated into a prototype push-pull power amplifier.

The investigation and design of a microwave transmission line balun has led to the identification of its open-circuit even-mode impedance. As will be seen in the next chapter, this observation requires the modes of operation inside a microwave push-pull power amplifier to be reconsidered.

Chapter 4

Push-Pull Operation at Microwave Frequencies

4.1 Introduction

In the previous chapter it was identified that the microwave transmission line balun presents an open circuit to even-mode signals. This is an important observation, the consequences of which will be investigated in this chapter. The conventional view on push-pull amplifiers, that a centre-tapped output transformer presents a short circuit to the harmonics components, is not the case when transmission line baluns are used. It is also worth noting that the transmission line balun presents a finite resistance to odd-mode signals, so the third harmonic will not be a short circuit either.

As was shown in Chapter 3, if the half-wavelength resonance has not been suppressed, the even-mode impedance is a short circuit at the resonant frequency. In this chapter however, it is assumed that the resonance has been suppressed and that the even-mode impedance is an open circuit.

Because of the unique impedances presented by a transmission line balun, the mode of operation inside a push-pull amplifier must be reconsidered. None of the existing modes of power amplifier operation outlined in Chapter 2 can be applied to the transistors inside a push-pull amplifier at microwave frequencies. New modes of operation that describe the behaviour of the push-pull amplifier at microwave frequencies are introduced in this chapter.

These new modes of operation were first introduced through the development of factorised time-domain current and voltage waveforms in [65] (included in Appendix B). It will be seen that at certain bias points the push-pull waveforms bear a resemblance to existing modes such inverse Class F and inverse Class B, but it should be stressed that the impedance environment is unique to the push-pull mode of operation.

In this chapter a novel mathematical formulation is proposed to describe the time-

domain waveforms by defining the harmonic impedance environment in terms of odd- and even-mode excitation rather than tuned harmonics. Simulations were used to investigate these modes further, and experimental verification using harmonic load-pull measurements showed good agreement with the theoretical waveforms.

4.2 Benefits of the Push-Pull Topology at Microwave Frequencies

The push-pull configuration offers significant impedance matching benefits when compared to the single-ended topology. It has already been shown how the transmission line balun presents a 25 Ω impedance to each half of its balanced port. When used in a push-pull topology, this means that each transistor will be looking into a 25 Ω impedance environment rather than the standard 50 Ω. For high-power transistors whose loadline impedances are around or below 25 Ω, this provides a 2:1 impedance matching advantage over single-ended amplifiers. In addition, the output balun serves as a power combiner, allowing two transistors to be used and hence doubling the total output power of the overall amplifier. If two single-ended transistors were combined in parallel, their output impedance would be half that of a single transistor, and so the required impedance matching ratio would be doubled. It can therefore be reasonably stipulated that for a given output power level the push-pull configuration provides a 4:1 matching advantage over a standard single-ended design.

The advantage of the push-pull modes of operation is not only in the efficiency and output power of the waveforms, as will be seen later in this chapter, but in the fact that they can be maintained over the entire bandwidth of the transmission line balun, which is significantly larger than for conventional matching networks. In theory, a push-pull PA using transmission line baluns does not suffer from the same inherent bandwidth limitations as a harmonically tuned single-ended PA mode, such as Class F. This is an important observation, and is a result of the properties of transmission line baluns. In contrast to a conventional output matching network, a balun is able to present two impedances at the same frequency, depending on the mode of excitation. This eliminates the problems of conflicting harmonic impedances that limit the bandwidth of harmonically tuned PAs and were outlined in Section 2.3.3.

4.3 Waveform Formulations

The analysis of the theoretical time-domain waveforms begins with mathematical expressions. In the following discussions of time-domain waveforms, the first three harmonics are considered. This is partly because the inclusion of higher harmonics results in an ever-diminishing improvement in the amplifier's performance, and partly because three

harmonics represents the practical limit that can be measured using the active harmonic load-pull system at Cardiff University.

In existing work on factorised waveforms [14,15], the analysis assumes a fixed current (or voltage, for inverted modes) and allows the impedances to be varied to shape the voltage. In this work a different approach is employed, whereby the impedances are fixed and the current is varied, shaping the output voltage. This was done on the assumption that an ideal balun would present frequency-independent impedances, and that these impedances were being presented to the transistor at the current generator plane. It is recognised that this is a highly simplified representation of a real-world scenario, but it nonetheless serves as a useful starting point.

It is important that neither the voltage nor current waveforms can dip below zero, as this would not be permitted in a real transistor. There are no restrictions placed on the upper limit that the voltage can reach. It was assumed that the peak voltage will always be lower than the transistor's breakdown voltage, a reasonable assumption when considering GaN technology. This same assumption is made when discussing other PA modes with high peak voltages, such as Class J and inverse Class F, as well as switched modes.

4.3.1 Voltage Waveforms

The push-pull waveform expressions permit only two impedances to be defined; odd- and even-mode, as this is what would be presented by an ideal balun. The odd-mode impedance will be presented to odd-order excitations, i.e. the fundamental frequency component and the third harmonic (and fifth, seventh etc. harmonics if higher-order components were being considered). The even-mode impedance will be presented to even-order excitations, in this case the second harmonic component only.

A suitable voltage expression was required to contain components at all three harmonics, since although there will be no second harmonic current, second harmonic voltage is permissible. This is analogous to the situation for the third harmonic in the Class F mode and for the second harmonic in the inverse Class F mode.

The factorised voltage waveform equation is shown in (4.1). α and β are parameters which are initially unbounded and which generate a set of 'zero-grazing' voltage waveforms having fundamental, second and third harmonics. Only cosinusoidal terms are required, as the scope of the present work only extends to resistive terminations. When (4.1) is expanded, the individual harmonic components can be described by (4.2) to (4.5).

$$V(\omega t) = (1 + \alpha \cos(\omega t))^2 (1 + \beta \cos(\omega t)) \tag{4.1}$$

$$V_{DC} = 1 + \alpha\beta + \frac{\alpha^2}{2} \tag{4.2}$$

$$V_{f_0} = 2\alpha + \beta + \frac{3\alpha^2\beta}{4} \tag{4.3}$$

$$V_{2f_0} = \alpha\beta + \frac{\alpha^2}{2} \tag{4.4}$$

$$V_{3f_0} = \frac{\alpha^2\beta}{4} \tag{4.5}$$

4.3.2 Current Waveforms

The ideal transmission line balun presents an even-mode open circuit, which does not permit even-order harmonic currents to flow, and so the current waveform expression is only required to contain a fundamental and third harmonic component.

$$I(\omega t) = 1 + k(\cos(\omega t) - \gamma\cos(3\omega t)) \tag{4.6}$$

The parameter γ relates to the bias condition of a transistor, where $\gamma = 0$ corresponds to a raised cosinusoidal current waveform, or Class A bias. As the transistor is biased deeper into Class AB and eventually Class B, the third harmonic current component increases and has a 'squaring-off' effect on the waveform. The parameter k is a scaling factor to ensure that the zero-grazing condition is met for a given value of γ.

4.3.3 Microwave Transmission Line Balun Impedances

The next stage in the analysis is to take account of the impedance restrictions imposed by the balun. These restrictions are shown in (4.7) and (4.8).

$$Z_{odd} = Z_{f_0} = Z_{3f_0} = Z_{5f_0} ... = Z_B \tag{4.7}$$

$$Z_{even} = Z_{2f_0} = Z_{4f_0} = Z_{6f_0} ... = \infty \tag{4.8}$$

Z_B is the odd mode impedance of the balun when one half of the balanced output is measured with respect to ground. For the ideal transmission line baluns considered in Chapter 3, Z_B will have a value of 25 Ω. Using (4.1), (4.6) and (4.7), β can be defined in terms of α and γ by setting the fundamental and third harmonic impedances to be equal.

$$Z_{f_0} = \frac{V_{f_0}}{I_{f_0}} = \frac{2\alpha + \beta + \frac{3\alpha^2\beta}{4}}{k} = \frac{8\alpha + 4\beta + 3\alpha^2\beta}{4k} \tag{4.9}$$

$$Z_{3f_0} = \frac{V_{3f_0}}{I_{3f_0}} = \frac{\frac{\alpha^2\beta}{4}}{-k\gamma} = \frac{\alpha^2\beta}{-4k\gamma} \tag{4.10}$$

It is then possible to set $Z_{f_0} = Z_{3f_0}$ in accordance with (4.7);

$$\frac{8\alpha + 4\beta + 3\alpha^2\beta}{4k} = \frac{\alpha^2\beta}{-4k\gamma} \tag{4.11}$$

$$8\alpha + 4\beta + 3\alpha^2\beta = \frac{-\alpha^2\beta}{\gamma} \tag{4.12}$$

$$4\beta + 3\alpha^2\beta + \frac{\alpha^2\beta}{\gamma} = -8\alpha \tag{4.13}$$

$$\beta(4 + 3\alpha^2 + \frac{\alpha^2}{\gamma}) = -8\alpha \tag{4.14}$$

$$\beta = \frac{-8\alpha}{4 + 3\alpha^2 + \frac{\alpha^2}{\gamma}} \tag{4.15}$$

By defining β in terms of α and γ, it is now possible to investigate the performance of this mode of operation by varying these two parameters.

4.3.4 Theoretical Performance

The equations introduced in the previous sections define the current and voltage waveforms for different values of γ, whilst ensuring that the impedance conditions imposed by the balun are met. It is now possible to plot the drain efficiency against the parameter α, as shown in Fig. 4.1. Notably, this shows that the maximum drain efficiency occurs at the value of $\alpha = -\sqrt{2}$ for all values of γ. Figure 4.2 plots drain efficiency against γ, and shows that the maximum theoretical efficiency is 71.65% at $\gamma = 0.12$.

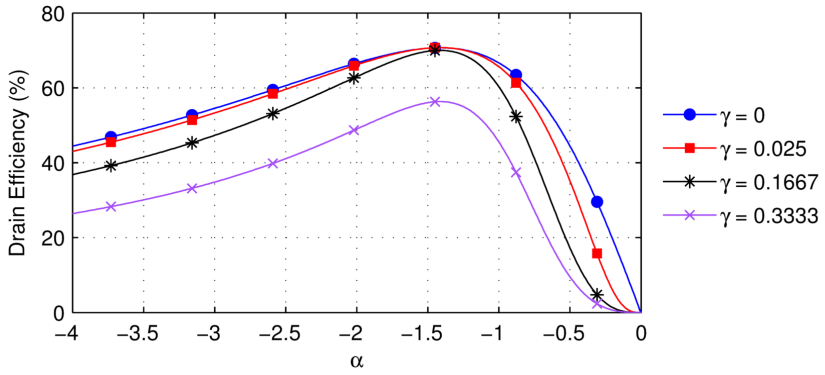

Figure 4.1: Drain efficiency plotted against α for different values of γ

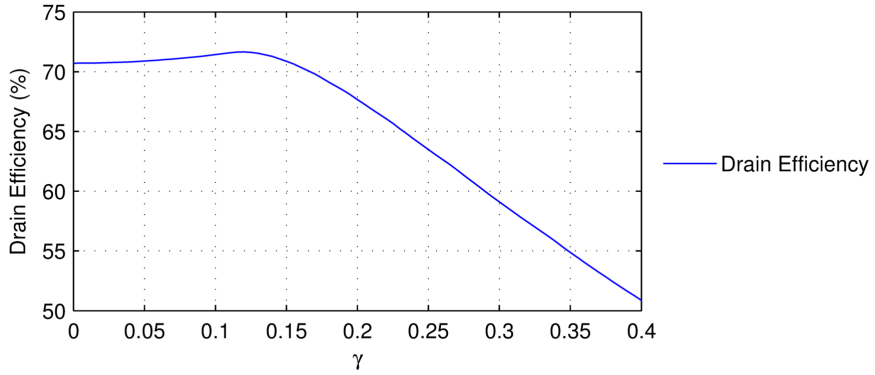

Figure 4.2: Drain efficiency plotted against γ with $\alpha = -\sqrt{2}$

It is possible to calculate the output power of the push-pull mode compared to the Class A mode, which was introduced in Chapter 2. Referring back to Fig. 2.3, the Class A mode has a peak-to-peak voltage swing of 2, and peak-to-peak current swing of 1. Using (4.16), it can be calculated that the output power is 0.25.

$$P = \frac{V_{pp} I_{pp}}{8} \tag{4.16}$$

For the push-pull mode with γ set to zero, the fundamental current swing is still 1, but the fundamental voltage swing is increased to $2\sqrt{2}$. This can be shown by substituting $\alpha = -\sqrt{2}$ and $\gamma = 0$ into (4.3) and (4.15), and this increase in fundamental voltage results in an output power of 0.354, a 1.5 dB increase in fundamental power compared to Class A. This is a significant increase in output power, and is a notable benefit of the push-pull mode at microwave frequencies.

The output power is plotted against γ in Fig. 4.3. The output power has been normalised to the Class A case under full drive (maximum power) conditions. Figure 4.3 shows that there is a significant increase in power for a device operating in the push-pull mode compared to the Class A case over a wide range of γ values.

Figure 4.4 shows how this power advantage is realised. At low values of γ, the second harmonic component is flattening the voltage waveform 'troughs' and allowing an increase in fundamental voltage. At higher values of γ, the third harmonic current component is flattening the current waveform and allowing the fundamental current component to be increased compared to Class A. As shown in Fig. 4.3, the maximum output power is realised at $\gamma = 0.12$ and subsequently decreases with increasing values of γ.

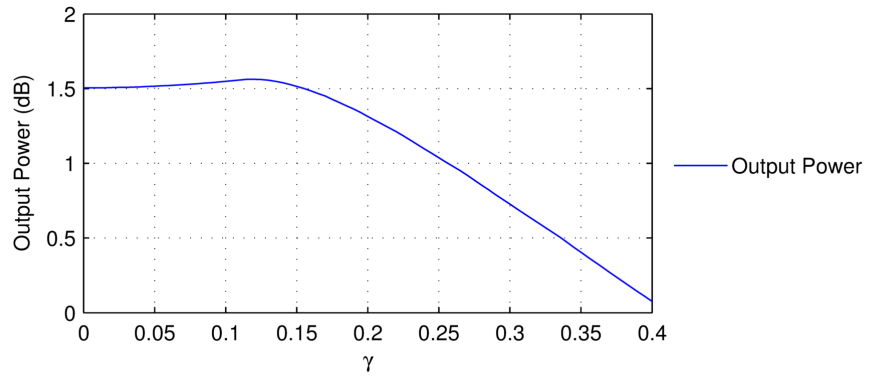

Figure 4.3: Output power plotted against γ with $\alpha = -\sqrt{2}$ (normalised to Class A)

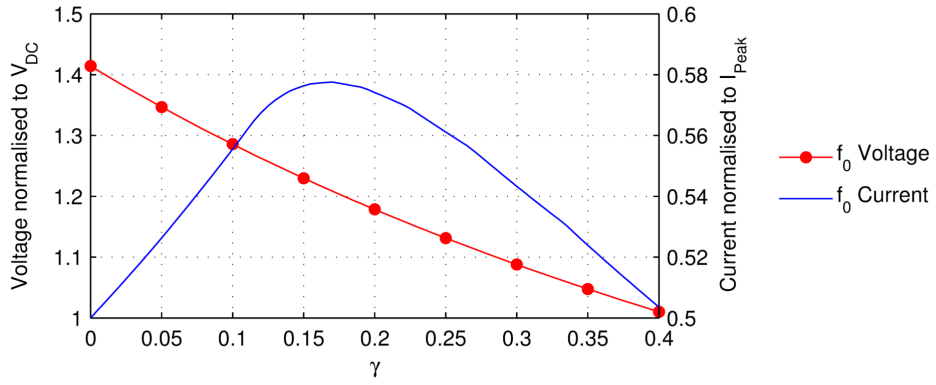

Figure 4.4: Fundamental frequency voltage and current components plotted against γ

4.3.5 Theoretical Time-Domain Waveforms

Theoretical waveforms are generated directly from (4.1) and (4.6) and are plotted in Figs. 4.5, 4.6 and 4.7, with drain efficiencies of 70.71%, 71.65% and 63.49%, respectively.

A case of particular interest is when γ is close to zero. It can be seen from Fig. 4.5 that the waveforms bear a resemblance to the waveforms of the 'inverted Class B' mode, which has a sinusoidal current waveform and a half-wave rectified voltage waveform. It must be stressed, however, that the waveforms of Fig. 4.5 are unique. The inverted Class B mode is implemented by biasing the transistor in Class A and presenting the harmonic frequencies with an open-circuit. The difference between the two modes is that the third harmonic impedance in the push-pull case is a finite resistance instead of the open circuit of the inverted Class B mode. Due to the need for an open circuit at all harmonics, the inverted Class B mode would also be subject to the same bandwidth limitations as the 'conventional' PA modes outlined in Chapter 2.

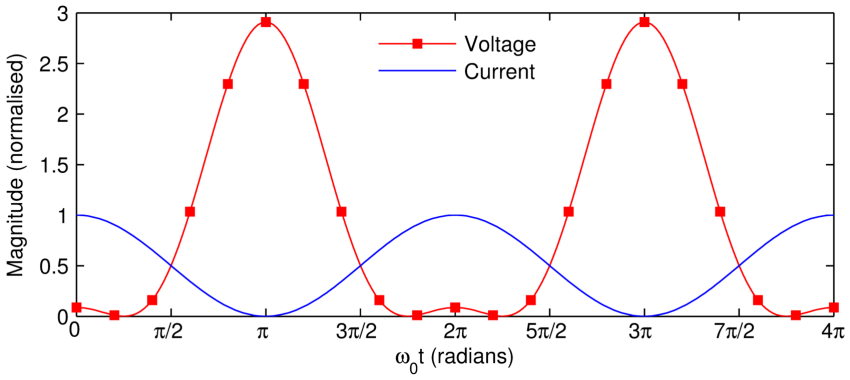

Figure 4.5: Time domain theoretical waveforms for $\gamma = 0.001$ and $\alpha = -\sqrt{2}$

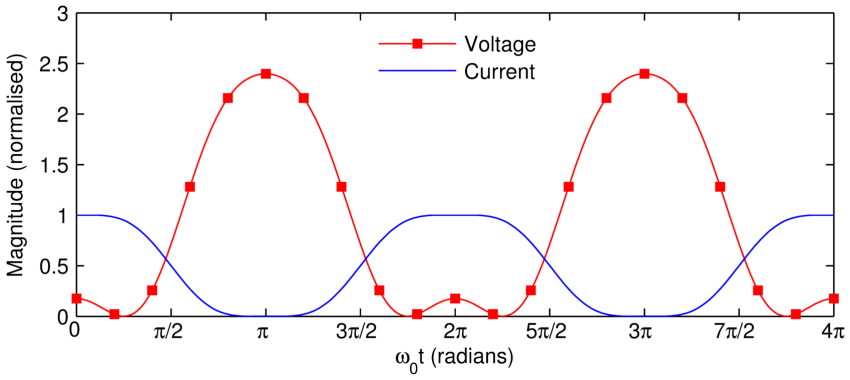

Figure 4.6: Time domain theoretical waveforms for $\gamma = 0.12$ and $\alpha = -\sqrt{2}$

Fig. 4.6 shows the case for $\gamma = 0.12$. This particular set of waveforms has an output power of 1.56 dB (normalised to Class A) and a drain efficiency of 71.65%. It can be seen from Fig. 4.6 that the current is at the 'maximally flat' state. Interestingly, this

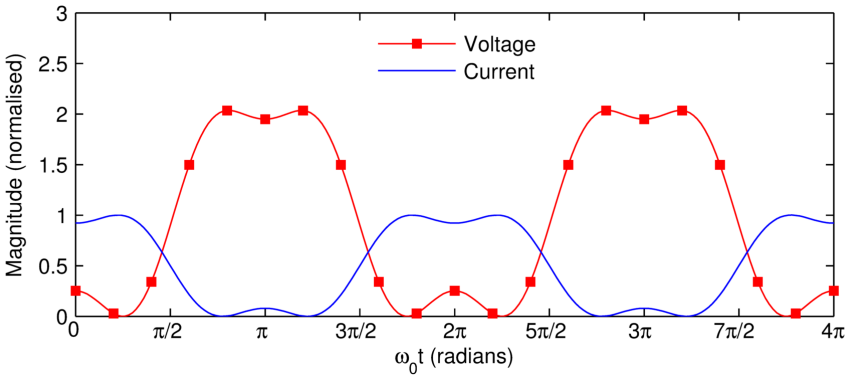

Figure 4.7: Time domain theoretical waveforms for $\gamma = 0.25$ and $\alpha = -\sqrt{2}$

is not the point at which the fundamental current component is at its maximum. As can be seen in Fig. 4.4, maximum fundamental current occurs at $\gamma = 0.17$. There are similarities with the work of Raab, where for Class F the maximum power waveforms are not maximally flat but instead "exhibit slight ripples" [8].

The waveforms of Fig. 4.7 are a unique set of waveforms that look significantly different to any presented in the current literature. These waveforms may be more suitable when voltage breakdown is a problem, as their peak voltage is no higher than that of the Class A mode. It will also be seen in Section 4.4 that the power back-off characteristics differ with different bias conditions. Where voltage breakdown is not a problem, waveforms with small values of γ are preferable.

Inverted modes are, in effect, the natural modes for push-pull PAs using transmission line baluns. The analytical expressions predict that a push-pull PA, with the transistors biased in a high quiescent current state, can be implemented over multi-octave bandwidths with drain efficiencies above 70%.

All of the theoretical waveforms assume that the full range of voltage and current swing is being utilised. To evaluate other parameters such as power back-off (PBO), and gain compression, nonlinear circuit simulations are used.

4.4 Simulations

4.4.1 Purpose of Simulations

The purpose of carrying out circuit simulations was twofold. Firstly, circuit simulations can serve as initial verification of the theoretical modes of operation presented in the previous section. Secondly, it is quicker and easier to investigate other performance characteristics of the modes of operation, such as back-off power and gain compression, using a circuit simulator compared to mathematical analysis.

4.4.2 Simulation Setup

Load-pull simulations were carried out using the nonlinear harmonic balance simulator in AWR Microwave Office. The simulation schematic is shown in Fig. 4.8. The HBTUNER2 component allows arbitrary impedances to be specified at the first three harmonic frequencies, and also incorporates an integrated ideal bias tee for biasing the transistor under test. An additional tuner is included in order to control the fourth harmonic impedance.

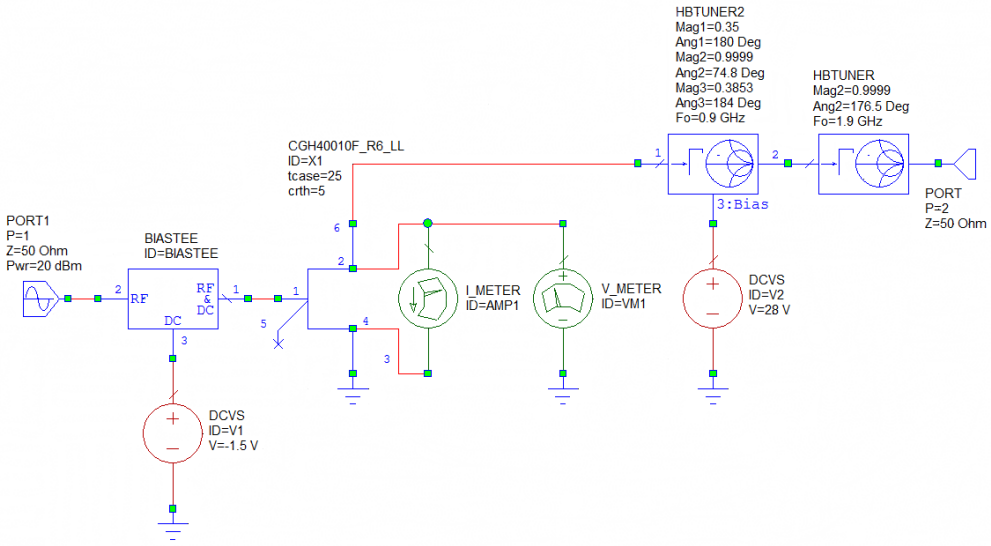

Figure 4.8: Circuit schematic for load-pull simulations in AWR Microwave Office

The large signal transistor model used in the simulations was the CGH40010F_R6_LL model provided by Cree. The simulations were carried out at a fundamental frequency of 900 MHz in order to match the fundamental frequency at which the active harmonic load-pull measurements were conducted (presented in Section 4.5).

Load-pull is carried out at the output of the transistor, whilst all the input harmonics are terminated into 50 Ω. This emulates the load-pull measurement setup at Cardiff University.

4.4.3 Transistor Reference Planes

As discussed in Chapter 2, a real transistor will not behave as an ideal voltage-controlled current source (VCCS). There will be reactive impedances within the transistor itself, such as C_{DS}, and those caused by the bond wires and transistor package.

It is necessary to define the different reference planes referred to in the following sections. A basic model of the reactive circuit elements for a packaged transistor is shown in Fig. 4.9. The most significant element is the drain-source capacitor, C_{DS}.

On the left hand side of Fig. 4.9, the transistor is first assumed to be an ideal voltage-controlled current source. This is referred to as the 'current generator' (I_{GEN}) reference plane. When the drain-source capacitor is included in the model of the transistor, along with other elements that are internal to the transistor chip, this is referred to as the 'device' plane. The ceramic package introduces components such as bond wires and metal tabs that are represented by additional circuit elements. Once all of these elements have been included, this outermost reference plane is termed the 'package' plane.

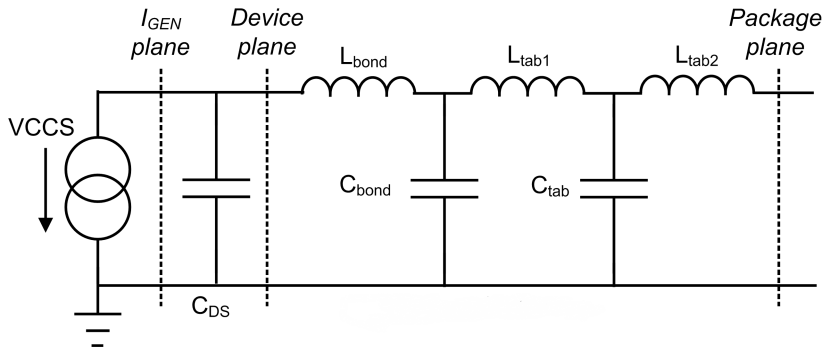

Figure 4.9: Transistor reference planes

When load-pull measurements are made, it is only possible to measure at the package plane. However, if a sufficiently accurate model of the package exists, it is possible to remove the effects of the package to effectively measure at the device plane. This is a process known as de-embedding. Similarly, if it is possible to model the intrinsic components such as C_{DS}, these can be de-embedded to provide a reasonable estimate of measurements at the current generator plane.

The same de-embedding process can be applied to circuit simulations, as most transistor vendors will provide models referenced to the package plane. However, recently released transistor models from Cree allow voltage and current meters to be placed directly at the current generator plane. These are shown connected to transistor ports 2 and 4 in Fig. 4.8. Therefore, in simulation, it is possible to view voltage and current waveforms at the current generator reference plane. It is these models that are used in the following simulations.

4.4.4 Power Sweep Simulations

The characteristics of the transistor in backed-off power conditions were investigated at two bias voltages; -1.5 V and -3.0 V. It should be noted that γ will change with input power, due to the generation of third harmonic current as the transistor compresses.

As shown in Fig. 4.10, the higher quiescent current case (V_{GS} = -1.5 V) exhibits more gain, as expected. It is also worth noting the 'soft' compression characteristics of the GaN transistor. Figure 4.11 shows that eventually the two operating conditions reach the same output power level. The higher γ value, corresponding to a V_{GS} value of -3.0 V, shows better performance in terms of efficiency when the input power is backed off. This can be observed from Fig. 4.12.

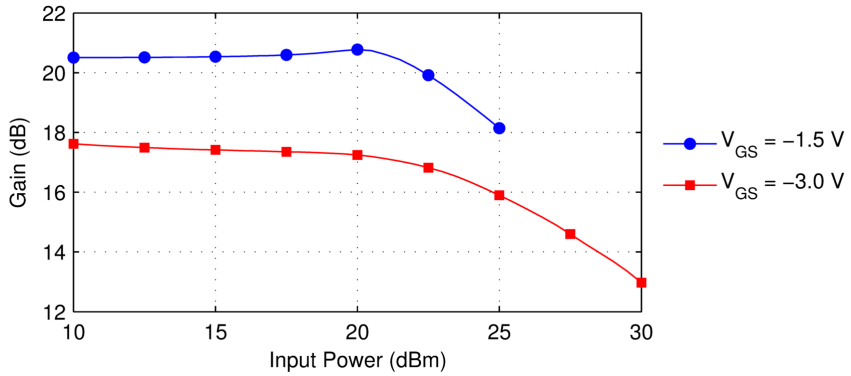

Figure 4.10: Gain versus input power for two bias points

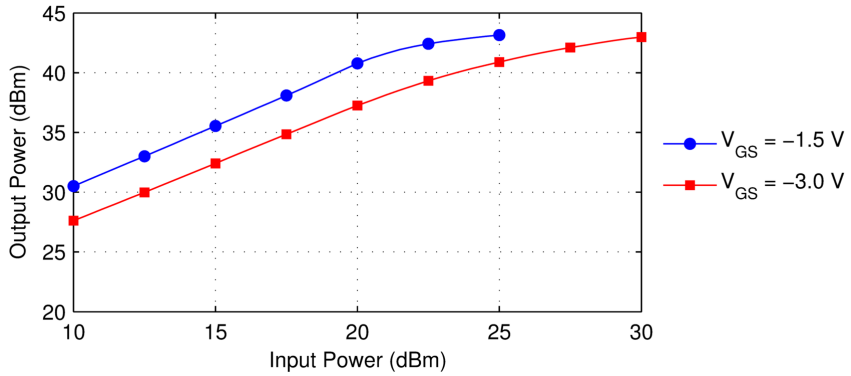

Figure 4.11: Output power versus input power for two bias points

Time-Domain Waveform Simulations

For the waveforms of Fig. 4.13 γ is close to zero, corresponding to a raised sinusoidal current waveform. It can be observed that there is a small amount of second harmonic voltage contributing to the 'peaking' of the voltage waveform and the 'flattening' of

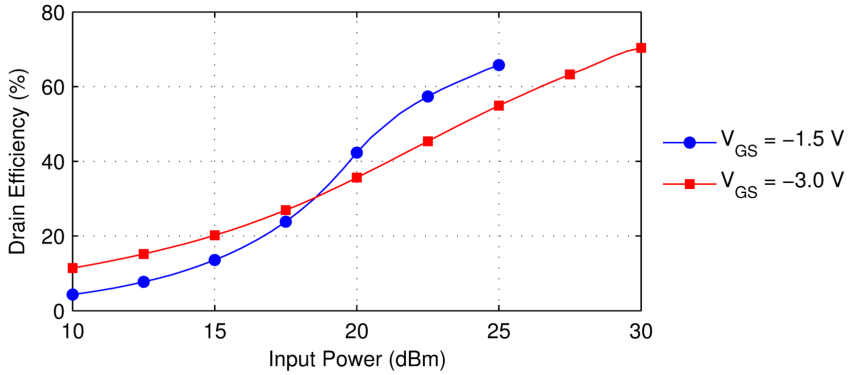

Figure 4.12: Drain efficiency versus input power for two bias points

the trough of the waveform. The associated output power, gain and efficiency was 42.1 dBm, 20.3 dB and 54.2% respectively. The efficiency is lower than the theoretical 70.7% for $\gamma = 0$, however this can be explained by the presence of the knee voltage in the transistor model.

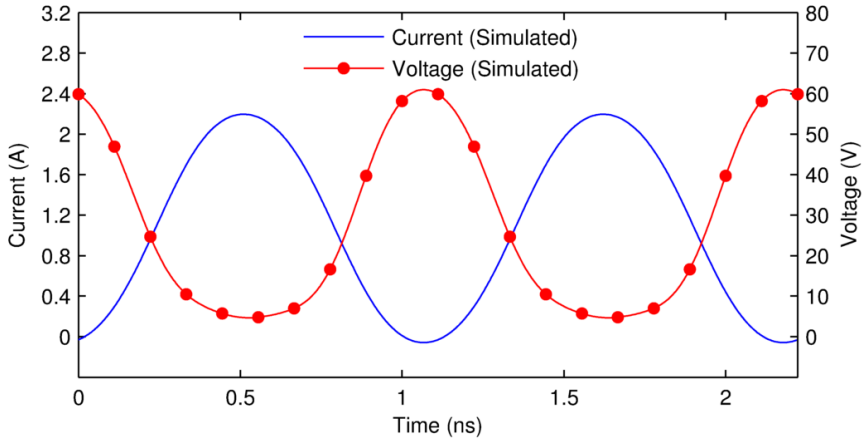

Figure 4.13: Simulated current and voltage waveforms for $\gamma = 0.0235$

As γ is increased to 0.1050, achieved in practice by reducing the gate bias voltage, the waveforms of Fig. 4.14 are produced. The output power and drain efficiency are 42.15 dBm and 57.8% respectively, which is comparable to the results of Fig. 4.13, however the gain has reduced by approximately one decibel to 19.35 dB. The current is slightly flattened by the third harmonic current in order to remain above zero. This third harmonic current is multiplied by Z_{odd} to produce a third harmonic voltage which flattens the peaks of the voltage waveform.

Figure 4.15 shows the results for a γ value of 0.1811. The voltage and current waveforms are flattened by the increased third harmonic components, and the gain is reduced to 18.10 dB. The output power is 41.90 dBm and the drain efficiency is 58.7%.

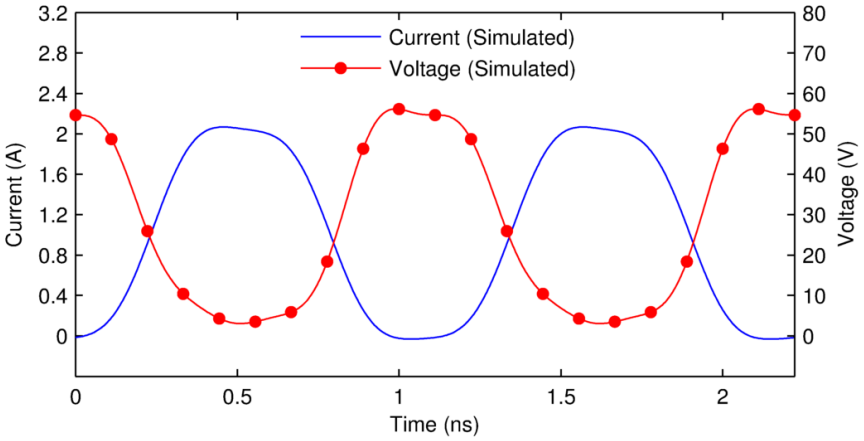

Figure 4.14: Simulated current and voltage waveforms for $\gamma = 0.1050$

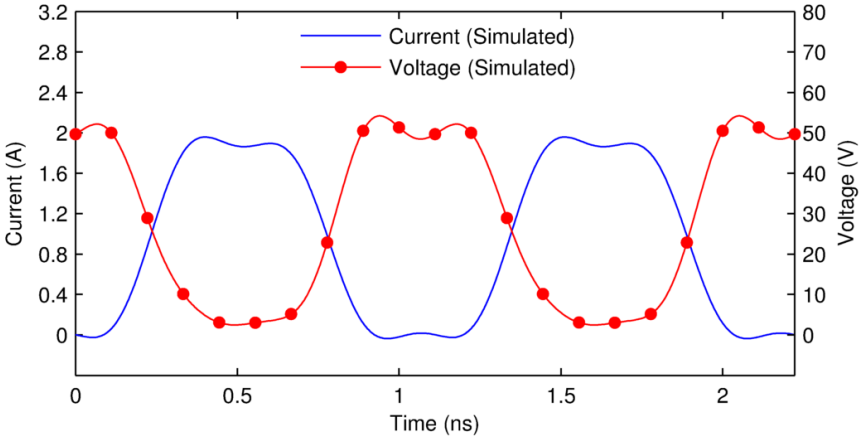

Figure 4.15: Simulated current and voltage waveforms for $\gamma = 0.1811$

For the waveforms of Figure 4.16, the output power has dropped fairly significantly to 40.32 dBm. The third harmonic current is a considerable fraction of the fundamental current, with a γ value of 0.2681. The drain efficiency is 55.9% and the gain is 16.5 dB. This reduced performance at higher values of γ again suggests that inverted modes (low γ) are better suited to the push-pull topology. Figure 4.16 shows some unexpected asymmetry, which could be a result of de-embedding.

Good performance is simulated without distorting the waveforms. There is reasonable agreement with theory, although the efficiencies are lower in simulation due to the inclusion of knee voltage in the transistor model.

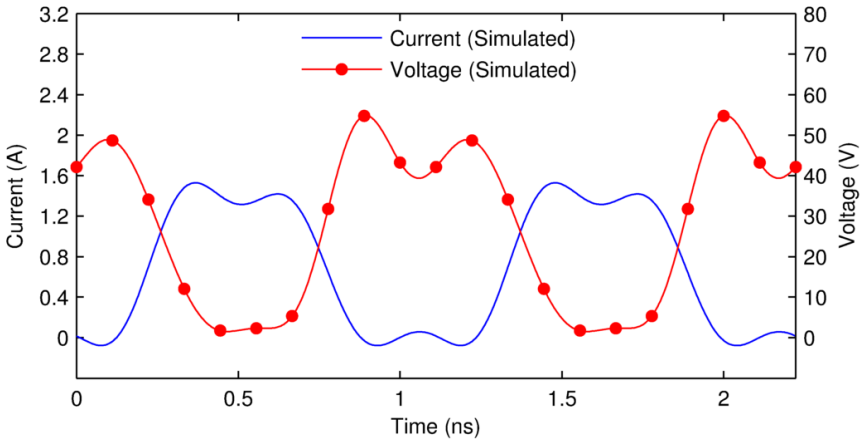

Figure 4.16: Simulated current and voltage waveforms for $\gamma = 0.2681$

4.5 Load-Pull Measurements

Section 4.4 demonstrated that the push-pull mode of operation could be realised in simulation, and so the next stage was to investigate whether these modes could be achieved using a real transistor.

4.5.1 Measurement Setup

Using the active harmonic load-pull system developed at Cardiff University, measurements were made on a Cree CGH40010F gallium nitride (GaN) power transistor at 900 MHz. The package reactances and the transistor's drain-source capacitance were de-embedded such that specific output loads could be presented to the first three harmonics at the current generator plane.

The load-pull system is not described in detail here owing to the abundance of existing literature documenting the system [66–69]. However, a simple block diagram of the open-loop active harmonic load-pull system is shown in Fig. 4.17. A digital sampling oscilloscope (DSO) samples incident and reflected travelling waves (a- and b-waves) in the time-domain, which can be transformed to voltage and current waveforms through knowledge of the system impedance, which is 50 Ω.

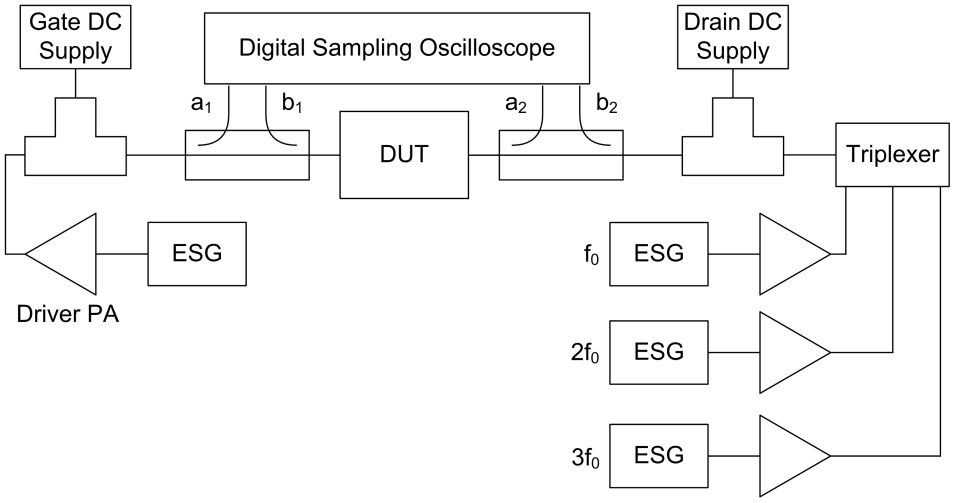

Figure 4.17: Active harmonic load pull system block diagram

Whilst the number of harmonics that can be *measured* depends on the upper frequency limit of the DSO and the accuracy of calibration at higher harmonics, the number of harmonics whose impedances can be *controlled* by the measurement system is limited to three. It is theoretically possible to control the fourth harmonic impedance and higher, however practical limitations in the load-pull software and the equipment available meant the load-pull control was limited to the fundamental, second and third harmonics. The fourth harmonic and above are measured, however they will be presented with an arbi-

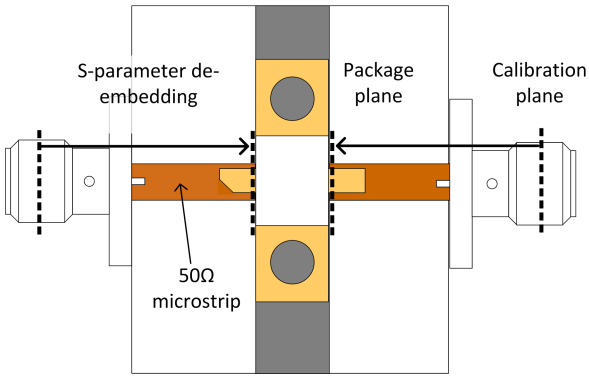

Figure 4.18: Test fixture de-embedding

trary impedance which is a product of the system impedance, the effects of the cables in the load-pull system and the package and device reactances.

4.5.2 Calibration and Test Fixture De-embedding

The load-pull system was calibrated using a thru-open-short-match (TOSM) calibration procedure [70]. The calibration kit used was an Agilent 85052D 3.5 mm kit, where resulting calibration plane is approximately in the middle of the cable and calibration standard mating interface. In order to move the reference plane to the 'package plane', where de-embedding can be carried out, it is first necessary to de-embed the transistor test fixture. This can be done by measuring the test fixture's S-parameters and mathematically removing them from the measured results, which has the effect represented in Fig. 4.18. An alternative approach would be to calibrate directly to the device plane by using a set of microstrip calibration standards. The calibration was verified by measuring a different set of 3.5 mm calibration standards and comparing measurements to the calibration standards' known characteristics.

The large-signal aspect of the calibration is done by making a large-signal measurement using a power meter as a reference, and scaling the travelling waves measured by the DSO.

4.5.3 Transistor Package De-embedding

As discussed in Section 4.4.3, recently released transistor models from Cree allow voltage and current meters to be placed directly at the current generator plane in simulation. Therefore, it is possible to view simulated voltage and current waveforms at the current generator reference plane.

However this is not possible for load-pull measurements, and so S-parameter de-embedding is necessary using estimated values for the intrinsic and extrinsic elements. For these measurements the package model of Fig. 4.9 was used, with associated values

Package Model Element	Value
C_{DS}	1.22 pF
L_{bond}	0.55 nH
C_{bond}	0.25 pF
L_{tab1}	0.1 nH
C_{tab}	0.25 pF
L_{tab2}	0.1 nH

Table 4.1: Package model element values for Cree CGH40010F

provided in Table 4.1. Cree do not provide details of their intrinsic and extrinsic de-embedding models, so the values were obtained from previous work at Cardiff University using the same transistor [71]. For a more accurate model of package and device circuit elements, it should be possible to compare simulated waveforms at the current generator and package planes and 'reverse engineer' a more accurate model for these elements than the one that was used. This improved model could then be used for de-embedding measured data. However, as the transistor models with current-generator plane ports were only made available in May 2013, this was not possible to do when the load-pull measurements were conducted.

4.5.4 Measured Waveforms

Two sets of measurements are presented in this section. The odd-mode impedance in both cases was 50 Ω, the even mode impedance was a high impedance approximating an open circuit and the drain voltage was 28 V.

In Figs. 4.19 and 4.20 the same measured data is plotted with the number of harmonic frequencies included set to three and five, respectively. Having calculated the value of γ for the measured waveform, the theoretical waveform is generated and scaled up to a drain supply voltage of 28 V, in order to be compared to the measured data. A gate-source voltage of -2.0 V gave a corresponding γ value of 0.076.

The measured fundamental output power of Fig. 4.19 was 40.8 dBm, drain efficiency was 73.7% and transducer gain was 18.2 dB. This is very impressive performance that demonstrates the viability of of the push-pull mode of operation. In Fig. 4.19, when three harmonics are included, the agreement between theoretical and measured waveforms is good. When viewing only three harmonics, it appears as though the voltage dips into the knee region, however it can be seen in Fig. 4.20 that the higher harmonics are flattening the voltage trough to reduce this. It can be seen that the current is not

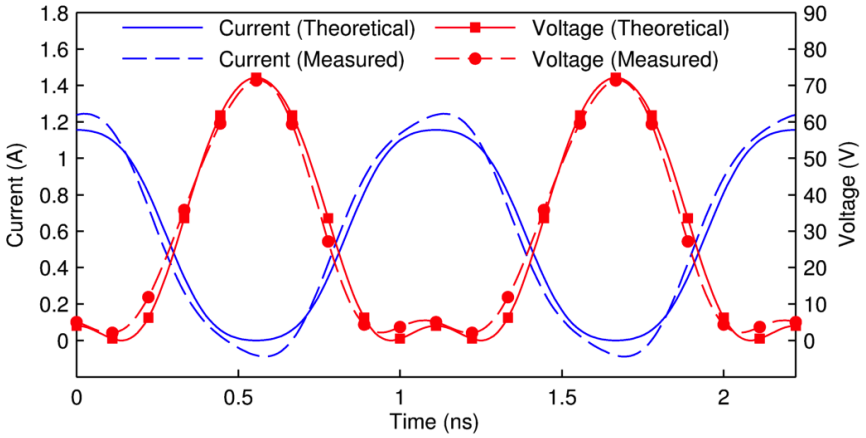

Figure 4.19: Measured and theoretical waveforms for $\gamma = 0.076$ (3 harmonics)

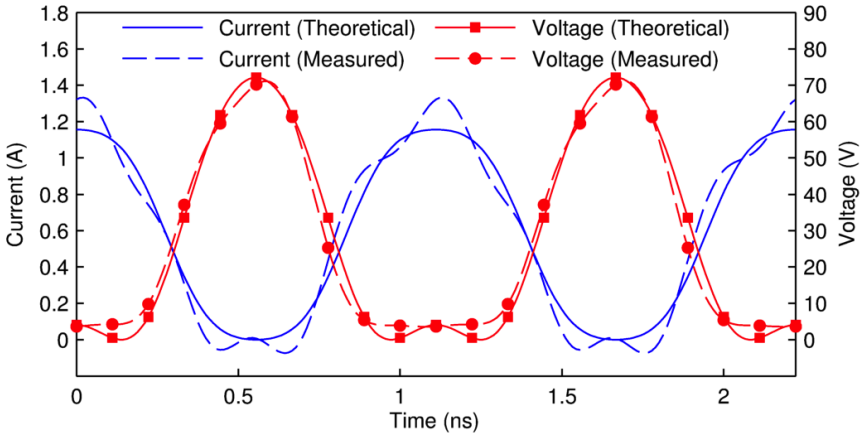

Figure 4.20: Measured and theoretical waveforms for $\gamma = 0.076$ (5 harmonics)

sinusoidal, especially when all five harmonics are included. The peaking of the current in Fig. 4.20 cannot be controlled due to the limitations of the measurement setup. The current appears to be crossing zero when three harmonics are included, but this does seem to reduce when the higher harmonics are included. Large signal calibration error could provide further explanation for the zero-crossing current waveform.

A second set of waveforms is presented in Figs. 4.21 and 4.22 at a γ value of 0.219. The measured output power was 39.4 dBm, drain efficiency was 68.1% and transducer gain was 15.8 dB. The gate-source voltage was -3.1 V.

As would be expected, the gain at the higher value of γ is reduced, as is the drain efficiency. As with the $\gamma = 0.076$ case, the fourth harmonic is flattening the current to reduce the amount by which the current dips below zero. The higher harmonics are also preventing the voltage waveform from entering the knee region. When three harmonics are considered, the agreement between theoretical and measured waveforms is good. Although not achieving the performance figures of the other measured waveforms, the

waveforms of Figs. 4.21 and 4.22 should have improved drain efficiency under backed-off conditions.

It can be observed that the measured waveforms and drain efficiencies closely match those predicted by theory for two different bias voltages. It is believed that the measured drain efficiency is slightly higher than that predicted by theory due to the beneficial effect of the current at the fourth harmonic, which flattens the current waveform and allows the fundamental current component to be increased.

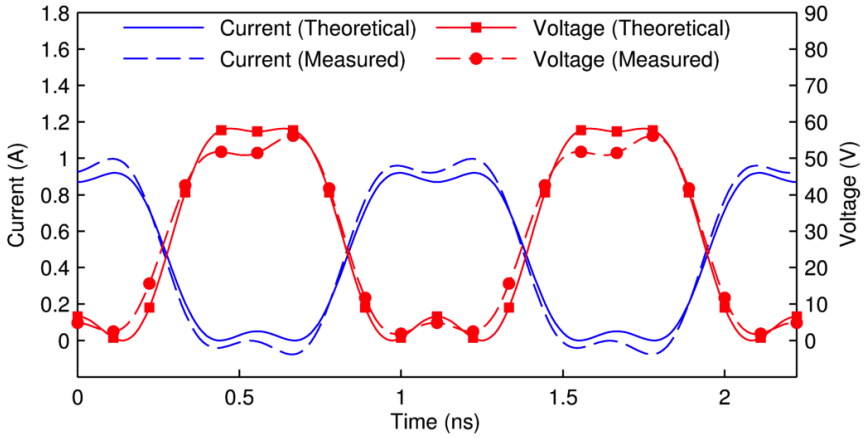

Figure 4.21: Measured and theoretical waveforms for $\gamma = 0.219$ (3 harmonics)

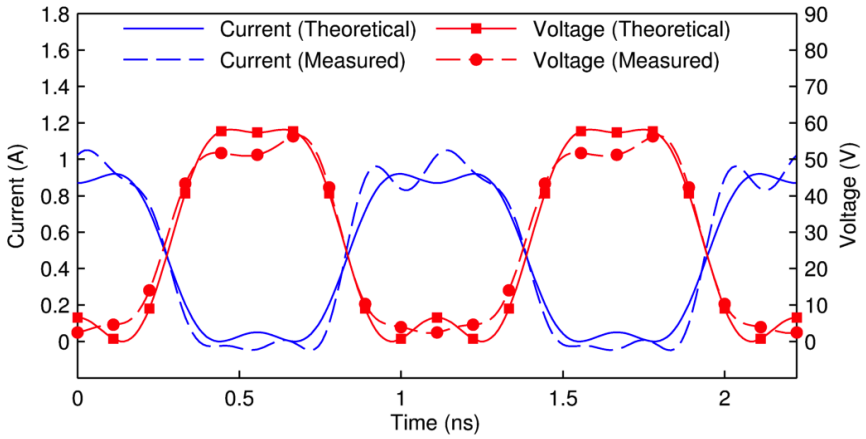

Figure 4.22: Measured and theoretical waveforms for $\gamma = 0.219$ (5 harmonics)

4.6 Chapter Summary

In this chapter, new modes of operation inside a push-pull power amplifier with transmission line baluns have been identified and investigated. The resulting waveforms have been found to differ significantly from the Class B waveforms that are usually associated with the push-pull mode of operation. This difference results from the open-circuited even-mode impedance presented by a microwave transmission line balun.

The new modes of operation demonstrate high efficiency performance and significantly higher output power than the Class A mode. In addition, due to the microwave transmission line balun, these modes can be realised over significantly broader bandwidths than conventional PA modes.

Using the 'factorised waveform' approach, the time-domain RF waveforms have been predicted by theory and show good agreement with simulation and measurement. It has been demonstrated that for push-pull amplifiers at microwave frequencies, the waveforms share many of the characteristics of the 'inverted' modes of operation, an important observation that has significant consequences for the PA designer.

This chapter has demonstrated the potential for multi-octave, high power, high efficiency microwave push-pull amplifiers that use transmission line baluns. Such amplifiers will be introduced in the next chapter.

Chapter 5

Push-Pull Power Amplifier Prototypes

5.1 Introduction

In this chapter the design, manufacture and measurement of two prototype push-pull power amplifiers is presented. These amplifiers were developed in order to demonstrate that the push-pull topology is a promising solution to the challenge of designing high-power, high-efficiency multi-octave power amplifiers.

The design and simulation of the amplifiers is described, with measured results demonstrating the performance that is currently achievable. In addition, the bespoke measurement systems used for characterising these amplifiers are discussed.

The first prototype amplifier was presented at the International Microwave Symposium in June 2012 [72], whilst the second prototype was presented at the ARMMS conference in April 2013 [73].

The first prototype amplifier achieved a minimum output power of 20 W between 250 MHz and 3.1 GHz, with an output power of 40 W and a minimum of 45% drain efficiency between 700 MHz and 2 GHz. The development of these amplifiers shows that the push-pull topology is a feasible solution to the challenges of broadband power amplifier design, and that extremely competitive performance figures can be obtained.

5.2 Push-Pull Power Amplifier Version 1

5.2.1 Design Goals

The objective was to build an amplifier with a bandwidth significantly larger than one octave, with a significant portion of the frequency range being above 1 GHz. As outlined in Chapter 2, there are many examples of broadband push-pull power amplifiers in the literature, however very few of these operate above 1 GHz.

For the first version of the prototype amplifier (abbreviated to v1 for brevity), a target output power of at least 20 W was specified. Again, this was to differentiate this work from other broadband techniques that, whilst achieving impressive operating bandwidths, are limited to relatively modest output power levels. It is worth mentioning this as the task of efficient power combining over large bandwidths is non-trivial. The initial frequency range to design across was 750 MHz to 3 GHz, a bandwidth of two octaves. The aim was to measure the efficiency that could be achieved whilst meeting the bandwidth and power requirements, with the results of Chapter 4 suggesting that good efficiency should be achievable in a practical amplifier.

5.2.2 Choice of Transistor

As discussed in Chapter 2, gallium nitride transistors have many desirable properties for high-power, broad-bandwidth power amplifiers. The two major perceived drawbacks of GaN, cost and reliability, are not significant concerns when designing a prototype amplifier for research, rather than commercial or military, purposes.

Of the commercial GaN vendors, Cree was chosen as the preferred supplier. The Centre for High Frequency Engineering at Cardiff University has both an existing relationship with Cree and a familiarity with its GaN devices through research involving load-pull measurements and prototype power amplifiers [13, 15, 74].

Two Cree transistors were considered; model number CGH40010F, referred to as the '10 W transistor' for simplicity and model number CGH40025F, referred to as the '25 W transistor'. These are both packaged transistors, meaning that the GaN transistors have been die attached and wire bonded to a package, which makes them easier to handle and interface with a printed circuit board. Because of this, packaged devices are more convenient than 'bare die' transistors, however the package introduces additional reactances that can limit the transistor's performance. The performance disadvantage was judged to be acceptable when compared to the extra expense, manufacturing time and inconvenience that a 'chip-and-wire' approach would result in.

The choice of whether to use the 10 W transistor or 25 W transistor largely rested on the optimum output impedance for both of the devices. The closer to 25 Ω the optimum impedance was, the fewer matching elements would be required and hence the better the performance would be over multi-octave bandwidths.

Loadline Matching

There are a number of different methods that can be used for determining a transistor's optimum output impedance. For maximum output power, loadline matching is the simplest method. Loadline matching involves calculating the impedance that will result in the voltage and current waveforms swinging across their full ranges without clipping

Property	Value
V_{dc}	28 V
V_k	5 V
I_{dc}	1 A

Table 5.1: Basic properties of Cree CGH40010F

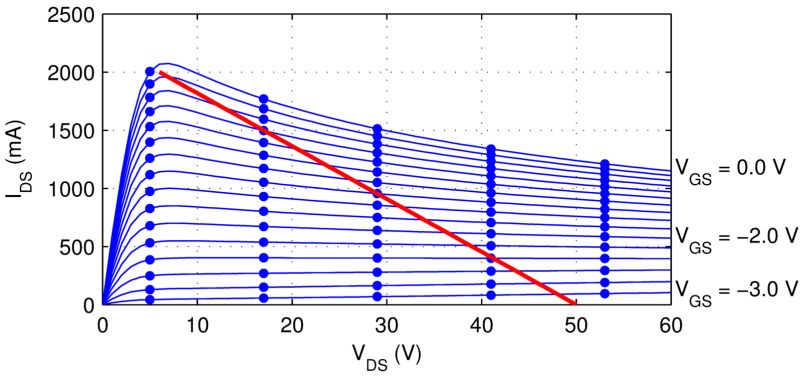

Figure 5.1: Simulated output DC I-V characteristic of Cree 10 W transistor with loadline

or entering the 'knee' region. The great advantage of loadline matching is that a value of R_{opt} can be obtained whilst knowing relatively little information about the transistor.

Using (5.1) from [4] and the transistor properties in Table 5.1, R_{opt} is calculated as 22 Ω for the 10 W transistor, and the resulting loadline is shown in Fig. 5.1.

For the 25 W transistor, the DC drain supply voltage and the knee voltage remain the same, but the DC current changes to 1.8 A, which results in an R_{opt} value of 12.2 Ω, as shown in Fig. 5.2. According to the loadline method, the 10 W transistor provides the closest optimum impedance to 25 Ω.

$$R_{opt} = \frac{V_{dc} - V_k}{I_{dc}} \tag{5.1}$$

It should be noted that the DC I-V curves have a negative gradient due to the simulated thermal effects at higher power levels. These are not necessarily the same characteristics that will be observed at microwave frequencies, as the transistor will only be at peak power, and hence experience a rise in temperature, for a small percentage of the overall time. Pulsed DC I-V measurements would result in a more accurate model of the transistor's output characteristics.

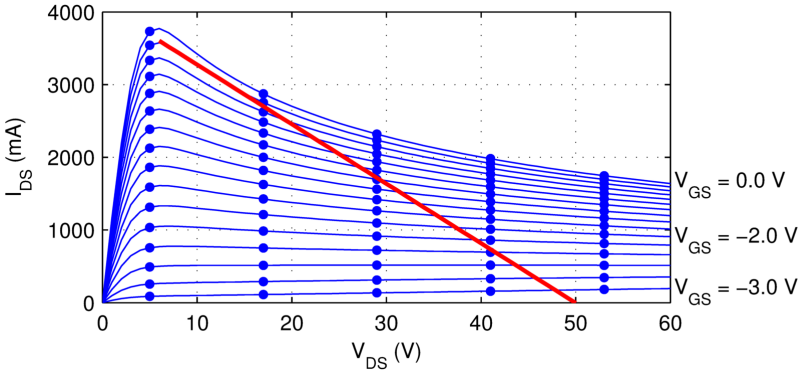

Figure 5.2: Simulated output DC I-V characteristic of Cree 25 W transistor with loadline

Load-Pull Measurements

Whilst loadline matching is a quick, convenient and useful method of determining a transistor's optimum output impedance, a more accurate method is to measure R_{opt} for an actual transistor, using the same load-pull measurement system that was introduced in Chapter 4.

It is difficult to categorically define a single value for optimum impedance, as it is dependent on input power, bias, frequency, harmonic impedances and many other factors. It is also worth noting the difficulty in calibrating the system for high power measurements due to the sensitivity of the receiver and the maximum power that the calibration standards can withstand. Measuring a transistor under all possible operating conditions is a time-consuming exercise, and so an approximate value was chosen from one set of load-pull measurements.

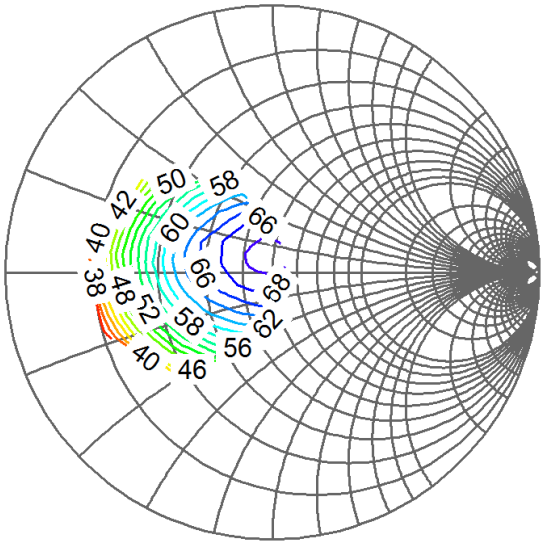

Figure 5.3: Measured drain efficiency contours for the 25 W transistor at 2 GHz

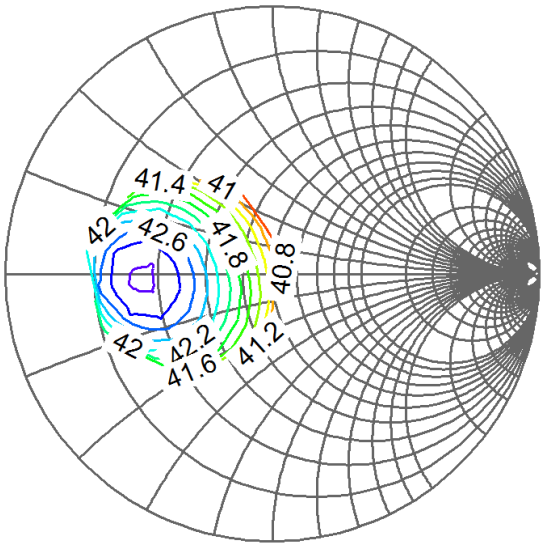

Figure 5.4: Measured output power contours for the 25 W transistor at 2 GHz

Load-pull measurements were conducted on a CGH40025F transistor at 2 GHz. The fundamental impedance was swept whilst the second harmonic impedance was held at an open circuit and the third harmonic impedance was 25 Ω. As Figs. 5.3 and 5.4 show, the optimum impedance is not the same for maximum output power and maximum efficiency. In Fig. 5.3, the highest measured drain efficiency was 71.7% at $Z_{f_0} = 55.8 + j7.8\ \Omega$. The maximum output power measured was 43.01 dBm at $Z_{f_0} = 19.0 + j1.7\ \Omega$. A value between 19 Ω and 56 Ω represents a compromise between optimum output power and efficiency. The load-pull sweeps of Figs. 5.3 and 5.4 reveal that a fundamental impedance of 25 Ω results in an output power of 46.7 dBm and drain efficiency of 63.7%. These load-pull measurements show that 25 Ω is a good compromise between output power and efficiency, and hence that the 25 W transistor should be chosen over the 10 W transistor for this design.

Another reason to use the 25 W transistor is to increase the overall output power of the amplifier, which enables a more favourable comparison with conventional single-ended amplifiers. To achieve a similar output power of between 40 W and 50 W from a single-ended, single-transistor amplifier would significantly increase the matching ratio and hence reduce its bandwidth. This serves to highlight the inherent advantages of the push-pull topology that were outlined in Chapter 4.

5.2.3 Differential Input Ports

It was decided to drive the prototype amplifier using differential inputs instead of one single-ended input. This provided the opportunity to investigate the operation of the push-pull power amplifier in greater depth. For example, as will be shown in Section

5.2.10, it is possible to vary the amplitude and phase balance between the two halves of the differential input in order to measure the effect on output power, efficiency and gain.

5.2.4 Output Balun Design

The output balun design was largely the same as the prototype balun described in Chapter 3. It was decided to use these baluns due to the familiarity with their design, manufacture and assembly. Compared to the balun of Chapter 3, a thicker coaxial cable was used, increasing the outer diameter from 1.19 mm to 2.20 mm. This was mainly due to the increased power handling capability of the thicker cable, which was 69.8 W at 5 GHz compared to 20.7 W [75]. The thicker coaxial cable also reduced the loss from 2.59 dB/m to 1.51 dB/m. The datasheet for the coaxial cable is included in Appendix I.

It was decided to set the balun length to 40 mm, resulting in a half-wavelength resonant frequency of 3.75 GHz. This set the resonant frequency outside the intended operating range of the amplifier, to avoid the need for ferrite beads, which as Chapter 3 shows increase the insertion loss of the baluns.

An alternative approach would have been to set the balun length at a value closer to 80 mm, placing the resonant frequency around 1.875 GHz, deliberately in the middle of the amplifier's passband. Ferrite beads could then have been used to suppress the half-wavelength resonance, thus demonstrating that the design methodology of Chapter 3 could be applied in to a power amplifier design. However, it was decided against this approach, as it was thought that better overall amplifier performance would be achieved by keeping the resonance out-of-band and hence removing the need for ferrite beads.

In addition, as it is relatively straightforward to disassemble the balun and add ferrite beads at a later date, it was decide to make initial measurements without the beads, and to add them later if necessary.

5.2.5 Simulations

Nonlinear harmonic balance simulations were conducted during the power amplifier design. A large-signal model from Cree was used to model the transistors, and measured S-parameter data of the output balun was imported into the simulator.

Input return loss ($|S_{11}|$) is a commonly specified parameter in PA design, and is usually important when considering the PA as part of a transmitter chain, however it was not considered during this design. This was because it would be unlikely that this PA would be used in a transmitter chain in its present form, and instead there would either be a differential driver stage or a balun at its input.

Capacitors to ground were included close to the gate tabs to increase the gain at

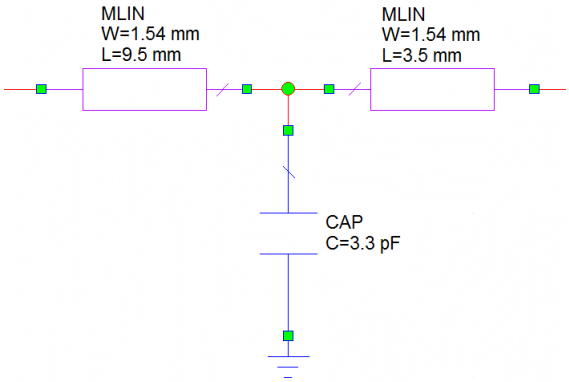

Figure 5.5: Transmission lines and capacitor to ground at input of PA v1

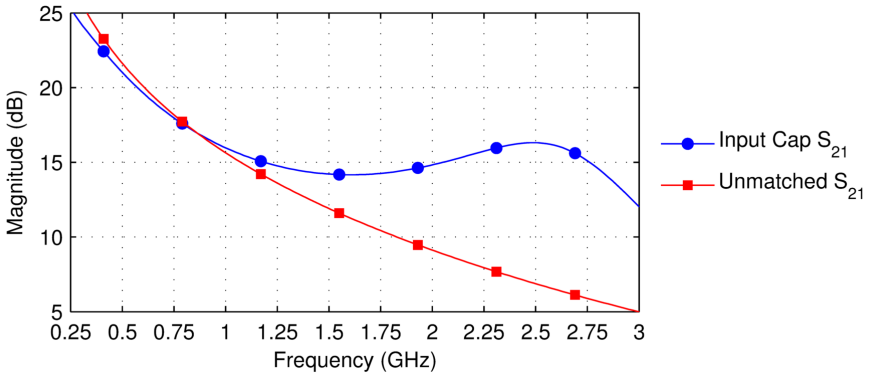

Figure 5.6: Simulated small-signal gain of PA v1

the high-end of the frequency range, and to flatten the gain across the bandwidth. The distance between the capacitors and the gate tabs were tuned, and the network is shown in Fig. 5.5. The input transmission lines had a characteristic impedance of 50 Ω. As shown in Fig. 5.6, the capacitors at the input greatly improve the gain at higher frequencies compared to the unmatched transistor. It would be extremely difficult to achieve flat gain across such a wide bandwidth without feedback or a 'lossy' match at lower frequencies, both of which would lower the overall gain. It was decided that the preferred approach would be to try and maximise gain at all frequencies and compensate for the gain variation by adjusting the input power to achieve a constant output power.

In simulation, no lumped-element matching components at the output could improve performance in one part of the band without significantly worsening performance in another. The microstrip line lengths were tuned to optimise amplifier performance, with the characteristic impedance of the output transmission lines set to 25 Ω. The simulated large-signal performance is shown in Fig. 5.7, and suggests that 60% efficiency should be achievable across a bandwidth greater than a decade. For the simulations of Fig. 5.7, the input power was varied to compensate for the gain variation of the amplifier, and

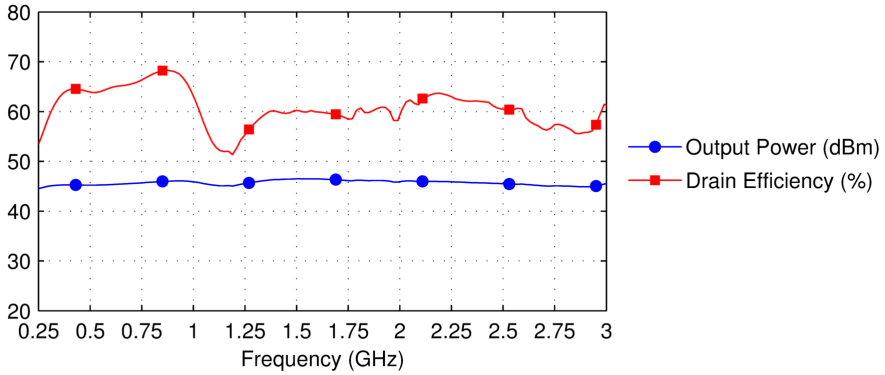

Figure 5.7: Simulated large-signal performance of PA v1

the phase offset between the two inputs was 180°.

The final layout of the power amplifier is shown in Fig. 5.8. The simplicity of the design is one of the advantages of using the push-pull topology in conjunction with GaN transistors, as a 25 Ω impedance environment combined with a 25 Ω optimum output impedance should eliminate the need for conventional matching. It is worth noting the output voltage probe, which will be discussed further in Section 5.2.11.

5.2.6 Manufacture

The manufacture of the prototype amplifier used the same equipment as the manufacture of the transmission line baluns of Chapter 3. A high-precision PCB (printed circuit board) milling machine was used to mill away the copper in order to define the microstrip lines. The milling machine was then used to create the balun channel in the aluminium that the coaxial cable sits above, as well as the small rectangular 'pockets' in which the transistors sit. The depth of the transistor gaps was set to allow the transistor package tabs to align with the top of the microstrip line. The assembled amplifier is shown in Fig. 5.9.

5.2.7 Stability and S-Parameter Measurements

Initially it was found that the PA was unstable at certain bias points. A 50 Ω resistor was added to each of the gate bias feeds to prevent instability. Once these resistors had been added, no further stability problems were observed.

S-parameters were measured using a four-port VNA in the same manner as the transmission line baluns. This involves measuring the individual S-parameters at each port, with only one port being excited at a time, and then mathematically transforming the S-parameters into 'mixed-mode S-parameters' [76]. This is valid at low power levels where the amplifier is assumed to be linear, however would not be a valid technique at

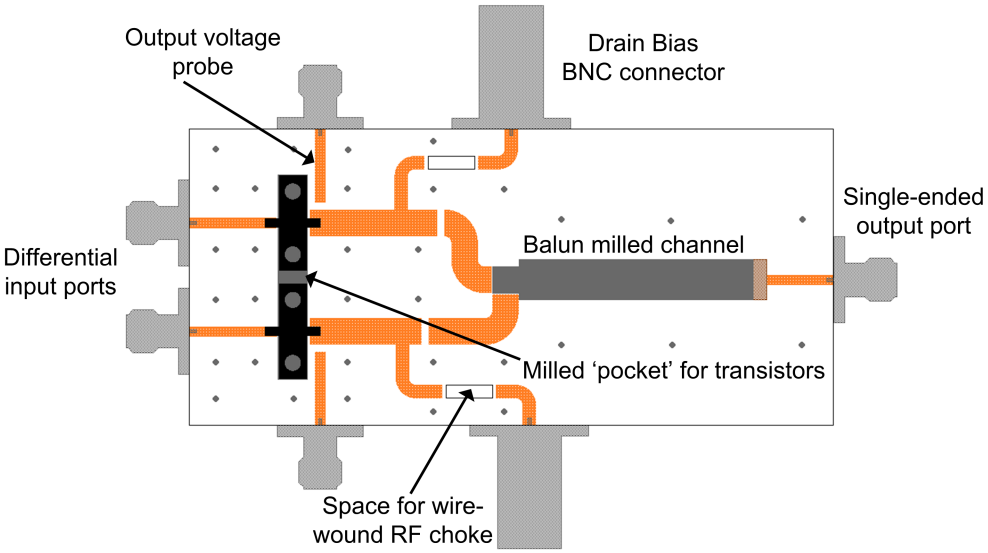

Figure 5.8: Layout of push-pull PA v1

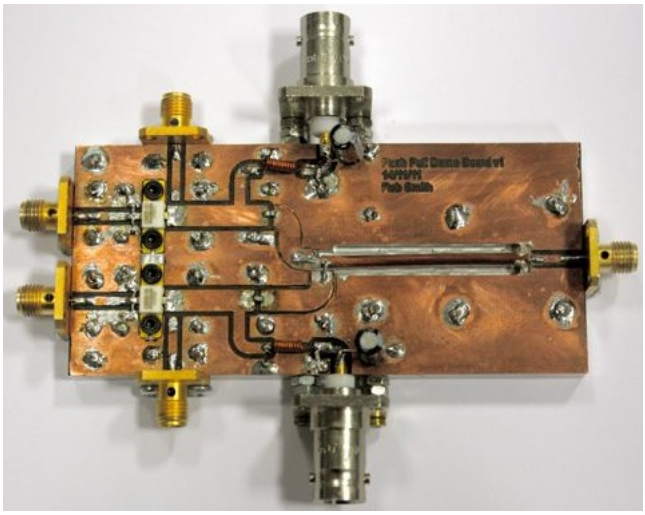

Figure 5.9: Photograph of assembled push-pull PA v1

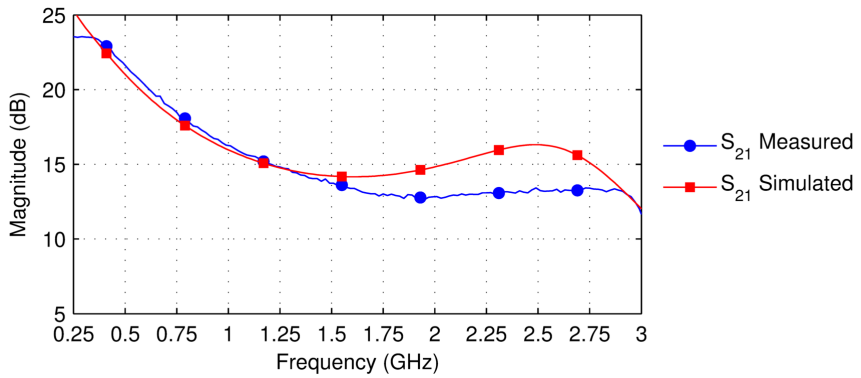

Figure 5.10: Measured mixed-mode S_{21} of PA v1

higher power levels. As will be seen in Section 5.2.8, a bespoke measurement system was developed for measuring the PA under large-signal conditions.

At this stage, the values and positions of the parallel input matching capacitors were tuned to give optimum performance, and the mixed-mode S_{21} measurements are shown in Fig. 5.10. There was a minimum of 12 dB gain across the measured bandwidth. At higher frequencies the gain was lower than was predicted in simulation, however it did show a similar roll-off with frequency.

5.2.8 Large Signal Measurement Setup

The differential inputs of the PA create practical difficulties when measuring its large-signal performance. It is necessary to ensure that a 180° phase difference and equal amplitude balance is maintained across the wide frequency range over which the amplifier is to be tested. 180° hybrid couplers and baluns are limited in bandwidth, and are unlikely to provide ideal amplitude and phase balance. In addition, it is difficult to vary the amplitude and phase balance in order to measure their effect on performance.

To overcome these difficulties, it was decided to use two electronic signal generators (ESGs) that were phase-locked together. Electronic signal generators have a 10 MHz reference signal input and output port, which allows them to be phase locked with other instruments through the use of a built-in phase-locked loop (PLL). In this way, an arbitrary phase difference can be specified. The problem with this approach is that the phase difference between the two phase-locked ESGs is initially unknown, and is frequency dependent. In addition, there is a phase shift associated with each path between the ESG and the PA input. If the phase shifts in the two paths are different, which is likely due to different cable lengths, differences in driver PA characteristics and any variation in directional couplers, there will be an unknown phase difference between the two input ports of the PA.

This problem can be overcome by the measurement setup shown in Fig. 5.11. By

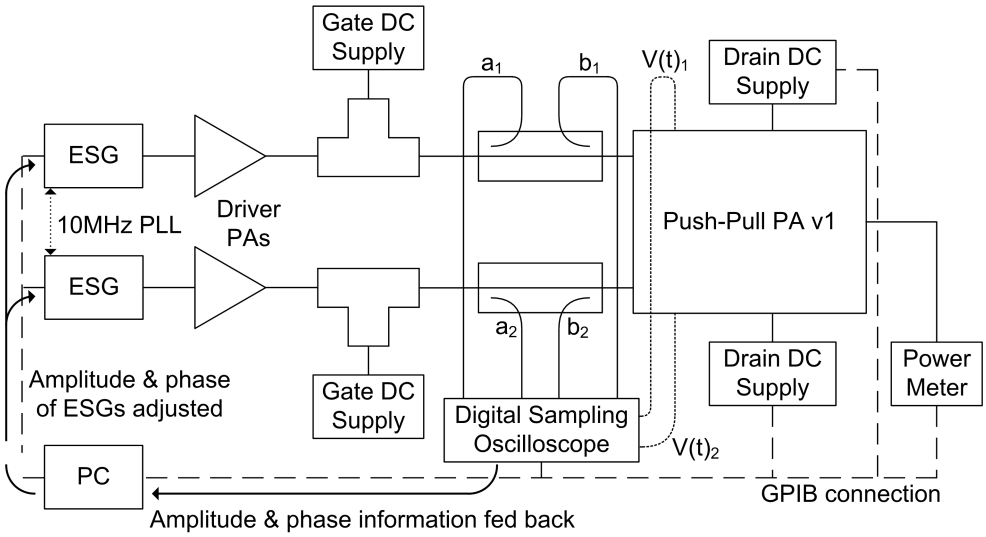

Figure 5.11: Block diagram of setup for measuring PA with differential inputs

using a digital sampling oscilloscope (DSO) to measure the amplitude and phase at each input, a software-controlled feedback loop ensures that the desired phase relationship between the inputs is achieved. Bespoke software was written in C# to control the ESGs, as well as collect measured data from the DC power supplies and RF power meter. An example screenshot from the program's graphical user interface (GUI) is shown in Fig. 5.12. Because the software can be programmed to sweep certain parameters and store the measured data, this frees the user from having to manually measure each point of interest.

The disadvantage of this measurement setup is that the digital sampling oscilloscope takes a relatively long time to capture a measurement, and as it can take a number of iterations to converge on the desired amplitude and phase balance, this further slows the measurement procedure. As can be seen from Fig. 5.11, this setup also requires a significant amount of hardware to implement.

The input ports were calibrated using the same procedure that was used for the load-pull measurements in Section 4.5, and indeed the existing software was used. A TOSM calibration was used at small signal, and a power meter was used to calibrate the absolute power level. The only difference is that this measurement system has two input ports, rather than one input and one output port. As with the load-pull measurements of Section 4.5, a different set of calibration standards was measured in order to verify the calibration.

5.2.9 Large Signal Measurement Results

The large-signal measurements were made using the system shown in Fig. 5.11. The phase between the differential input ports was varied to optimise performance. The

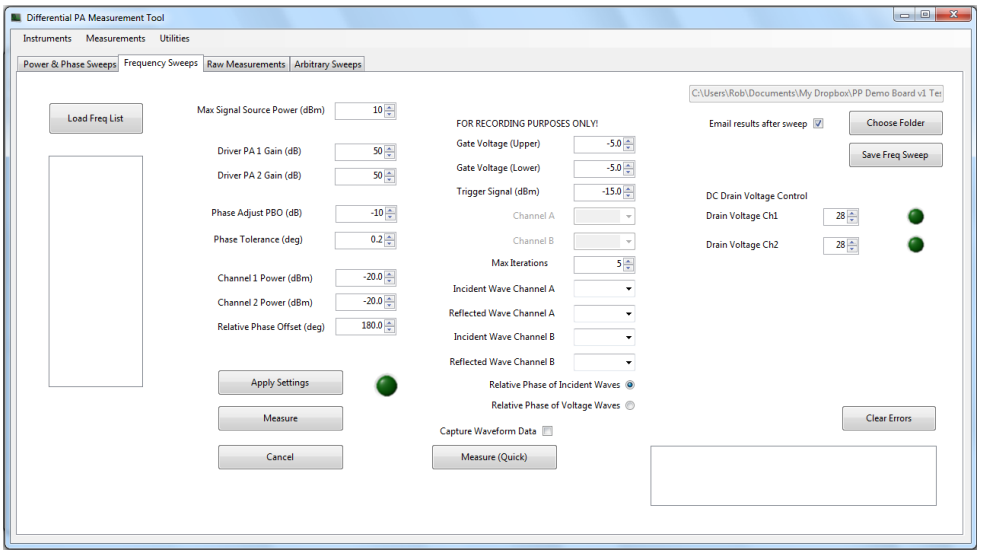

Figure 5.12: Screenshot of measurement system software

input power was set to compensate for the gain variation of the amplifier and achieve 40 W of output power where possible.

It can be seen in Fig. 5.13 there is good output power and efficiency across a very wide bandwidth. The output power is 46 dBm (40 W) between 700 MHz and 2 GHz, with drain efficiencies greater than 45%. The output power decreases above 2 GHz, probably due to the increased effects of the drain-source capacitance and package reactances at higher frequencies, but remains above 20 W between 250 MHz and 3.1 GHz, a bandwidth greater than a decade.

At lower frequencies, the PA is performing particularly well, with a minimum of 60% drain efficiency and 11 dB of transducer gain measured between 350 MHz and 1 GHz. This level of performance would be impressive even if considered in isolation, without taking into account the extended bandwidth of the amplifier.

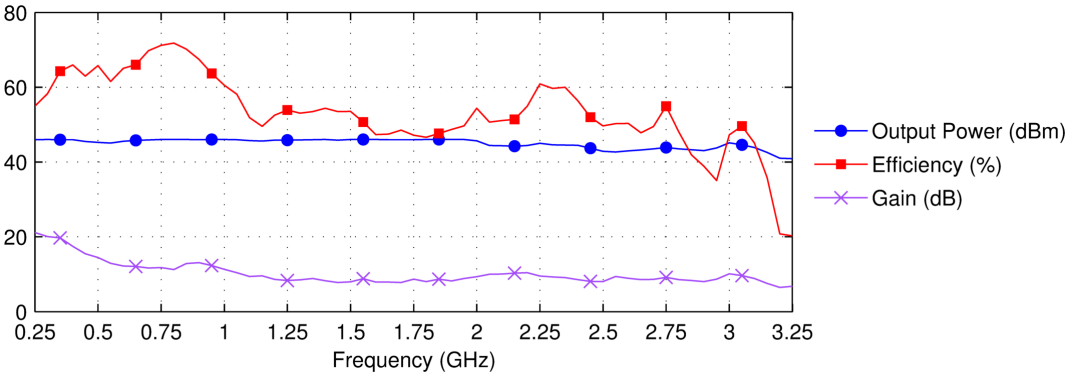

Figure 5.13: Large signal measurement results for push-pull PA v1

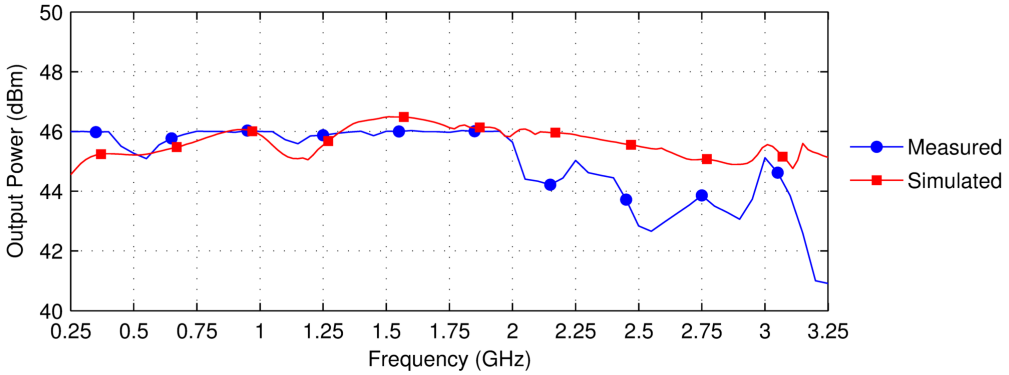

Figure 5.14: Measured and simulated output power for push-pull PA v1

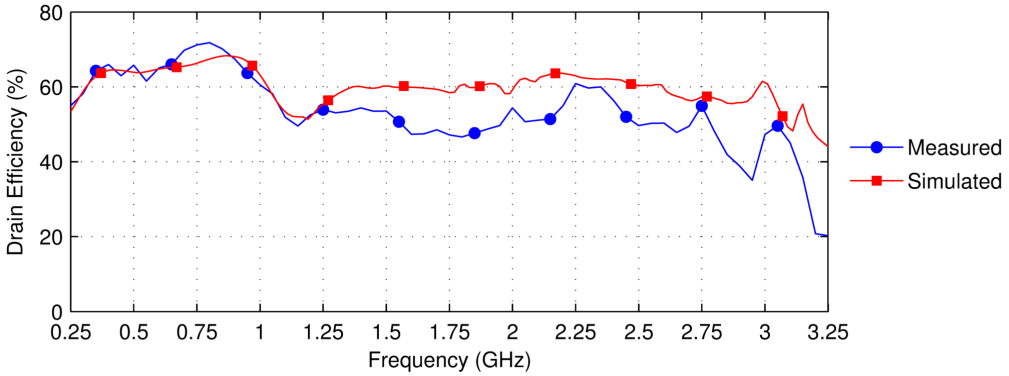

Figure 5.15: Measured and simulated drain efficiency for push-pull PA v1

It can be seen in Fig. 5.14 that there is reasonably good agreement between simulated and measured output power. The output power of the measured amplifier rolls off with frequency, however below 2 GHz the performance matches that which was predicted by simulation. It should be noted that the simulation and measurement conditions are not identical, as the input power at each measured point was adjusted to produce 40 W of output power, and this adjustment was not possible in simulation. The input phase of the measured PA was also adjusted to optimise performance, whereas the input phase of the simulated PA was 180° across the bandwidth. In Fig. 5.15, the agreement between simulated and measured drain efficiency is good at lower frequencies, with better efficiency being predicted by simulation at higher frequencies.

These performance figures are very encouraging and show that the push-pull configuration is worth pursuing as an amplifier topology for achieving high-power, high efficiency performance across bandwidths well in excess of an octave. The bandwidth that this amplifier is operating over should not be underestimated, especially when considering the output power levels. For an initial prototype, this was a highly satisfactory outcome. It is believed that at the time of publication, the combination of bandwidth, output power and efficiency was the best reported to date at frequencies above 1 GHz.

5.2.10 Amplitude Balance Measurements

The measurement system described in Section 5.2.8 and shown in Fig. 5.11 provides the ability to specify arbitrary powers and phases at each input port of the PA. This allows each input port to be driven with a different amount of power whilst still maintaining a 180° phase offset. The relationship between the differential input powers is the 'amplitude balance', and is specified so that 0 dB represents an equal amount of power at each input, negative amplitude balance represents more power at the 'upper' input port and positive amplitude balance represents more power at the 'lower' input port. It is specified in dB, so that, for example, 3 dB means that there is twice as much power at one input than at the other. For all the measurement points in an amplitude balance sweep, *the total input power is the same*. Table 5.2 shows an example of how the input power at each port is calculated for a total input power of 1 W (30 dBm).

Similar measurements could be made for phase balance. For this amplifier, it was determined that amplitude balance measurements were more relevant, due to the characteristics of the balun being used. The balun measurements of Chapter 3 showed that the phase balance was close to 180° at all frequencies, however the power split between the differential ports was relatively uneven.

Amplitude Balance	Input A (dBm)	Input B (dBm)	Input A (W)	Input B (W)	Total Power (W)
- 3.0 dB	25.236	28.236	0.334	0.666	1
- 2.5 dB	25.562	28.062	0.360	0.640	1
- 2.0 dB	25.876	27.876	0.387	0.613	1
- 1.5 dB	26.175	27.675	0.415	0.585	1
- 1.0 dB	26.461	27.460	0.443	0.557	1
- 0.5 dB	26.733	27.233	0.471	0.529	1
0.0 dB	26.990	26.990	0.500	0.500	1
0.5 dB	27.233	26.733	0.529	0.471	1
1.0 dB	27.461	26.461	0.557	0.443	1
1.5 dB	27.675	26.175	0.585	0.415	1
2.0 dB	27.876	25.876	0.613	0.387	1
2.5 dB	28.062	25.562	0.640	0.360	1
3.0 dB	28.236	25.236	0.666	0.334	1

Table 5.2: Amplitude balance and corresponding input powers for a total input power of 1 W

Figures 5.16 and 5.17 show a set of amplitude balance measurements at 1 GHz with V_{GS} equal to -2.4 V and phase difference equal to 180°. The amplifier was measured at intervals of 0.5 dB between -3 dB and +3 dB. It can be seen that the maximum output power is achieved at an amplitude balance of between -2 dB and -1.5 dB, i.e. with more power being input into the lower half of the amplifier. On first glance, it may be surprising that the optimum performance is not achieved at an equal amplitude balance. However, given that the microwave transmission line baluns of Chapter 3 did not have a equal amplitude balance across most of the bandwidth, it can be seen how some adjustment may be needed to maximise performance. Considering that the difference in input power is varied significantly, it can be seen that the PA is relatively tolerant to a change in amplitude balance. For this particular case, there is an performance advantage in ensuring that more input power is being injected into the lower half of the amplifier.

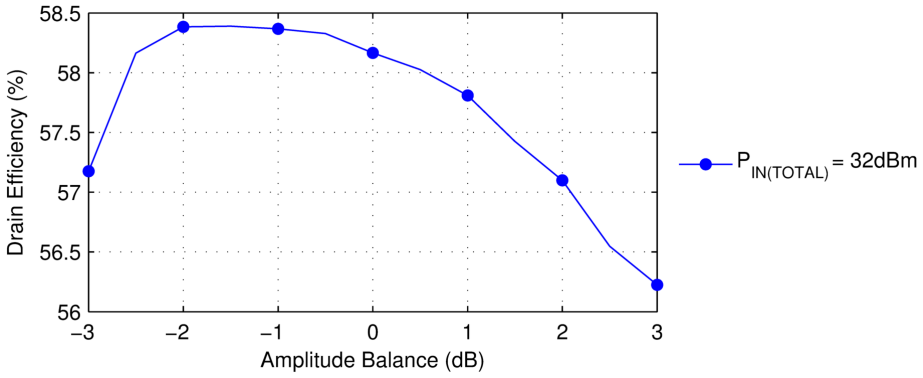

Figure 5.16: Drain efficiency against amplitude balance at 1 GHz

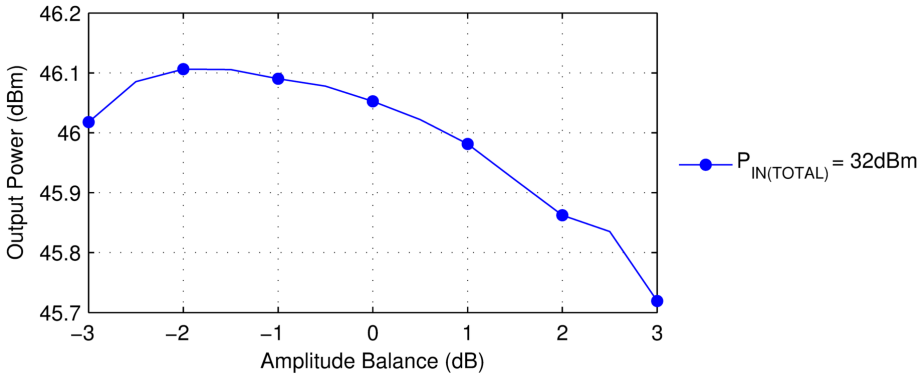

Figure 5.17: Output power against amplitude balance at 1 GHz

Figures 5.18 and 5.19 show that for 2 GHz and V_{GS} of -3.2 V the optimum output power and efficiency were achieved with an even power split between the two inputs. It can also be observed that there is a fairly symmetrical roll-off in performance. Again, the PA can be seen to be relatively tolerant to a change in amplitude balance, given

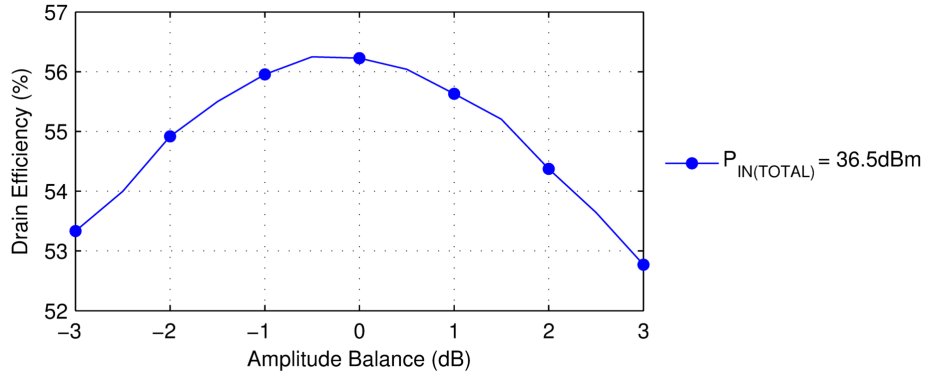

Figure 5.18: Drain efficiency against amplitude balance at 2 GHz

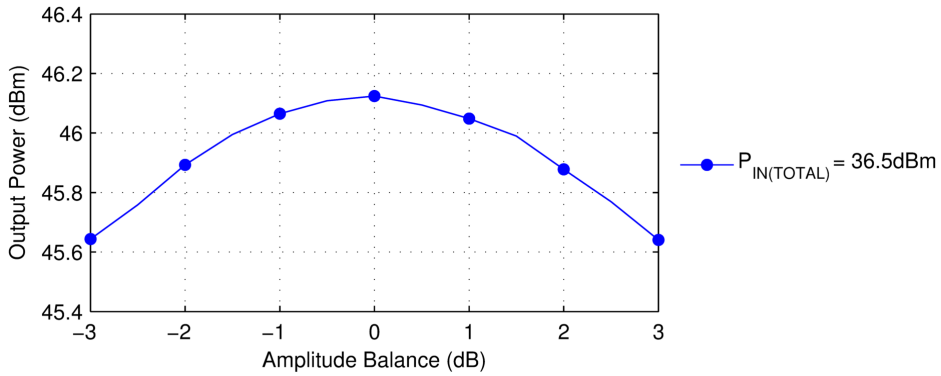

Figure 5.19: Output power against amplitude balance at 2 GHz

that the difference between maximum and minimum output power for Fig. 5.19 is only 0.5 dB.

It is speculated that the amplitude balance is not overly critical to the overall amplifier performance as the transistors influence each other through the coupling between the balanced ports of the output balun. It is possible that the output power from one transistor is fed back through the balun to effectively 'load-pull' the other transistor, similar to the effect observed in Doherty amplifiers.

From the initial measurements, no overall trend could be identified for optimum amplitude balance versus bias or frequency. As measurements were only taken at five widely-spaced frequency points, this is perhaps not surprising. With data at more frequency points, it may be possible to determine a relationship between frequency and amplitude balance, which could aid with input balun design or the dynamic control of amplitude balance. The differential measurement system is a useful tool for further investigation of the push-pull mode of operation.

5.2.11 Output Voltage Waveform Measurements

To gain further insight into the characteristics of the prototype amplifier, voltage probing microstrip lines were included close to the drain tab of the transistors, as shown in Fig. 5.20. When a suitable resistor is soldered across the gap between the main microstrip line and the voltage probing microstrip line a voltage divider is formed and the time-domain waveforms can be measured using a digital sampling oscilloscope. This can be used to study the waveforms at the output of each transistor relative to each other and to highlight and diagnose any performance issues. Further modifications to the measurement software were required to support simultaneous measurements on six channels.

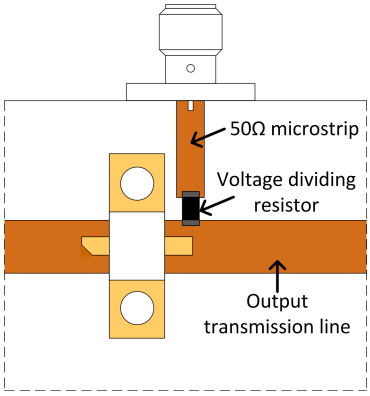

Figure 5.20: Voltage probe (not to scale)

An example of a set of time-domain voltage waveforms is shown in Fig. 5.21. Although every effort was made to keep the path lengths equal, these measurements have to be regarded as qualitative rather than quantitative due to the lack of a rigorous calibration procedure. These measurements can only measure voltage waveforms, and without time-domain current waveforms only limited analysis of the PA operation can be conducted.

Despite the limitations of these measurements, they can, at the very least, confirm that the two transistors are operating approximately 180° out of phase, and that both are contributing to the total output power of the amplifier. This may not be a surprising result, but it is a reassuring discovery nonetheless. If the performance of the amplifier at this frequency had been significantly lower than expected, the voltage waveform measurement would help to determine whether the two transistors were operating similarly.

Another set of voltage waveform measurements is shown in Fig. 5.22. Again, the 180° phase difference is evident, however in this case the waveforms are quite different between the two transistors. It can also be seen that these waveforms appear to have more harmonic content compared to the waveforms of Fig. 5.21.

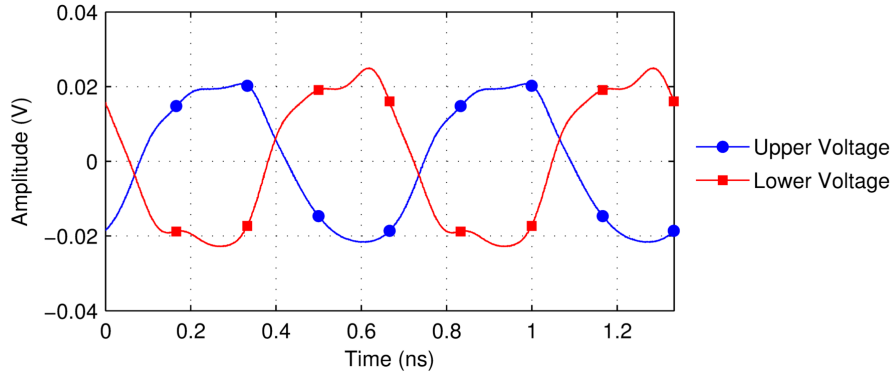

Figure 5.21: Measured time-domain output voltage waveforms at 1.5 GHz and 0 dB amplitude balance

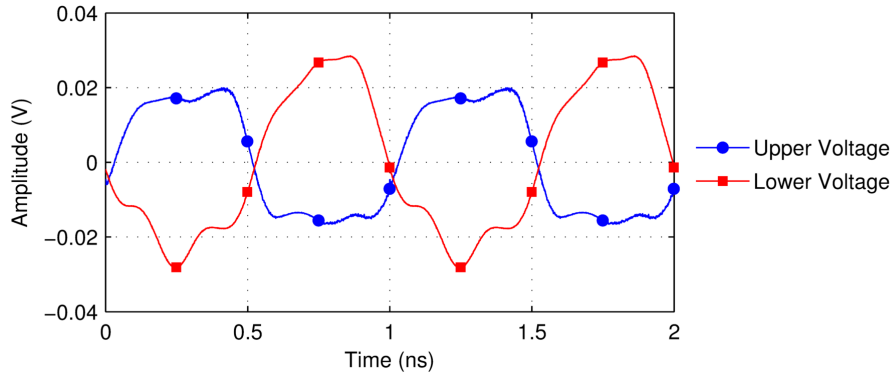

Figure 5.22: Measured time-domain output voltage waveforms at 1 GHz and -3 dB amplitude balance

It should be recognised that using more sophisticated, less intrusive methods of measuring time-domain voltages [77], this work could be extended to gain valuable information about the operation of the push-pull amplifier at microwave frequencies. For example, voltage waveform measurements could be made to verify the push-pull modes of operation introduced in Chapter 4, and could be compared to simulated waveforms in AWR Microwave Office.

5.3 Push-Pull Power Amplifier Version 2

5.3.1 Design Goals

The performance goals for the first prototype were also used as targets for the second prototype, with three additional requirements.

The first prototype power amplifier made use of differential inputs, which allowed the effects of amplitude and phase balance to be tested. However, the measurement procedure was much more time consuming than for standard single-input PA measurements and also required a relatively complex and costly measurement setup. For the second prototype it was decided to include an input balun with the option of switching to differential inputs if desired. The disadvantage of the input balun is that the loss in the input side of the PA is increased and so the overall gain of the amplifier is reduced. In addition, the amplitude and phase balance cannot be tuned to optimise performance.

With the addition of an input balun, and hence a single-ended input, the input return loss ($|S_{11}|$) became of interest, and a target of less than -10 dB at all frequencies was set. The third requirement was to integrate gate bias networks into the amplifier, in order to obviate the need for external bias tees.

The overall aim of the second prototype was to achieve similar performance figures to the first prototype whilst creating a more 'usable' power amplifier.

5.3.2 Choice of Transistor

It was decided to use the same CGH40025F transistors as PA v1. As the balun design was unchanged, the same reasoning for selecting the 25 W transistor based on load-pull measurements could be applied. By using the same transistor, it also facilitated a direct comparison between the amplifiers, and hence an evaluation of the effect of the input balun and input matching.

5.3.3 Design

As previously stated, the target for input matching was an input return loss ($|S_{11}|$) of less than -10 dB at all frequencies. This is a typical input match target for broadband power amplifiers. The strategy was to match the high end of the frequency band, where there is less available gain, and use a 'lossy' resistive match at the low end to flatten the gain and provide the necessary return loss. This was only achievable by including a resistive element in the input matching network, which reduced the gain of the amplifier.

The input matching network was developed by first designing into a single-ended topology. The initial matching network, using ideal lossless components, is shown in Fig. 5.23. The matching network is oriented such that the input balun is at Port 1, and the gate tab of the transistor is at Port 2. The first element, moving from right

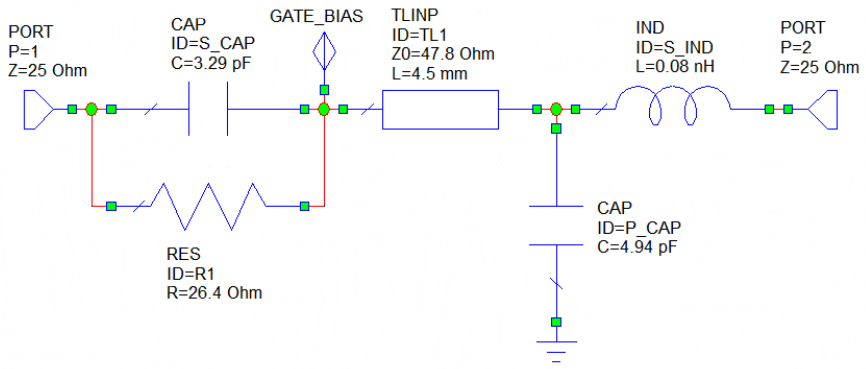

Figure 5.23: PA v2 input matching network (ideal lumped elements)

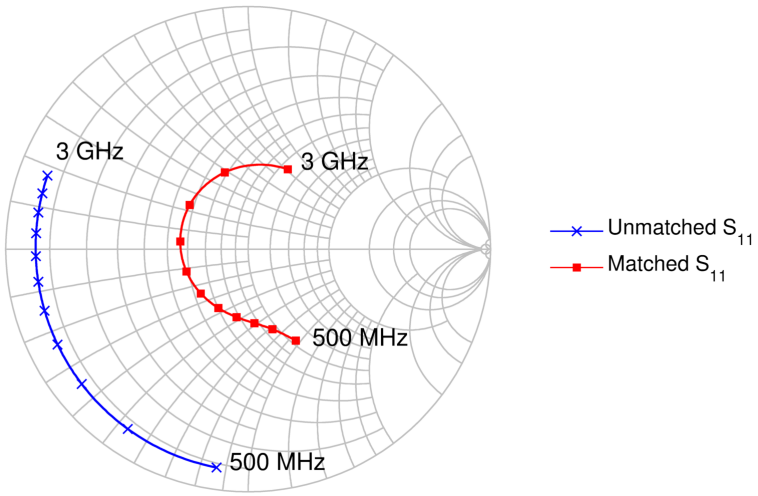

Figure 5.24: S_{11} of CGH40025F transistor with and without input matching network

to left, is a series inductor and shunt capacitor (low-pass filter) network that shifts the high frequency end of S_{11} towards the centre of the Smith Chart. The next element is a length of transmission line that rotates S_{11}. Finally, a parallel combination of capacitor and resistor serves to provide a 'lossy' match at the low end of the frequency band. The effect of the input matching network is shown in Fig. 5.24, which demonstrates how S_{11} is shifted towards the centre of the Smith Chart and hence increases the input return loss.

The input matching procedure was done into both a 50 Ω and 25 Ω impedance environment. The advantages of the 25 Ω environment can be seen in Figs. 5.25 and 5.26 through higher gain values and a better input match.

Ideally, a power amplifier would have both a good input match and flat gain across the entire operational bandwidth. However, this is very rarely possible, especially over the extended bandwidths being considered here. Therefore, it was decided to prioritise input match over gain flatness in this design. The consequence of this is that the input

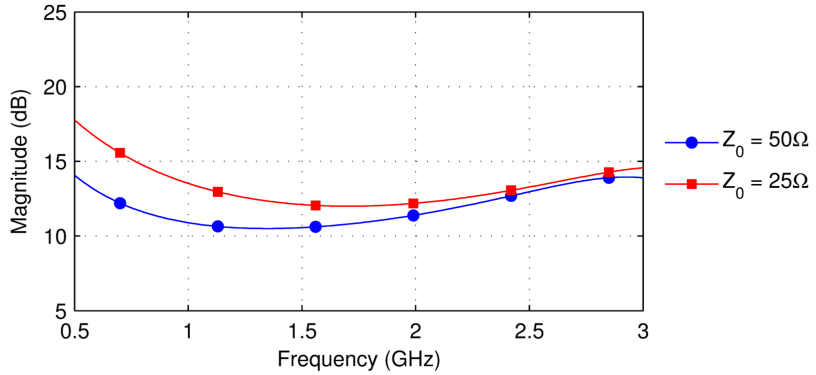

Figure 5.25: Simulated S_{21} of CGH40025F with input matching network of Fig. 5.23

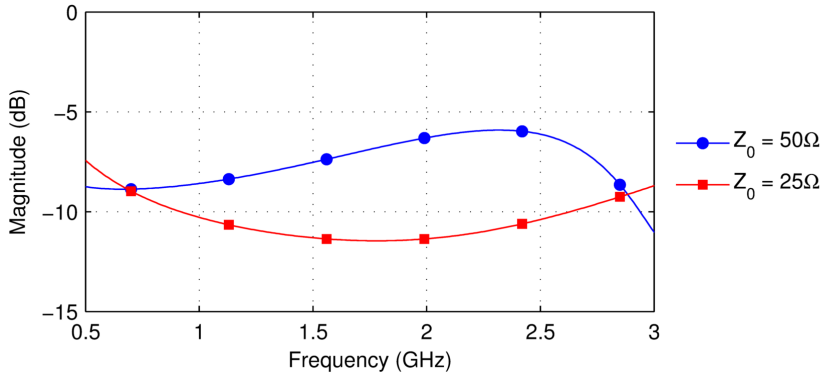

Figure 5.26: Simulated S_{11} of CGH40025F with input matching network of Fig. 5.23

power has to be varied with frequency in order to achieve a constant output power. In the simulator, this was achieved by fitting a fifth-order polynomial to S_{21} then inverting the sign of the polynomials. This compensated for the gain variation with frequency, and resulted in an approximately constant output power. The input power variation with frequency is shown in Fig. 5.27.

As with the first prototype amplifier, no combination of lumped element matching components at the output could be found to improve the overall amplifier performance. The transmission line lengths and widths were tuned to optimise performance across the operating bandwidth. The final layout is shown in Fig. 5.28. The simulated large-signal performance is shown in Fig. 5.29, and shows a constant output power of around 46 dBm across the entire bandwidth. The predicted drain efficiency is lower than for PA v1, however 40% drain efficiency up to 3 GHz would still be impressive performance given the bandwidth of the amplifier.

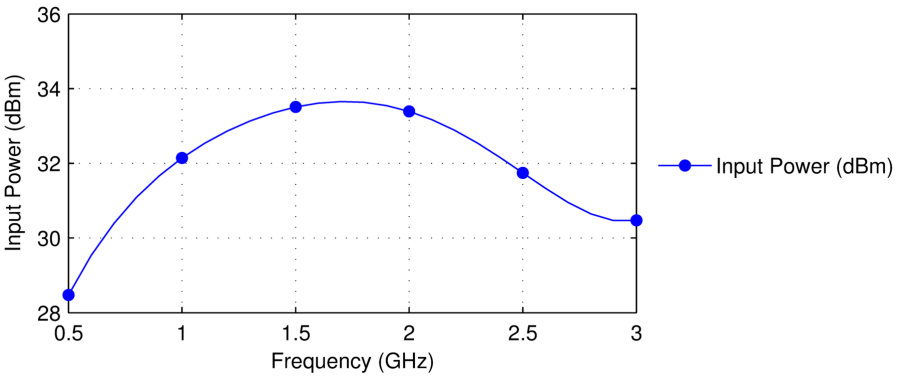

Figure 5.27: Input power variation with frequency

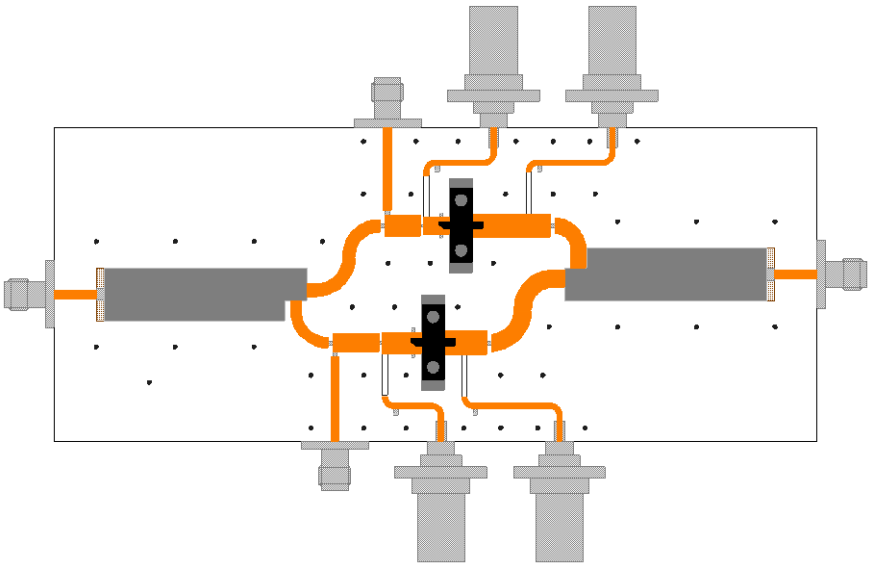

Figure 5.28: Layout of PA v2

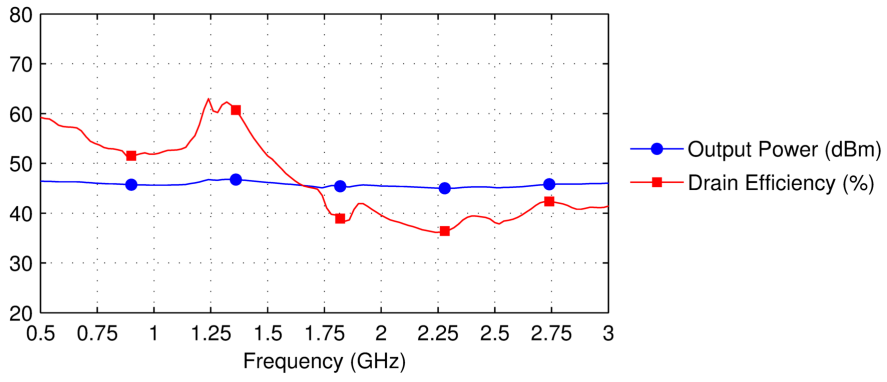

Figure 5.29: Simulated large-signal performance of PA v2

5.3.4 Manufacture

The manufacturing and assembly process was the same as for the first prototype, with two minor improvements. The holes for grounding via pins were drilled using the milling machine, rather than being drilled manually, which resulted in more uniform and reliable ground connections. Also, the layout was changed so that all the microstrip lines had a 1.0 mm border around them, which is wide enough to ensure against accidental shorting of the microstrip line to ground and narrow enough to allow 0402-size surface mount components to be attached between the microstrip and the ground. This was not possible in PA v1, with the result that at some points the gaps had to be widened manually using a scalpel. The assembled amplifier is shown in Fig. 5.30.

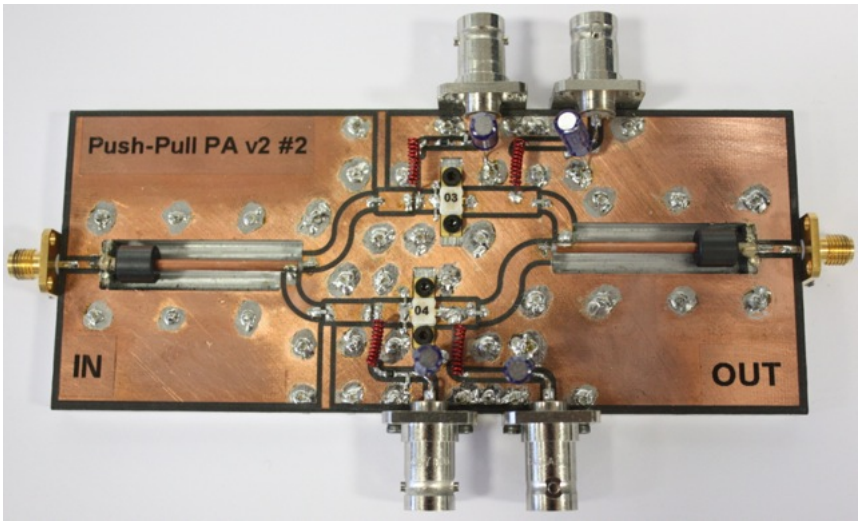

Figure 5.30: Photograph of assembled push-pull PA v2 (ferrite beads included)

5.3.5 Stability and Initial S-Parameter Measurements

Due to the initial instability of PA v1, gate resistors were included as part of the gate bias networks at the design stage of PA v2. Under all bias conditions that were tested, the power amplifier was stable.

Figure 5.31 shows that, apart from a dip around 1.9 GHz, the gain of the amplifier was greater than 11 dB up to 3 GHz for two of the bias conditions. The third bias condition, with the lowest quiescent current, had less gain, as would be expected. The dip was unexpected and did not appear during simulation. Further investigation of this effect is discussed in Section 5.3.8. Apart from the dip in performance at 1.9 GHz, Fig. 5.32 shows that the agreement between measured and simulated S_{21} is good across the entire band.

Figure 5.33 shows that there is an input return loss of less than -10 dB over most of the bandwidth, the only exceptions being around 1.9 GHz and at the high end of

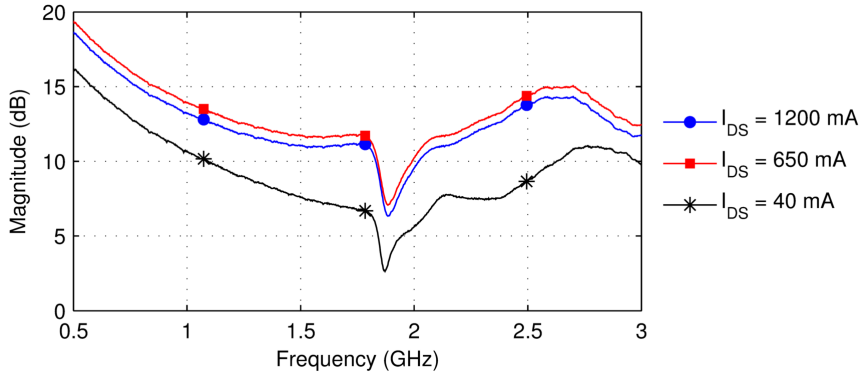

Figure 5.31: S_{21} of PA v2 at different bias levels

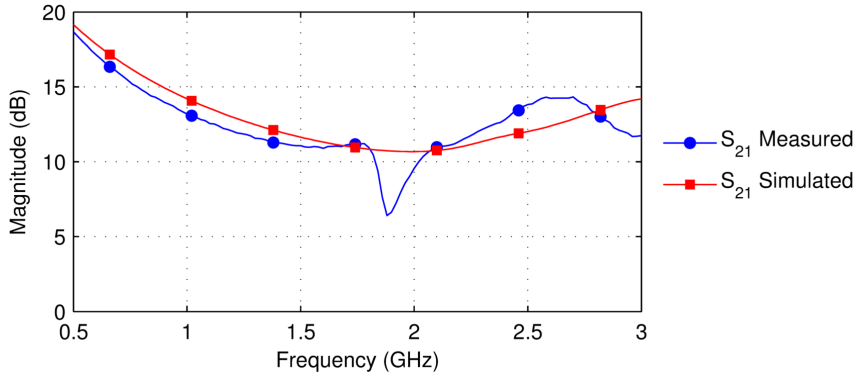

Figure 5.32: Comparison of measured and simulated S_{21} of PA v2

the band. This was judged to be acceptable performance given the bandwidth of the amplifier.

5.3.6 Large Signal Measurement Setup

Because of the single-ended input on the second prototype, the large-signal measurement setup (shown in Fig. 5.34) is significantly simpler than for the first prototype. There is no requirement to measure input phase, and so a power meter can be used in place of the digital sampling oscilloscope. This has the advantage of significantly reducing the measurement time and requiring fewer calibration steps. The calibration consisted of characterising the coupling factor of the directional coupler at the input across the frequencies to be measured at. In addition, the attenuation between the output of the PA and the power meter (not shown) is characterised. It can be seen that less hardware is required to implement this measurement setup compared to the measurement system used for PA v1. Due to the integrated gate bias networks, bias tees on the input ports are no longer required. A feedback loop ensures the required incident input power is provided, and data from the DC supplies and power meters is acquired.

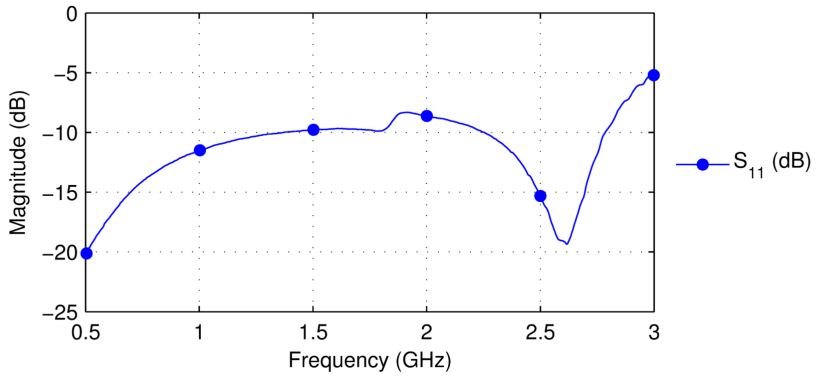

Figure 5.33: Measured S_{11} of PA v2

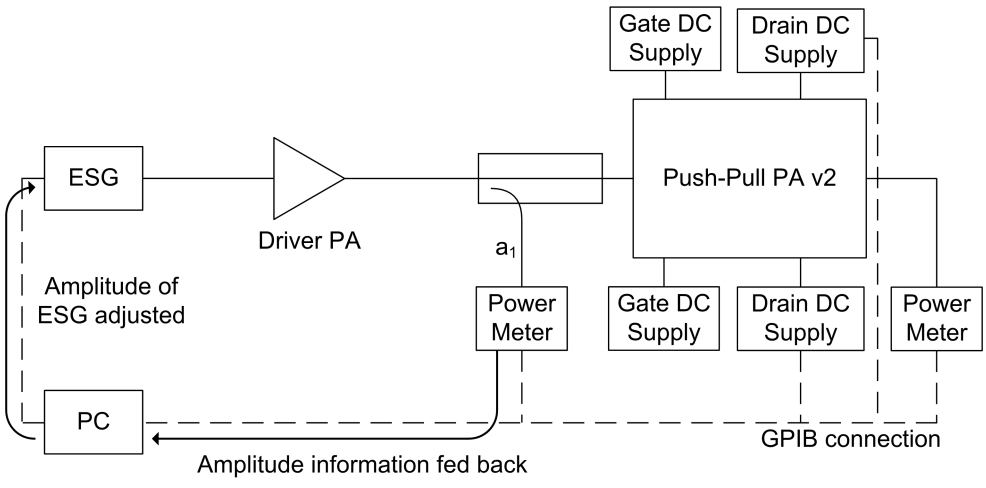

Figure 5.34: Block diagram of setup for measuring PA v2 (single-ended input)

5.3.7 Large Signal Measurement Results

Large-signal measurements were made at 100 MHz intervals between 0.5 GHz and 2.5 GHz, and are shown in Fig. 5.35. Excellent large-signal performance can be seen between 0.5 GHz and 1.5 GHz, a 3:1 bandwidth. The output power over this range is between 44.5 dBm and 46.5 dBm, with drain efficiencies around 60% for much of the band, falling to 44% at 1.5 GHz. At the time of writing, large-signal measurements below 500 MHz were unavailable, but it is predicted that the performance would be similar to that of PA v1, with usable performance down to around 300 MHz. Between 1.3 GHz and 2.5 GHz the performance is lower than predicted in simulation, and also lower than that achieved with PA v1. It is thought that this is partially because, unlike the first prototype, it was not possible to vary the input amplitude and phase balance to optimise performance. Large-signal measurements were not available above 2.5 GHz.

It can be seen in Fig. 5.36 that the decrease in output power at 1.9 GHz was not predicted in simulation, however there is good agreement with simulation below 1.2 GHz. The input power was the same for both simulation and measurement. The drain efficiency is actually higher than predicted by simulation below 1.2 GHz, as shown in Fig. 5.37.

The dip in performance at 1.9 GHz that was visible in the small-signal measurements is also present in the large-signal measurements, resulting in an output power of 42.0 dBm and drain efficiency of 23.9%. As mentioned in Section 5.3.3, the input power was varied with frequency in order to compensate for the gain variation of the PA.

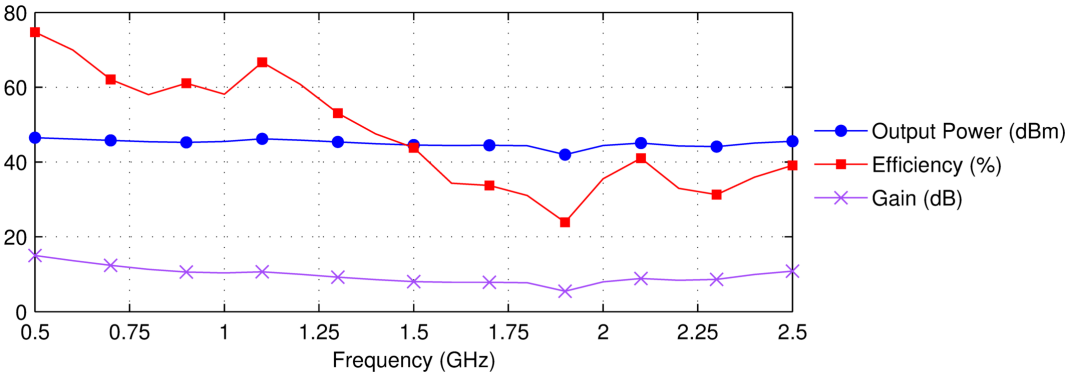

Figure 5.35: Large signal measurement results for push-pull PA v2

5.3.8 S-Parameter Measurements - Addition of Ferrite

Up until this point, it had not been necessary to add ferrite beads to the baluns on the prototype amplifiers. From the start it had been decided to measure the amplifiers without ferrite beads in order to reduce loss, with the option of adding them if deemed necessary. However, from the initial measured results of PA v2 it was clear that there

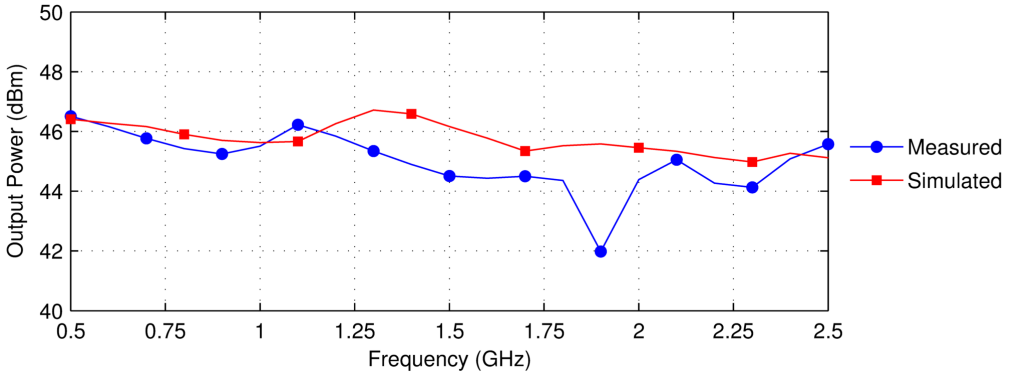

Figure 5.36: Measured and simulated output power for PA v2

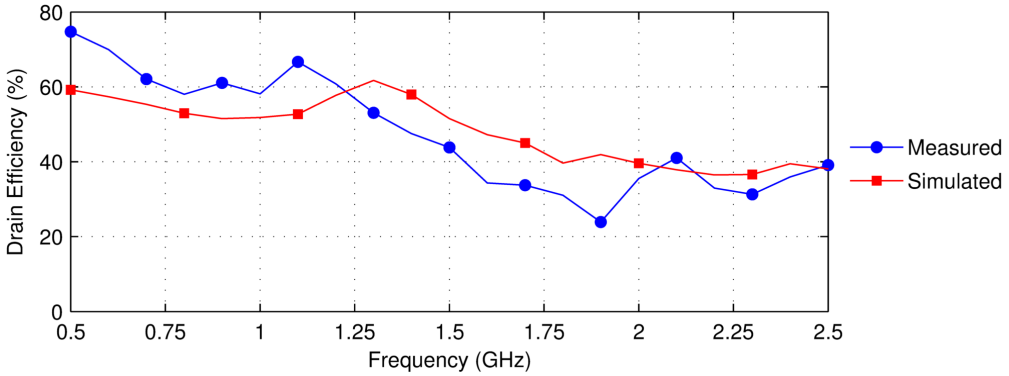

Figure 5.37: Measured and simulated drain efficiency for PA v2

was an unexpected dip in performance. Given that the frequency it occurred at was around 1.9 GHz, approximately half the frequency of where the half-wavelength resonance occurred, it was thought that the half-wavelength resonant frequency was having an adverse effect on the second harmonic. It was decided to add ferrite beads to the input and output baluns, to see if they could remove the dip in performance.

The coaxial cable used for PA v2 was AtlanTec CSR-086, which has an overall outer diameter of 2.20 mm. This is the same cable that was used for PA v1, and was selected for its greater maximum power handling and lower loss compared to thinner cables. The disadvantage of using this coaxial cable is that most of the ferrite beads available would not fit over this diameter of cable and so the only choice of ferrite bead was part number 2661000801 from Fair-Rite.

The S-parameter measurements of PA v2 with ferrite included are shown in Fig. 5.38. Ferrite beads were added to the output balun, and then to the input and output balun, to see whether they had any effect on the dip. It would appear that the ferrite has no effect on the dip in performance, suggesting that either the dip is caused by other factors or that the particular ferrite bead model is ineffective. This second explanation is unlikely as even if the ferrite's equivalent resistance was not equal to Z_{OUTER} it should

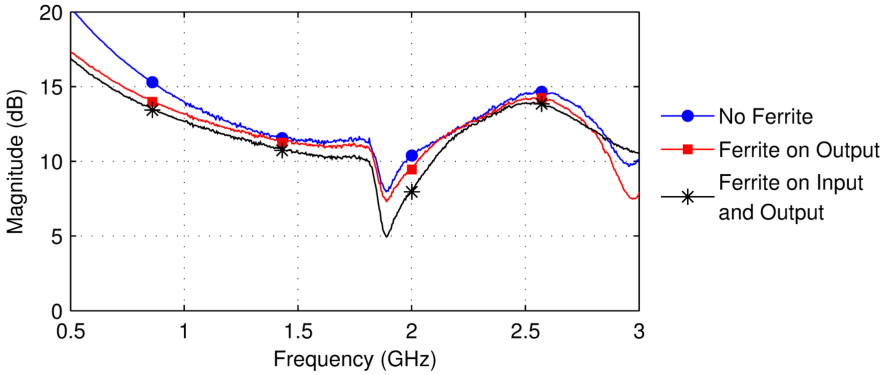

Figure 5.38: S_{21} of push-pull PA v2 with ferrite included

have some noticeable flattening effect.

It would be possible to use a thinner cable for the input balun, where power handling is not a primary consideration, which increases the number of beads available for use at the input. Further options include sourcing different COTS ferrite beads, or having ferrite beads shaped to custom dimensions, as discussed in Section 7.3.1.

Whilst the cause of the dip in performance is unknown at the time of writing, future work provides an opportunity to gain better understanding of the operation of the push-pull topology at microwave frequencies. This is discussed in more detail in Section 7.2.2.

5.4 Chapter Summary

In this chapter two prototype push-pull power amplifiers have been presented, along with bespoke measurement systems for evaluating their performance.

The impressive performance of PA v1 shows the potential for using the push-pull topology at frequencies greater than 1 GHz, an area where it has rarely been used. It is believed that at the time of publication, the combination of bandwidth, output power and efficiency was the best reported to date at frequencies above 1 GHz. Usable performance was achieved across a decade bandwidth, with especially good performance at lower frequencies.

The second prototype greatly improves practicality and usability, but does not achieve the same level of performance. Efficiency figures of around 60% are achieved up to 1.2 GHz, which was achieved without the ability to tune the amplitude and phase balance. The output power between 0.5 GHz and 1.2 GHz is close to that predicted in simulation, and the efficiency is higher than predicted, however the performance rolls off at higher frequencies and there is a noticeable dip at 1.9 GHz. The addition of ferrite beads did not have the expected effect of removing this dip, and further work is needed to investigate this. The second prototype was a more practical power amplifier, with a good input match across most of the bandwidth.

The measurement system software that was written to allow large-signal differential input measurements opens up the possibility for furthering knowledge of the push-pull amplifier. Examples of amplitude balance measurements and output voltage waveform measurements have been presented, and the insight gained from these measurements has been discussed.

It may be surprising to the reader that the resonance suppression techniques of Chapter 3 were not utilised in the design of the power amplifier prototypes presented in this chapter. However, for these particular designs, the upper bandwidth limit was the transistor and the low-pass response of its package, as discussed previously. The best performance could be obtained by designing the half-wavelength resonance of the balun to be above the cut-off frequency of the packaged transistor. For a design where the bandwidth is limited by the half-wavelength resonance, the theory and procedure of suppressing the resonance using ferrite should provide an effective technique of extending the bandwidth. The design choices made in this chapter in no way invalidate the design methodology of Chapter 3.

The realisation of prototype amplifiers serves to demonstrate that the push-pull topology is a promising solution to the challenge of designing high-power, high-efficiency multi-octave power amplifiers.

Chapter 6

Conclusions

The aim of the work presented in this thesis was to investigate the push-pull topology as a method of achieving high power, high efficiency performance across a wide bandwidth at microwave frequencies. The uses for such an amplifier include wireless communication and military applications, as discussed in the introduction.

There are four main conclusions that can be drawn as a result of the work presented in this thesis.

The first, and most important, conclusion is that the push-pull topology has been shown to be a valid method of simultaneously achieving high efficiency and high output power over multi-octave bandwidths at microwave frequencies. Two prototype power amplifiers were developed to demonstrate the achievable performance, and there is potential to improve performance, as will be discussed in Chapter 7. The amplifiers compare favourably to those reviewed in the literature, and the first prototype was believed at the time to give the best combination of efficiency, output power and bandwidth at the particular frequencies of operation. The push-pull amplifier is not traditionally used at microwave frequencies, and it is hoped that these results will lead to more widespread investigation into its use.

The second conclusion that can be drawn is that the mode of operation inside the push-pull power amplifier at microwave frequencies is significantly different to the conventional 'textbook' view of the push-pull amplifier. Instead of two Class B amplifiers operating 180° out of phase, the transistors are presented with an open circuit at the even-order harmonics and a resistive impedance at the odd-order harmonics, which has a profound effect on the performance figures and time-domain waveforms. It has been shown in Chapter 4 that the push-pull mode of operation resembles an 'inverted mode', and shows an increase in output power of 1.5 dB compared to Class A. Perhaps most importantly, these modes of operation can be maintained over much wider bandwidths than conventional PA modes. This is due to the transmission line balun's ability to present two different impedances at the same frequency, depending on whether the

excitation is odd- or even-mode.

In Chapter 3 it was shown that the bandwidth of a coaxial cable transmission line balun can be greatly extended through the addition of ferrite beads. The conventional use for this material has been to enhance the low-frequency performance by making use of its reactive permeability, however it has been shown that the resistive permeability can be utilised to suppress the half-wavelength resonance of the balun. This dual role of ferrite materials can greatly extend the balun's bandwidth, at the expense of increased loss. The balun is the key component in the push-pull power amplifier, and so extending the bandwidth of the balun enables the development of multi-octave microwave power amplifiers. This design methodology could also potentially be applied to the design of baluns for other applications, such as mixers.

Lastly, a measurement system was developed to further investigate the characteristics of the microwave push-pull power amplifier. The amplitude and phase balance of the differential inputs could be varied in order to evaluate the effect that this has on the amplifier's large-signal performance. The output voltage waveforms could be measured using the same system, and applications for this have been discussed. The software also captures the measured data, removing the need for the measurements to be conducted manually.

This thesis has introduced a number of novel contributions that have resulted in interesting and valuable developments in the area of push-pull power amplifiers. These contributions enable a vast number of possible future developments, some of which are discussed in the next chapter.

Chapter 7

Future Work

7.1 Introduction

In the preparation of this thesis, a large amount of work has been completed across a wide variety of areas. For instance, assembly of prototype coaxial cable transmission line baluns has been interspersed with programming an automated power amplifier measurement system in C#. This inevitably means that there are many areas where there is much left to investigate, and some of the most interesting and intriguing of these will be outlined in this chapter.

The development of a third prototype amplifier is documented first. At the time of writing, this amplifier was not available for measurement, so only simulated results can be presented. The advantages of chip-and-wire assembly are discussed, and investigation into the 'dual-mode' of operation is presented.

In addition, five further directions for future work are suggested, spanning the range of balun developments to push-pull amplifier measurements. It should be noted that there are many more possibilities for investigation that are not discussed here.

7.2 Push-Pull Power Amplifier Version 3

7.2.1 Chip-and-wire Assembly

Attempting to achieve multi-octave, high-efficiency operation at high power levels is significantly hampered by the reactances introduced by the package of the transistor. By shifting the optimum output impedance to a lower value, these reactive elements make the task of impedance matching more difficult, as outlined in Section 2.3.2.

One approach to overcome this limitation is to use an unpackaged, or 'bare die' transistor in a 'chip-and-wire' assembly. The semiconductor wafer is sawn up into individual die, which are then attached directly to the circuit board using eutectic solder, and the gate and drain pads are wire-bonded to the transmission lines.

In effect, removing the package is equivalent to eliminating the reactances L_{tab1}, L_{tab2} and C_{tab} in Fig. 4.9. As a series inductor combined with a parallel capacitor acts as a low-pass filter, removing these elements should improve the high-frequency response of the amplifier. A secondary benefit is the reduced loss from eliminating the package.

A chip-and-wire approach also results in higher gain values, due to lower inductance in the source path to ground, and also due to reduced feedback from the output to the input.

One downside to a chip-and-wire design is that the circuit designer has to take greater responsibility for the thermal management compared to a packaged device design. The quality of the die attach is critical, especially for GaN devices, which dissipate a lot of heat in a relatively small area. The absence of a package also means the transistor is at greater risk to damage from its environment. Bond wires, in particular, are thin and fragile and hence are susceptible to accidental damage.

However, for the development of the third prototype amplifier, PA v3, the benefits of a chip-and-wire assembly were judged to outweigh the disadvantages, and so this approach was pursued.

7.2.2 'Dual-mode' Push-Pull

During the simulation stage of the design of PA v3, it was found that the addition of output matching capacitors to ground significantly improved the high frequency performance. However, this resulted in a significant dip in performance around the centre of the amplifier's operating bandwidth. This dip in performance can be seen in Figs. 7.1 and 7.2.

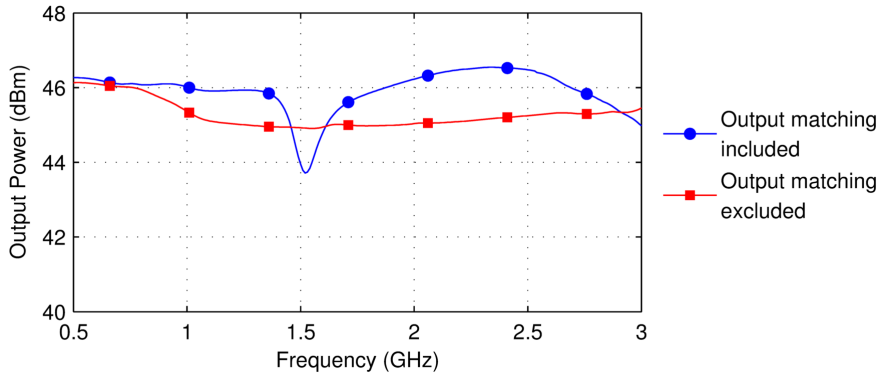

Figure 7.1: Output power of PA v3 preliminary simulations

The frequency at which the dip occurs is designated the 'transition frequency'. Investigation into the time-domain waveforms revealed that at frequencies less than the transition frequency the mode of operation was similar to a non-inverted mode, as shown in the waveforms of Fig. 7.3. This is indicated by the half-wave rectified shape of the

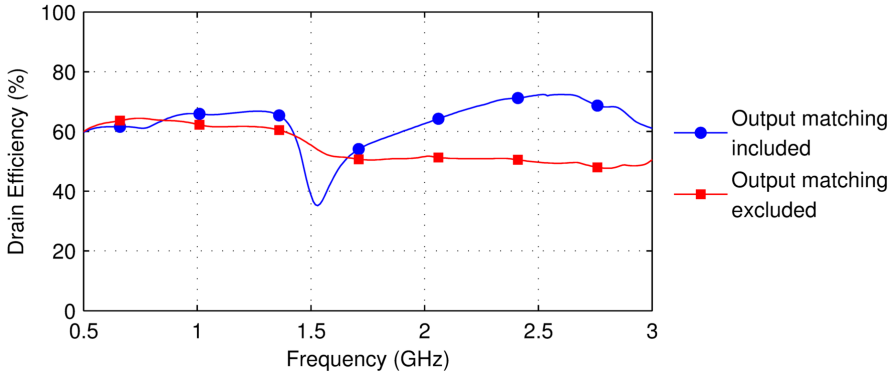

Figure 7.2: Drain efficiency of PA v3 preliminary simulations

current waveform, and sinusoidal nature of the voltage waveform, which is flattened by a third harmonic voltage contribution. Above the critical 'transition frequency', the waveforms, shown in Fig. 7.4, were more similar to an inverted mode of operation. The current can be observed to be approximately sinusoidal, with the voltage resembling a half-wave rectified sinusoid. In this way, it can be observed that the PA is, in effect, working in a 'dual mode' of non-inverted operation below the transition frequency and inverted above it.

The harmonic voltage magnitudes at the transition frequency are greatly increased compared to the rest of the band, resulting in the highly irregular waveforms of Fig. 7.5 and reduced output power and efficiency. The variation in fundamental and harmonic voltage magnitudes with frequency is shown in Fig. 7.6.

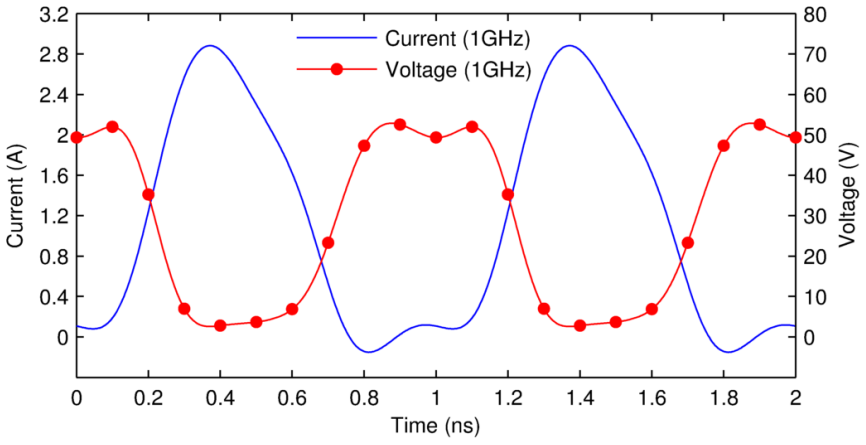

Figure 7.3: Simulated time-domain waveforms below the transition frequency

This is a highly interesting phenomenon, however it should be noted that it would be necessary to build a prototype amplifier with the transition frequency deliberately included to verify that this dip in performance could be observed through measurement.

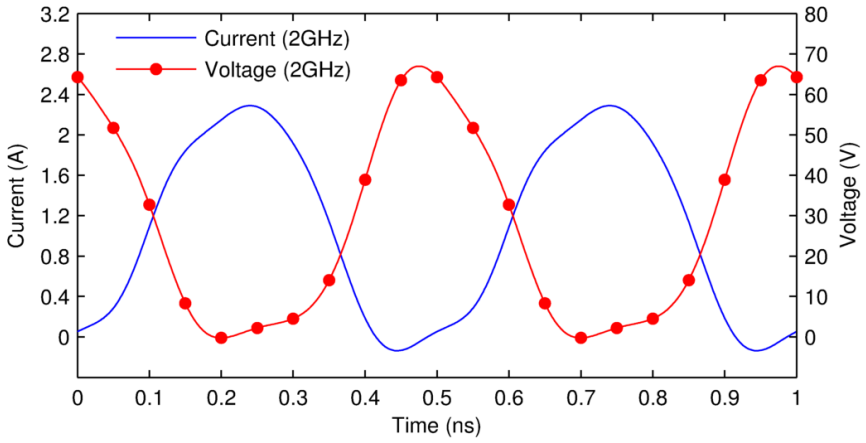

Figure 7.4: Simulated time-domain waveforms above the transition frequency

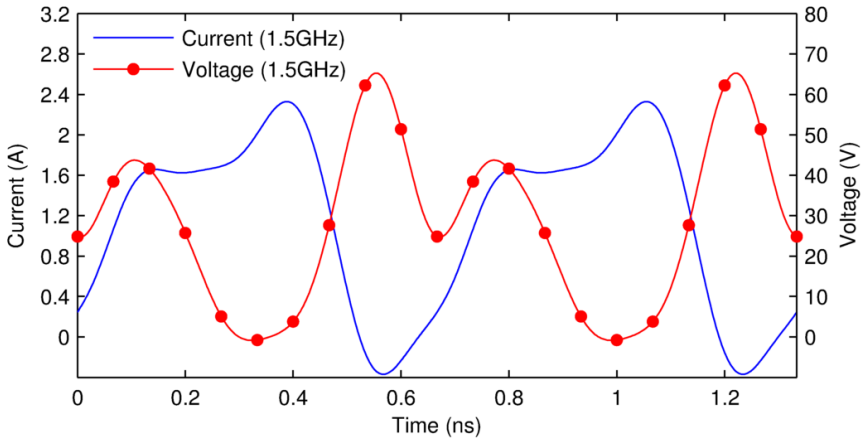

Figure 7.5: Simulated time-domain waveforms at the transition frequency

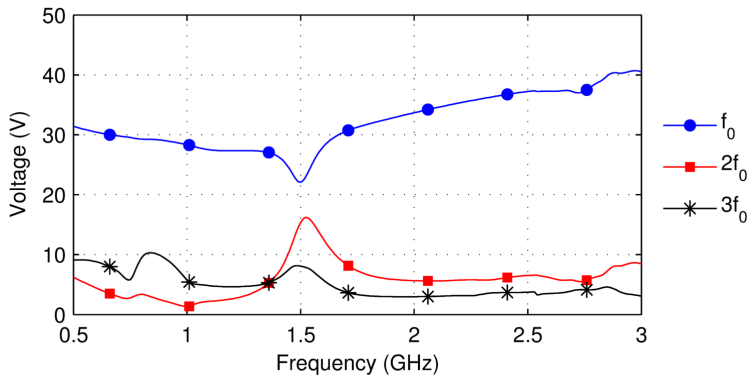

Figure 7.6: Harmonic voltage magnitudes with output matching included

It is possible that this dip is related to the one observed in the measured results of PA v2, although this cannot be determined at present.

If the 'dual mode' is discovered to be present in prototype amplifiers, this suggests that frequency-dependent biasing should be investigated, as the biasing requirements differ for inverted and non-inverted modes of operation. Analysis of the waveforms should be able to provide information on the optimum condition for each frequency. It is unlikely that one bias point is optimum for all frequencies, especially over the bandwidths being considered in this thesis.

7.2.3 Design and Simulated Results

It was decided that, as with the first two prototype designs, good performance at all frequencies across the band would be targeted, as opposed to a 'dual-band' design with a dip in performance at the transition frequency. Efforts were made to eliminate the dip in performance without removing the output matching capacitors and hence compromising the performance across the rest of the bandwidth. The best performance was obtained by implementing a 'virtual ground' between the two halves of the amplifier, where the output matching capacitors were connected together via an area of copper microstrip which was not grounded. Interestingly, this was also required for the input matching capacitors, and further investigation is needed to establish why this is. The final layout is shown in Fig. 7.7, and the simulated performance compared to the second prototype amplifier is shown in Figs. 7.8 and 7.9.

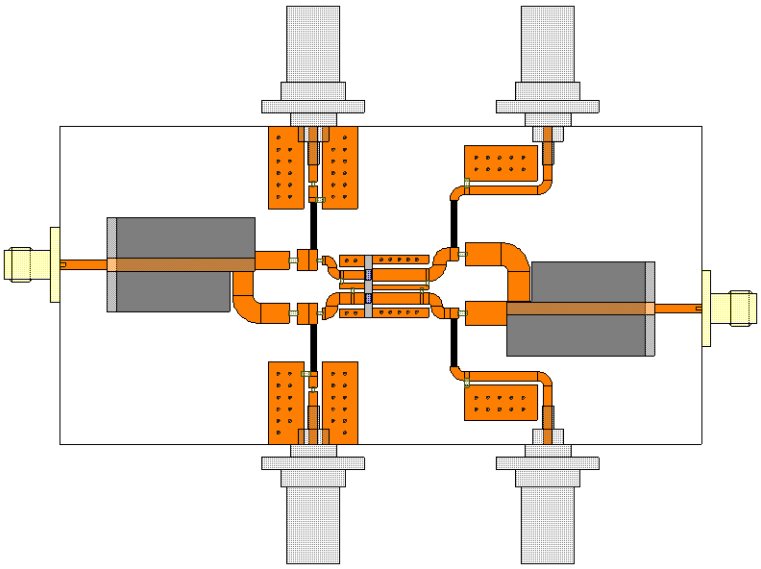

Figure 7.7: Layout of PA v3

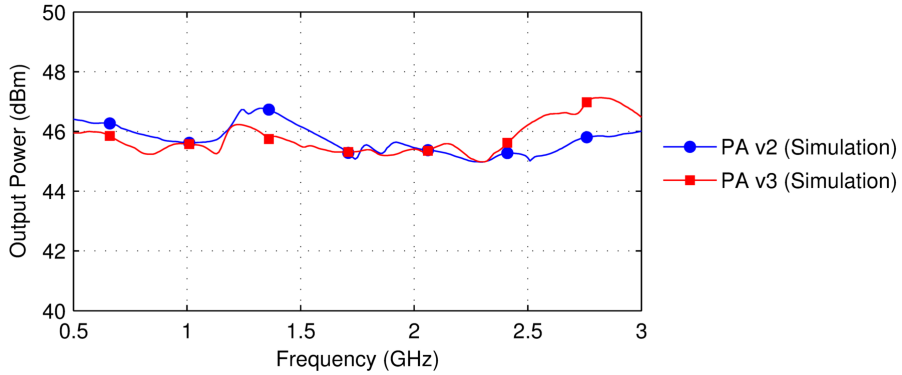

Figure 7.8: Comparison of simulated output power for PA v2 and PA v3

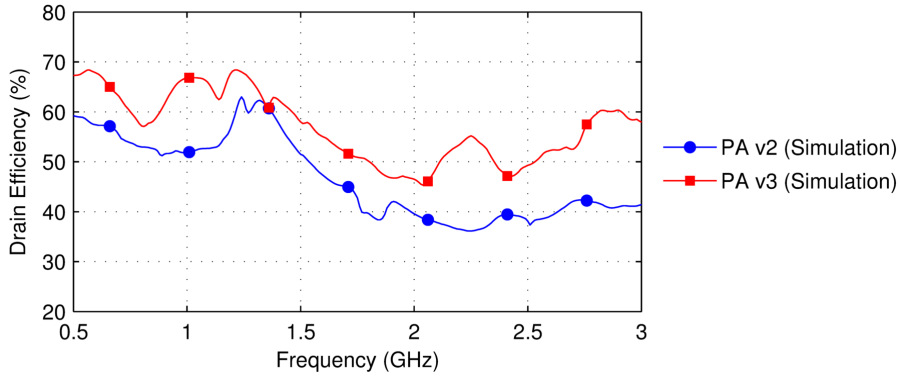

Figure 7.9: Comparison of simulated drain efficiency for PA v2 and PA v3

It can be seen in Fig. 7.8 that the output power is similar to PA v2 across most of the band, which is to be expected, but that it is improved at higher frequencies. However, the drain efficiency, shown in Fig. 7.9, is significantly improved across almost all of the bandwidth. This is a very promising result, and shows the potential performance improvements of the chip-and-wire approach combined with appropriate output matching. It should be noted that this is simulated data, however it is hoped that the improved performance in simulation will be realised in practice and reflected in the measured results.

7.3 Additional Future Work

In this section, a number of potential areas for future research are outlined.

7.3.1 Ferrite Materials

In Chapter 3, three different types of ferrite material were evaluated for use in suppressing the half-wavelength resonance of a coaxial cable balun, all manufactured by Fair-Rite. However, there are many more ferrite manufacturers from whom ferrite beads could be evaluated, which may be found to be more suitable for this application. As it is possible for ferrite materials to be machined to custom dimensions, it would also be useful to investigate the effect of varying the ferrite bead's length and inner and outer diameters.

The design of custom ferrite beads would be greatly aided by 3D electromagnetic simulations. 3D electromagnetic simulations using COMSOL were briefly described in Chapter 3 as a method of simulating the outer characteristic impedance of a transmission line balun. The simulation of ferrite material was also attempted using COMSOL, however it was found that it was extremely difficult to define a ferrite material's characteristics in the simulator, largely due to the fact that most of its parameters are frequency-dependent. This requires mathematical expressions for the frequency relationship to be developed, which is a time-consuming process. If it were possible to simulate the ferrite beads accurately in a 3D EM simulator, it should be possible to design a complete transmission line balun whose half-wavelength resonance is suppressed using ferrite. This would result in shorter development times and fewer prototype baluns being required due to a more comprehensive design methodology.

Another possible development would be to investigate ferrite beads of different materials on the same balun to optimise both resonance suppression and low frequency performance. For example, #73 material ferrite could be used to improve low-end performance, with unaffected resonance suppression, whilst #61 material could be used to suppress the half-wavelength resonance. In this way the optimum combination of ferrite beads could be found.

7.3.2 Alternatives to Coaxial Cable Baluns

One problem with the transmission line baluns used in this thesis is that they are difficult to manufacture and assemble reliably. As each balun is assembled by hand, the quality of the assembly is variable and it can be difficult to find faults in the balun once the whole PA has been assembled.

Planar baluns can be manufactured more reliably, but in general these do not perform as well as coaxial cable baluns. This largely stems from the fact that the inner transmission line is no longer shielded from the ground plane, as happens in the coaxial cable case. A vertical balun design, an example of which is shown in Fig. 7.10, could

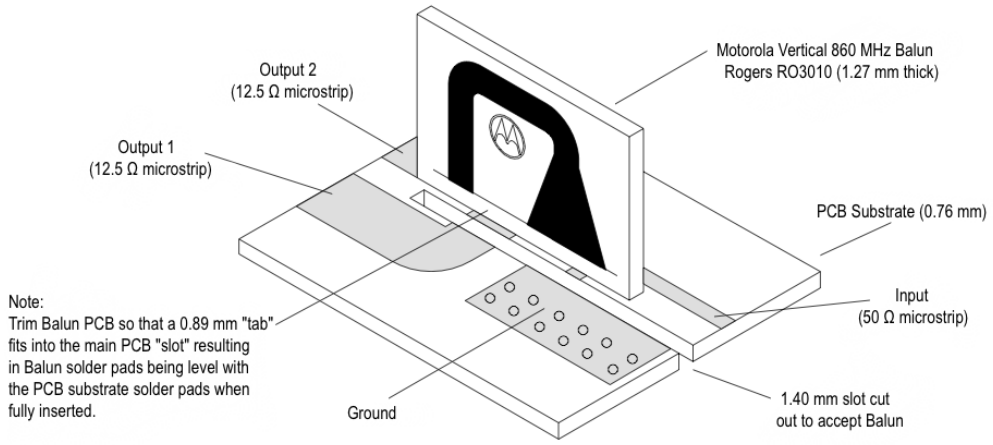

Figure 7.10: Example of vertical balun (adapted from [78])

be used to partially resolve this problem by moving the inner conductor further from the ground plane. It would also reduce the overall circuit board area, but is less practical than a standard horizontal planar balun.

7.3.3 Continuous Push-Pull Mode

The time-domain waveforms relating to the mode of operation inside a microwave push-pull power amplifier were presented in Chapter 4. However, this work was based on an ideal microwave transmission line balun, which presents an open circuit to even-order harmonics and a resistance to odd-order harmonics. However, as has been previously recognised, this does not account for the fact that C_{DS} and other reactances will shift these impedances away from their theoretical values. Refinements to the existing theory could lead to better understanding of microwave push-pull amplifiers, and ultimately to better designs. The voltage waveform formulations can be extended to account for a reactive element in the second harmonic;

$$V(\omega t) = (1 + \alpha\cos(\omega t))^2(1 + \beta\cos(\omega t))(1 - \lambda\sin(\omega t)) \tag{7.1}$$

By introducing an extra term in the voltage expression, a continuous version of the push-pull waveform expression is formed, shown in (7.1). The resulting waveforms for different values of λ are shown in Fig. 7.11. In the same way as the Class JB continuum and the continuous Class F mode, a reactive component is added to the fundamental impedance to compensate for a second harmonic reactance of opposite sign. As with the other continuous modes, all the waveforms shown in Fig. 7.11 have the same output power and efficiency.

The continuous push-pull concept has not been verified either through simulation or measurement, and this would be required to validate the preliminary extension to the

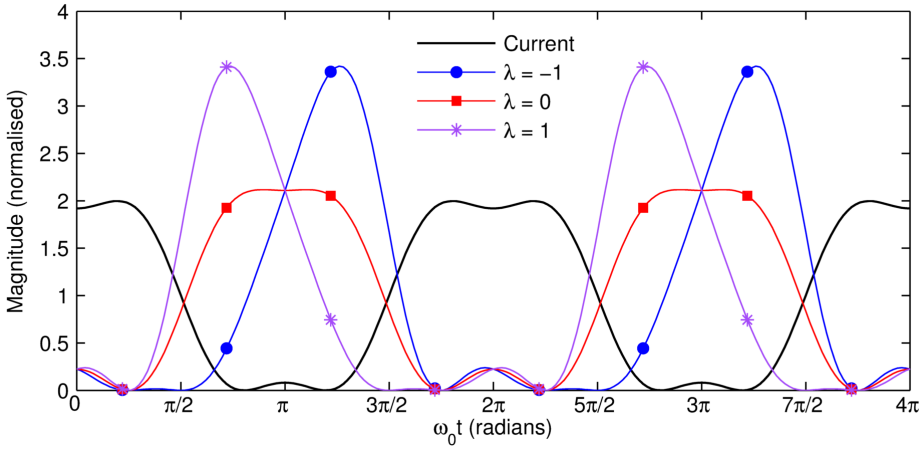

Figure 7.11: 'Continuous' push-pull mode voltage and current waveforms

theory presented. However, this is an exciting extension to the basic push-pull mode theory, and also serves to demonstrate another application for the continuous modes of operation.

7.3.4 Higher Power PAs and Impedance Transforming Baluns

The push-pull configuration was used to investigate multi-octave bandwidth applications, but its 4:1 impedance advantage can also be utilised for narrow-band applications, especially where high-power transistors are to be used. In narrower band applications, there is the possibility of combining the impedance-transforming advantages of the push-pull topology with Doherty or envelope tracking techniques to improve back-off efficiency, or with the balanced amplifier configuration for improved return loss and additional power combining.

As outlined in Chapter 1, high output powers are desirable for a number of reasons. For communications systems, the increased signal power improves SNR and hence data capacity, and for radar and jamming systems the increased signal power increases effective range. The main challenge in developing higher power amplifiers is matching to the low optimum impedances of high-power transistors.

Impedance-transforming transmission line baluns, based on the quarter-wave transformer, were discussed in Chapter 3. It was seen that higher impedance transformation ratios were possible, albeit with a greatly reduced bandwidth. Another possible approach is to investigate 'Guanella' baluns, based on the classic 1944 paper [79]. The essence of the technique is to combine a number of transformer 'building blocks' so as to increase the overall transformation ratio. Each 'building block' is a basic 1:1 balun (or 2:1, depending on the position of ground at the balanced port). These building blocks are connected in series at the unbalanced end of the balun and in parallel at the balanced

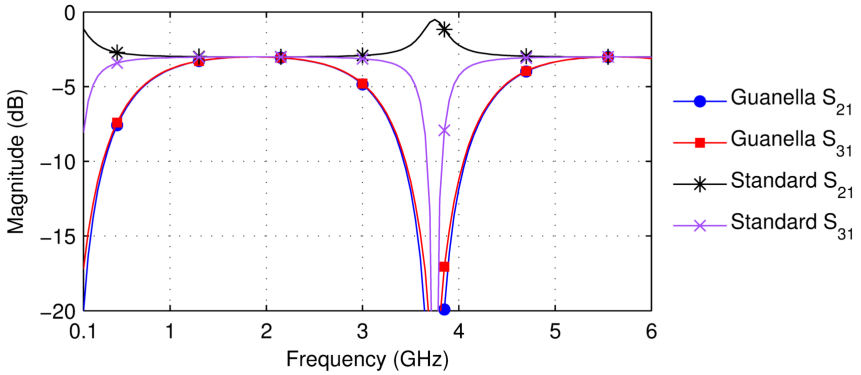

Figure 7.12: Guanella 8:1 balun compared to 'standard' 2:1 balun

end of the balun.

Figure 7.12 shows that the bandwidth of a simulated Guanella balun is reduced compared to the 'standard' transmission line balun considered in the rest of the thesis. However, its bandwidth is significantly wider than that of the quarter-wave impedance-transforming baluns of Chapter 3, and its impedance transformation ratio is 8:1, compared to 2:1 for the standard transmission line balun. Assuming a 50 Ω external impedance environment, this balun would potentially be suitable for matching to transistors with an optimum impedance of 6.25 Ω. This would allow the concepts presented in this thesis to be extended to higher power levels through the use of larger transistors.

As well as developing higher power amplifiers using GaN, another advantage in developing baluns with higher transformation ratios is to enable the use of different semiconductor materials, such as LDMOS, which have lower optimum impedances for the same output power compared to GaN. The implementation of push-pull power amplifiers using LDMOS transistors would yield significant cost savings.

It would also be interesting to investigate whether ferrite materials could be used to extend the bandwidth of Guanella impedance transforming baluns using the same design methodology presented in Chapter 3 for 'standard' coaxial cable transmission line baluns.

7.3.5 Amplitude Balance and Voltage Probing Measurements

The measurement system for making amplitude balance and voltage probing measurements was described in Chapter 5, along with preliminary results. These initial investigations could be taken forward to develop a powerful methodology for understanding microwave push-pull power amplifier operation. Initial measurements showed that performance improvements could be realised by setting the optimum amplitude balance, and that voltage probing measurements could be used to study the behaviour of the amplifiers.

The primary focus for further amplitude balance work would be to establish whether there is a correlation between the optimum amplitude balance and frequency, as initial measurements were only made at a small number of widely spaced frequency points. This data could be used to improve the design of the matching networks or baluns, or to provide motivation for the development of an active amplitude balance control system.

Follow-on work could also investigate the relationship between optimum phase balance and frequency, and how tuning the phase balance could improve the performance of the amplifier.

A voltage probe, whether in the form of a simple voltage divider or an electric field probe, could provide valuable insight into optimum amplitude and phase balances through waveform analysis. Identifying why a particular amplitude or phase balance value results in the highest performance would be useful for the designer. It should be noted that it would be necessary to develop a robust calibration procedure for the voltage probe before detailed analysis of the time-domain waveforms would be possible.

The ability to measure voltages would also be useful for verifying the push-pull mode of operation theory introduced in Chapter 4, and could be combined with future work into the 'continuous push-pull mode' discussed in Section 7.3.3. It may also be of interest to study the waveforms' harmonic content to provide further insight.

7.4 Chapter Summary

The push-pull topology provides many opportunities for future work, some of which are ongoing at the time of writing.

The simulations of push-pull PA v3 show the advantages of the chip-and-wire assembly, and also highlight a potential new opportunity to better understand push-pull operation at microwave frequencies over significant bandwidths.

There are many other opportunities for future research across all the areas covered in this thesis. Further ferrite material investigations and alternative balun designs could yield significant performance improvements. The continuous push-pull mode has been introduced, and the potential for using impedance-transforming baluns to achieve higher power levels has been outlined. Finally, it is suggested that amplitude and phase balance measurements and time-domain voltage-probing measurements could be used to further extend knowledge of push-pull operation at microwave frequencies.

It has been shown in this chapter how the work presented in this thesis may be continued and expanded upon, and it is hoped that valuable research could develop from these suggestions.

References

[1] Oxford English Dictionary Online, "microwave, n. and adj." in *Oxford English Dictionary*. Oxford University Press, 2013 (accessed August 28, 2013), http://www.oed.com/view/Entry/118111?rskey=hQVY5E&result=1.

[2] *3GPP TS 36.101 E-UTRA: User Equipment (UE) radio transmission and reception*, 3GPP Std.

[3] Agilent Technologies, "Agilent 2-Port and 4-Port PNA-X Network Analyzer N5242A datasheet," Datasheet, June 2010.

[4] S. C. Cripps, *RF Power Amplifiers for Wireless Communications*, 2nd ed. Artech House Publishers, 2006.

[5] S. Maas, *Nonlinear Microwave and RF Circuits*, 2nd ed. Artech House Publishers, 2003.

[6] S. C. Cripps, *Advanced Techniques in RF Power Amplifier Design*. Artech House Publishers, 2002.

[7] P. J. Tasker, "Practical waveform engineering," *Microwave Magazine, IEEE*, vol. 10, no. 7, pp. 65–76, Dec. 2009.

[8] F. Raab, "Maximum efficiency and output of class-F power amplifiers," *Microwave Theory and Techniques, IEEE Transactions on*, vol. 49, no. 6, pp. 1162–1166, Jun 2001.

[9] C. Bowick, *RF Circuit Design*. Newnes, 1982.

[10] S. C. Cripps, "A theory for the prediction of GaAs FET load-pull power contours," in *Microwave Symposium Digest, 1983 IEEE MTT-S International*, June 1983, pp. 221 – 223.

[11] H. W. Bode, *Network Analysis and Feedback Amplifier Design*. Van Nostrand, New York, 1945.

[12] R. M. Fano, "Theoretical limitations on the broadband matching of arbitrary impedances," Massachusetts Institute of Technology, Tech. Rep., January 1948.

[13] P. Wright, J. Lees, P. J. Tasker, J. Benedikt, and S. C. Cripps, "An efficient, linear, broadband Class-J-mode PA realised using RF waveform engineering," in *International Microwave Symposium*, 2009, pp. 653 – 656.

[14] S. Cripps, P. Tasker, A. Clarke, J. Lees, and J. Benedikt, "On the continuity of high efficiency modes in linear RF power amplifiers," *Microwave and Wireless Components Letters, IEEE*, vol. 19, no. 10, pp. 665–667, Oct. 2009.

[15] V. Carrubba, J. Lees, J. Benedikt, P. J. Tasker, and S. C. Cripps, "A novel highly efficient broadband continuous class-F RFPA delivering 74% average efficiency for an octave bandwidth," in *Microwave Symposium Digest (MTT), 2011 IEEE MTT-S International*, June 2011, pp. 1 – 4.

[16] V. Carrubba, A. L. Clarke, M. Akmal, J. Lees, J. Benedikt, P. J. Tasker, and S. C. Cripps, "On the extension of the continuous class-F mode power amplifiers," *IEEE Transactions on Microwave Theory and Techniques*, vol. 59, pp. 1294–1303, 2011.

[17] V. Carrubba, "Novel highly efficient broadband continuous power amplifier modes," PhD thesis, Centre for High Frequency Engineering, School of Engineering, Cardiff University, 2012.

[18] J. L. B. Walker, Ed., *Handbook of RF and Microwave Power Amplifiers*. Cambridge University Press, 2012.

[19] R. Pengelly, S. Wood, J. Milligan, S. Sheppard, and W. Pribble, "A review of GaN on SiC high electron-mobility power transistors and MMICs," *Microwave Theory and Techniques, IEEE Transactions on*, vol. 60, no. 6, pp. 1764 –1783, June 2012.

[20] Y.-F. Wu, A. Saxler, M. Moore, R. Smith, S. Sheppard, P. Chavarkar, T. Wisleder, U. Mishra, and P. Parikh, "30-W/mm GaN HEMTs by field plate optimization," *Electron Device Letters, IEEE*, vol. 25, no. 3, pp. 117 – 119, March 2004.

[21] P. H. Aaen, J. A. Plá, and J. Wood, *Modeling and Characterization of RF and Microwave FETs*. Cambridge University Press, 2007.

[22] C. Campbell, A. Balistreri, M. Kao, D. Dumka, and J. Hitt, "GaN takes the lead," *Microwave Magazine, IEEE*, vol. 13, no. 6, pp. 44 –53, Sept.-Oct. 2012.

[23] J. Lees, J. Benedikt, K. Hilton, J. Powell, R. Balmer, M. Uren, T. Martin, and P. Tasker, "Experimental gallium nitride microwave Doherty amplifier," *Electronics Letters*, vol. 41, no. 23, pp. 1284–1285, Nov. 2005.

[24] C. Campbell, C. Lee, V. Williams, M.-Y. Kao, H.-Q. Tserng, P. Saunier, and T. Balisteri, "A wideband power amplifier MMIC utilizing GaN on SiC HEMT technology," *Solid-State Circuits, IEEE Journal of*, vol. 44, no. 10, pp. 2640–2647, Oct. 2009.

[25] D. Meharry, R. Lender, K. Chu, L. Gunter, and K. Beech, "Multi-Watt wideband MMICs in GaN and GaAs," in *Microwave Symposium, 2007. IEEE/MTT-S International*, June 2007, pp. 631–634.

[26] S. Lin, M. Eron, and A. Fathy, "Development of ultra wideband, high efficiency, distributed power amplifiers using discrete GaN HEMTs," *Circuits, Devices & Systems, IET*, vol. 3, no. 3, pp. 135 –142, June 2009.

[27] K. Kobayashi, Y. Chen, I. Smorchkova, B. Heying, W.-B. Luo, W. Sutton, M. Wojtowicz, and A. Oki, "Multi-decade GaN HEMT cascode-distributed power amplifier with baseband performance," in *Radio Frequency Integrated Circuits Symposium, 2009. RFIC 2009. IEEE*, June 2009, pp. 369 –372.

[28] D. M. Pozar, *Microwave Engineering*. Wiley, New York, 2005.

[29] R. Pengelly, "Application of feedback techniques to the realisation of hybrid and monolithic broadband low-noise-and-power GaAs FET amplifiers," *Electronics Letters*, vol. 17, no. 21, pp. 798 –799, Oct. 1981.

[30] J. L. B. Walker, Ed., *Classic Works in RF Engineering: Combiners, Couplers, Transformers and Magnetic Materials*. Artech House Publishers, 2005.

[31] Krytar, "Model 3005070 datasheet," Datasheet, 2012.

[32] Krytar "Model 1831 datasheet," Datasheet, 2012.

[33] J. Kuhn, F. van Raay, R. Quay, R. Kiefer, W. Bronner, M. Seelmann-Eggebert, M. Schlechtweg, M. Mikulla, O. Ambacher, and M. Thumm, "Balanced microstrip AlGaN/GaN HEMT power amplifier MMIC for X-band applications," in *Microwave Integrated Circuit Conference, 2008. EuMIC 2008. European*, Oct. 2008, pp. 95 – 98.

[34] H. Le, Y.-C. Shih, V. Hwang, T. Chi, K. Kasel, and D. Wang, "An X-band high-efficiency MMIC power amplifier with 20-dB return losses," *Solid-State Circuits, IEEE Journal of*, vol. 26, no. 10, pp. 1383 –1389, Oct. 1991.

[35] S. C. Cripps, "Pulling power [microwave bytes]," *Microwave Magazine, IEEE*, vol. 11, no. 4, June 2010.

[36] C. M. Andersson, J. Moon, C. Fager, B. Kim, and N. Rorsman, "Decade bandwidth high efficiency GaN HEMT power amplifier designed with resistive harmonic loading," in *Microwave Symposium Digest (MTT), 2012 IEEE MTT-S International*, June 2012, pp. 1 –3.

[37] K. Krishnamurthy, T. Driver, R. Vetury, and J. Martin, "100 W GaN HEMT power amplifier module with $>$ 60% efficiency over 100-1000 MHz bandwidth," in *Microwave Symposium Digest (MTT), 2010 IEEE MTT-S International*, May 2010, pp. 940 –943.

[38] K. Krishnamurthy, J. Martin, D. Aichele, and D. Runton, "A decade bandwidth 90 W GaN HEMT push-pull power amplifier for VHF / UHF applications," in *Compound Semiconductor Integrated Circuit Symposium (CSICS), 2011 IEEE*, Oct. 2011, pp. 1 –4.

[39] L. Bacque, P. Bouysse, W. Rebernak, C. Poumier, L. Lapierre, G. Nanfack-Nkondem, G. Neveux, D. Barataud, and R. Quere, "High-current high-speed dynamic bias control system applied to a 100-W wideband push-pull amplifiers," *Microwave Theory and Techniques, IEEE Transactions on*, vol. 56, no. 12, pp. 2798 –2807, Dec. 2008.

[40] J. Sim, J. Lim, M. Park, S.-W. Seo, and B.-I. Mah, "A 100Watt ultra-broadband power amplifier using silicon LDMOSFETs," in *Microwave Conference Proceedings (APMC), 2010 Asia-Pacific*, Dec. 2010, pp. 418 –421.

[41] J. Cho, K. Lim, S. You, M. Seo, K. Kim, J. Sim, M. Park, and Y. Yang, "Design of a 100 Watt high-efficiency power amplifier for the 10-500MHz band," in *Microwave Conference, 2009. APMC 2009. Asia Pacific*, 2009, pp. 285 –288.

[42] A. Ezzeddine and H. Huang, "10W ultra-broadband power amplifiers," in *Microwave Symposium Digest, 2008 IEEE MTT-S International*, 2008, pp. 643 –646.

[43] K. Krishnamurthy, D. Lieu, R. Vetury, and J. Martin, "A 0.1-1.8 GHz, 100 W GaN HEMT power amplifier module," in *Compound Semiconductor Integrated Circuit Symposium (CSICS), 2010 IEEE*, Oct. 2010, pp. 1 –4.

[44] J.-W. Lee, L. Eastman, and K. Webb, "A gallium-nitride push-pull microwave power amplifier," *Microwave Theory and Techniques, IEEE Transactions on*, vol. 51, no. 11, pp. 2243 – 2249, Nov. 2003.

[45] J.-W. Lee and K. Webb, "Broadband GaN HEMT push-pull microwave power amplifier," *Microwave and Wireless Components Letters, IEEE*, vol. 11, no. 9, pp. 367 –369, Sept. 2001.

[46] A. Chen, A. Pham, and R. Leoni, "A 6-18 GHz push-pull power amplifier with wideband even-order distortion cancellation in LCP module," in *Microwave Symposium, 2007. IEEE/MTT-S International*, June 2007, pp. 1079 –1082.

[47] I. Takenaka, K. Ishikura, H. Takahashi, K. Asano, J. Morikawa, K. Satou, K. Kishi, K. Hasegawa, K. Tokunaga, F. Emori, and M. Kuzuhara, "L/S-band 140-W push-pull power AlGaAs/GaAs HFETs for digital cellular base stations," *Solid-State Circuits, IEEE Journal of*, vol. 34, no. 9, pp. 1181 –1187, Sep 1999.

[48] A. Stameroff, A.-V. Pham, and R. Leoni, "High efficiency push-pull inverse class F power amplifier using a balun and harmonic trap waveform shaping network," in *Microwave Symposium Digest (MTT), 2010 IEEE MTT-S International*, May 2010, pp. 521 –525.

[49] A. Stameroff and A.-V. Pham, "Wide bandwidth inverse class F power amplifier with novel balun harmonic matching network," in *Microwave Symposium Digest (MTT), 2012 IEEE MTT-S International*, June 2012, pp. 1 –3.

[50] H. T. Jeong, M. H. Yeon, S. W. Kim, and I. S. Chang, "Design of the Doherty amplifier with push-pull structure using balun transformer," in *Microwave Symposium Digest, 2004 IEEE MTT-S International*, vol. 2, June 2004, pp. 851 – 854 Vol.2.

[51] J. Sevick, *Transmission Line Transformers*, 3rd ed. Noble Publishing, Atlanta, 1996.

[52] A. Riddle, "Ferrite and wire baluns with under 1 dB loss to 2.5 GHz," in *Microwave Symposium Digest, 1998 IEEE MTT-S International*, vol. 2, Jun. 1998, pp. 617 – 620 vol.2.

[53] E. C. Snelling, *Soft Ferrites - Properties and Applications*. Butterworth, Boston MA, 1988.

[54] G. Hofbauer, "An ultra-wideband microwave balun using a tapered coaxial coil structure working from kHz range to beyond 26.5 GHz," in *Microwave Symposium Digest, 2005 IEEE MTT-S International*, June 2005.

[55] A. Chen, A.-V. Pham, and I. Leoni, R.E., "Development of low-loss broad-band planar baluns using multilayered organic thin films," *Microwave Theory and Techniques, IEEE Transactions on*, vol. 53, no. 11, pp. 3648 – 3655, Nov. 2005.

[56] J. Horn and G. Boeck, "An ultra broadband ferriteless planar transmission line transformer," in *Microwave Conference, 2003. 33rd European*, vol. 2, 2003, pp. 551 – 553.

[57] F. Raab, "Model for the low-frequency performance of ferrite-loaded balun transformers," in *Microwave Symposium, 2007. IEEE/MTT-S International*, June 2007, pp. 7 –10.

[58] P. Gomez-Jimenez, P. Otero, and E. Marquez-Segura, "Analysis and design procedure of transmission-line transformers," *Microwave Theory and Techniques, IEEE Transactions on*, vol. 56, no. 1, pp. 163 –171, Jan. 2008.

[59] N. Marchand, "Transmission line conversion transformers," *Electronics*, vol. 17, pp. 142 – 145, 1944.

[60] G. Oltman, "The compensated balun," *Microwave Theory and Techniques, IEEE Transactions on*, vol. 14, no. 3, pp. 112 – 119, Mar. 1966.

[61] W. Roberts, "A new wide-band balun," *Proceedings of the IRE*, vol. 45, no. 12, pp. 1628 –1631, Dec. 1957.

[62] H. Ta, A. Stameroff, and A.-V. Pham, "Development of a defected ground structure wide bandwidth balun on multilayer organic substrate," in *Microwave Conference Proceedings (APMC), 2010 Asia-Pacific*, Dec. 2010, pp. 1641 –1644.

[63] R. M. Smith, J. Lees, P. J. Tasker, J. Benedikt, and S. C. Cripps, "A design methodology for the realization of multi-decade baluns at microwave frequencies," in *Microwave Symposium Digest (MTT), 2011 IEEE MTT-S International*, 2011.

[64] D. Jiles, *Introduction to Magnetism and Magnetic Materials*, 2nd ed. Chapman & Hall, 1998.

[65] R. M. Smith, J. Lees, P. J. Tasker, J. Benedikt, and S. C. Cripps, "A novel formulation for high efficiency modes in push-pull power amplifiers using transmission line baluns," *Microwave and Wireless Components Letters, IEEE*, vol. 22, no. 5, pp. 257 – 259, May 2012.

[66] J. Benedikt, R. Gaddi, P. J. Tasker, and M. Goss, "High-power time-domain measurement system with active harmonic load-pull for high-efficiency base-station amplifier design," *Microwave Theory and Techniques, IEEE Transactions on*, vol. 48, no. 12, pp. 2617–2624, Dec 2000.

[67] D. J. Williams, "Non-linear measurement system and techniques for RF power amplifier design," PhD thesis, Centre for High Frequency Engineering, School of Engineering, Cardiff University, September 2003.

[68] Z. Aboush, J. Lees, J. Benedikt, and P. J. Tasker, "Active harmonic load-pull system for characterizing highly mismatched high power transistors," in *Microwave Symposium Digest, 2005 IEEE MTT-S International*, June 2005, pp. 1311 – 1314.

[69] A. Sheikh, P. J. Tasker, J. Lees, and J. Benedikt, "The impact of system impedance on the characterization of high power devices," in *Microwave Conference, 2007. European*, 2007, pp. 949–952.

[70] M. Hiebel, *Fundamentals of Vector Network Analysis*, 5th ed. Rohde & Schwarz, 2011.

[71] P. Wright, "Development of novel design methodologies for the efficiency enhancement of RF power amplifiers in wireless communications," PhD thesis, Centre for High Frequency Engineering, School of Engineering, Cardiff University, September 2010.

[72] R. M. Smith, J. Lees, P. J. Tasker, J. Benedikt, and S. C. Cripps, "A 40W push-pull power amplifier for high efficiency, decade bandwidth applications at microwave frequencies," in *Microwave Symposium Digest (MTT), 2012 IEEE MTT-S International*, June 2012, pp. 1 – 3.

[73] R. M. Smith and S. C. Cripps, "Broadband push-pull power amplifier design at microwave frequencies," in *Automated RF and Microwave Measurement Society Conference*, April 2013.

[74] Z. Yusoff, J. Lees, J. Benedikt, P. Tasker, and S. Cripps, "Linearity improvement in RF power amplifier system using integrated Auxiliary Envelope Tracking system," in *Microwave Symposium Digest (MTT), 2011 IEEE MTT-S International*, 2011, pp. 1 – 4.

[75] "Coaxial cable: Semi-flex & semi-rigid," AtlanTec RF, Datasheet.

[76] D. Bockelman and W. Eisenstadt, "Combined differential and common-mode scattering parameters: theory and simulation," *Microwave Theory and Techniques, IEEE Transactions on*, vol. 43, no. 7, pp. 1530 – 1539, July 1995.

[77] N. Dehghan, S. Cripps, A. Porch, and J. Lees, "An improved electric field probe with applications in high efficiency PA design and diagnostics," in *81st ARFTG Microwave Measurement Conference*, June 2013, pp. 38 – 41.

[78] "RF Power Field-Effect Transistor," Freescale Semiconductor, Technical Data MRF374A, May 2006, rev. 5.

[79] G. Guanella, "New method of impedance matching in radio-frequency circuits," *Brown-Boveri Review*, vol. 31, pp. 327–329, Sept. 1944.

[80] *IEEE Standard Letter Designations for Radar-Frequency Bands*, IEEE Aerospace & Electronic Systems Society Std. 521, 2002.

Appendix A

'A Design Methodology for the Realization of Multi-Decade Baluns at Microwave Frequencies'

R. M. Smith, J. Lees, P. J. Tasker, J. Benedikt, and S. C. Cripps

IEEE MTT-S International Microwave Symposium 2011

June 2011, Baltimore, MD, USA

A Design Methodology for the Realization of Multi-Decade Baluns at Microwave Frequencies

R. M. Smith, J. Lees, P. J. Tasker, J. Benedikt and S. C. Cripps

Centre for High Frequency Engineering, Cardiff University, Cardiff, CF24 3AA, U.K.

Email: smithrm3@cardiff.ac.uk

***Abstract* — A new methodology is presented for designing baluns exhibiting multi-decade bandwidths at microwave frequencies. Simulations show that resistors terminating the outer transmission line suppress the half-wavelength resonance and greatly extend the bandwidth. Using linear measurements at microwave frequencies, ferrite beads have been shown to behave as resistors with a small reactance, suitable for terminating the outer transmission line. This paper shows that ferrite beads can perform the dual role of improving magnetic coupling at low frequency and suppressing resonance at higher frequencies. The design methodology was applied to produce a balun that operates between 30MHz and 6GHz, displays less than 1dB of power loss up to 4.4GHz, and delivers an impedance transformation of 2:1.**

***Index Terms* — Broadband amplifiers, design methodology, ferrites, impedance matching, transmission lines, wideband.**

I. Introduction

This paper describes the design and realization of an ultra-broadband balun, spanning more than two decades of bandwidth with low loss and a resonance-free flat frequency response. A key element in this work has been the evolution of an *a priori* design methodology, based on detailed measurement and understanding of the function of the ferrite elements in the final structure.

Baluns are used for a range of applications including push-pull amplifiers, balanced mixers and antenna feeds. One of three primary functions of the balun is to convert an unbalanced signal to a balanced signal (or vice versa). The second is a 2:1 impedance transformation, and the third is a suppression of even-mode signals.

Up to VHF frequencies, baluns make use of inductive coupling between wires, and ferrite materials are widely used to improve this coupling. However, most ferrite materials display rapidly decreasing real permeability at 100MHz and above [1], and therefore above this frequency baluns are based on the properties of transmission lines.

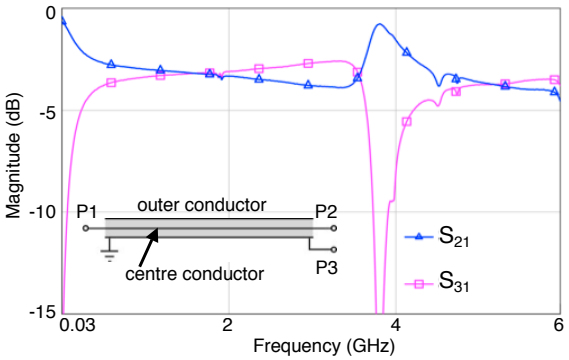

Fig. 1. Typical frequency response of a ferrite-less coaxial cable balun.

The transmission line properties force the voltage difference across the inner and outer conductor to remain constant along its length, so that a differential voltage appears across the balanced termination at the remote end. This structure has two bandwidth limitations. Firstly, the outer conductor forms a short-circuited stub with the ground plane, causing mid-band resonances, and secondly it appears as a short circuit on the unbalanced input at the lower end of the frequency band. The frequency response of a typical coaxial-cable balun is shown in Fig. 1.

The use of ferrimagnetic materials to improve the low frequency performance of transmission line baluns is widespread and described in [2]-[3]. A model for the ferrite-loaded balun at low frequencies is presented in [4]. At low frequencies, multi-octave bandwidths can be achieved through the use of ferrite materials [5], however the decreasing inductance of these materials greatly reduces the effectiveness of this technique at microwave frequencies. For some ultra-broadband baluns the ground plane is required to be as far away from the structure as possible for optimum performance [6], limiting the practical use of the device.

In this paper, a novel design methodology for ultra-broadband, low-loss baluns is presented. The low-frequency performance and resonance problems are overcome, and because the ground plane is integrated into the structure the balun is suitable for use in practical applications. The constructed balun exhibits low power loss and constant phase imbalance through a bandwidth of 30MHz to 6GHz.

II. Balun Modeling

The transmission line balun is modeled by the circuit shown in Fig. 2. It comprises two parallel transmission lines; one is formed between the centre and the outer conductors of the coaxial cable, the other between the outer conductor and the ground plane. The outer transmission line resonates at the half-wavelength frequency, limiting the bandwidth. Increasing the characteristic impedance of the outer transmission line, Z_{OUTER}, reduces the amplitude imbalance between the balanced

978-1-61284-757-3/11/$26.00 C2011 IEEE

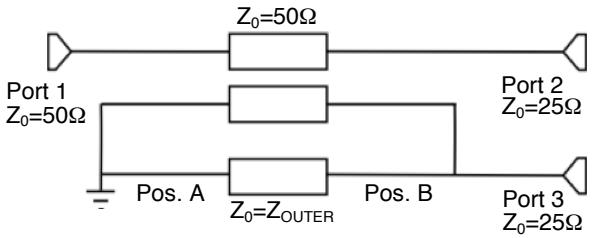

Fig. 2. Circuit model of a coaxial cable balun.

ports. For non-ferrite baluns, a higher Z_{OUTER} also increases the Q-factor of the resonance and hence increases the bandwidth.

The key innovation in this work is the introduction of a terminating resistor at the unbalanced end of the outer transmission line (position A in Fig. 2). Fig. 3 shows that when the resistance is equal to the characteristic impedance of the outer transmission line (Z_{OUTER}) the resonance is eliminated entirely and a flat insertion loss is achieved over multiple decades.

It should be noted that introducing resistance at the unbalanced end of the outer transmission line increases amplitude imbalance between the balanced ports. Additional resistance can be added at the balanced end of the outer transmission line (position B in Fig. 2) to increase the shunt impedance terminations across Ports 2 and 3 and reduce this imbalance. According to simulation, the resistance at position B should be as high as possible to reduce amplitude imbalance.

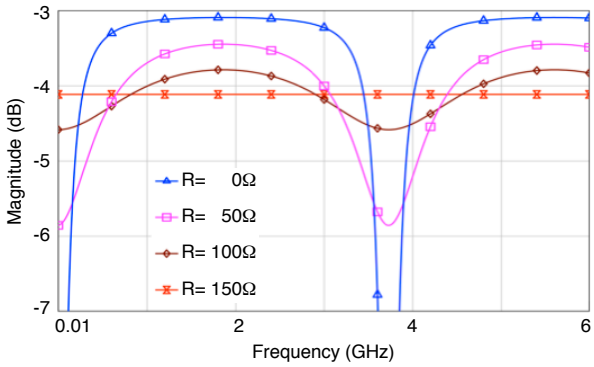

Fig. 3. Effect of resistor at the unbalanced end of the outer transmission line (Z_{OUTER}=150Ω).

III. Measurements

A. Ferrite Measurements

In this section we show that the terminating resistor can be realized in practice using a ferrite bead. Manufacturer data is readily available on ferrites up to 100MHz or 1GHz, but is rarely, if ever, available for higher frequencies. In this section we show that simple 2-port S-parameter measurements using a

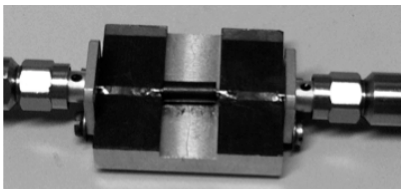

Fig. 4. Test fixture for measuring ferrite beads.

Vector Network Analyzer (VNA) can be used to characterize ferrite beads well into the GHz range. Fig. 4 shows the measurement configuration, which is a single bead placed on a single piece of wire having the same length as the bead, a so-called "bead-on-lead". It should be noted that due to the measurement configuration, 50Ω should be subtracted from the measured value to obtain the bead's true resistance.

S-parameter measurements were made between 30MHz and 6GHz on several beads made from Fair-Rite NiZn #61-material. As Fig. 5 shows, the inductive properties of the ferrite bead decrease, and essentially vanish, at higher frequencies. This shows that the imaginary permeability, which manifests itself as a resistance, becomes much higher than the real permeability at microwave frequencies. As noted in [4], the reactance becomes capacitive at the higher end of the frequency range. Crucially, these measurements show that at higher frequencies the bead-on-lead behaves like a resistance with a small series resonant reactance.

The measured resistances can be used to select the most appropriate ferrite bead for a given characteristic impedance. We consider this use of a ferrite bead as a terminating resistor, rather than as a high permeability core to boost even mode impedance, to be an entirely novel aspect of this work.

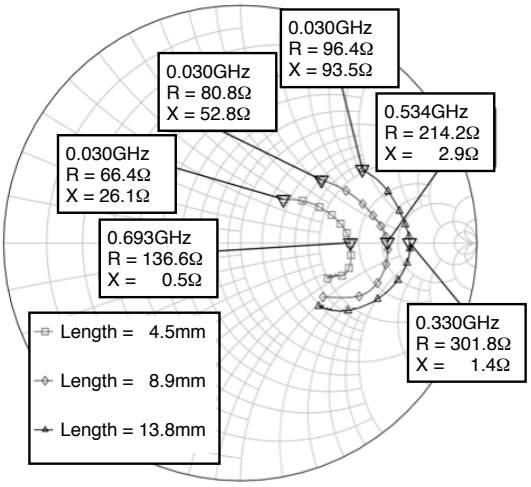

Fig. 5. Frequency response of three #61-material 'beads-on-leads' of different lengths between 30MHz and 6GHz.

978-1-61284-757-3/11/$26.00 C2011 IEEE

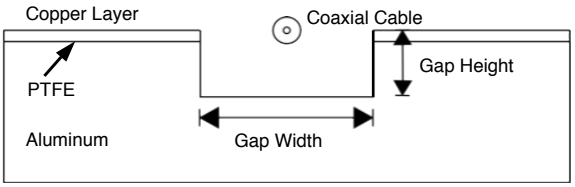

Fig. 6. Cross-section of coaxial cable test fixture and balun.

B. Coaxial Cable Measurements

The test fixture, shown in Fig. 6, was constructed from Rogers PTFE circuit board backed with a thick layer of aluminum. By milling a gap in the aluminum layer, the characteristic impedance between the outer conductor of the coaxial cable and the ground plane could be set. Two-port S-parameter measurements were made to test the effect of varying width and depth on Z_{OUTER}. Using (1), Z_{OUTER} was calculated from the measured value,

$$Z_{OUTER} = \sqrt{Z_{measured} \cdot Z_{load}} \,. \qquad (1)$$

TABLE I
Z_{OUTER} FOR GAP WIDTH OF 7.5MM

	Outer Coaxial Cable Diameter	
Gap Depth	0.86mm	1.19mm
2mm	136Ω	116Ω
3mm	157Ω	137Ω

Table I shows that thinner coaxial cable and greater test fixture depth result in a higher characteristic impedance of the 'outer' transmission line. As mentioned earlier, increased characteristic impedance (Z_{OUTER}) decreases balanced port amplitude imbalance. These measurements show that a trade-off is needed between test fixture size and balun power loss, which increases for smaller coaxial cable diameters.

IV. DESIGN METHODOLOGY

The ferrite and coaxial cable measurements described in the previous section are now used in a design procedure to increase the usable bandwidth of a coaxial-cable balun to multiple decades. To verify this design procedure a balun was constructed with a target frequency range of 30MHz to 6GHz, a greater than double-decade bandwidth. The assumption made in the design methodology is that that commercial off-the-shelf (COTS) ferrite beads and coaxial cable are used. The balun was constructed using the same method as the coaxial cable test fixture in the previous section, shown in Fig. 6.

The first stage in the design is to select the coaxial cable diameter and length. Transmission line properties, on which the fundamental operation of this design depends, require that the length of cable should be a substantial fraction of a wavelength. A longer cable therefore exhibits better low frequency performance, but the longer length increases the power loss. A trade-off can be made between low-frequency performance and loss when setting the cable length.

When selecting the coaxial cable diameter, measurements show that a trade-off must be made between Z_{OUTER} and power loss. Thicker coaxial cable exhibits less power loss but also requires a greater gap depth, and so a larger overall structure, to achieve the same value of Z_{OUTER}.

Once the cable diameter has been selected, Z_{OUTER} is set by the width and depth of the gap. Whilst a high value of Z_{OUTER} is preferable, as described earlier, a greater ferrite resistance is required to suppress the resonances, and with COTS components this requires series connection of the ferrite "resistors" which may limit the high-end performance. Simple 2D electromagnetic simulations can be used to calculate the required width and depth of the gap.

Using measurements made in the previous section, it is then possible to select ferrite beads to place at the unbalanced end of the outer transmission line and hence eliminate the resonance. The resonant frequency can be easily calculated from the cable's length, then a ferrite bead which satisfies the condition $R=Z_{OUTER}$ at that frequency can be chosen.

For the constructed balun, the resonant frequency was 3.75GHz and Z_{OUTER}=135Ω. Three ferrite beads, which as Fig. 7 shows have R=43Ω at 3.75GHz, were placed in series to give a combined resistance of 129Ω. The beads provide a terminating resistance approximately equal to Z_{OUTER}.

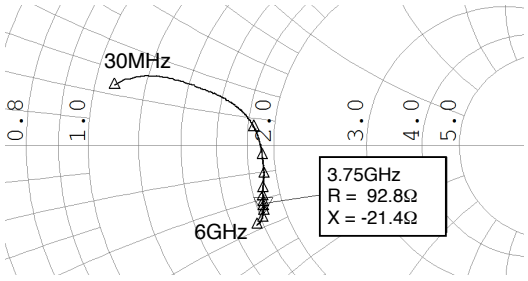

Fig. 7. Frequency response of #61-material bead used on balun.

V. BALUN MEASUREMENTS

The realized balun is shown in Fig. 8. Three-port S-parameter measurements were made on the constructed balun between 30MHz and 6GHz, with both balanced ports terminated into 25Ω. A resistance of 43Ω was used at the balanced end of the cable to increase the shunt impedance. Although simulations showed that making the balanced-end ferrite resistance as high as possible was beneficial, in practice it was found that doing this significantly increased the power loss at 3GHz and above.

Figs. 9 and 10 show the performance of the ferrite-loaded balun. Comparing Fig. 9 to Fig. 1, it should be noted that the resonance has been eliminated entirely, and the performance

978-1-61284-757-3/11/$26.00 C2011 IEEE

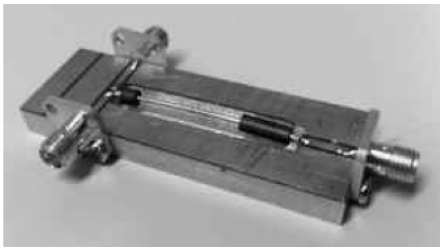

Fig. 8. Constructed balun including ferrite beads.

at the low-end of the band has been greatly improved. At UHF and below, it is clear the ferrite is still performing its 'traditional' role as an inductor. The insertion loss of the balun is relatively flat across the full 30MHz to 6GHz bandwidth. It is possible that the series connection of ferrite beads is diminishing the performance at higher frequencies, as mentioned in Section IV.

It should be noted that some of the insertion loss results from an uneven power split between the inner and outer transmission lines, and that this could be reduced by increasing Z_{OUTER}. This amplitude imbalance would not have been apparent if back-to-back measurements had been conducted, as is often the case in published balun measurements. In most practical applications, this imbalance can be compensated and has minimal impact on the final balanced performance. The power loss is less than 1dB up to 4.4GHz, and the balun remains usable up to 6GHz.

The balun when used in a push-pull amplifier would serve as a power combiner and matching network, giving an effective 2:1 impedance transformation over the entire bandwidth. Such a feat of matching would be impossible using conventional filter-style matching networks that are commonly used in GHz frequency amplifiers. Compared to parallel combining, this technique offers a 4:1 impedance advantage.

VI. Conclusion

A novel design procedure is presented for multi-decade coaxial cable baluns based on a new understanding of the dual role of ferrite beads. Measured beads are shown to act as series resistors at microwave frequencies, and so can be used to suppress resonances on the outer transmission line. At VHF and UHF, the established practice of using ferrite beads to improve magnetic coupling is used. Using this new design method, a balun was constructed that exhibits flat, low-loss performance between 30MHz and 6GHz. The power loss in the balun is less than 1dB up to 4.4GHz. The development of the balun opens up the possibility of a push-pull power amplifier operating over a bandwidth greater than two decades. Using detailed measurements and an understanding of the individual components of the balun, an *a priori* design methodology was developed.

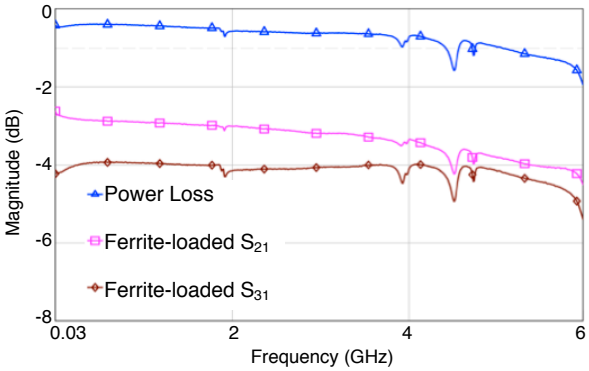

Fig. 9. Power loss, S_{21} and S_{31} of the ferrite-loaded balun.

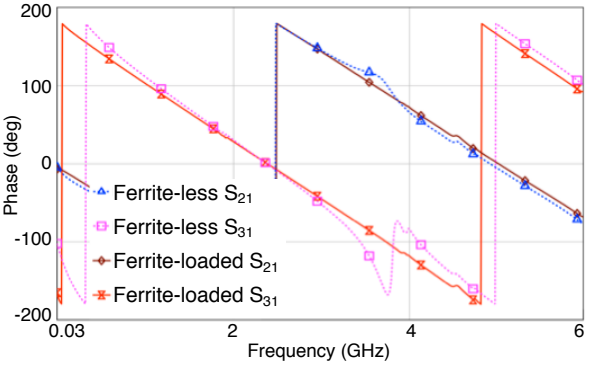

Fig. 10. Phase response of S_{21} and S_{31} for the ferrite-loaded balun (solid line) compared to the ferrite-less balun (dotted line).

Acknowledgement

The authors wish to thank Roke Manor Research Limited for sponsoring this work.

References

[1] E.C. Snelling, *Soft Ferrites: Properties and Applications*, 2nd ed, London: Butterworths, 1988.

[2] J. Horn, and G. Boeck, "Ultra broadband ferrite transmission line transformer," *2003 IEEE MTT-S Int. Microwave Symp. Dig.*, vol. 1, pp. 433-436, June 2003.

[3] K. Krishnamurthy, T. Driver, R. Ventury, and J. Martin, "100W GaN HEMT power amplifier module with >60% efficiency over 100-1000MHz bandwidth," *2010 IEEE MTT-S Int. Microwave Symp. Dig.*, pp. 940-943, June 2010.

[4] F. H. Raab, "Model for the low-frequency performance of ferrite-loaded balun transformers," *2007 IEEE MTT-S Int. Microwave Symp. Dig.*, pp. 7-10, June 2007.

[5] J. Sevick, *Transmission Line Transformers*, 3rd ed, Noble Publishing, 1996.

[6] G.A. Hofbauer, "An ultra-wideband microwave balun using a tapered coaxial coil structure working from kHz range to beyond 26.5GHz," *2005 IEEE MTT-S Int. Microwave Symp. Dig.*, vol. 4, pp. 551-554, June 2005.

978-1-61284-757-3/11/$26.00 C2011 IEEE

Appendix B

'A Novel Formulation for High Efficiency Modes in Push-Pull Power Amplifiers Using Transmission Line Baluns'

R. M. Smith, J. Lees, P. J. Tasker, J. Benedikt, and S. C. Cripps

IEEE Microwave and Wireless Components Letters

Vol. 22, no. 5, pp. 257 - 259, May 2012

A Novel Formulation for High Efficiency Modes in Push-Pull Power Amplifiers Using Transmission Line Baluns

Robert M. Smith, *Student Member, IEEE*, Jonathan Lees, Paul J. Tasker, *Senior Member, IEEE*, Johannes Benedikt, and Steve C. Cripps, *Fellow, IEEE*

***Abstract*—Push-pull power amplifiers (PAs) operating at HF through to GHz frequencies typically employ a transmission line balun structure. This letter demonstrates that their performance characteristics in high efficiency PA applications are critically different from conventional transformers. For the first time, the effect of the even-mode open-circuit termination on the output waveforms is measured. A novel mathematical formulation is proposed to describe the time-domain waveforms by defining the harmonic impedance environment in terms of odd and even mode excitation rather than tuned harmonics. Experimental verification using harmonic load-pull measurements showed good agreement with the theoretical waveforms generated from factorized waveform expressions.**

***Index Terms*—Balun, high-efficiency, load-pull, microwave amplifiers, power amplifiers (PAs), push-pull.**

I. Introduction

THIS letter outlines the general formulation for high-efficiency modes in a push-pull power amplifier (PA) that differ significantly from existing theory. Push-pull amplifiers employ a balun structure, either based on magnetic coupling or transmission line coupling. A simple transmission line balun (TLB) structure, based on a piece of coaxial cable, has the generic form shown in Fig. 1. A method of suppressing the half-wavelength resonance of such a balun, whilst minimizing the insertion loss [1], has made multi-decade microwave push-pull PAs a more realizable prospect.

The bandwidth potential of the push-pull configuration has been shown at lower frequencies through the use of magnetically coupled transformers [2], and at higher frequencies through transmission line baluns with harmonic traps to short-circuit the even harmonics [3]. At microwave frequencies, transmission line baluns are required due to the low-frequency nature of magnetically coupled transformers.

The use of transmission line baluns in the design of push-pull amplifiers will result in important differences when compared to the classical push-pull amplifier, in which two anti-phased half-wave rectified current waveforms are combined using a magnetically coupled balun transformer to form a complete sinusoid. Classical theory assumes that the even voltage harmonics at each device are shorted by the action of a center-tapped output transformer, but it is not clear whether this cancellation will still take place when the ideal transformers are substituted with TLBs.

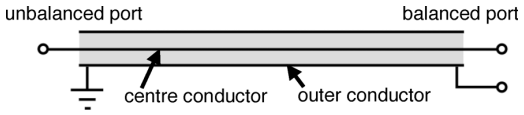

Fig. 1. Simple schematic of a coaxial cable transmission line balun.

The key property of the matched transmission line balun is that it maintains constant signal voltage amplitude along its length. Thus, if at one end the outer sheath is connected to a common ground point, and the remote end is connected to a balanced load with the centre tap returned to the common ground point, the voltage at the balanced end will be forced to be differential about ground. As a result, an odd-mode excitation at the balanced port will result in combined power at the unbalanced port. It is also clear, albeit less familiar, that the balanced port will not support an even-mode current component, since the transmission line properties require the inner and outer conductor terminal currents to be equal and opposite. When using such baluns in a push-pull amplifier design, the even harmonic current components in the transistors will thus be presented with an *open-circuit* termination rather than a short. This even-mode open-circuit termination has been previously recognized [4], but to the best of the authors' knowledge, the time-domain waveforms inside a microwave push-pull PA have never been explicitly addressed or measured. This letter reconsiders the voltage and current waveforms present in a push-pull amplifier, based on these less familiar harmonic loading conditions.

II. Waveform Formulations

The concept of using factorized expressions to describe voltage waveforms was first introduced by Cripps [5] and since has been used to describe families of voltage waveforms with high efficiencies maintained over extended bandwidth.

For the first time, this analytical approach is used to describe the current and voltage waveforms in a push-pull PA.

Manuscript received August 19, 2011; revised January 01, 2012; accepted February 29, 2012. Date of publication April 16, 2012; date of current version May 04, 2012. This work was supported by the Engineering and Physical Sciences Research Council (EPSRC) and by Roke Manor Research Limited, Romsey, United Kingdom (www.roke.co.uk).

The authors are with the Centre for High Frequency Engineering, School of Engineering, Cardiff University, Cardiff CF24 3AA U.K. (e-mail: smithrm3@cardiff.ac.uk).

Color versions of one or more of the figures in this letter are available online at http://ieeexplore.ieee.org.

Digital Object Identifier 10.1109/LMWC.2012.2191273

The push-pull waveform expressions permit two impedances to be defined; odd- and even-mode, corresponding to odd and even harmonic excitation at the output of a push-pull amplifier. A suitable voltage expression was required to contain components at all three harmonics, since although there will be no second harmonic current, second harmonic voltage is permissible. This is analogous to the situation for the third harmonic in the Class F case. A "design space" of appropriate voltage waveforms can be defined as

$$V = (1 + \alpha\cos(\omega t))^2 \cdot (1 + \beta\cos(\omega t)) \quad -1 < \beta < 1 \quad (1)$$

where α and β are "slack" parameters which generate a set of "zero-grazing" voltage waveforms having fundamental, second and third harmonics. Experience at GHz frequencies has shown that the restriction to three harmonics represents a good practical approximation using current semiconductor power technologies. In (1), only cosinusoidal terms are required, as the scope of the present work only extends to resistive terminations.

The voltage expression in (1) can be expanded, to give the following expressions for the harmonic components

$$\begin{aligned} V_{\mathrm{DC}} &= 1 + \alpha\beta + \frac{\alpha^2}{2} \\ V_{f_0} &= 2\alpha + \beta + \frac{3\alpha^2\beta}{4} \\ V_{2f_0} &= \alpha\beta + \frac{\alpha^2}{2} \\ V_{3f_0} &= \frac{\alpha^2\beta}{4}. \end{aligned} \quad (2)$$

An expression for the time-domain current waveforms is now developed. As previously mentioned, the current waveforms are not allowed to contain even harmonic components. Fundamental and odd harmonic impedances are however equal. The current waveform can therefore be described by

$$I(\theta) = 1 + k(\cos(\omega t) - \gamma\cos 3(\omega t)) \quad (3)$$

$$\gamma \cdot I_1 = -I_3 \quad (4)$$

where k is a scaling factor to restore the zero-grazing condition for a given value of γ. γ relates to the bias condition of a transistor, where $\gamma = 0$ corresponds to a raised cosinusoidal current waveform, or Class-A bias. As a transistor is biased deeper into Class-AB and eventually Class-B, the third harmonic current component increases and has a 'squaring-off' effect on the waveform.

The next stage in the analysis is to take account of the impedance restrictions imposed by the balun

$$\begin{aligned} Z_1 = Z_3 = Z_5 \ldots = Z_B \\ Z_2 = Z_4 = Z_6 \ldots = \infty \end{aligned} \quad (5)$$

where Z_B is the odd mode impedance of the balun when one half of the balanced output is measured with respect to ground.

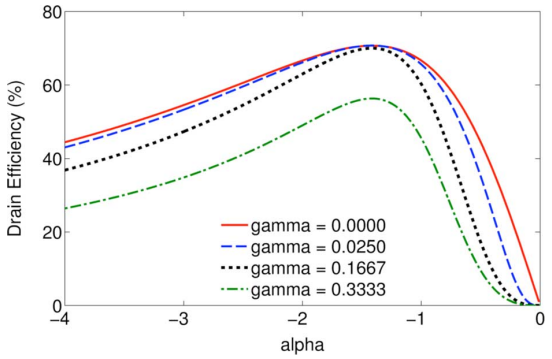

Fig. 2. Drain efficiency plotted against α for different values of γ.

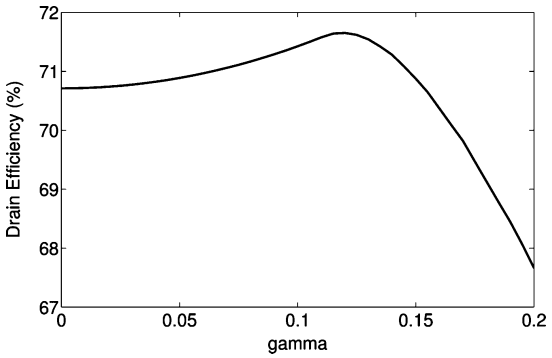

Fig. 3. Drain efficiency plotted against γ with $\alpha = -\sqrt{2}$.

Using (2), (3) and (5), β can be defined in terms of α and γ by setting the fundamental and third harmonic impedances to be equal

$$\beta = \frac{-2\alpha}{1 + \frac{3\alpha^2}{4} + \frac{\alpha^2}{4\gamma}}. \quad (6)$$

The above equations define the current and voltage waveforms, whilst ensuring that the impedance conditions imposed by the balun are met. It is now possible to plot the drain efficiency against the slack parameter α, as shown in Fig. 2. Notably, this shows that the maximum drain efficiency occurs at the value of $\alpha = -\sqrt{2}$ for all values of γ. Fig. 3 plots drain efficiency against γ, and shows that the maximum theoretical efficiency is 71.65% at $\gamma = 0.012$.

A case of particular interest is when γ is close to zero. This corresponds to a raised cosinusoidal current waveform, which typically allows 3 dB additional power gain when compared to deep Class-AB operation. The theoretical waveforms for this case, shown in Fig. 4, closely resemble inverted Class B waveforms, though it should be noted that the third harmonic impedance in this case is a finite resistance instead of an open circuit. As such, the push-pull configuration provides a method of presenting an open-circuit second harmonic impedance over a much broader bandwidth as compared to a single-ended topology. Inverted modes are, in effect, the 'natural' modes for push-pull PAs using transmission line baluns. The analytical

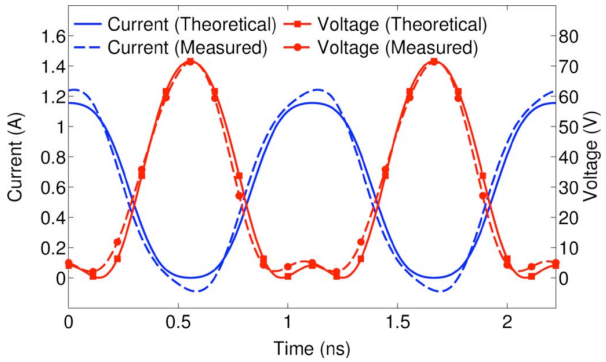

Fig. 4. Theoretical and measured device plane RF voltage and current waveforms for $\gamma = 0.076$.

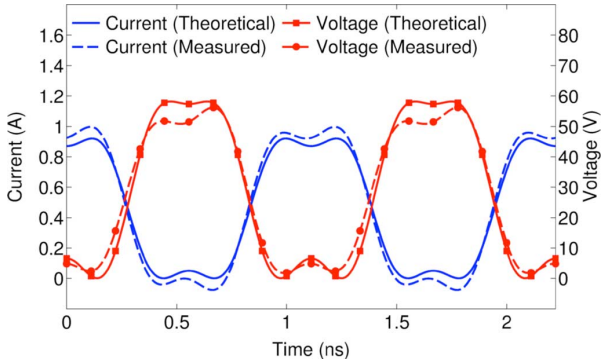

Fig. 5. Theoretical and measured device plane RF voltage and current waveforms for $\gamma = 0.219$.

expressions predict that a push-pull PA, with the transistors biased in a high quiescent current state, can be implemented over multi-octave bandwidths with drain efficiencies of 70%. However, due to the high quiescent current, the drain efficiency would decrease more rapidly than conventional Class-AB mode when input power is backed off.

Theoretical waveforms are generated directly from (1) and (3) and are plotted in Figs. 4 and 5, with drain efficiencies of 71.1% and 66.1%, respectively. The theoretical waveforms have been scaled to enable comparison with measurements.

III. Measurements

Using the active harmonic load-pull system developed at Cardiff University [6], measurements were made on a Cree CGH40010F Gallium Nitride (GaN) power transistor at 900 MHz. Package parasitics and drain-source capacitance were de-embedded, such that specific output loads could be presented to the first three harmonics at the current generator plane. For both sets of measurements, the odd-mode impedance was 50 Ω, the even mode impedance was an open circuit and the drain voltage was 28 V.

For the results of Fig. 4, measured output power was 40.8 dBm, drain efficiency was 73.7% and transducer gain was 18.2 dB. A gate voltage of -2.0 V gave a corresponding γ value of 0.076. For the waveforms presented in Fig. 5, measured output power was 39.4 dBm, drain efficiency was 68.1% and transducer gain was 15.8 dB. A gate voltage of -3.1 V gave a corresponding γ value of 0.219.

It can be observed that the measured waveforms and drain efficiencies closely match those predicted by theory for two different bias voltages. It is believed that the measured drain efficiency is slightly higher than that predicted by theory due to the beneficial effect of the current at the fourth harmonic (not shown), which flattens the current waveform and allows the fundamental current component to be increased.

In theory, a push-pull PA using TLBs has no inherent bandwidth limitation, a key advantage over harmonically tuned single-ended PA modes. This is an important observation, and is a result of the properties of transmission line baluns. In contrast to a conventional output matching network, a balun is able to present two impedances at the same frequency, depending on the mode of excitation. This eliminates the 'crossover' frequency problem that usually limits the bandwidth of harmonically tuned PAs.

IV. Conclusion

For the first time, the 'factorized waveform' approach has been applied to the time-domain RF waveforms of push-pull PAs that use transmission line baluns. The effect of the harmonic loading conditions presented by a transmission line balun has been measured on a GaN transistor for two bias conditions. In both cases, good agreement between the theoretical and measured waveforms is observed. These measurements demonstrate the potential for multi-octave microwave push-pull amplifiers that make use of the impedances presented by a transmission line balun.

References

[1] R. M. Smith, J. Lees, P. J. Tasker, J. Benedikt, and S. C. Cripps, "A design methodology for the realization of multi-decade baluns at microwave frequencies," in *IEEE MTT-S Int. Dig.*, Jun. 2011, pp. 1–4.

[2] K. Krishnamurthy, T. Driver, R. Vetury, and J. Martin, "100 W GaN HEMT power amplifier module with $>60\%$ efficiency over 100–1000 MHz bandwidth," in *IEEE MTT-S Int. Dig.*, Jun. 2010, pp. 940–943.

[3] T. S. Wooten and L. E. Larson, "A decade bandwidth, low voltage, medium power Class B push-pull Si/SiGe HBT power amplifier employing through-wafer vias," in *Proc. RFIC Symp.*, 2008, pp. 519–522.

[4] S. A. Maas, *Microwave Mixers*, 2nd ed. Norwood, MA: Artech House, 1993, p. 256.

[5] S. C. Cripps, P. J. Tasker, A. L. Clarke, J. Lees, and J. Benedikt, "On the continuity of high efficiency modes in linear RF power amplifiers," *IEEE Microw. Wireless Compon. Lett.*, vol. 19, no. 10, pp. 665–667, Oct. 2009.

[6] J. Benedikt, R. Gaddi, P. J. Tasker, M. Goss, and M. Zadeh, "High power time domain measurement system with active harmonic load-pull for high efficiency base station amplifier design," in *IEEE MTT-S Int. Dig.*, 2000, vol. 3, pp. 1459–1462.

Appendix C

'Design of High Efficiency, Multi-Octave Microwave Push-Pull Power Amplifiers'

R. M. Smith and S. C. Cripps

Automated RF and Microwave Measurement Society Conference (ARMMS)

April 2012, Oxford, UK

DESIGN OF HIGH EFFICIENCY, MULTI-OCTAVE MICROWAVE PUSH-PULL POWER AMPLIFIERS

Robert Smith and Professor Steve C. Cripps

Centre for High Frequency Engineering, Cardiff University

smithrm3@cardiff.ac.uk

Abstract - Using differential linear measurements, the harmonic impedance conditions presented by simple transmission line baluns are identified. These impedances are shown to differ significantly from the harmonic conditions usually associated with push-pull amplifiers. When taking into account these impedance conditions, a family of waveforms corresponding to the theoretical waveforms inside a push-pull amplifier can be described mathematically and measured using a harmonic load-pull system. The wideband nature of transmission line baluns can be utilised to design and build push-pull microwave power amplifiers that can operate over multiple octaves and at higher efficiencies than conventional broadband amplifiers. This concept has been demonstrated through the design and test of a push-pull PA prototype that uses packaged GaN HEMTs.

1. Introduction

The design of high-efficiency, broadband power amplifiers at microwave frequencies has always presented significant challenges to microwave engineers. A trade-off between bandwidth and efficiency is necessary, and higher power devices increase the transformation ratio required of the matching network. Two common approaches to designing power amplifiers for bandwidths greater than an octave are Class A designs, usually employing some feedback, and distributed amplifiers, commonly used at higher frequencies. Both of these approaches yield low efficiencies, however. At microwave frequencies, most amplifier designs are based around a single-ended configuration. However, at lower frequencies the push-pull configuration is used far more widely. To understand this difference in approaches, it is necessary to consider the structures that perform the balanced-to-unbalanced transformation, or 'balun' function. At lower frequencies, magnetically coupled centre-tapped transformers are used. They act as low-loss power combiners and present a short circuit to even-mode signals. Unfortunately, the properties of the ferrite materials used in these transformers prevent operation above the VHF or UHF bands. As Fig. 2 shows, the reactive permeability (also known as real permeability) decreases dramatically as frequency increases.

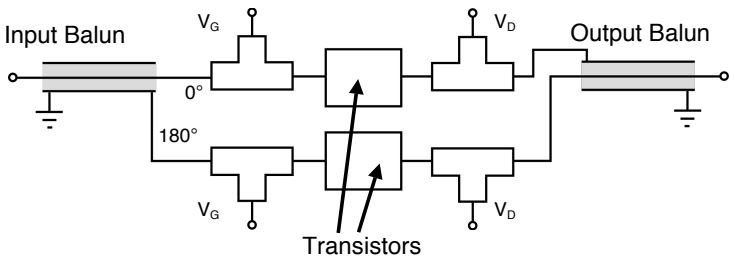

Fig. 1: Push-pull power amplifier configuration, showing back-to-back balun arrangement.

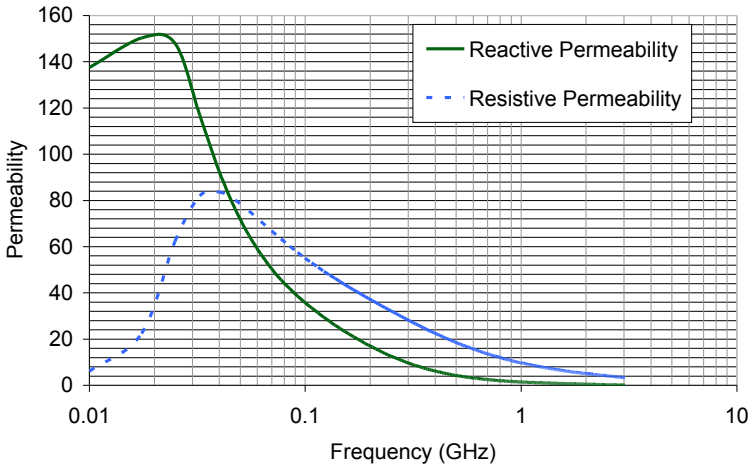

Fig. 2: Permeability versus frequency for Fair-Rite material no. 61 (measured data courtesy of Fair-Rite, www.fair-rite.com).

At microwave frequencies, the use of transmission line baluns is necessary. The limitations of these baluns, and how these can be addressed, are discussed in the next section.

2. Transmission Line Baluns

We identified early on in the project that the key component to be investigated in the design of broadband, high efficiency push-pull power amplifiers was the balun. The operational bandwidth of the balun has a large impact on the bandwidth of the amplifier as a whole, and the insertion loss of the output balun is critical in achieving high efficiency performance. The baluns we have been considering for this project are simple coaxial cable designs, such as the one shown in Fig. 3. The balun is made from low-loss RT/duroid 5880 circuit board backed with aluminium. A channel is milled in the aluminium to set the outer transmission line characteristic impedance. The cable used was 50Ω semi-rigid coaxial cable with a diameter of 1.19mm (47mil). This design was chosen to allow investigation into the effect of ferrite beads on the balun performance, as described below.

We can model the balun using the circuit schematic in Fig. 4. We use a standard floating transmission line to model the coaxial cable itself. We then model the transmission line between the outer of the coaxial cable and the ground plane using a parasitic transmission line, which we refer to as the 'outer' transmission line.

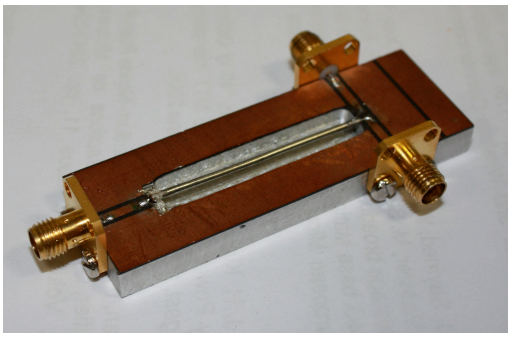

Fig. 3: Simple coaxial cable transmission line balun.

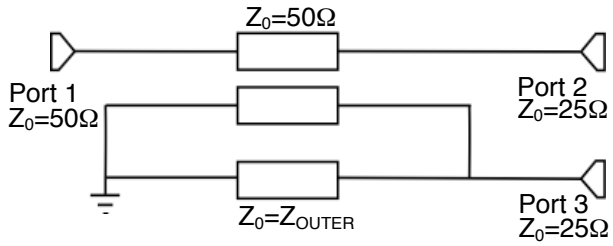

Fig. 4: Circuit model for the simple coaxial cable transmission line balun.

2.1 Bandwidth Extension

As can be seen in Fig. 5, there are two key areas where the transmission line balun is not performing the unbalanced-to-balanced transformation; at the low frequency end of the band, and at around 3.75GHz. The low frequency performance can be explained by the inability of the transmission lines to couple, as the length of the transmission lines is no longer a substantial fraction of a wavelength. The resonance at 3.75GHz occurs as the coaxial cable length is half of the wavelength of the signal, and therefore the 'outer' transmission line is a short circuit. Ferrite beads can be added to the coaxial cable in order to boost the magnetic coupling at the low frequency end of the bandwidth. This is a familiar result and is widely used.

A less familiar role that the ferrite beads can perform is the suppression of the half-wavelength resonance. This was first presented in [1]. Referring back to Fig. 2, it can be seen that although the reactive permeability has decreased to negligible values at 1GHz, there is some resistive permeability remaining. In other words, at microwave frequencies the ferrite beads can act as resistors on the outer transmission line. By adding resistance to the end of the outer transmission line, the impedance of the outer transmission line at the resonant frequency is a finite resistance rather than a short circuit. The effect of adding ferrite beads to the coaxial cable can be seen in Fig. 6. The low frequency performance has been improved, and the resonance is no longer present. It is worth noting that there is an uneven power split between the two halves of the balanced port, and that there is a 180° phase difference (not shown). The performance of the balun extends from 30MHz to 6GHz, a bandwidth greater than two decades.

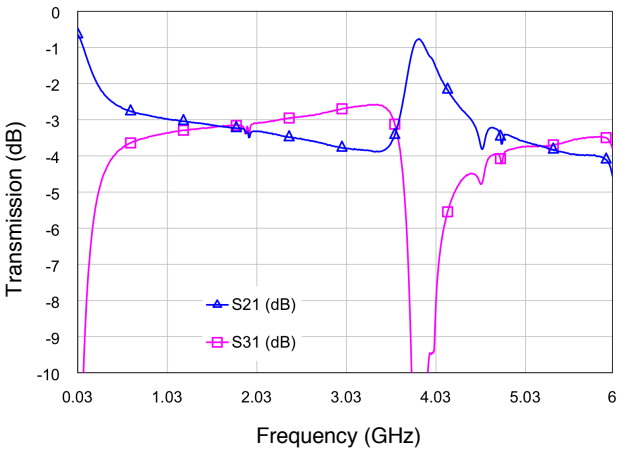

Fig. 5. Unbalanced to balanced transmission magnitude.

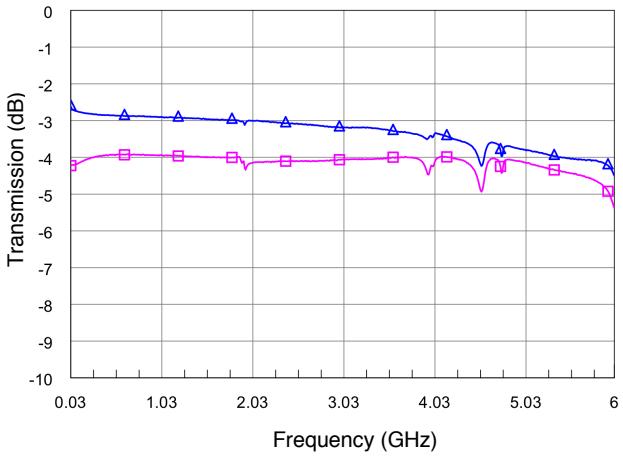

Fig. 6. Unbalanced to balanced transmission magnitude, with ferrite beads added.

2.2 Impedances Presented by a Transmission Line Balun

Both magnetically coupled transformers used at VHF frequencies and transmission line baluns present different impedances at their balanced ports depending on whether the excitation is common-mode (even-mode) or differential-mode (odd-mode). For the magnetically coupled transformer balun, the even-mode impedance is close to a short circuit, and hence any second harmonic currents are cancelled. In contrast, a simple transmission line balun presents an open-circuit to even-mode signals, i.e. even harmonics. This is a significant observation, as it affects the operation of the PA and needs to be accounted for in the design.

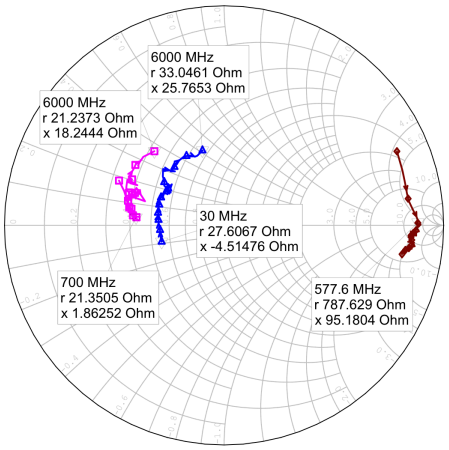

Fig. 7. Odd and even mode impedances of a transmission line balun.

The measured odd- and even-mode impedances of a transmission line balun are shown in Fig. 7. The two traces around 25Ω are the odd-mode impedances presented by each half of the balanced port. The high-impedance trace is the even-mode impedance presented by the balanced port. The balun's open circuit at the even harmonics has previously been identified in [2] for mixer applications, but seems to have received limited attention for power amplifier applications.

3. Push-Pull PA Modes of Operation

As the balun impedances differ significantly from the traditional push-pull impedance conditions, the waveforms inside a push-pull PA using microwave baluns were reconsidered. The waveform analysis will be published in a forthcoming issue of IEEE Microwave and Wireless Components Letters [3]. Using the factorised waveform approach first described by Cripps [4], analytical expressions for the voltage and current time-domain waveforms inside a push-pull PA were developed. Due to the open-circuit at the even harmonics, the waveforms bear a closer resemblance to inverted modes than conventional PA modes, as shown in Fig. 8. The maximum theoretical drain efficiency for push-pull amplifiers using ideal transmission line baluns was found to be 71.7%. This is lower than the 78.5% drain efficiency theoretically possible using magnetically coupled centre-tapped transformers, but higher than alternative broadband approaches such as single-ended Class A or distributed architectures.

The impedances of an ideal balun were emulated using the active hamonic load-pull measurement system at Cardiff University [5], and the measured waveforms were found to verify the theoretical waveforms.

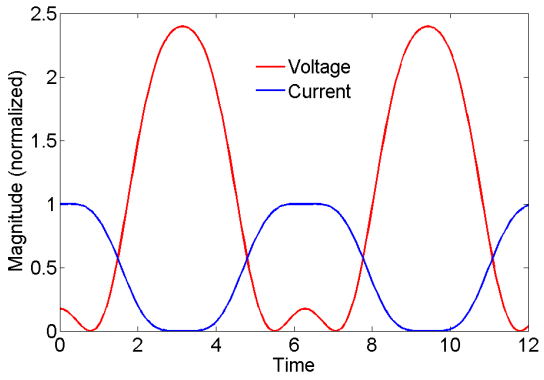

Fig. 8. Theoretical push-pull waveforms for a shallow Class AB bias.

The analysis of the waveforms shows that although the push-pull mode of operation yields lower efficiencies than harmonically tuned modes, the efficiencies are higher than those that could be achieved by the Class A or distributed amplifier approaches. Because the odd- and even-mode impedances are maintained over the operational bandwidth of the balun, this means that the push-pull mode can be maintained over multiple octaves, in contrast to harmonically tuned modes that are limited to less than an octave of bandwidth.

4. Push-Pull Power Amplifier Prototype

A prototype power amplifier was built and tested to investigate whether the theoretical performance could be realised in practise. It should be noted that the PA only consisted of an output stage, and so may not be regarded as a 'complete' PA. The full design and measurements of the PA will be published at the next International Microwave Symposium [6].

The output balun provided a 2:1 impedance transformation ratio at the fundamental frequency, which greatly reduces the matching requirement. Two Cree CGH400025F packaged GaN HEMTs were used, whose optimum output impedances are close to 25Ω. This, in theory, reduces the need for conventional matching networks.

The prototype power amplifier exhibited 46dBm output power and greater than 45% drain efficiency between 700MHz and 2GHz. Between 250MHz and 3.1GHz, a minimum of 43dBm output power is achieved. High drain efficiencies of at least 60% were measured between 350MHz and 1GHz, a greater than octave bandwidth. The PA was observed to have the soft gain compression characteristics that are typical of GaN-based amplifiers.

The half-wavelength resonance was designed to be outside the fundamental frequency band, and for the initial measurements no ferrite was added to the balun. The PA was designed with differential inputs, to allow the effects of phase and amplitude imbalance to be measured. Due to the minimal output matching on the PA, it is anticipated that these results can be improved upon, especially if a chip-and-wire approach is adopted for a future PA.

5. Conclusions

The potential for using the push-pull configuration to realise high-efficiency, broadband microwave power amplifiers was investigated. A key component in the amplifier is the balun, whose operational bandwidth can be increased with the addition of ferrite beads. The odd- and even-mode impedances presented by a transmission line balun were used to evaluate the voltage and current waveforms at the output of the transistors through the factorised waveform approach. The wideband nature of transmission line baluns can be utilised to design and build push-pull microwave power amplifiers that can operate over multiple octaves and at higher efficiencies than conventional broadband amplifiers. This concept has been demonstrated through the design and test of a push-pull PA prototype, which has produced encouraging preliminary results.

Acknowledgement

The authors wish to thank Roke Manor Research Limited (www.roke.co.uk) and EPSRC for sponsoring this work. We would also like to thank Cree for supplying the GaN devices used in this work.

References

[1] R. M. Smith, J. Lees, P. J. Tasker, J. Benedikt, and S. C. Cripps, "A Design Methodology for the Realization of Multi-Decade Baluns at Microwave Frequencies," in *IEEE MTT-S International Microwave Symposium Digest*, June 2011, Baltimore, MD.

[2] S. A. Maas, Microwave Mixers. Norwood, MA., Artech House Publishers, 2nd ed., 1993.

[3] R. M. Smith, J. Lees, P. J. Tasker, J. Benedikt, and S. C. Cripps, "A Novel Formulation for High Efficiency Modes in Push-Pull Power Amplifiers using Transmission Line Baluns," to be published in *IEEE Microwave and Wireless Components Letters*, accepted 29th Feb 2012.

[4] S. C. Cripps, P.J. Tasker, A. L. Clarke, J. Lees and J. Benedikt, "On the Continuity of High Efficiency Modes in Linear RF Power Amplifiers", in *IEEE Microwave and Wireless Components Letters*, vol. 19, no. 10, pp. 665-667, Oct. 2009.

[5] J. Benedikt, R. Gaddi, P. J. Tasker, M. Goss and M. Zadeh, "High Power Time Domain Measurement System with Active Harmonic Load-Pull for High Efficiency Base Station Amplifier Design", in *IEEE MTT-S International Microwave Symposium Digest,* 2000, vol. 3, pp 1459-1462.

[6] R. M. Smith, J. Lees, P. J. Tasker, J. Benedikt, and S. C. Cripps, "A 40W Push-Pull Power Amplifier for High Efficiency, Decade Bandwidth Applications at Microwave Frequencies", to be presented at the *IEEE MTT-S International Microwave Symposium*, June 2012, Montreal, Canada.

Appendix D

‘A 40W Push-Pull Power Amplifier for High Efficiency, Decade Bandwidth Applications at Microwave Frequencies’

R. M. Smith, J. Lees, P. J. Tasker, J. Benedikt, and S. C. Cripps

IEEE MTT-S International Microwave Symposium 2012

June 2012, Montreal, Quebec, Canada

A 40W Push-Pull Power Amplifier for High Efficiency, Decade Bandwidth Applications at Microwave Frequencies

R. M. Smith, J. Lees, P. J. Tasker, J. Benedikt and S. C. Cripps

Centre for High Frequency Engineering, Cardiff University, Cardiff, CF24 3AA, U.K.
Email: smithrm3@cardiff.ac.uk

***Abstract* — A high-efficiency push-pull power amplifier has been designed and measured across a bandwidth of 250MHz to 3.1GHz. The output power was 46dBm with a drain efficiency of above 45% between 700MHz and 2GHz, with a minimum output power of 43dBm across the entire band. In addition, a minimum of 60% drain efficiency and 11dB transducer gain was measured between 350MHz and 1GHz. The design was realized using a coaxial cable transmission line balun, which provides a broadband 2:1 impedance transformation ratio and reduces the need for bandwidth-limiting conventional matching. The combination of output power, bandwidth and efficiency are believed to be the best reported to date at these frequencies.**

***Index Terms* — Balun, high efficiency, microwave amplifiers, power amplifiers, push-pull, wideband.**

I. Introduction

Designing a power amplifier (PA) to deliver high efficiency over a bandwidth of greater than an octave is a significant challenge at microwave frequencies, and the challenge increases as the power level is raised. The conventional approach for designing broadband microwave power amplifiers has been to use a single device biased in Class A, usually with some feedback, however this approach generally yields low efficiency amplifiers. At higher frequencies a distributed architecture is frequently used, but this is also not a high efficiency approach. Previous works on push-pull power amplifiers have either presented wide bandwidths but modest efficiencies and output powers [1] or high power and efficiency over limited bandwidths [2].

A high-power, push-pull PA is presented in [3]. Using ferrite-based magnetically coupled transformers, high efficiency and output power is maintained across a bandwidth of 100MHz to 1GHz. However, attempts to extend this performance above 1GHz will be limited by the ferrite materials currently available for constructing transformers.

For applications above 1GHz, it is necessary to use an alternative design of balun that uses the properties of a transmission line rather than magnetic coupling.

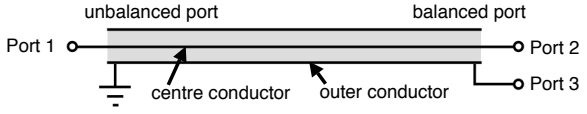

Fig. 1. Simple schematic of a coaxial cable transmission line balun.

Such a balun may be made from a straight piece of coaxial cable mounted above a ground plane, where the length of the cable is chosen to be less than a half wavelength at the specified upper frequency limit. This structure has a wide useable bandwidth, which can be further extended as described in [4], albeit with increased insertion loss.

In this paper, we describe the design and manufacture of a push-pull power amplifier output stage using a ferrite-less coaxial cable balun that outputs 40W (46dBm) output power at greater than 45% drain efficiency between 700MHz and 2GHz. Furthermore, the amplifier output power is above 43dBm between 250MHz and 3.1GHz, a bandwidth greater than a decade. These results clearly demonstrate the advantages of the push-pull configuration in designing high efficiency PAs for broadband microwave applications.

II. Advantages of the Push-Pull Configuration

Single-ended power amplifiers designed to operate over significant bandwidths tend to use transistors biased in Class A with filter-based matching networks, the design of which is well documented [5]. As the required transformation ratio between the 50Ω system impedance and the optimum device impedance increases, the Q factor of the matching network also increases and hence the bandwidth is reduced. This is particularly problematic for higher power devices, where the output impedance of a device can be of the order of one Ohm or less, and a high transformation ratio is required.

The push-pull configuration, where two transistors are operated 180° out of phase, greatly alleviates the limitations of conventional matching networks. The simple transmission line balun of Fig. 1 presents an odd-mode impedance of approximately 25Ω to each half of the balanced output, as shown in Fig. 2. The impedance presented to Port 3 of the balanced output decreases at low frequencies as the length of coaxial cable ceases to be a substantial fraction of a wavelength. At higher frequencies, the Port 3 impedance tends towards a short circuit due to the half-wavelength resonance.

The 2:1 transformation ratio is maintained over the operational bandwidth of the balun. It can therefore be reasonably stipulated that in an equal power comparison, using identical device types, the push-pull configuration not only offers a 4:1 benefit in matching Q-factor, but also achieves this using a structure that is inherently much broader band than filter-based matching networks.

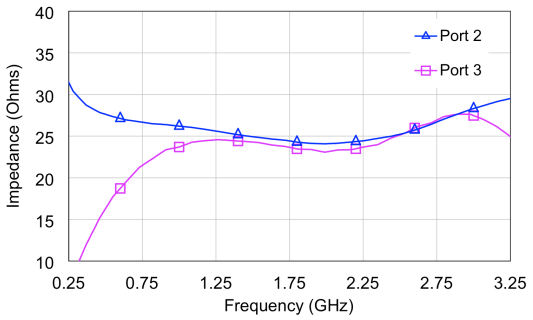

Fig. 2. Measured odd-mode impedance presented to each half of the balanced output port of a coaxial cable transmission line balun.

Due to its transmission line properties, the balun will not support any even-mode current component and thus presents an open circuit termination to signals at the even harmonic frequencies. This represents an important difference between high frequency push-pull design using transmission line baluns, and low frequency designs based on magnetically coupled transformers, since in the latter case the even harmonic voltages at each device will be conveniently cancelled. A key element in this design is to recognize, and design for, even harmonic open circuit terminations at the balanced balun port.

III. Load-Pull Transistor Measurements

To investigate the effects of the transmission line balun impedance conditions on a real device, a three-harmonic active load-pull measurement system was used to measure a Cree CGH40025F Gallium Nitride (GaN) high electron-mobility transistor (HEMT). The odd-mode impedance of an ideal balun, 25Ω, was presented to the fundamental and third harmonics, with an open circuit presented to the second harmonic. A model of the package parasitic components and an estimation of the drain-source capacitance (C_{DS}) were used to de-embed the waveforms to the current generator plane.

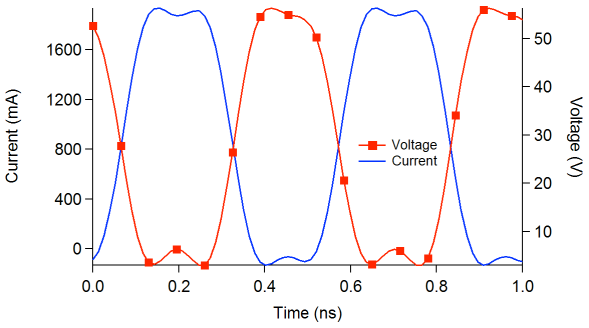

Fig. 3. Measured device plane RF voltage and current waveforms when presented with ideal balun impedances.

The waveforms shown in Fig. 3 were measured at 2GHz with the transistor operating in Class AB bias. As expected, due to the open circuit even-mode impedance, the current waveform contains no second harmonic component, but the third harmonic component has a small 'squaring off' effect, increasing the efficiency compared to a pure sinusoid.

The drain efficiency of this waveform is 65.80%, demonstrating the performance that would be achievable if the ideal balun impedances could be presented to the transistor at the current generator plane. In practice, C_{DS} and package parasitics, in addition to non-ideal balun structures will lower the drain efficiency.

IV. Design of Push-Pull Broadband Power Amplifier

The same Cree GaN HEMTs that were measured on the active harmonic load-pull system were used for the realized push-pull power amplifier. As has been previously outlined, filter-based matching networks limit the performance of the power amplifier for very broadband applications. For this design, a very simple matching topology was sufficient, based on the fact that the individual transistor loadline resistance was close to the odd-mode balun impedance of 25Ω.

The amplifier was designed with differential input ports, since a multistage design will very likely retain differential operation in at least the first driver stage. We also wished to allow for future investigations into the effects of input amplitude and phase imbalance. The current generator plane impedances presented by the differential output matching network are shown in Fig. 4. Note that the even harmonic impedances are reactive, due to the action of the balun. Although the spread of reactance over a decade bandwidth is not optimum for Class AB operation, the impedance environment is largely compatible with the 'Class B-J' design space described in [6].

A simple shunt-capacitor matching network was used at the inputs of the PA to increase the gain at higher frequencies.

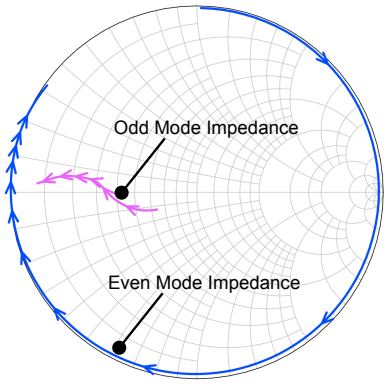

Fig. 4. Odd- and even-mode impedances presented to the transistor at the current generator plane from 400MHz to 3.25GHz.

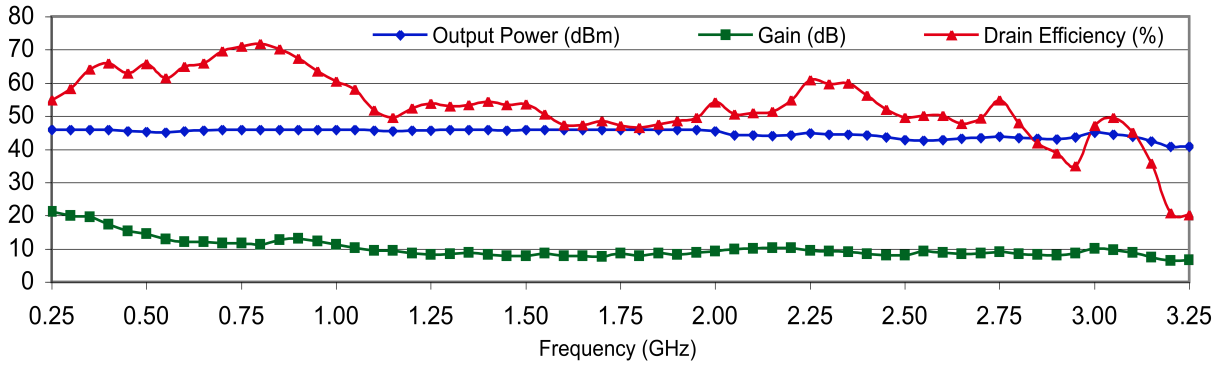

Fig. 5. Measured output power, transducer gain and drain efficiency of the realized push-pull output stage power amplifier.

It is expected that the output matching can be further improved by compensating for the package parasitic reactances at higher frequencies; this was not implemented in the present design since a chip-and-wire hybrid approach may be used in the future.

V. Realized Push-Pull Power Amplifier Performance

The design described in the previous section was manufactured on low-loss aluminium-backed circuit board. The slot required for the coaxial cable balun was milled directly into the aluminium, which served as the ground plane. The realized push-pull PA is shown in Fig. 6.

The output stage was driven by two signal sources with 180° phase offset. As can be seen in Fig. 5, the prototype push-pull PA exhibits 46dBm output power and greater than 45% drain efficiency between 700MHz and 2GHz. The PA has a minimum output power of 43dBm and high efficiency between 250MHz and 3.1GHz. In addition, a transducer gain and drain efficiency of over 11dB and 60% respectively were measured between 350MHz and 1GHz. Considering that packaged devices were used, the bandwidth and power levels presented are especially noteworthy.

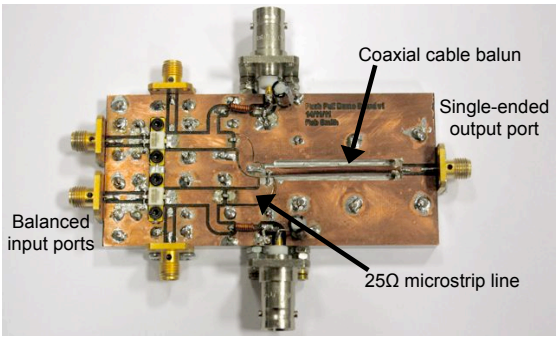

Fig. 6. Push-pull power amplifier with integrated coaxial cable transmission line balun at output.

VI. Conclusion

In order to realize a broadband, high-efficiency push-pull power amplifier at microwave frequencies, a coaxial cable transmission line balun was used to present a 2:1 impedance transformation ratio over a very wide bandwidth. When used with transistors with a comparable loadline resistance, the need for conventional filter-based matching is greatly reduced.

The bandwidth potential of the push-pull configuration has been demonstrated through the measurement of a prototype output stage PA. Output powers greater than 43dBm and high drain efficiencies were measured over a bandwidth greater than a decade. To the best of the authors' knowledge, the combination of bandwidth, output power and efficiency is the best reported to date.

Acknowledgement

The authors wish to thank Roke Manor Research for sponsoring this work and Cree Inc. for supplying the devices.

References

[1] A. K. Ezzeddine and H. C. Huang, "10W Ultra-Broadband Power Amplifier," in *2008 IEEE MTT-S Int. Microw. Symp. Dig.*, pp. 643 - 646, June 2008.

[2] I. Takenaka *et al.*, "L/S-Band 140-W Push–Pull Power AlGaAs/GaAs HFETs for Digital Cellular Base Stations," in *IEEE J. Solid-State Circuits*, pp. 1181-1187, Sept 1999.

[3] K. Krishnamurthy *et al.*, "100 W GaN HEMT Power Amplifier Module with > 60% Efficiency over 100-1000 MHz Bandwidth," in *2010 IEEE MTT-S Int. Microw. Symp. Dig.*, pp. 940 - 943, June 2010.

[4] R. M. Smith *et al.*, "A Design Methodology for the Realization of Multi-Decade Baluns at Microwave Frequencies", in *IEEE MTT-S Int. Microw. Symp. Dig., 2011*, June 2011.

[5] Cripps, S. C., "RF Power Amplifiers for Wireless Communications," 2nd Edition, Artech House Publishers, 2006.

[6] Cripps, S. C. *et al.*, "On the Continuity of High Efficiency Modes in Linear RF Power Amplifiers," in *IEEE Microw. Wireless Component Letters*, vol. 19, no. 10, pp. 665-667, Oct. 2009.

Appendix E

'Broadband Push-Pull Power Amplifier Design at Microwave Frequencies'

R. M. Smith and S. C. Cripps

Automated RF and Microwave Measurement Society Conference (ARMMS)

April 2013, Oxford, UK

Winner of the Steve Pugh Memorial Prize for Best Paper.

Broadband Push-Pull Power Amplifier Design at Microwave Frequencies

Robert Smith and Prof. Steve Cripps
Centre for High Frequency Engineering, Cardiff University
smithrm3@cardiff.ac.uk

A broadband, high efficiency push-pull power amplifier is presented between 0.5GHz and 1.5GHz. Coaxial cable transmission line baluns are utilised to transform the impedance environment of the transistors down to 25Ω, greatly simplifying the matching, whilst still providing a 50Ω environment to interface with other components. Using packaged GaN HEMT transistors, typical output powers of 45dBm and efficiencies of 44% to 75% have been measured across a 3:1 bandwidth. The small signal input match is less than -10dB and small signal gain is greater than 10dB across the entire band.

1 Introduction

Achieving broadband operation at microwave frequencies is a challenge which has confronted power amplifier designers for many years. If high-power operation and reasonable power efficiency is also required, the challenge is significantly increased. High-efficiency operation using continuous modes such as Continuous Class F can be shown to extend to a bandwidth of an octave [1], however for larger bandwidths a different approach is required. The push-pull configuration has demonstrated excellent performance at frequencies below 1GHz [2] but is rarely found at higher frequencies. In this paper two prototype push-pull power amplifiers are presented, demonstrating encouraging performance across significant bandwidths.

2 The Microwave Push-Pull Approach

Previous work [3] has demonstrated the advantages of the push-pull configuration at microwave frequencies, where it is not traditionally used. The transmission line baluns that convert an unbalanced signal to a balanced signal, and vice versa, also transform the system reference impedance down by a factor of two. For an amplifier designed to interface with a 50Ω system, the individual transistors are presented with a 25Ω system impedance. This is an advantage when matching high-power transistors, which typically have an optimum output impedance much lower than 50Ω. The output balun also serves as a power combiner, so that double the output power is produced by the overall amplifier. Therefore, for a particular transistor it can be stated that the push-pull configuration offers a 4:1 advantage compared to a conventional, single-ended amplifier.

The other advantage of the push-pull amplifier is that its operation can be maintained across a very wide bandwidth. Baluns present odd- or even-mode impedances, depending on how they are excited, and these impedances can be maintained over very wide bandwidths. The operational bandwidth of the amplifier is highly dependent on the balun components. The insertion loss of the baluns should be kept to a minimum, as loss in the output balun will decrease output power and efficiency, and loss in the input balun will reduce gain and power-added efficiency (PAE). The baluns used in this work are simple coaxial cable transmission line baluns, such as the one shown in Fig. 1.

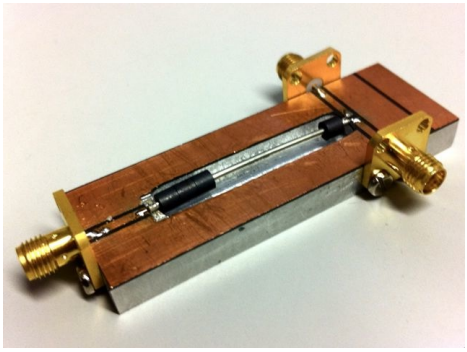

Figure 1: Coaxial cable transmission line balun

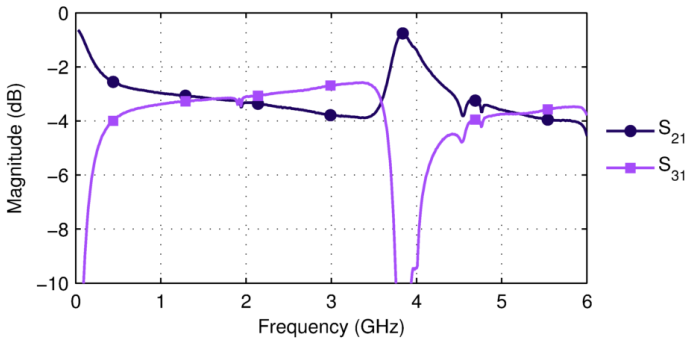

Figure 2: S_{21} and S_{31} of coaxial cable balun without ferrite

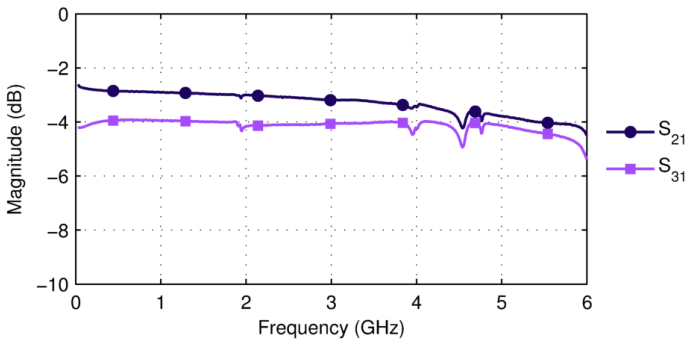

Figure 3: S_{21} and S_{31} of coaxial cable balun with ferrite

It has been shown in [4] that for coaxial cable baluns, ferrite beads can be used to suppress the balun's half-wavelength resonance. This increases the upper cut-off frequency of the balun and hence increases its bandwidth. The effect of adding ferrite beads to the coaxial cable can be seen by comparing Fig. 2 to Fig. 3. The low frequency performance has been improved, and the resonance is no longer present. The performance of the balun extends from 30MHz to 6GHz. The insertion loss of the balun is shown in Fig. 4. It can be seen that insertion loss is increased when ferrite is added, but that the bandwidth of the balun is also increased.

There are many methods of implementing baluns, including in planar form. An excellent source of information on the various types of baluns at RF and microwave frequencies can be found in [5].

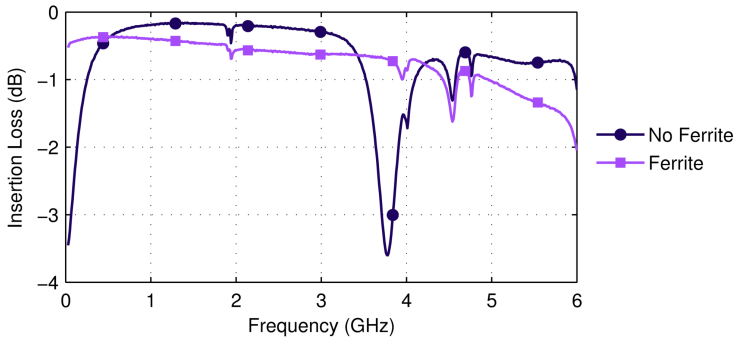

Figure 4: Insertion loss of coaxial cable balun with and without ferrite

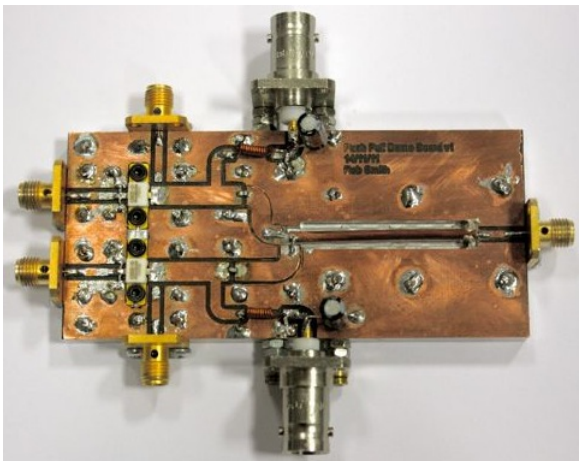

Figure 5: Prototype amplifier v1

3 Prototype Amplifier v1

A prototype power amplifier was presented in [6] in order to demonstrate the performance that could be achieved by the push-pull configuration in practice. The PA, shown in Fig. 5, consists of a single output stage, and is driven by differential inputs.

The output balun provided a 2:1 impedance transformation ratio at the fundamental frequency, which greatly reduces the matching requirement. Two Cree CGH400025F packaged GaN HEMTs were used, and load-pull measurements indicated that their optimum output impedances were close to 25Ω. GaN transistors are well suited to broadband applications, due to their low drain-source capacitance (C_{DS}) and high output impedances compared to LDMOS or GaAs. This reduces the need for conventional matching networks. Gate bias tees were omitted to simplify the design.

Fig. 6 shows the amplifier's performance across frequency, where the phase between the inputs has been varied to obtain optimum performance. The input power is also varied with frequency in order to compensate for the amplifier's gain variation with frequency and hence keep the output power constant.

The prototype power amplifier exhibited 46dBm (40W) output power and greater than 45% drain efficiency between 700MHz and 2GHz. Between 250MHz and 3.1GHz, a minimum of 43dBm (20W) output power is achieved. High drain efficiencies of at least 60% were measured between 350MHz and 1GHz.

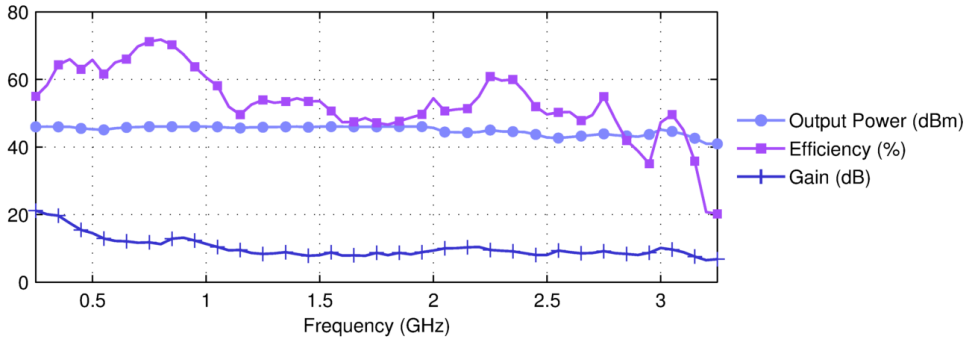

Figure 6: Large signal measurements of PA v1

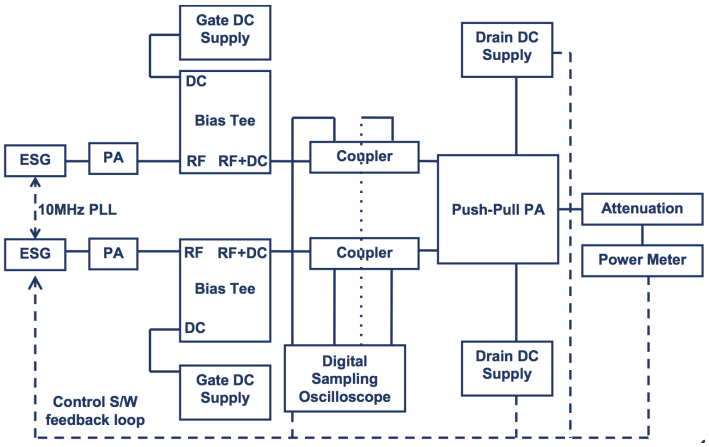

Figure 7: Push-pull power amplifier measurement setup with differential input

3.1 Differential Measurement Setup

The differential input provides an opportunity to investigate the push-pull power amplifier in greater depth. In order to measure the effect of amplitude and phase balance, a measurement setup had to be developed that was capable of providing the necessary phase difference between the inputs. The setup is shown in Fig. 7.

Two Electronic Signal Generators (ESGs) are phase locked together to provide a differential input. When the phase lock between the ESGs is established, there is an arbitrary phase difference. This phase difference is measured using a digital sampling oscilloscope, and the measurement software changes the phase of one of the ESGs to achieve the desired phase difference. Similarly, the amplitude of each ESG can be varied in order to set the amplitude balance of the differential input.

3.2 Amplitude and Phase Balance

Fig. 8 shows the variation in output power of the PA with amplitude balance. The total power driving the PA is the same for all cases, as shown in Table 1.

It can be seen that the PA is relatively tolerant to a change in amplitude balance. There is clearly an advantage to trying to set the amplitude balance correctly, but the amplifier's operation is not dependent on achieving a particular balance. The variation in output power is only 0.4dBm for a wide range of amplitude balance conditions. It is speculated that the transistors influence each other through the coupling between the two halves of the balanced port of the output balun. The output

Amplitude Balance	Input A (dBm)	Input B (dBm)	Input A (W)	Input B (W)	Total Power (W)	P (dBm)
- 3.0 dB	25.236	28.236	0.334	0.666	1	30
- 2.5 dB	25.562	28.062	0.360	0.640	1	30
- 2.0 dB	25.876	27.876	0.387	0.613	1	30
- 1.5 dB	26.175	27.675	0.415	0.585	1	30
- 1.0 dB	26.461	27.460	0.443	0.557	1	30
- 0.5 dB	26.733	27.233	0.471	0.529	1	30
0.0 dB	26.990	26.990	0.500	0.500	1	30
0.5 dB	27.233	26.733	0.529	0.471	1	30
1.0 dB	27.461	26.461	0.557	0.443	1	30
1.5 dB	27.675	26.175	0.585	0.415	1	30
2.0 dB	27.876	25.876	0.613	0.387	1	30
2.5 dB	28.062	25.562	0.640	0.360	1	30
3.0 dB	28.236	25.236	0.666	0.334	1	30

Table 1: Amplitude balance and corresponding input powers for a total input power of 1W

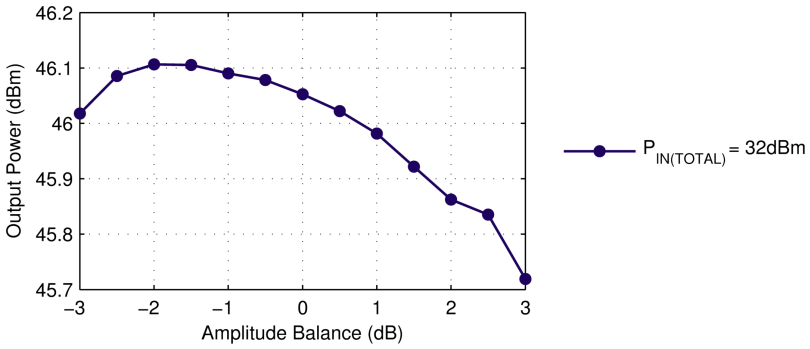

Figure 8: Output power variation with amplitude balance

power from one transistor is fed back through the balun to effectively 'load-pull' the other transistor. Further work will be done to investigate this effect.

4 Prototype Amplifier v2

The first prototype provided promising results, but is not suited to practical implementation. Several factors make it difficult to use in practical applications, the primary one being its differential inputs. For this reason, the second prototype included an input balun, so that the amplifier could be driven by a single-ended input. A target input return loss of -10dB was set. This was only achievable by including a resistive element in the input matching network, which reduced the gain of the amplifier. As with the first prototype, the output match consisted of minimal components, as the 25Ω impedance environment provides a reasonable match for this particular device. Gate bias networks were integrated into the amplifier, obviating the need for external bias tees.

The second prototype used the same GaN transistors as the first. For larger devices with lower impedances, the 25Ω environment reduces the matching ratio and increases bandwidth compared to

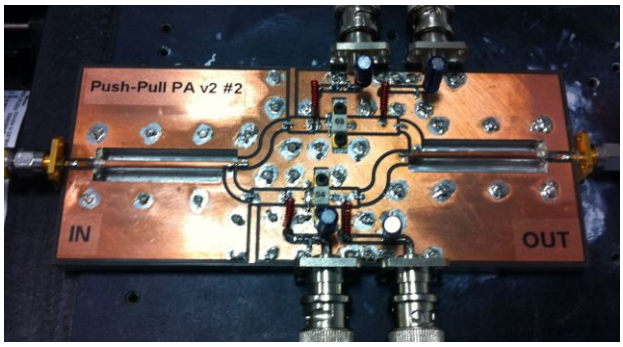

Figure 9: Prototype amplifier v2

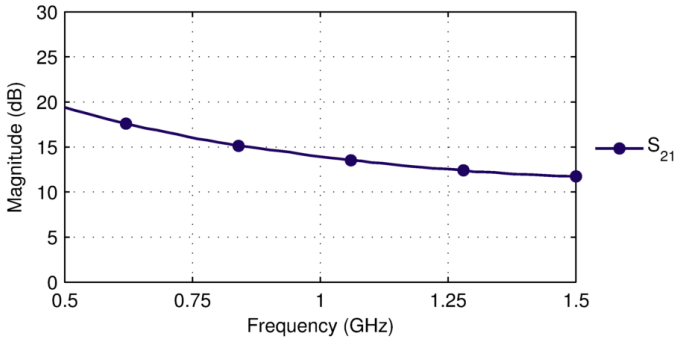

Figure 10: S_{21} of PA v2

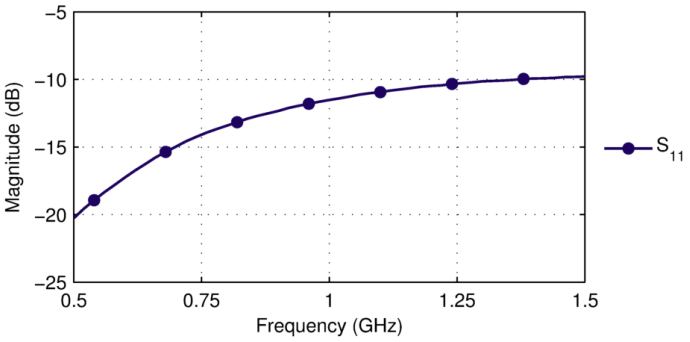

Figure 11: S_{11} of PA v2

a single-ended design into 50Ω. The disadvantage of the input balun is that the loss in the input side of the PA is increased and so the overall gain of the amplifier is reduced.

4.1 Small-Signal Measurements

Between 500MHz and 1.5GHz, a small signal gain greater than 12dB was measured, as shown in Fig. 10. The input match, shown in Fig. 11, was better than -10dB across most of the band, but degrades with frequency.

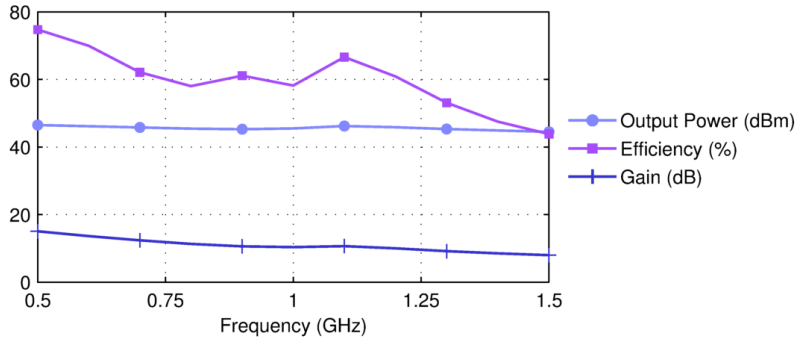

Figure 12: Large signal measurements of PA v2

4.2 Large-Signal Measurements

Preliminary large signal measurements for the second prototype amplifier are shown in Fig. 12. Measurements were made at 100MHz intervals from 0.5GHz to 1.5GHz. Over a 3:1 bandwidth, the efficiency is around 60% for much of the band, falling to 44% at 1.5GHz. Unlike the first prototype, it was not possible to vary the amplitude and phase balance to optimise performance. The output power varies between 44.5dBm and 46.5dBm. Input power is varied with frequency in order to compensate for the gain variation of the PA.

One problem with using coaxial cable baluns is the difficulty in assembling the baluns reliably. As each balun is assembled by hand, the quality of the assembly is variable and it is difficult to find faults in the balun once the whole PA has been assembled. Planar baluns can be manufactured more reliably, but in general these do not perform as well as coaxial cable baluns.

Further measurements are to be carried out on the amplifier to establish its performance under different conditions, included modulated signals.

5 Conclusions

The advantages of the push-pull configuration for microwave power amplifiers have been outlined. Two prototype amplifiers have been shown to exhibit good performance across wide bandwidths. This shows that the push-pull configuration has potential for use in the realisation of very broadband amplifiers at microwave frequencies, an area where it has rarely been used. It is probable that further improvement can be achieved by adopting a chip-and-wire approach, and by further investigation into the balun structures. The push-pull configuration was used to investigate broadband applications, but its 4:1 impedance advantage can also be utilised for narrow-band applications, especially where high-power transistors are to be used.

Acknowledgement

The authors wish to thank Roke Manor Research Limited (www.roke.co.uk) for sponsoring this work, and Cree (www.cree.com) for supplying the GaN devices.

References

[1] V. Carrubba, J. Lees, J. Benedikt, P. Tasker, and S. Cripps, "A novel highly efficient broadband continuous class-F RFPA delivering 74% average efficiency for an octave bandwidth," in *Microwave Symposium Digest (MTT), 2011 IEEE MTT-S International*, June 2011, pp. 1 –4.

[2] K. Krishnamurthy, T. Driver, R. Vetury, and J. Martin, "100 W GaN HEMT power amplifier module with $>$ 60% efficiency over 100-1000 MHz bandwidth," in *Microwave Symposium Digest (MTT), 2010 IEEE MTT-S International*, May 2010, pp. 940 –943.

[3] R. M. Smith, J. Lees, P. J. Tasker, J. Benedikt, and S. C. Cripps, "A novel formulation for high efficiency modes in push-pull power amplifiers using transmission line baluns," *Microwave and Wireless Components Letters, IEEE*, vol. 22, no. 5, pp. 257 – 259, May 2012.

[4] ——, "A design methodology for the realization of multi-decade baluns at microwave frequencies," in *Microwave Symposium Digest (MTT), 2011 IEEE MTT-S International*, 2011.

[5] J. L. B. Walker, Ed., *Classic Works in RF Engineering: Combiners, Couplers, Transformers and Magnetic Materials*. Artech House Publishers, 2005.

[6] R. M. Smith, J. Lees, P. J. Tasker, J. Benedikt, and S. C. Cripps, "A 40W push-pull power amplifier for high efficiency, decade bandwidth applications at microwave frequencies," in *Microwave Symposium Digest (MTT), 2012 IEEE MTT-S International*, June 2012, pp. 1 –3.

Appendix F

List of symbols and abbreviations

A, mA	Amperes, milliAmperes
AM	Amplitude Modulation
AWR	Applied Wave Research (developers of Microwave Office)
BJT	Bipolar Junction Transistor
C	Capacitance (F)
c	Speed of light in a vacuum ($\approx 3 \times 10^8$ m/s)
CAD	Computer-Aided Design
CAPEX	Capital Expenditure
Class F^{-1}	Inverse Class F
COTS	Commercial Off The Shelf
dB	Decibels
dBm	Decibels referenced to 1mW
DC	Direct Current
D.E.	Drain Efficiency (P_{RF} / P_{DC})
DSO	Digital Sampling Oscilloscope
DUT	Device Under Test
ECM	Electronic Counter Measures
E_c	Electric field for breakdown (V/cm)

E_g	Energy Gap (eV)
EM	Electromagnetic
EMI	Electromagnetic Interference
ESG	Electronic Signal Generator
eV	Electron Volts
EW	Electronic Warfare
F, pF	Farads, picoFarads
FEM	Finite Element Method
FET	Field Effect Transistor
Freq., f	Frequency
GaAs	Gallium Arsenide
GaN	Gallium Nitride
GUI	Graphical User Interface
H, nH	Henries, nanoHenries
HBT	Hetrojunction Bipolar Transistor
HEMT	High Electron Mobility Transistor
HFET	Hetrostructure FET
Hz, GHz	Hertz, Gigahertz
I, i	Current
I-V	Current-voltage relationship
III-V	Compound semiconductor of Group III and Group V elements
I_{dq}	Quiescent drain current
I_{MAX}	Maximum drain current
InP	Indium Phosphide
ISM	Industrial, Scientific, Medical
K	Thermal conductivity

L	Inductance (H)
LDMOS	Laterally Diffused Metal Oxide Semiconductor
LNA	Low Noise Amplifier
LTE	Long Term Evolution
MAG	Maximum Available Gain
MMIC	Monolithic Microwave Integrated Circuit
NDPA	Nonlinear Distributed Power Amplifier
OPEX	Operational Expenditure
PA	Power Amplifier
PAE	Power Added Efficiency
PAR	Peak-to-Average Ratio
PBO	Power Back Off
PCB	Printed Circuit Board
PLL	Phase Locked Loop
Q-factor	Quality Factor
R	Resistance (Ω)
RF	Radio Frequency
S-parameters	Scattering parameters
Si	Silicon
SiC	Silicon Carbide
SiGe	Silicon Germanium
SNR	Signal-to-Noise Ratio
TOSM	Thru-Open-Short-Match
V	Voltage / Volts
VCCS	Voltage Controlled Current Source
V_{DS}	Drain-source voltage

V_{GS}	Gate-source voltage
VNA	Vector Network Analyser
W mW	Watts, milliwatts
X	Reactance
Z	Impedance
Z_0	Characteristic Impedance
ε_r	Relative Permittivity
η	Efficiency
μ	Permeability
Ω	Ohms

Appendix G

Radar Band Designations

Radar Band Letter Designation	Frequency Range
High Frequency (HF)	3 - 30 MHz
Very High Frequency (VHF)	30 - 300 MHz
Ultra High Frequency (UHF)	300 MHz - 1000 MHz
L-band	1 - 2 GHz
S-band	2 - 4 GHz
C-band	4 - 8 GHz
X-band	8 - 12 GHz
Ku-band	12 - 18 GHz
K-band	18 - 27 GHz
Ka-band	27 - 40 GHz
V-band	40 - 75 GHz
W-band	75 - 110 GHz
mm	110 - 300 GHz

Reproduced from [80].

Appendix H

Cree CGH40025F Datasheet

CGH40025

25 W, RF Power GaN HEMT

Cree's CGH40025 is an unmatched, gallium nitride (GaN) high electron mobility transistor (HEMT). The CGH40025, operating from a 28 volt rail, offers a general purpose, broadband solution to a variety of RF and microwave applications. GaN HEMTs offer high efficiency, high gain and wide bandwidth capabilities making the CGH40025 ideal for linear and compressed amplifier circuits. The transistor is available in a screw-down, flange package and solder-down, pill packages.

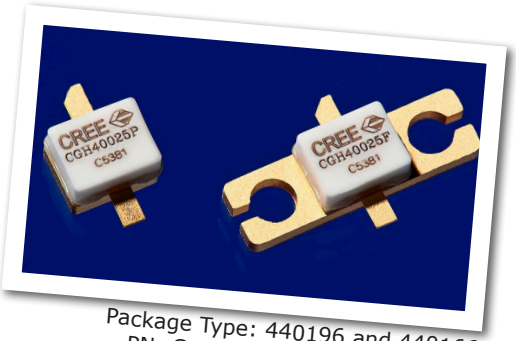

Package Type: 440196 and 440166
PN: CGH40025P and CGH40025F

FEATURES

- Up to 6 GHz Operation
- 15 dB Small Signal Gain at 2.0 GHz
- 13 dB Small Signal Gain at 4.0 GHz
- 30 W typical P_{SAT}
- 62 % Efficiency at P_{SAT}
- 28 V Operation

APPLICATIONS

- 2-Way Private Radio
- Broadband Amplifiers
- Cellular Infrastructure
- Test Instrumentation
- Class A, AB, Linear amplifiers suitable for OFDM, W-CDMA, EDGE, CDMA waveforms

RoHS COMPLIANT

Large Signal Models Available for SiC & GaN

Absolute Maximum Ratings (not simultaneous) at 25˚C Case Temperature

Parameter	Symbol	Rating	Units
Drain-Source Voltage	V_{DSS}	84	Volts
Gate-to-Source Voltage	V_{GS}	-10, +2	Volts
Storage Temperature	T_{STG}	-65, +150	˚C
Operating Junction Temperature	T_J	225	˚C
Maximum Forward Gate Current	I_{GMAX}	7.0	mA
Soldering Temperature[1]	T_S	245	˚C
Screw Torque	τ	60	in-oz
Thermal Resistance, Junction to Case[2]	$R_{\theta JC}$	4.8	˚C/W
Case Operating Temperature[2,3]	T_C	-40, +150	˚C

Note:
[1] Refer to the Application Note on soldering at www.cree.com/products/wireless_appnotes.asp
[2] Measured for the CGH40025F at P_{DISS} = 28 W.
[3] See also, the Power Dissipation De-rating Curve on Page 6.

Electrical Characteristics (T_C = 25˚C)

Characteristics	Symbol	Min.	Typ.	Max.	Units	Conditions
DC Characteristics[1]						
Gate Threshold Voltage	$V_{GS(th)}$	-3.8	-3.3	-2.3	V_{DC}	V_{DS} = 10 V, I_D = 7.2 mA
Gate Quiescent Voltage	$V_{GS(Q)}$	–	-3.0	–	V_{DC}	V_{DS} = 28 V, I_D = 250 mA
Saturated Drain Current	I_{DS}	5.8	7.0	–	A	V_{DS} = 6.0 V, V_{GS} = 2.0 V
Drain-Source Breakdown Voltage	V_{BR}	120	–	–	V_{DC}	V_{GS} = -8 V, I_D = 7.2 mA
RF Characteristics[2] (T_C = 25˚C, F_0 = 3.7 GHz unless otherwise noted)						
Small Signal Gain	G_{SS}	12	13	–	dB	V_{DD} = 28 V, I_{DQ} = 250 mA
Power Output[3]	P_{SAT}	20	30	–	W	V_{DD} = 28 V, I_{DQ} = 250 mA
Drain Efficiency[4]	η	55	62	–	%	V_{DD} = 28 V, I_{DQ} = 250 mA, P_{SAT}
Output Mismatch Stress	VSWR	–	–	10 : 1	Ψ	No damage at all phase angles, V_{DD} = 28 V, I_{DQ} = 250 mA, P_{OUT} = 25 W CW
Dynamic Characteristics						
Input Capacitance	C_{GS}	–	9.0	–	pF	V_{DS} = 28 V, V_{gs} = -8 V, f = 1 MHz
Output Capacitance	C_{DS}	–	2.6	–	pF	V_{DS} = 28 V, V_{gs} = -8 V, f = 1 MHz
Feedback Capacitance	C_{GD}	–	0.4	–	pF	V_{DS} = 28 V, V_{gs} = -8 V, f = 1 MHz

Notes:
[1] Measured on wafer prior to packaging.
[2] Measured in CGH40025-TB.
[3] P_{SAT} is defined as I_G = 0.72 mA.
[4] Drain Efficiency = P_{OUT} / P_{DC}

Cree, Inc.
4600 Silicon Drive
Durham, NC 27703
USA Tel: +1.919.313.5300
Fax: +1.919.869.2733
www.cree.com/wireless

Typical Performance

Small Signal Gain and Return Loss vs Frequency of the CGH40025F in the CGH40025-TB

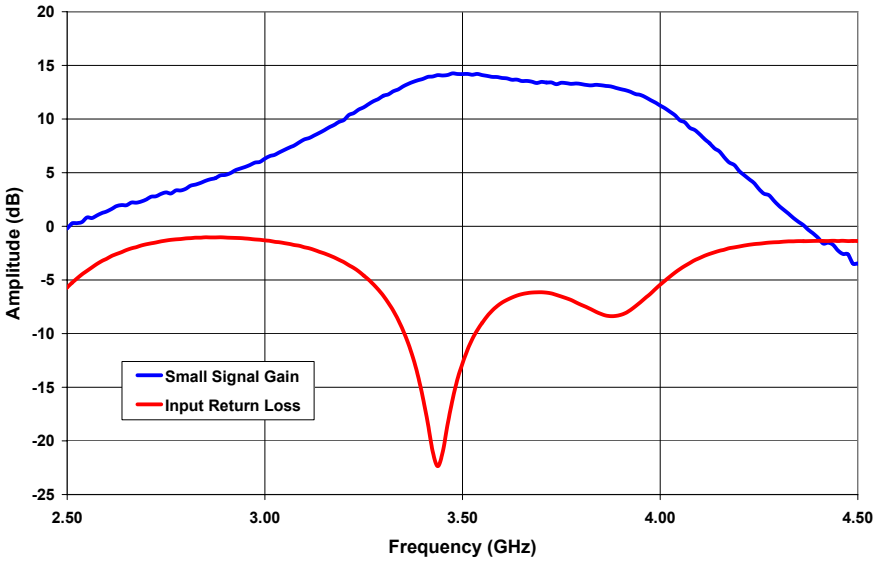

P_{SAT}, Gain, and Drain Efficiency vs Frequency of the CGH40025F in the CGH40025-TB
V_{DD} = 28 V, I_{DQ} = 250 mA

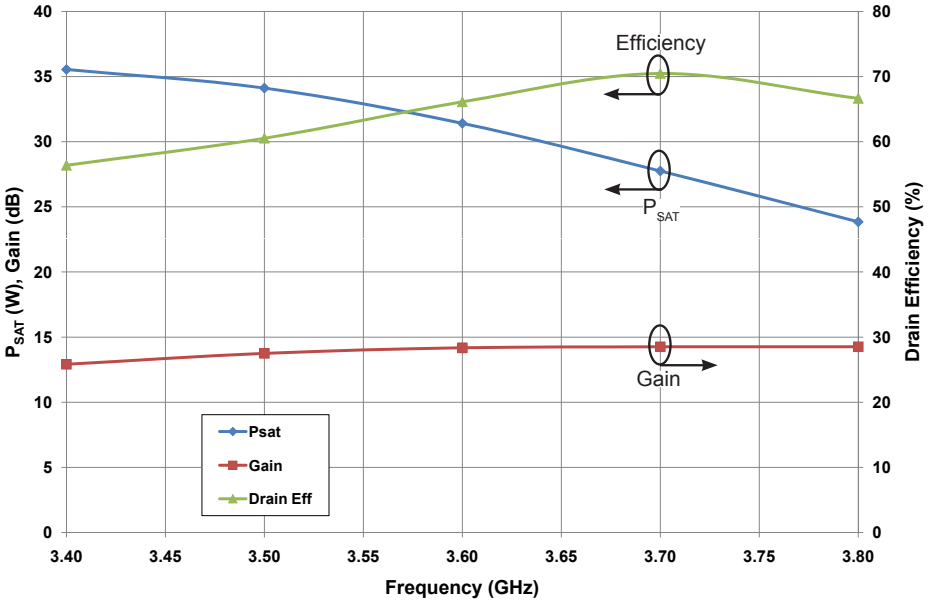

Cree, Inc.
4600 Silicon Drive
Durham, NC 27703
USA Tel: +1.919.313.5300
Fax: +1.919.869.2733
www.cree.com/wireless

Typical Performance

Swept CW Data of CGH40025 vs. Output Power with Source and Load Impedances Optimized for P_{SAT} Power in CGH40025-TB
V_{DD} = 28 V, I_{DQ} = 250 mA, Freq = 3.7 GHz

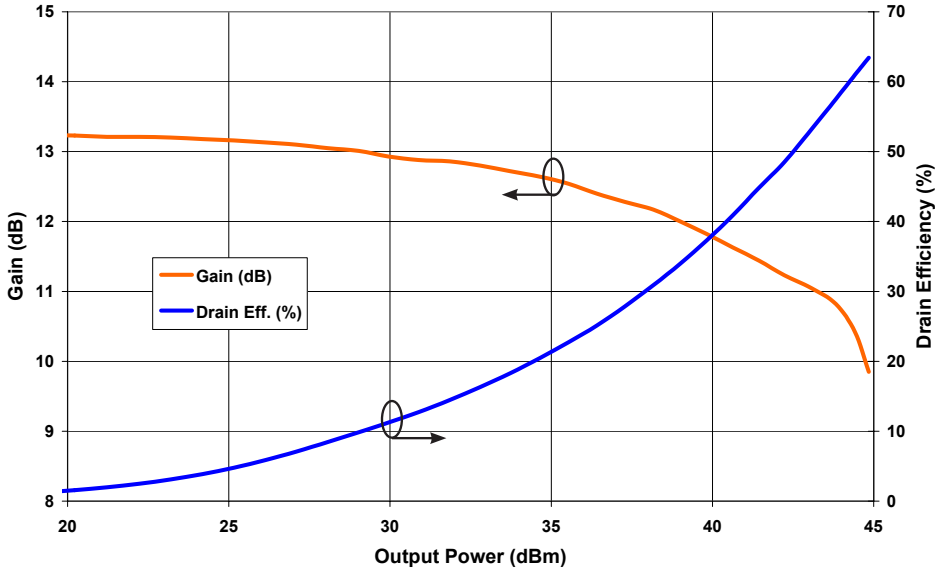

Maximum Available Gain and K Factor of the CGH40025
V_{DD} = 28 V, I_{DQ} = 250 mA

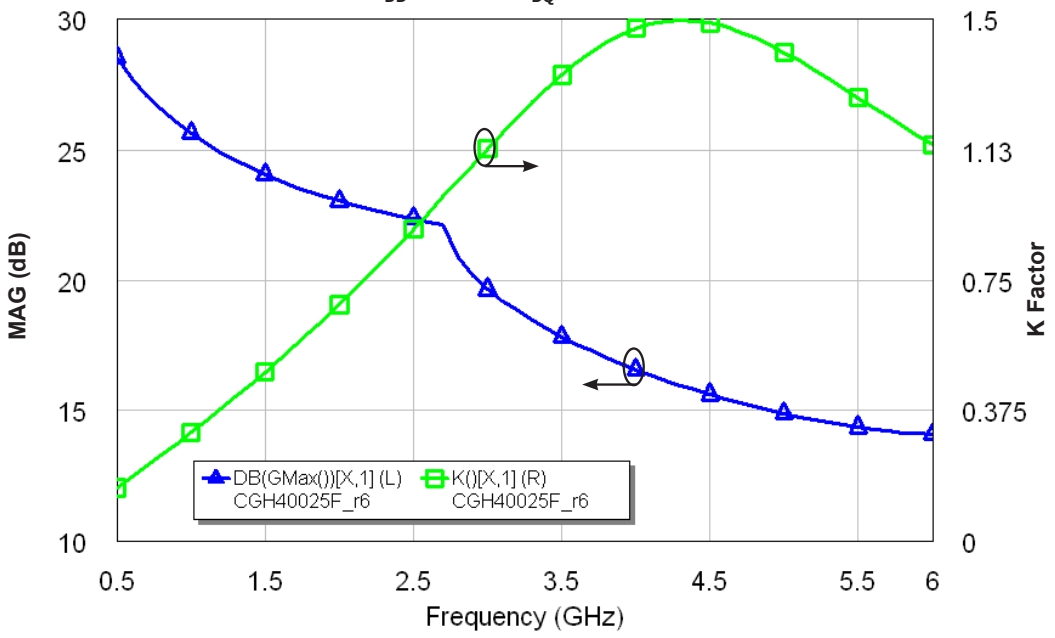

Cree, Inc.
4600 Silicon Drive
Durham, NC 27703
USA Tel: +1.919.313.5300
Fax: +1.919.869.2733
www.cree.com/wireless

Typical Noise Performance

Simulated Minimum Noise Figure and Noise Resistance vs Frequency of the CGH40025F
V_{DD} = 28 V, I_{DQ} = 250 mA

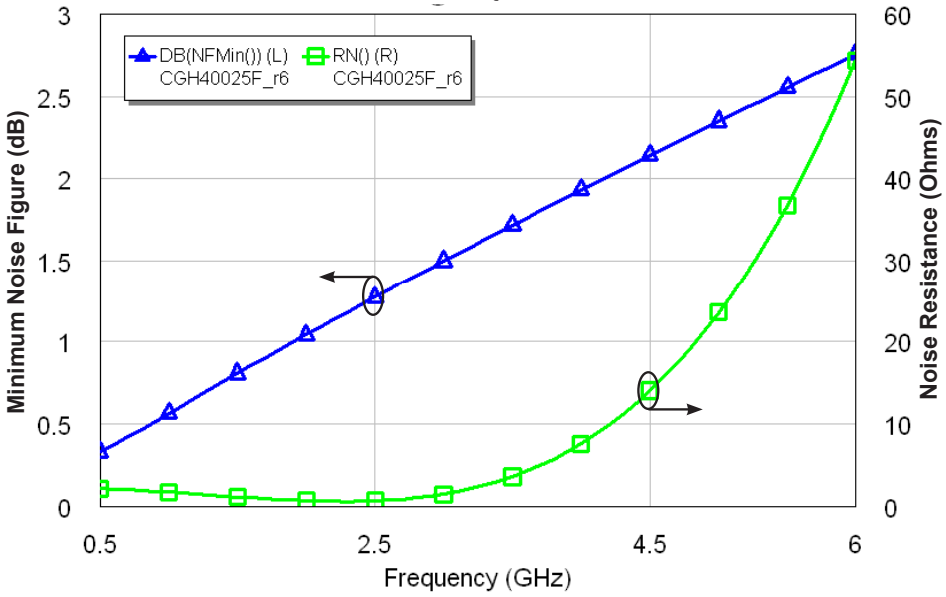

Electrostatic Discharge (ESD) Classifications

Parameter	Symbol	Class	Test Methodology
Human Body Model	HBM	1A > 250 V	JEDEC JESD22 A114-D
Charge Device Model	CDM	1 < 200 V	JEDEC JESD22 C101-C

Cree, Inc.
4600 Silicon Drive
Durham, NC 27703
USA Tel: +1.919.313.5300
Fax: +1.919.869.2733
www.cree.com/wireless

Source and Load Impedances

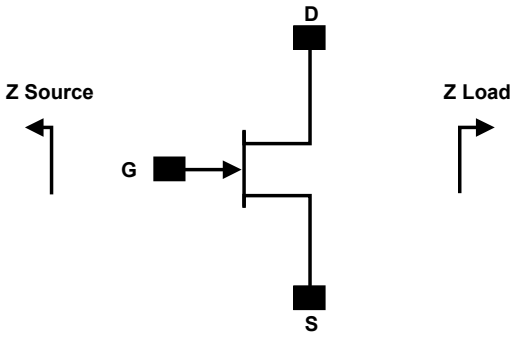

Frequency (MHz)	Z Source	Z Load
500	7.75 + j15.5	20 + j5.2
1000	3.11 + j5.72	17 + j6.66
1500	2.86 + j1.63	16.8 + j3.2
2500	1.2 - j3.26	9.41 + j3.2
3500	1.31 - j7.3	5.85 - j0.51

Note 1. V_{DD} = 28V, I_{DQ} = 250mA in the 440166 package.
Note 2. Optimized for power gain, P_{SAT} and PAE.
Note 3. When using this device at low frequency, series resistors should be used to maintain amplifier stability.

CGH40025 Power Dissipation De-rating Curve

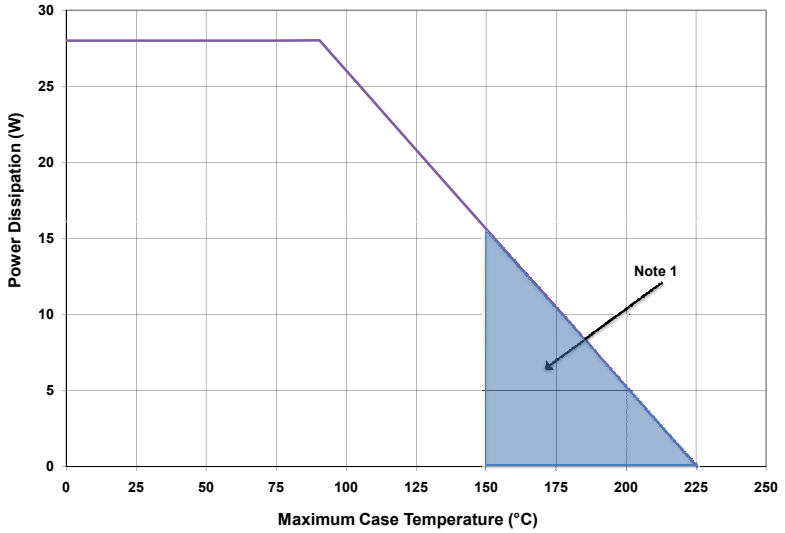

Note 1. Area exceeds Maximum Case Operating Temperature (See Page 2).

Cree, Inc.
4600 Silicon Drive
Durham, NC 27703
USA Tel: +1.919.313.5300
Fax: +1.919.869.2733
www.cree.com/wireless

CGH40025-TB Demonstration Amplifier Circuit Schematic

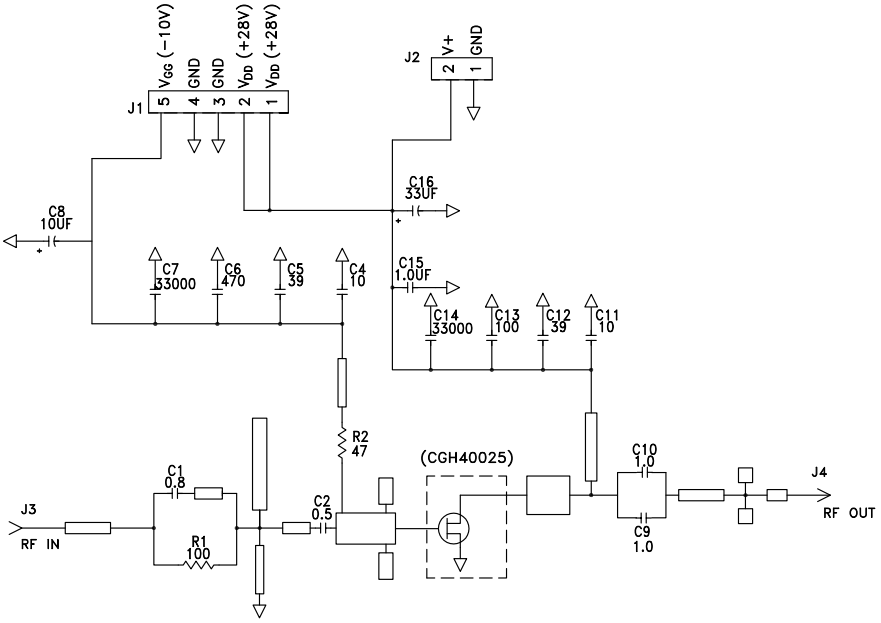

CGH40025-TB Demonstration Amplifier Circuit Outline

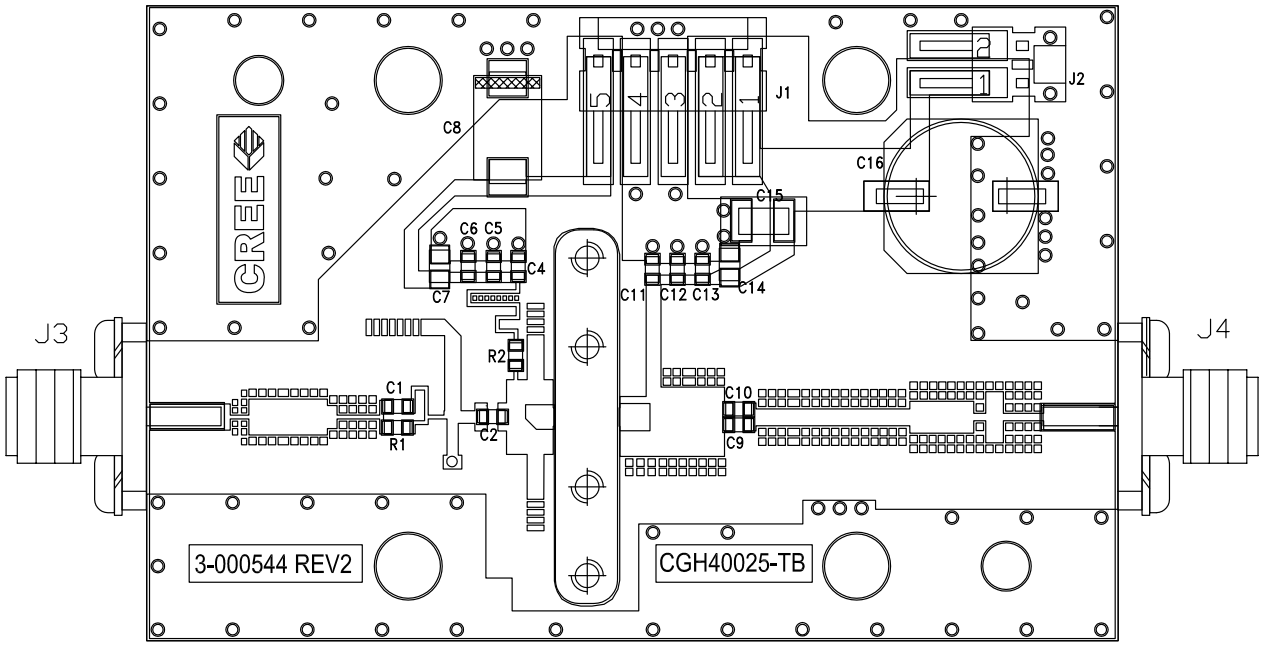

Cree, Inc.
4600 Silicon Drive
Durham, NC 27703
USA Tel: +1.919.313.5300
Fax: +1.919.869.2733
www.cree.com/wireless

CGH40025-TB Demonstration Amplifier Circuit Bill of Materials

Designator	Description	Qty
R2	RES,1/16W,0603,1%,47 OHMS	1
R1	RES,1/16W,0603,1%,100 OHMS	1
C6	CAP, 470PF, 5%,100V, 0603	1
C16	CAP, 33 UF, 20%, G CASE	1
C15	CAP, 1.0UF, 100V, 10%, X7R, 1210	1
C8	CAP 10UF 16V TANTALUM	1
C13	CAP, 100.0pF, +/-5%, 0603	1
C1	CAP, 0.8pF, +/-0.1pF, 0603	1
C2	CAP, 0.5pF, +/-0.1pF, 0603	1
C9,C10	CAP, 1.0pF, +/-0.1pF, 0603	2
C4,C11	CAP, 10.0pF,+/-5%, 0603	2
C5,C12	CAP, 39pF, +/-5%, 0603	2
C7,C14	CAP,33000PF, 0805,100V, X7R	2
J3,J4	CONN SMA STR PANEL JACK RECP	2
J1	HEADER RT>PLZ .1CEN LK 5POS	1
-	PCB, RO4350B, Er = 3.48, h = 20 mil	1
-	CGH40025F or CGH40025P	1

CGH40025-TB Demonstration Amplifier Circuit

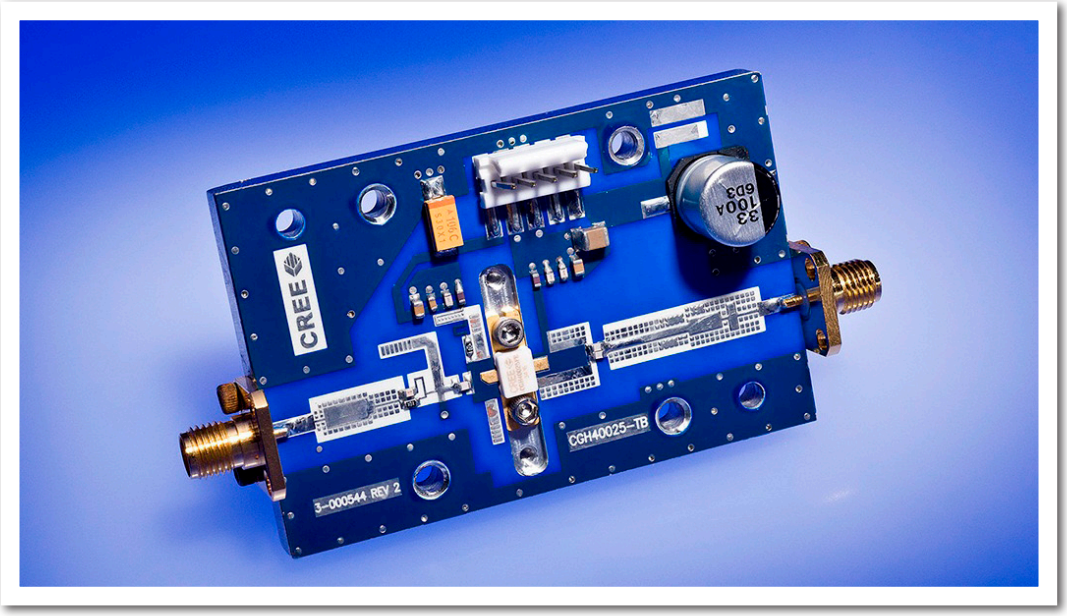

Cree, Inc.
4600 Silicon Drive
Durham, NC 27703
USA Tel: +1.919.313.5300
Fax: +1.919.869.2733
www.cree.com/wireless

Typical Package S-Parameters for CGH40025
(Small Signal, V_{DS} = 28 V, I_{DQ} = 100 mA, angle in degrees)

Frequency	Mag S11	Ang S11	Mag S21	Ang S21	Mag S12	Ang S12	Mag S22	Ang S22
500 MHz	0.902	-151.72	11.80	92.09	0.025	6.22	0.393	-140.34
600 MHz	0.901	-157.13	9.89	87.31	0.025	2.28	0.402	-143.54
700 MHz	0.900	-161.20	8.49	83.18	0.025	-0.99	0.412	-145.64
800 MHz	0.900	-164.41	7.42	79.49	0.025	-3.82	0.424	-147.11
900 MHz	0.901	-167.04	6.58	76.10	0.024	-6.33	0.436	-148.22
1.0 GHz	0.902	-169.26	5.89	72.93	0.024	-8.60	0.449	-149.12
1.1 GHz	0.903	-171.19	5.33	69.93	0.024	-10.69	0.462	-149.91
1.2 GHz	0.904	-172.89	4.86	67.07	0.023	-12.61	0.476	-150.65
1.3 GHz	0.905	-174.43	4.45	64.33	0.023	-14.39	0.489	-151.38
1.4 GHz	0.906	-175.84	4.10	61.68	0.022	-16.06	0.503	-152.12
1.5 GHz	0.907	-177.14	3.80	59.12	0.022	-17.61	0.517	-152.87
1.6 GHz	0.909	-178.36	3.54	56.64	0.022	-19.05	0.531	-153.65
1.7 GHz	0.910	-179.52	3.30	54.22	0.021	-20.38	0.545	-154.46
1.8 GHz	0.912	179.38	3.09	51.87	0.021	-21.62	0.558	-155.29
1.9 GHz	0.913	178.33	2.90	49.58	0.020	-22.75	0.571	-156.15
2.0 GHz	0.914	177.30	2.73	47.34	0.020	-23.78	0.584	-157.04
2.1 GHz	0.916	176.31	2.58	45.15	0.019	-24.70	0.596	-157.95
2.2 GHz	0.917	175.34	2.44	43.02	0.019	-25.52	0.608	-158.88
2.3 GHz	0.918	174.39	2.31	40.92	0.018	-26.22	0.620	-159.82
2.4 GHz	0.920	173.46	2.19	38.88	0.018	-26.82	0.631	-160.78
2.5 GHz	0.921	172.54	2.09	36.87	0.017	-27.29	0.642	-161.76
2.6 GHz	0.922	171.63	1.99	34.91	0.016	-27.64	0.652	-162.74
2.7 GHz	0.923	170.73	1.90	32.98	0.016	-27.85	0.662	-163.73
2.8 GHz	0.925	169.84	1.82	31.09	0.015	-27.92	0.672	-164.73
2.9 GHz	0.926	168.95	1.74	29.24	0.015	-27.85	0.681	-165.73
3.0 GHz	0.927	168.07	1.67	27.41	0.014	-27.61	0.690	-166.74
3.2 GHz	0.929	166.30	1.54	23.86	0.013	-26.63	0.706	-168.76
3.4 GHz	0.931	164.54	1.42	20.42	0.013	-24.89	0.721	-170.79
3.6 GHz	0.932	162.78	1.33	17.08	0.012	-22.30	0.735	-172.82
3.8 GHz	0.934	161.00	1.24	13.84	0.011	-18.80	0.748	-174.85
4.0 GHz	0.935	159.21	1.16	10.67	0.011	-14.40	0.759	-176.88
4.2 GHz	0.936	157.39	1.10	7.58	0.010	-9.18	0.769	-178.90
4.4 GHz	0.937	155.55	1.04	4.55	0.010	-3.38	0.778	179.07
4.6 GHz	0.938	153.67	0.98	1.57	0.010	2.65	0.787	177.04
4.8 GHz	0.939	151.77	0.94	-1.36	0.011	8.52	0.794	175.00
5.0 GHz	0.939	149.82	0.89	-4.25	0.011	13.87	0.801	172.96
5.2 GHz	0.939	147.82	0.86	-7.11	0.012	18.48	0.807	170.90
5.4 GHz	0.939	145.78	0.82	-9.95	0.013	22.25	0.812	168.83
5.6 GHz	0.940	143.68	0.79	-12.78	0.014	25.17	0.817	166.74
5.8 GHz	0.939	141.53	0.77	-15.59	0.016	27.32	0.821	164.62
6.0 GHz	0.939	139.31	0.74	-18.41	0.017	28.77	0.825	162.48

Download this s-parameter file in ".s2p" format at http://www.cree.com/products/wireless_s-parameters.asp

Cree, Inc.
4600 Silicon Drive
Durham, NC 27703
USA Tel: +1.919.313.5300
Fax: +1.919.869.2733
www.cree.com/wireless

Typical Package S-Parameters for CGH40025
(Small Signal, V_{DS} = 28 V, I_{DQ} = 250 mA, angle in degrees)

Frequency	Mag S11	Ang S11	Mag S21	Ang S21	Mag S12	Ang S12	Mag S22	Ang S22
500 MHz	0.917	-157.22	12.62	91.45	0.018	7.56	0.458	-158.97
600 MHz	0.916	-161.92	10.57	87.33	0.018	4.70	0.465	-160.93
700 MHz	0.916	-165.46	9.07	83.78	0.018	2.41	0.472	-162.19
800 MHz	0.916	-168.28	7.94	80.58	0.018	0.51	0.478	-163.04
900 MHz	0.916	-170.61	7.05	77.64	0.017	-1.12	0.485	-163.64
1.0 GHz	0.916	-172.60	6.33	74.88	0.017	-2.55	0.493	-164.09
1.1 GHz	0.917	-174.33	5.74	72.25	0.017	-3.82	0.500	-164.45
1.2 GHz	0.917	-175.88	5.24	69.73	0.017	-4.94	0.508	-164.77
1.3 GHz	0.918	-177.28	4.82	67.30	0.017	-5.95	0.516	-165.06
1.4 GHz	0.918	-178.57	4.46	64.94	0.017	-6.84	0.525	-165.36
1.5 GHz	0.919	-179.78	4.14	62.65	0.016	-7.63	0.533	-165.67
1.6 GHz	0.919	179.09	3.87	60.41	0.016	-8.31	0.542	-165.99
1.7 GHz	0.920	178.01	3.62	58.22	0.016	-8.90	0.550	-166.35
1.8 GHz	0.921	176.98	3.40	56.07	0.016	-9.39	0.559	-166.73
1.9 GHz	0.921	175.99	3.21	53.97	0.015	-9.77	0.568	-167.14
2.0 GHz	0.922	175.03	3.03	51.90	0.015	-10.06	0.577	-167.59
2.1 GHz	0.923	174.09	2.87	49.87	0.015	-10.24	0.585	-168.07
2.2 GHz	0.924	173.17	2.73	47.87	0.014	-10.31	0.594	-168.57
2.3 GHz	0.924	172.27	2.60	45.91	0.014	-10.27	0.602	-169.11
2.4 GHz	0.925	171.39	2.47	43.97	0.014	-10.12	0.610	-169.67
2.5 GHz	0.926	170.51	2.36	42.07	0.014	-9.85	0.619	-170.26
2.6 GHz	0.926	169.65	2.26	40.19	0.013	-9.46	0.626	-170.88
2.7 GHz	0.927	168.79	2.16	38.34	0.013	-8.95	0.634	-171.52
2.8 GHz	0.928	167.93	2.08	36.52	0.013	-8.31	0.642	-172.17
2.9 GHz	0.928	167.08	1.99	34.72	0.013	-7.54	0.649	-172.85
3.0 GHz	0.929	166.24	1.92	32.94	0.013	-6.65	0.656	-173.55
3.2 GHz	0.930	164.54	1.78	29.45	0.012	-4.49	0.670	-175.00
3.4 GHz	0.931	162.85	1.66	26.05	0.012	-1.85	0.683	-176.50
3.6 GHz	0.932	161.14	1.55	22.72	0.012	1.19	0.695	-178.06
3.8 GHz	0.933	159.42	1.46	19.46	0.012	4.55	0.706	-179.66
4.0 GHz	0.933	157.68	1.38	16.27	0.012	8.08	0.716	178.70
4.2 GHz	0.934	155.91	1.31	13.12	0.012	11.64	0.726	177.02
4.4 GHz	0.934	154.11	1.24	10.03	0.013	15.08	0.735	175.30
4.6 GHz	0.935	152.28	1.18	6.97	0.013	18.26	0.743	173.56
4.8 GHz	0.935	150.41	1.13	3.95	0.014	21.09	0.750	171.78
5.0 GHz	0.935	148.49	1.08	0.96	0.015	23.50	0.756	169.97
5.2 GHz	0.935	146.53	1.04	-2.00	0.016	25.48	0.762	168.12
5.4 GHz	0.935	144.52	1.00	-4.96	0.017	27.02	0.768	166.24
5.6 GHz	0.935	142.45	0.97	-7.90	0.018	28.12	0.773	164.32
5.8 GHz	0.934	140.31	0.94	-10.84	0.020	28.83	0.777	162.36
6.0 GHz	0.934	138.12	0.91	-13.79	0.021	29.18	0.781	160.36

Download this s-parameter file in ".s2p" format at http://www.cree.com/products/wireless_s-parameters.asp

Cree, Inc.
4600 Silicon Drive
Durham, NC 27703
USA Tel: +1.919.313.5300
Fax: +1.919.869.2733
www.cree.com/wireless

Typical Package S-Parameters for CGH40025
(Small Signal, V_{DS} = 28 V, I_{DQ} = 400 mA, angle in degrees)

Frequency	Mag S11	Ang S11	Mag S21	Ang S21	Mag S12	Ang S12	Mag S22	Ang S22
500 MHz	0.924	-159.12	12.64	91.13	0.015	8.27	0.485	-163.72
600 MHz	0.923	-163.56	10.58	87.23	0.015	5.84	0.491	-165.34
700 MHz	0.923	-166.92	9.08	83.86	0.015	3.96	0.497	-166.41
800 MHz	0.923	-169.60	7.95	80.83	0.015	2.43	0.502	-167.13
900 MHz	0.923	-171.82	7.06	78.03	0.015	1.16	0.508	-167.65
1.0 GHz	0.923	-173.72	6.34	75.40	0.015	0.08	0.514	-168.05
1.1 GHz	0.923	-175.39	5.75	72.89	0.015	-0.84	0.520	-168.36
1.2 GHz	0.924	-176.88	5.26	70.48	0.015	-1.62	0.526	-168.63
1.3 GHz	0.924	-178.24	4.84	68.15	0.015	-2.29	0.533	-168.88
1.4 GHz	0.924	-179.50	4.48	65.89	0.015	-2.85	0.539	-169.13
1.5 GHz	0.925	179.33	4.17	63.68	0.014	-3.31	0.546	-169.38
1.6 GHz	0.925	178.22	3.89	61.52	0.014	-3.67	0.553	-169.65
1.7 GHz	0.926	177.17	3.65	59.41	0.014	-3.93	0.560	-169.94
1.8 GHz	0.926	176.16	3.43	57.34	0.014	-4.09	0.568	-170.26
1.9 GHz	0.927	175.18	3.24	55.30	0.014	-4.16	0.575	-170.60
2.0 GHz	0.927	174.24	3.07	53.29	0.014	-4.13	0.582	-170.97
2.1 GHz	0.928	173.32	2.91	51.32	0.013	-4.00	0.589	-171.36
2.2 GHz	0.928	172.41	2.76	49.38	0.013	-3.76	0.597	-171.79
2.3 GHz	0.929	171.53	2.63	47.46	0.013	-3.43	0.604	-172.24
2.4 GHz	0.929	170.65	2.51	45.57	0.013	-2.99	0.611	-172.71
2.5 GHz	0.929	169.79	2.40	43.71	0.013	-2.44	0.618	-173.22
2.6 GHz	0.930	168.93	2.30	41.87	0.013	-1.79	0.625	-173.75
2.7 GHz	0.930	168.08	2.20	40.05	0.012	-1.04	0.632	-174.30
2.8 GHz	0.931	167.24	2.12	38.26	0.012	-0.18	0.638	-174.87
2.9 GHz	0.931	166.40	2.04	36.48	0.012	0.77	0.645	-175.47
3.0 GHz	0.932	165.56	1.96	34.73	0.012	1.82	0.651	-176.08
3.2 GHz	0.932	163.88	1.82	31.28	0.012	4.18	0.663	-177.37
3.4 GHz	0.933	162.20	1.70	27.91	0.012	6.83	0.675	-178.72
3.6 GHz	0.934	160.51	1.60	24.60	0.012	9.69	0.686	179.86
3.8 GHz	0.934	158.80	1.51	21.35	0.012	12.64	0.696	178.39
4.0 GHz	0.935	157.07	1.42	18.16	0.013	15.58	0.706	176.88
4.2 GHz	0.935	155.32	1.35	15.01	0.013	18.40	0.715	175.31
4.4 GHz	0.935	153.53	1.29	11.91	0.014	21.01	0.723	173.70
4.6 GHz	0.935	151.70	1.23	8.84	0.014	23.33	0.730	172.05
4.8 GHz	0.935	149.84	1.17	5.80	0.015	25.32	0.737	170.36
5.0 GHz	0.935	147.93	1.13	2.79	0.016	26.96	0.743	168.63
5.2 GHz	0.935	145.98	1.09	-0.20	0.017	28.24	0.749	166.86
5.4 GHz	0.935	143.97	1.05	-3.19	0.018	29.16	0.754	165.05
5.6 GHz	0.934	141.91	1.01	-6.16	0.020	29.75	0.759	163.20
5.8 GHz	0.934	139.78	0.98	-9.14	0.021	30.02	0.763	161.30
6.0 GHz	0.933	137.58	0.96	-12.12	0.023	29.99	0.767	159.35

Download this s-parameter file in ".s2p" format at http://www.cree.com/products/wireless_s-parameters.asp

Cree, Inc.
4600 Silicon Drive
Durham, NC 27703
USA Tel: +1.919.313.5300
Fax: +1.919.869.2733
www.cree.com/wireless

Product Dimensions CGH40025F (Package Type — 440166)

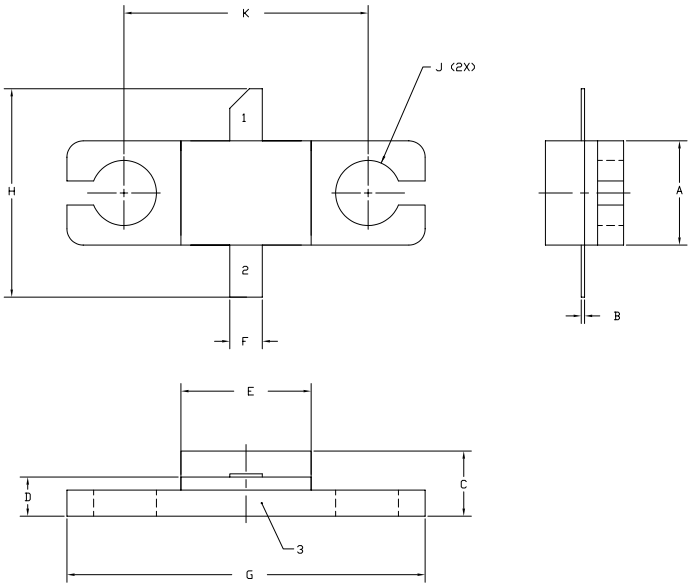

NOTES:

1. DIMENSIONING AND TOLERANICING PER ANSI Y14.5M, 1982.
2. CONTROLLING DIMENSION: INCH.
3. ADHESIVE FROM LID MAY EXTEND A MAXIMUM OF 0.020" BEYOND EDGE OF LID.
4. LID MAY BE MISALIGNED TO THE BODY OF THE PACKAGE BY A MAXIMUM OF 0.008" IN ANY DIRECTION.
5. ALL PLATED SURFACES ARE NI/AU

	INCHES		MILLIMETERS	
DIM	MIN	MAX	MIN	MAX
A	0.155	0.165	3.94	4.19
B	0.004	0.006	0.10	0.15
C	0.115	0.135	2.92	3.43
D	0.057	0.067	1.45	1.70
E	0.195	0.205	4.95	5.21
F	0.045	0.055	1.14	1.40
G	0.545	0.555	13.84	14.09
H	0.280	0.360	7.87	8.38
J	ø .100		2.54	
K	0.375		9.53	

PIN 1. GATE
PIN 2. DRAIN
PIN 3. SOURCE

Product Dimensions CGH40025P (Package Type — 440196)

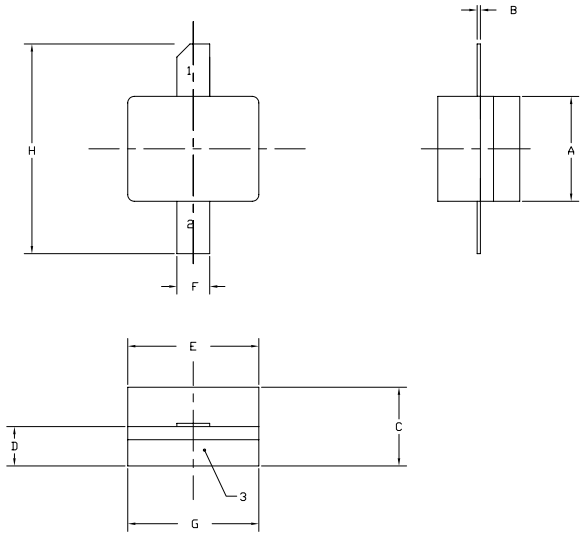

NOTES:

1. DIMENSIONING AND TOLERANICING PER ANSI Y14.5M, 1982.
2. CONTROLLING DIMENSION: INCH.
3. ADHESIVE FROM LID MAY EXTEND A MAXIMUM OF 0.020" BEYOND EDGE OF LID.
4. LID MAY BE MISALIGNED TO THE BODY OF THE PACKAGE BY A MAXIMUM OF 0.008" IN ANY DIRECTION.
5. ALL PLATED SURFACES ARE NI/AU

	INCHES		MILLIMETERS	
DIM	MIN	MAX	MIN	MAX
A	0.155	0.165	3.94	4.19
B	0.003	0.006	0.10	0.15
C	0.115	0.135	2.92	3.17
D	0.057	0.067	1.45	1.70
E	0.195	0.205	4.95	5.21
F	0.045	0.055	1.14	1.40
G	0.195	0.205	4.95	5.21
H	0.280	0.360	7.112	9.114

PIN 1. GATE
PIN 2. DRAIN
PIN 3. SOURCE

Cree, Inc.
4600 Silicon Drive
Durham, NC 27703
USA Tel: +1.919.313.5300
Fax: +1.919.869.2733
www.cree.com/wireless

Disclaimer

Specifications are subject to change without notice. Cree, Inc. believes the information contained within this data sheet to be accurate and reliable. However, no responsibility is assumed by Cree for any infringement of patents or other rights of third parties which may result from its use. No license is granted by implication or otherwise under any patent or patent rights of Cree. Cree makes no warranty, representation or guarantee regarding the suitability of its products for any particular purpose. "Typical" parameters are the average values expected by Cree in large quantities and are provided for information purposes only. These values can and do vary in different applications and actual performance can vary over time. All operating parameters should be validated by customer's technical experts for each application. Cree products are not designed, intended or authorized for use as components in applications intended for surgical implant into the body or to support or sustain life, in applications in which the failure of the Cree product could result in personal injury or death or in applications for planning, construction, maintenance or direct operation of a nuclear facility.

For more information, please contact:

Cree, Inc.
4600 Silicon Drive
Durham, NC 27703
www.cree.com/wireless

Ryan Baker
Marketing
Cree, Wireless Devices
919.287.7816

Tom Dekker
Sales Director
Cree, Wireless Devices
919.313.5639

Cree, Inc.
4600 Silicon Drive
Durham, NC 27703
USA Tel: +1.919.313.5300
Fax: +1.919.869.2733
www.cree.com/wireless

Appendix I

AtlanTecRF Coaxial Cable Datasheet

Coaxial Cable
Semi-Flex & Semi-Rigid

- .034, .047, .086, .141, .250 ins. O/D
- Copper, Aluminium & Composite
- Choice of Plating
- Lengths to 50ft, 15m
- Choice of Impedance
- Very Cost Effective

General Specifications	
Impedance	50 ohms
Outer Conductor Material	See table
Dielectric Material	PTFE
Centre Conductor Material	Table code
Silver Plated Copper-clad Steel	SPST
Silver Plated Copper	SPC
Operating Temperature Range	-55+125C
Attenuation data is at	+20C, Sea level, dB/100m max.
Power Rating data is at	5GHz, +20C, Sea level, CW, watts
Power Rating	Increases for frequencies below 5GHz Decreases for frequencies above 5GHz Please contact factory for additional information

Part Number	Nom. O/Dins.	Type (1)	Outer Conductor Material (2)	Overall Outer Dia. (mm)	Centre Conductor Material	Centre Conductor Dia. (mm)	Attenuation (dB/100m) max.					Inside Bend Radius (mm) min.	Power at 5GHz (watts) max.
							0.5 (GHz)	1 (GHz)	5 (GHz)	10 (GHz)	20 (GHz)		
ASF-047	.047	SF	C/TC	1.19	SPST	0.29	79	112	258	373	544	4.00	19.1
ASF-086	.086	SF	C/TC	2.10	SPST	0.51	45	64	151	222	329	6.00	52.2
ASF-141	.141	SF	C/TC	3.52	SPST	0.92	26	39	92	138	210	8.00	126.7
ASF-250	.250	SF	C/TC	6.10	SPC	1.65	17	25	63	98	N/A	30.00	210.0
ASR-086	.086	SF	A/TP	2.20	SPST	0.51	45	64	151	222	329	7.63	52.2
ASR-141	.141	SF	A/TP	3.58	SPST	0.92	26	38	91	137	209	12.50	126.7
ASR-250	.250	SF	A/TP	6.35	SPC	1.65	16	24	61	94	N/A	22.23	265.3
CSR-034	.034	SR	PC	0.86	SPST	0.20	112	159	362	520	752	3.00	11.1
CSR-047	.047	SR	PC	1.19	SPST	0.29	79	113	259	374	544	4.20	24.7
CSR-086	.086	SR	PC	2.20	SPST	0.51	45	64	151	222	329	7.63	69.8
CSR-141	.141	SR	PC	3.58	SPST	0.92	26	38	91	137	209	12.50	174.4
CSR-250	.250	SR	PC	6.35	SPC	1.65	16	24	61	94	N/A	22.23	364.4
CSR-034T	.034	SR	C/TP	0.86	SPST	0.20	112	159	362	520	752	3.00	9.5
CSR-047T	.047	SR	C/TP	1.19	SPST	0.29	79	113	259	374	544	4.20	20.7
CSR-086T	.086	SR	C/TP	2.20	SPST	0.51	45	64	151	222	329	7.63	57.2
CSR-141T	.141	SR	C/TP	3.58	SPST	0.92	26	38	91	137	209	12.50	140.4
CSR-250T	.250	SR	C/TP	6.35	SPC	1.65	16	24	61	94	N/A	22.23	290.0

(1) SF = Semi Flexible, SR = Semi Rigid
(2) C/TC = Copper/Tin Composite, A/TP = Aluminium, Tin Plated, PC = Plain Copper, C/TP = Copper, Tin Plated

Data for Capacitance, Corona, Voltage Withstand and Moding Frequency is also available. Please contact factory for additional information.
Options: • Alternative Impedances
- FEP Jacket for Semi-Flexible types
- Silver Plated Copper Outer Conductor for Semi-Rigid types
- Silver Plated Copper Centre Conductor for some .086 and .141 types
- Low Loss versions are also available – See separate data sheet.
- Fully Flexible Cables are also available – See separate data sheet.

Note:
Material options will affect electrical and mechanical performance, including attenuation and power rating.
Please contact factory for additional information.

We reserve the right to change standard product specifications without notice but will be pleased to consider control drawings for quotation.